Interference cancellation in MIMO and massive MIMO systems

Abdelhamid Ladaycia

UNIVERSITÉ PARIS 13 | USPC Université Sorbonne Paris Cité

Galilée Ecole doctorale

THÈSE

pour obtenir le grade de

Docteur de l'université Paris 13, Sorbonne Paris Cité

Discipline : "Doctorat de sciences pour l'ingénieur"

présentée et soutenue publiquement par

Abdelhamid LADAYCIA

le 01 Juillet 2019

Annulation d'interférences dans les systèmes MIMO et MIMO massifs (Massive MIMO)

Directeur de thèse : **Prof. Anissa Mokraoui**

Co-directeur de thèse : **Prof. Karim Abed-Meraim**

Co-directeur de thèse : **Prof. Adel Belouchrani**

JURY

Pierre Duhamel,	Directeur de recherches CNRS, Ecole Centrale Supélec	Président
Philippe Ciblat,	Professeur, Telecom Paristech	Examinateur
Jean Pierre Delmas,	Professeur, Telecom SudParis	Rapporteur
Mohammed Nabil El Korso,	Maître de conférences HDR, Université Paris Naterre	Rapporteur
Gabriel Dauphin,	maître de conférences, Université Paris 13	Examinateur
Anissa Mokraoui,	Professeur, Université Paris 13	Examinateur
Karim Abed-Meraim,	Professeur, Université d'Orléans	Examinateur
Adel Belouchrani,	Professeur, ENP d'Alger	Examinateur

L2TI LABORATOIRE DE TRAITEMENT ET TRANSPORT DE L'INFORMATION UNIVERSITE PARIS 13

L'Université Paris 13 est membre de : USPC Université Sorbonne Paris Cité

CAMPUS CONDORCET Paris-Aubervilliers

It is with my deepest gratitude and appreciation that I dedicate this thesis

To my parents;
To my wife.

To my son Mouetez Billah;
To my daughters Alaa and Acile;
To brothers and sisters.

for their constant source of love,
support and encouragement.

Acknowledgments

> *None of us got to where we are alone. Whether the assistance we received was obvious or subtle, acknowledging someone's help is a big part of understanding the importance of saying thank you.*
>
> Harvey Mackay.

Time goes by so fast and it has been already four years since the first time I came to France for a huge turning point in my life. Doing a PhD thesis in France in general and at University Sorbone, Paris 13 in particular has been one of the most enjoyable time in my life. Without the guidance of the committee members, the help from my friends and the encouragement of my family, my thesis would not have been possible. Therefore, I would like to thank all people who have contributed in a variety of ways to this dissertation.

First of all, I would like to thank almighty Allah (SWT) for his countless blessing on me at every sphere of life. May he help us to follow Islam in its true spirit according to the teachings of his prophet Muhammed (PBUH).

Secondly, I would like to thank my country, Algeria, that gave me the opportunity to continue my study and offer me PhD scholarship. Especially the RD department (DRD) of CFDAT/MDN, I am greatly thankful to Mr. REMILI Kamel and Mr GUEROUI Fawzi.

I would like to express my deepest gratitude to my doctoral supervisors: Professor Anissa MOKRAOUI, Professor Karim ABED-MERAIM and Professor Adel BELOUCHRANI for their guidance and support in several years. It has been a great pleasure for me to work on an interesting PhD project and from which I have a great chance to improve my mathematical skills and work with various researchers from different institutions. I am thankful to them for listening patiently all my questions, sharing their knowledge to me and giving me a lot of outstanding advice to overcome numerous obstacles.

Beside my supervisors, I am deeply thankful to Professors Jean Pierre DELMAS and Mohammed Nabil EL KORSO, the two reviewers of my dissertation. It is a great honor for me to have my PhD thesis evaluated by these experts. I also want to express my gratitude to the president of my thesis committee Professor Pierre DUHAMEL and the two examinators Philippe CIBLAT and Gabriel DAUPHIN, for their insightful comments and encouragements.

Moreover, without hesitation, I would like to thank all my friends in L2TI laboratory (University Sorbonne, Paris 13) for their encouragement and support. They make my stay and study in this place more enjoyable. I am happy to share a lot of memorable moments with them.

Finally, I would also express my appreciation to my wife who provide unending inspiration. She is always supporting and encouraging me with their best effort.

Thank you very much, everyone !

Résumé

Les systèmes de communications MIMO (Multiple Input Multiple Output) utilisent des réseaux de capteurs qui peuvent s'étendre à de grandes dimensions (MIMO massifs) et qui sont pressentis comme solution potentielle pour les futurs standards de communications à très hauts débits.

Un des problèmes majeur de ces systèmes est le fort niveau d'interférences dû au grand nombre d'émetteurs simultanés. Dans un tel contexte, les solutions 'classiques' de conception de pilotes 'orthogonaux' sont extrêmement coûteuses en débit utile permettant ainsi aux solutions d'identification de canal dites 'aveugles' ou 'semi-aveugles' (abandonnées pour un temps dans les systèmes de communications civiles) de revenir au-devant de la scène comme solutions intéressantes d'identification ou de déconvolution de ces canaux MIMO.

Dans cette thèse, nous avons commencé par une analyse comparative des performances, en se basant sur les bornes de Cramèr-Rao (CRB), afin de mesurer la réduction potentielle de la taille des séquences pilotes et ce en employant les méthodes dites semi-aveugles basées sur l'exploitation conjointe des pilotes et des données. Les résultats d'analyse montrent que nous pouvons réduire jusqu'à 95% des pilotes sans affecter les performances d'estimation du canal.

Nous avons par la suite proposé de nouvelles méthodes d'estimation semi-aveugle du canal, éventuellement de faible coût, permettant d'approcher les performances limites (CRB). Nous avons proposé un estimateur semi-aveugle, LS-DF (Least Squares-Decision Feedback), basé sur une estimation des moindres carrés avec retour de décision qui permet un bon compromis performance / complexité numérique. Un autre estimateur semi-aveugle de type sous-espace a aussi été proposé ainsi qu'un algorithme basé sur l'approche EM (Expectation Maximization) pour lequel trois versions à coût réduit ont été étudiées. Dans le cas d'un canal spéculaire, nous avons proposé un algorithme d'estimation paramétrique se basant sur l'estimation des temps d'arrivés combinée avec la technique DF.

Mots Clés— MIMO/ massive MIMO, OFDM, CRB, semi-aveugle, méthode sous-espace, algorithme EM, LS-DF, canal spéculaire.

Abstract

Multiple Input Multiple Output (MIMO) systems use sensor arrays that can be of large-scale (we will then refer to them as massive MIMO systems) and are seen as a potential candidate for future digital communications standards at very high throughput.

A major problem of these systems is the high level of interference due to the large number of simultaneous transmitters. In such a context, 'conventional' orthogonal pilot design solutions are expensive in terms of throughput, thus allowing for the so-called 'blind' or 'semi-blind' channel identification solutions (forsaken for a while in the civil communications systems) to come back to the forefront as interesting solutions for identifying or deconvolving these MIMO channels.

In this thesis, we started with a comparative performance analysis, based on Cramèr-Rao Bounds (CRB), to quantify the potential size reduction of the pilot sequences when using semi-blind methods that jointly exploit the pilots and data. Our analysis shows that, up to 95% of the pilot samples can be suppressed without affecting the channel estimation performance when such semi-blind solutions are considered.

After that, we proposed new methods for semi-blind channel estimation, that allow to approach the CRB with relatively low or moderate cost. At first, we have proposed a semi-blind estimator, LS-DF (Least Squares-Decision Feedback), based on the decision feedback technique which allows a good compromise between performance and numerical complexity. Other semi-blind estimators have also been introduced based on the subspace technique and on the maximum likelihood approach, respectively. The latter is optimized via an EM (Expectation Maximization) algorithm for which three reduced cost versions are proposed. In the case of a specular channel model, we considered a parametric estimation method based on times of arrival estimation combined with the DF technique.

Keywords— MIMO/ massive MIMO, OFDM, CRB, semi-blind, subspace method, EM algorithm, LS-DF, specular channel.

Contents

List of Tables

List of Figures

Abbreviations

BPSK	Binary Phase Shift Keying signals
BS	Base Station
CCG	Circular Complex Gaussian
CFO	Carrier Frequency Offset
CG	Circular Gaussian
CP	Cyclic Prefix
CRB	Cramér-Rao Bound
CSI	Channel State Information
DA	Data-Aided
DFE	Decision Feedback Equalizer
DFT	Discrete Fourier Transform
DoA	Direction-of-Arrival
EM	Expectation Maximization
ESPRIT	Estimation of Signal Parameters via Rotational Invariance Technique
EVD	Eigenvalue Decomposition
FDD	Frequency Division Duplexing
FFT	Fast Fourier Transform
FIM	Fisher Information Matrix
HT-LTF	High Throughput Long Training Field
i.i.d.	independent and identically distributed
LS	Least-Squares
LS-DF	Least-Squares Decision Feedback
LTE	Long Term Evolution
MCFO	Multiple Carrier Frequency Offset
MIMO	Multiple-Input-Multiple-Output
MISO	Multiple-Input-Single-Output

ML	Maximum Likelihood
MSE	Mean Squared Error
MUSIC	MUltiple SIgnal Classification
NCG	Non Circular Gaussian
NCRB	Normalized Cramér-Rao Bound
NDA	Non Data-Aided
NO	Non Orthogonal
NRMSE	Normalized Root Mean Square Error
OFDM	Orthogonal Frequency Division Multiplexing
OMR	OFDM-based Multi-hop Relaying
OP	Only Pilots
PDF	Probability Density Function
PR	Partial Relaxation
QPSK	Quadrature Phase Shift Keying signals
SB	Semi-Blind
S-EM	Simplified Expectation Maximization
SER	Symbol Error Rate
SNR	Signal-to-Noise Ratio
SIMO	Single-Input-Multiple-Output
SISO	Single-Input-Single-Output
SOS	Second Order Statistics
SS	Subspace
SVD	Singular Value Decomposition
TDD	Time Division Duplexing
ToA	Time-of-Arrival
UAV	Unmanned Aerial Vehicle
VC	Virtual Carriers
w.r.t	with respect to
ZC	Zadoff-Chu
ZF	Zero-Forcing

Notations

A, a	non-bold letters are used to denote scalars
$\mathbf{a}$	boldface lower case letters are used for vectors
$\mathbf{A}$	boldface upper case letters are used for matrices
$\hat{\mathbf{A}}$, $\hat{\mathbf{a}}$	a hat is used to denote an estimate
$(.)^T$	transpose
$(.)^*$	complex conjugate
$(.)^H$	conjugate transpose
$\Re(.)$, $\Im(.)$	real and imaginary parts
$tr\{.\}$	trace
$\text{vec}(\mathbf{A})$	operator stacking the columns of a matrix into a vector
$\text{diag}(\mathbf{a})$	diagonal matrix constructed from a
$\text{diag}(\mathbf{A})$	operator stacking the diagonal of a matrix into a vector
$NC(\mu, \mathbf{C})$	Complex Gaussian distribution with mean μ and covariance $\mathbf{C}$
$E[.]$	the expectation of [.]
$\mathbf{I}_m$	m $\times$ m identity matrix
$\|.\|^2$	L2 norm
$\otimes$	Kronecker product
$\odot$	Element-wise product
$\oslash$	Element-wise division

Introduction

> *Creativity requires the courage to let go of certainties.*
> Erich Fromm

0.1 Overview

Over the last few decades, wireless communications have seen remarkable developments in many distinct fields. This started with academic research, where a lot of improvement and progress has been made. This is also evident in military applications, where traditional war and weapons have been replaced by autonomous weapons (like Unmanned Aerial Vehicles (UAV)) and electronic cybernetic war. The civilian field has also seen its part of wireless communications progress, in the sense that our lives have becomes more virtual and connected.

Mobile cellular communications are considered as the most common radio access application for wireless communications, whose remarkabale development can be divided into five generations envolving from the first generation (1G) to the fifth generation (5G) [1]. In the 1980s, the analog mobile radio systems were used and adopted for 1G mobile communications. With the appearance of digital technology, the second generation (2G) mobile communications standards and systems were developed. Digital systems in 2G are superior to the analog systems in terms of system capacity, link quality and additional services. Furthermore, unlike the 1G analog systems employed in different countries, Global System for Mobile communications (GSM) in 2G have been standardized and have spread all over the world [2]. The success of GSM in 2G motivated the development of the third generation (3G) communications systems which are the first mobile systems for broadband wireless communications. Thanks to the wideband Code Division Multiplexing Access (CDMA) techniques [3], new applications such as internet browsing and audio/video streaming have been developed and used in 3G communications. Despite the fact that 3G networks provided better service quality and boosted the system capacity, nowadays, the Long-Term Evolution (LTE) and LTE-Advanced (LTE-A) integrating the fourth generation (4G)

are deployed [4]. The flagship technologies of 4G systems are Multiple-Input Multiple-Output (MIMO) and Orthogonal Frequency Division Multiplexing (OFDM) [4].

The use of multiple antennas at the transmitter or at the receiver or at both (MIMO), can substantially increase data throughput and the reliability of radio communications [5, 6]. MIMO communications systems offer additional degrees of freedom provided by the spatial dimension, which can be exploited to either simultaneously transmit independent data-streams (spatial multiplexing) thereby increasing the data-rate, or multiplicative transmission of single data stream (spatial diversity) to increase the system reliability [5, 7].

On the other hand, multicarrier modulation techniques (OFDM) make the system robust against frequency-selective fading channels by converting the overall channel into a number of parallel flat fading channels, which helps to achieve high data rate transmission [8, 9]. Besides, the OFDM eliminates the inter-symbol interference and inter-carrier interference thanks to the use of a cyclic prefix and an orthogonal transform. Moreover, the combination of MIMO technology with OFDM called MIMO-OFDM systems, has enabled high speed data transmission and broadband multimedia services over wireless links [8, 10].

Another important development in wireless communications, apart from mobile cellular networks, is the Wireless Local Area Network (WLAN) [11]. The Institute of Electrical and Electronics Engineers (IEEE) 802.11 based WLAN is the most broadly deployed WLAN technology. Nowadays, WLAN services are widely used not only at homes and offices but also at restaurants, libraries and many other public services and locations. The standardization process of IEEE 802.11 based WLAN originated in the 1990s, and since it has evolved several times in order to increase its throughput, enhance its security and compatibility leading to several versions 802.11 b/a/g/n/ac [12, 13]. In 2009, the IEEE 802.11n standardization process was completed and adopted in Wi-Fi (WIreless FIdelity) transmissions offering high data rate, which primarily results from the use of multi-antennas (MIMO) and multi-subcarriers modulation (OFDM) techniques (MIMO-OFDM systems) [10].

The unprecedented usage of smart phone, tablets, super-phones etc., equipped with data-intensive applications like video streaming, graphics heavy social media interfaces and real time navigation services, has called for revolutionary changes the current 4G to the next generation wireless systems. Although 4G systems could be loaded with much more services, real time functionality and data than previous systems, there is still a dramatic gap between the people's practical requirements and what can be offered by the 4G technologies. To meet the strong demands from the explosive growth of cellular users and the associated potential services, currently

the fifth generation (5G) standard is under extensive investigation and discussion. With speeds of up to 10 gigabits per second, 5G is set to be as much as 100 times faster than 4G [14]. The two prime technologies for sustaining the requirements of 5G are the use of millimeter wave (mmWave) and massive MIMO systems [15].

With a higher number of Base Station (BS) antennas, around few hundreds, compared to the classical MIMO systems (8 antennas for the LTE), massive MIMO or large-scale MIMO systems can achieve huge gains in spectral and energy efficiencies [14, 16, 17]. Massive MIMO systems overcome several limitations of the traditional MIMO systems such as security, robustness and throughput rate [18, 15]. It has been demonstrated that massive MIMO systems hold greater promises of boosting system throughput by 10 times or more by simultaneously serving tens of users in the same time-frequency resource [18]. So that, both throughput and system capacity will be highly enhanced in order to satisfy the increasing amount of data exchange and demand for quality of service for the future cellular networks.

To fully realize the potentials of the aforementioned technologies, the knowledge of Channel State Information (CSI) is indispensable. To improve the system performance, it is essential that CSI is available at both transmitter and the receiver. The knowledge of CSI is used for coherent detection of the transmitted signals at the receiver side. On transmitter side, CSI, is crucial to design effective precoding schemes for inter-user interference cancellation. However, the perfect knowledge of CSI is not available in practice, therefore it has to be estimated. This thesis is concerned with efficient and low complexity channel estimation algorithms for MIMO-OFDM and massive MIMO-OFDM systems.

0.2 Channel estimation

The well conduct of wireless communications system's objective depends largely upon the availability of the knowledge of its environment. The propagation environment refers to the communications channel which provides the connection between the transmitter and the receiver. Thus, channel estimation is of paramount importance to equalization and symbol detection. Several channel models and channel estimation approaches have been developed in literature depending on their applications and on the selected standard. The estimation approaches can be divided into three main classes as follows:

0.2.1 Pilot-based channel estimation

Typically, channel estimation is performed by inserting, in the transmitted frame, a training sequences (called pilots) known a priori at the receiver, according to a known arrangement pattern in the frame (block, comb or lattice) [19, 20, 21]. At the receiver side then, by observing the output in correspondence of the pilot symbols, it is possible to estimate the channel. This knowledge is then fed into the detection process, to allow optimal estimation of the data. This approach (pilot-based channel estimation), is the most commonly used in communications standards [22, 13], for its low computational complexity and robustness. Its drawback consists of the fact that the pilot symbols do not carry useful information, therefore they represent a bandwidth waste. Moreover, most of the observations (those related to the unknown symbols) are discarded in the estimation process, thus representing a missed opportunity to enhance the accuracy of the channel estimate.

0.2.2 Blind channel estimation

Unlike pilot-based channel estimation, blind channel estimation methods are fully based on the statistical properties of the unknown transmitted symbols (i.e. no pilots are transmitted) [23, 24, 25]. This approach reduces the overhead but needs a large number of data symbols for statistical properties and powerful algorithms. Moreover, pilot-based approaches give better performance at low computational complexity than the blind ones.

0.2.3 Semi-blind channel estimation

Each channel estimation class has its own benefits and drawbacks. Generally, the first class (i.e. pilot-based channel estimator) provides a more accurate channel estimation than the blind estimation class. However, the second class, in most cases, increases the spectral efficiency compared to the first one. Therefore, it would be advantageous to retain the benefits of the two techniques through the use of Semi-Blind (SB) estimation methods [26, 27, 28, 29] which exploit both data and pilots to achieve the desired channel identification.

0.3 Thesis purpose and manuscript organization

The number of channel parameters to be estimated in MIMO and massive MIMO systems increases with the system dimension (i.e. number of transmitters and receivers). Hence, the pilot-based channel estimation techniques have a severe limitation due to the required longer size of the pilot sequences. However, the transmission of a longer pilot sequence is not desirable in a

communications system, since they do not carry useful information and represent a bandwidth waste. Furthermore, the wireless spectral resource is becoming more and more scarce and precious due to the limitation, by nature, of the spectrum allocated to wireless communications services.

In this context, this thesis proposes to use semi-blind channel estimation approach, which exploits all the transmitted signal's information (i.e. pilots and unknown data), to overcome the above-mentioned resource problems. Instead of using semi-blind estimation to improve the channel estimation performances, herein, we propose to keep the same performances of pilot-based estimation but reducing the pilot sequences. However, due to the complexity of the blind estimation part, semi-blind estimation increases the receiver complexity compared to pilot-based methods.

Thanks to the channel reciprocity property and according to the widely accepted Time Division Duplexing (TDD) protocol used in MIMO-OFDM and massive MIMO-OFDM systems [30, 31], CSI is estimated only during the uplink transmission (at the Base Station (BS)) then transmitted to the different users for channel equalization in the downlink. Hence, the 'semi-blind' complex channel estimation task could be easily achieved by the powerful calculator at the BS.

The study of the semi-blind solution, proposed in this thesis, is divided into two principal parts. The first part concerns the performance analysis of semi-blind channel estimation methods. The second part is dedicated to the derivation of semi-blind channel estimation algorithms.

0.3.1 Part I - Channel estimation limit Performance analysis

The first part of thesis focuses on the performance bounds analysis of the semi-blind and pilot-based channel estimation methods in the context of MIMO-OFDM and massive MIMO-OFDM systems. To obtain general comparative results independent from specific algorithms or estimation methods, this analysis is carried out using the estimation performance limits given by the Cramér-Roa-Bound (CRB).

The first contribution of this thesis is to quantify the rate of reduction of the transmitted pilots using semi-blind channel estimation while ensuring the same pilot-based channel estimation performance. Chapter 1 introduces the CRB derivations for semi-blind and pilot-based channel estimation approaches [32]. This performance analysis is performed for different data models (Circular Gaussian (CG), Non Circular Gaussian (NCG), Binary/Quadratic Phase Shift Keying (BPSK/QPSK)) and different pilot design schemes such as: block-pilot type arrangement, comb-type pilot arrangement and lattice-type arrangement. For the BPSK/QPSK case, a new approximation of the CRB is proposed to avoid heavy numerical integral calculations. Moreover,

in the massive MIMO context, an efficient computational technique to deal with the huge-size matrix manipulation needed for the CRB derivation is proposed exploiting the block diagonal structure of the covariance matrices.

The derived CRBs are then used to quantify the achievable rate of pilot compression allowed by the use of a semi-blind approach in the context of MIMO-OFDM and very large MIMO-OFDM systems. The main outcome of this analysis is that, using the semi-blind channel estimation method, one can reduce more than 95% of the pilot size.

In chapter 2, the CRBs derivation is extended to the massive MIMO-OFDM case taking into account multi-cell scenario and pilot contamination issue. Through this chapter, the effectiveness of semi-blind channel estimation approaches is investigated and shown that it is possible to efficiently solve the pilot contamination problem when considering BPSK/QPSK signals.

As a byproduct of the derived CRBs in MIMO-OFDM context, a derivation of CRBs in the case of Single-Input Multiple-Output (SIMO-OFDM) system for deterministic and stochastic Gaussian data model is proposed in chapter 3. A practical application of the derived CRB is proposed in this chapter, which consists of protecting the exchanged data between a drone and mobile stations against blind interceptions. To do so, one tunes the system parameters in such a way, the blind identification is not possible (too poor) while the semi-blind one allows the 'authorized' user to get a relatively good channel estimate and to restore properly the transmit data.

In chapter 4, two further investigations on the performance bounds, based on the derivation of CRB, of MIMO-OFDM channel estimation are proposed. The first one deals with the analytical derivation of the CRBs in the presence of Carrier Frequency Offset (CFO) for semi-blind channel estimation. The analysis and comparison of the CRBs with and without CFO shows that the CFO impacts advantageously the CRB of the semi-blind channel estimation mainly due to the CFO cyclostationarity propriety. The second investigation evaluates and compares the CRB for the estimation of the subcarrier channel coefficients with and without considering the OFDM structure (i.e. when taking into account the relation between these coefficients through the Fourier transform of the channel taps and when ignoring this relation in the estimation process). The latter highlights the significant gain associated to the time-domain channel estimation as compared to the frequency domain one which, somehow, disregards the OFDM structure.

0.3.2 Part II - Semi-blind channel estimation approaches

The second part of the thesis, once the theoretical limit semi-blind channel estimation performance based on the CRB is performed, proposes four semi-blind channel estimation algorithms. The major requirements of the proposed algorithms are: (i) low complexity, (ii) good performance to reach the CRB at moderate or high SNR.

The first considered estimator (LS-DF) is quite cheap as it uses a simple least squares (LS) estimation together with a decision feedback (DF) where the estimated data is re-injected to the channel estimation stage to enhance the estimation performance. In particular, we have taken advantage of this estimator to quantify the overall power consumption gain (about 66%) due to the pilot-size reduction associated to this semi-blind approach.

The second semi-blind channel estimator, proposed in this thesis, is based on the Maximum Likelihood (ML) technique. The latter is known to be powerful but also too expensive. Hence, for the ML cost optimization, new Expectation Maximization (EM) algorithms for the channel taps estimation are introduced in chapter 6. A main focus of chapter 6 is the reduction of the numerical complexity while preserving at best the channel estimation quality. To do so, three approximation/simplification approaches are proposed after introducing the exact version of the EM-MIMO algorithm, where the MIMO-OFDM system is treated as one block to estimate the overall channel vector through an iterative process.

The first approach consists of decomposing the MIMO-OFDM system into parallel MISO-OFDM systems. The EM algorithm is then applied in order to estimate the MIMO channel in a parallel way. The second approach takes advantage of the semi-blind context to reduce the EM cost from exponential to linear complexity by reducing the size of the search space. Finally, the last proposed approach uses a parallel interference cancellation technique to decompose the MIMO-OFDM system into several SIMO-OFDM systems. The latter are identified in a parallel scheme and with a reduced complexity.

In between the cheap LS-DF and the relatively expensive EM method, we have considered some intermediate solutions. Hence, in chapter 7, an efficient semi-blind subspace channel estimation, in the case of MIMO-OFDM system, is proposed for which an identifiability result is first established for the subspace based criterion. The proposed algorithm adopts the MIMO-OFDM system model without cyclic prefix and takes advantage of the circulant property of the channel matrix to achieve lower computational complexity and to accelerate the algorithm's convergence by generating a group of sub-vectors from each received OFDM symbol.

For the practical case of specular channel model, chapter 8 proposes a parametric approach

based on the Time-Of-Arrival (TOA) estimation using subspace methods for SISO-OFDM systems. At first the TOA estimation is achieved using only one OFDM pilot. The latter is used to generate a group of sub-vectors, with an appropriate windowing, to which one can apply subspace methods to estimate the TOA. Then a refining step based on the incorporation of the unknown data on the channel estimation process is considered. The semi-blind TOA estimation is done using a Decision Feedback process (as detailed in chapter 5), where a first estimate of the transmitted data is used with the existing pilot to enhance the TOA estimation performance.

At the end, in appendix A, we present joint channel and CFO estimation in a Multiple Input Single Output (MISO) communications system. This problem arises in OFDM based multi-relay transmission protocols such as the geo-routing one proposed by A. Bader et al. in 2012. Indeed, the outstanding performance of this multi-hop relaying scheme relies heavily on the channel and CFO estimation quality at the physical layer. In this work, two approaches are considered: The first is based on estimating the overall channel (including the CFO) as a time-varying one using an adaptive scheme under the assumption of small or moderate CFOs while the second one performs separately, the channel and CFO parameters estimation based on the considered data model.

0.4 List of publications

Based on the research work presented in this thesis, some papers have been published or submitted for publication to journals and conferences as following:

Journal papers:

1) Ladaycia, A. Mokraoui, K. Abed-Meraim, and A. Belouchrani, "Performance bounds analysis for semi-blind channel estimation in MIMO-OFDM communications systems," IEEE Transactions on Wireless Communications, vol. 16, no. 9, pp. 5925-5938, Sep. 2017.

2) A. Ladaycia, A. Belouchrani, K. Abed-Meraim and A. Mokraoui, "Semi-Blind MIMO-OFDM Channel Estimation using EM-like Techniques," IEEE Transactions on Wireless Communications, May. 2019. (submitted).

3) O. Rekik, A. Ladaycia, K. Abed-Meraim, and A. Mokraoui, "Performance Bounds Analysis for Semi-Blind Channel Estimation with Pilot Contamination in Massive MIMO-OFDM Systems," IET Communications, May. 2019. (submitted).

Conference Papers:

1) A. Ladaycia, A. Mokraoui, K. Abed-Meraim, and A. Belouchrani, "What semi-blind channel estimation brings in terms of throughput gain?" in 2016 10th ICSPCS, Dec. 2016, pp. 1-6, Gold Coast, Australia.

2) A. Ladaycia, A. Belouchrani, K. Abed-Meraim, and A. Mokraoui, "Parameter optimization for defeating blind interception in drone protection," in 2017 Seminar on Detection Systems Architectures and Technologies (DAT), Feb. 2017, pp. 1-6, Alger, Algeria.

3) A. Ladaycia, A. Mokraoui, K. Abed-Meraim, and A. Belouchrani, "Further investigations on the performance bounds of MIMO-OFDM channel estimation," in The 13th International Wireless Communications and Mobile Computing Conference (IWCMC 2017), June 2017, pp. 223-228, Valance, Spain.

4) A. Ladaycia, A. Mokraoui, K. Abed-Meraim, and A. Belouchrani, "Toward green communications using semi-blind channel estimation," in 2017 25th European Signal Processing Conference (EUSIPCO), Aug. 2017, pp. 2254-2258, Kos, Greece.

5) A. Ladaycia, K. Abed-Meraim, A. Bader, and M.S. Alouini, "CFO and channel estimation for MISO-OFDM systems," in 2017 25th European Signal Processing Conference (EUSIPCO), Aug. 2017, pp. 2264-2268, Kos, Greece.

6) A. Ladaycia, A. Mokraoui, K. Abed-Meraim, and A. Belouchrani, "Contributions à l'estimation semi-aveugle des canaux MIMO-OFDM," in GRETSI 2017, Sep. 2017, Nice, France.

7) A. Ladaycia, A. Belouchrani, K. Abed-Meraim, and A. Mokraoui, "EM-based semi-blind MIMO-OFDM channel estimation," in 2018 IEEE International Conference on Acoustics, Speech and Signal Processing (ICASSP2018), Apr. 2018, Alberta, Canada.

8) A. Ladaycia, K. Abed-Meraim, A. Mokraoui, and A. Belouchrani, "Efficient Semi-Blind Subspace Channel Estimation for MIMO-OFDM System," in 2018 26th European Signal Processing Conference (EUSIPCO), Sep. 2018, Rome, Italy.

9) O. Rekik, A. Ladaycia, K. Abed-Meraim, and A. Mokraoui, "Performance Bounds Analysis for Semi-Blind Channel Estimation with Pilot Contamination in Massive MIMO-OFDM Systems," in 2018 26th European Signal Processing Conference (EUSIPCO), Sep. 2018, Rome, Italy.

10) A. Ladaycia, M.Pesavento, A. Mokraoui, K. Abed-Meraim, and A. Belouchrani, "Decision feedback semi-blind estimation algorithm for specular OFDM channels," in 2019 IEEE International Conference on Acoustics, Speech and Signal Processing (ICASSP2019).

11) A. Ladaycia, A. Belouchrani, K. Abed-Meraim, and A. Mokraoui, "Efficient EM-algorithm for MIMO-OFDM semi blind channel estimation," in 2019 Conference on Electrical Engineering (CEE2019).

12) O. Rekik, A. Ladaycia, K. Abed-Meraim, and A. Mokraoui, "Semi-Blind Source Separation based on Multi-Modulus Criterion: Application for Pilot Contamination Mitigation in Massive MIMO Systems," in The 19th ISCIT, Ho Chi Minh City, Vietnam.

13) A. Ladaycia, A. Belouchrani, K. Abed-Meraim, and A. Mokraoui, "Algorithme EM efficace pour l'estimation semi-aveugle de canal MIMO-OFDM," in GRETSI 2019.

Part I

Performance bounds analysis for channel estimation using CRB

CHAPTER 1

Analysis of channel estimation performances limits of MIMO-OFDM communications systems

Knowledge is the conformity
of the object and the intellect.

Averroes (Ibn Rochd)

Abstract

The main objective of this chapter is to quantify the rate of reduction of the overhead due to the use of a semi-blind channel estimation. Different data models and different pilot design schemes have been considered in this study. By using the Cramér Rao Bound (CRB) tool, the estimation error variance bounds of the pilot-based and semi-blind based channel estimators for a MIMO-OFDM system are compared. In particular, for large MIMO-OFDM systems, a direct computation of the CRB is prohibitive and hence a dedicated numerical technique for its fast computation has been developed. The most important result is that, thanks to the semi-blind approach, one can skip about 95% of the pilot samples without affecting the channel estimation quality as shown in[1] [32].

[1] [32] Ladaycia, A. Mokraoui, K. Abed-Meraim, and A. Belouchrani, "Performance bounds analysis for semi-blind channel estimation in MIMO-OFDM communications systems," IEEE Transactions on Wireless Communications, vol. 16, no. 9, pp. 5925-5938, Sep. 2017.

Chapter content

1.1 Introduction

The combining of the Multiple-Input Multiple-Output (MIMO) technology with the Orthogonal Frequency Division Multiplexing (OFDM) (i.e. MIMO-OFDM) is widely deployed in wireless communications systems as in 802.11n wireless network [22], LTE and LTE-A [4]. Indeed, the use of MIMO-OFDM enhances the channel capacity and improves the communications reliability. In particular, it has been demonstrated in [14, 16], that thanks to the deployment of a large number of antennas in the base stations, the system can achieve high data throughput and provide very high spectral efficiency.

Using multicarrier modulation techniques (OFDM in this chapter) makes the system robust against frequency-selective fading channels by converting the overall channel into a number of parallel flat fading channels, which helps to achieve high data rate transmission [9]. Moreover, the OFDM eliminates the inter-symbol interference and inter-carrier interference thanks to the use of a cyclic prefix and an orthogonal transform. In such a system, channel estimation remains a current concern since the overall performance depends strongly on it, particularly for large MIMO systems where the channel state information becomes more challenging.

This chapter is dedicated to the comparative performance bounds analysis of the semi-blind channel estimation and the data-aided approaches in the context of MIMO-OFDM systems. To obtain general comparative results independent from specific algorithms or estimation methods, this analysis is conducted using the estimation performance limits given by the CRB[2]. Therefore, we begin by providing several CRB derivations for the different data models (Circular Gaussian (CG), Non Circular Gaussian (NCG), Binary/Quadratic Phase Shift Keying (BPSK/QPSK)) and different pilot design schemes (block, comb and lattice). For the particular case of large dimensional MIMO systems, we exploited the block diagonal structure of the covariance matrices to develop a fast numerical technique that avoids the prohibitive cost and the out of memory problems (due to the large matrix sizes) of the CRB computation. Moreover, for the BPSK/QPSK case, a realistic approximation of the CRB is introduced to avoid heavy numerical integral calculations. After computing all the needed CRBs, we use them to compare the performance of the semi-blind and pilot based approaches. It is well known that semi-blind techniques can help reduce the pilot size or improve the estimation quality [35]. However, to the best of our knowledge, this is the first study that thoroughly quantifies the achievable rate of pilot compression allowed by the use of a semi-blind approach in the context of MIMO-OFDM. A main outcome of this

[2]Note that the considered performance bounds are tight (i.e. they are reachable), as shown in [33, 34], and hence their use for the considered communications system analysis and design is effective.

analysis is that it highlights the fact that, by resorting to the semi-blind estimation, one can get rid of most of the pilot samples without affecting the channel identification quality. Also an important by-product of this study is the possibility to easily design semi-orthogonal pilot sequences in the large dimensional MIMO case thanks to their significant shortening.

This chapter is organized as follows. Section 1.2 introduces the basic concepts and data models of the MIMO-OFDM system. Section 1.3 briefly introduces the well known pilot-based channel estimation CRB while section 1.4 derives the analytical expressions of the semi-blind CRBs when block-type pilot arrangement is considered. Section 1.5 investigates the CRB for semi-blind channel estimation for comb-type and lattice-type pilots arrangement. The large MIMO computational issue is considered in section 1.6, where a new vector representation and treatment for the fast manipulation of block diagonal matrices are proposed. Section 1.7 analyzes the throughput gain of the semi-blind channel estimation as compared to pilot-based channel estimation. Finally, discussions and concluding remarks are drawn in section 1.8.

1.2 Mutli-carrier communications systems: main concepts

This section first introduces the MIMO-OFDM wireless communications scheme represented by its mathematical model. Given the context of this chapter related to channel estimation, this section also provides the commonly used pilot arrangement patterns available in the literature or already specified by communications standards.

1.2.1 MIMO-OFDM system model

The multi-carrier communications system, illustrated in Figure 1.1, is composed of N_t transmit antennas and N_r receive antennas using K sub-carriers. The transmitted signal is assumed to be an OFDM one. Each OFDM symbol is composed of K samples and is extended by the insertion of its last L samples in its front considered as a Cyclic Prefix (CP). The CP length is assumed to be greater or equal to the maximum multipath channel delay denoted N (i.e. $N \leq L$).

The received signal at the r-th antenna, after removing the CP and taking the K-point FFT of the received OFDM symbols, is given in time domain by:

$$\mathbf{y}_r = \sum_{i=1}^{N_t} \mathbf{F}\, \mathbf{T}(\mathbf{h}_{i,r}) \frac{\mathbf{F}^H}{K} \mathbf{x}_i + \mathbf{v}_r \qquad K \times 1, \tag{1.1}$$

where $\mathbf{F}$ represents the K-point Fourier matrix; $\mathbf{h}_{i,r}$ is the $N \times 1$ vector representing the channel taps between the i-th transmit antenna and the r-th receive antenna; $\mathbf{x}_i$ is the i-th OFDM symbol

of length K; and $\mathbf{T}(\mathbf{h}_{i,r})$ is a circulant matrix. $\mathbf{v}_r$ is assumed to be an additive white Circular Gaussian (CG) noise satisfying $E\left[\mathbf{v}_r(k)\mathbf{v}_r(i)^H\right] = \sigma^2_{\mathbf{v}}\mathbf{I}_K\delta_{ki}$; $(.)^H$ being the Hermitian operator; $\sigma^2_{\mathbf{v}}$ the noise variance; $\mathbf{I}_K$ the identity matrix of size $K \times K$ and δ_{ki} the Dirac operator.

The eigenvalue decomposition of the circulant matrix $\mathbf{T}(\mathbf{h}_{i,r})$ leads to:

$$\mathbf{T}(\mathbf{h}_{i,r}) = \frac{\mathbf{F}^H}{K}\mathrm{diag}\{\mathbf{W}\mathbf{h}_{i,r}\}\mathbf{F}, \tag{1.2}$$

where $\mathbf{W}$ is a matrix containing the N first columns of $\mathbf{F}$ and $\mathbf{diag}$ is the diagonal matrix composed by its vector argument. Finally equation (1.1) becomes:

$$\mathbf{y}_r = \sum_{i=1}^{N_t}\mathrm{diag}\{\mathbf{W}\mathbf{h}_{i,r}\}\mathbf{x}_i + \mathbf{v}_r. \tag{1.3}$$

This equation can be extended to the N_r receive antennas as follows:

$$\mathbf{y} = \boldsymbol{\lambda}\mathbf{x} + \mathbf{v}, \tag{1.4}$$

where $\mathbf{y} = \left[\mathbf{y}_1^T \cdots \mathbf{y}_{N_r}^T\right]^T$; $\mathbf{x} = \left[\mathbf{x}_1^T \cdots \mathbf{x}_{N_t}^T\right]^T$; $\mathbf{v} = \left[\mathbf{v}_1^T \cdots \mathbf{v}_{N_r}^T\right]^T$ with $\mathbf{v} \sim NC\left(0, \sigma^2_{\mathbf{v}}\mathbf{I}_{N_rK}\right)$; and $\boldsymbol{\lambda} = [\boldsymbol{\lambda}_1 \cdots \boldsymbol{\lambda}_{N_t}]$ with $\boldsymbol{\lambda}_i = \left[\boldsymbol{\lambda}_{i,1} \cdots \boldsymbol{\lambda}_{i,N_r}\right]^T$ where $\boldsymbol{\lambda}_{i,r} = \mathrm{diag}\{\mathbf{W}\mathbf{h}_{i,r}\}$.

Next sections address the analytical CRB derivations. In order to facilitate their calculations, equation (1.4) is rewritten in a most appropriate form and some notations are introduced: $\mathbf{h} = \left[\mathbf{h}_1^T \cdots \mathbf{h}_{N_r}^T\right]^T$ is a vector of size $N_rN_tN \times 1$ (where $\mathbf{h}_r = \left[\mathbf{h}_{1,r}^T \cdots \mathbf{h}_{N_t,r}^T\right]^T$); $\mathbf{X}_{D_i} = \mathrm{diag}\{\mathbf{x}_i\}$ is a diagonal matrix of size $K \times K$; $\mathbf{X} = \left[\mathbf{X}_{D_1}\mathbf{W} \cdots \mathbf{X}_{D_{N_t}}\mathbf{W}\right]$ of size $K \times NN_t$; and $\tilde{\mathbf{X}} = \mathbf{I}_{N_r} \otimes \mathbf{X}$ a matrix of size $N_rK \times NN_tN_r$ and $\otimes$ refers to the Kronecker product. According to these notations, equation (1.4) is rewritten as follows:

$$\mathbf{y} = \tilde{\mathbf{X}}\mathbf{h} + \mathbf{v}. \tag{1.5}$$

1.2.2 Main pilot arrangement patterns

Most wireless communications standards specify the insertion of training sequences (i.e. preamble) in the physical frame. These sequences are considered as OFDM pilot symbols and are known both by the transmitter and receiver (see e.g. [22]). Therefore the receiver exploits these pilots to estimate the propagation channel. These pilots can be arranged in different ways in the physical frame. This chapter focuses on three pilot patterns mainly adopted in communications systems. They are described in what follows.

Figure 1.2a illustrates the block-type pilot arrangement where the pilot OFDM symbols are periodically transmitted. This structure is well adapted to frequency-selective channels.

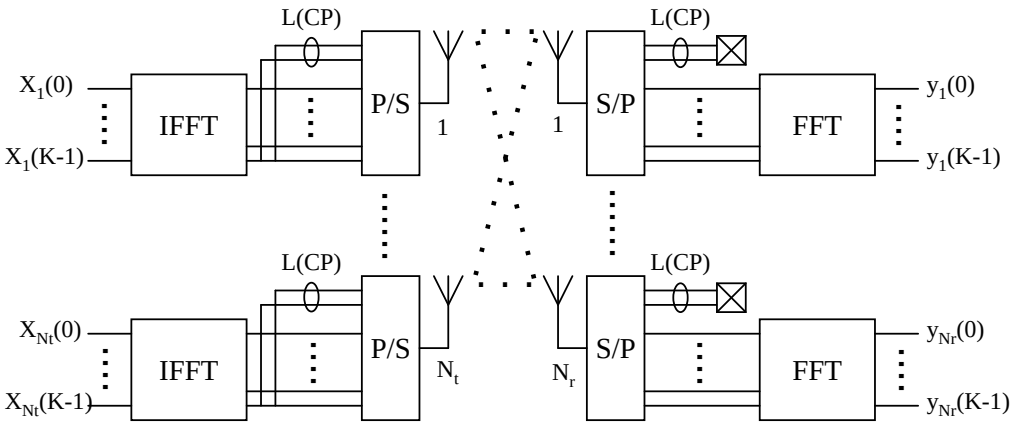

Figure 1.1: *MIMO-OFDM communications system*

Figure 1.2b concerns the comb-type pilot arrangement which is more adapted to fast fading channels. For this structure, specific and periodic sub-carriers are reserved as pilots in each OFDM symbol. Each OFDM symbol contains K_p sub-carriers dedicated to pilots and the remaining i.e. $K_d = K - K_p$ sub-carriers are dedicated to the data. Every OFDM symbol has pilot tones at the periodically-located sub-carriers.

Figure 1.2c represents a lattice-type pilot arrangement. In this structure the K_p sub-carrier positions are modified across the OFDM symbols in a diagonal way with a given periodicity. This arrangement is appropriate for time/frequency-domain interpolations for channel estimation. To be adapted to these two last pilot structures, equations (1.4) and (1.5) representing the MIMO-OFDM system model are modified as follows[3]:

$$\mathbf{y} = \begin{bmatrix} \boldsymbol{\lambda}_p & \boldsymbol{\lambda}_d \end{bmatrix} \begin{bmatrix} \mathbf{x}_p \\ \mathbf{x}_d \end{bmatrix} + \mathbf{v} = \begin{bmatrix} \tilde{\mathbf{X}}_p \\ \tilde{\mathbf{X}}_d \end{bmatrix} \mathbf{h} + \mathbf{v}. \tag{1.6}$$

where $\mathbf{x}_p$ and $\mathbf{x}_d$ represent the pilot and data symbol vectors, respectively. Similarly $\boldsymbol{\lambda}_p$ and $\boldsymbol{\lambda}_d$ are the corresponding system matrices.

In the sequel, to take into account the time index (ignored in equation (1.6)), we will refer to the t-th OFDM symbol by $\mathbf{y}(t)$ instead of $\mathbf{y}$.

1.3 CRB for block-type pilot-based channel estimation

This section introduces the well known analytical CRB bound [34] associated to the pilot-based channel estimation with the block-type pilot arrangement. The CRB is obtained as the inverse

[3]This rewriting considers implicitly a permutation of the OFDM sub-carriers which has no impact on our performance analysis.

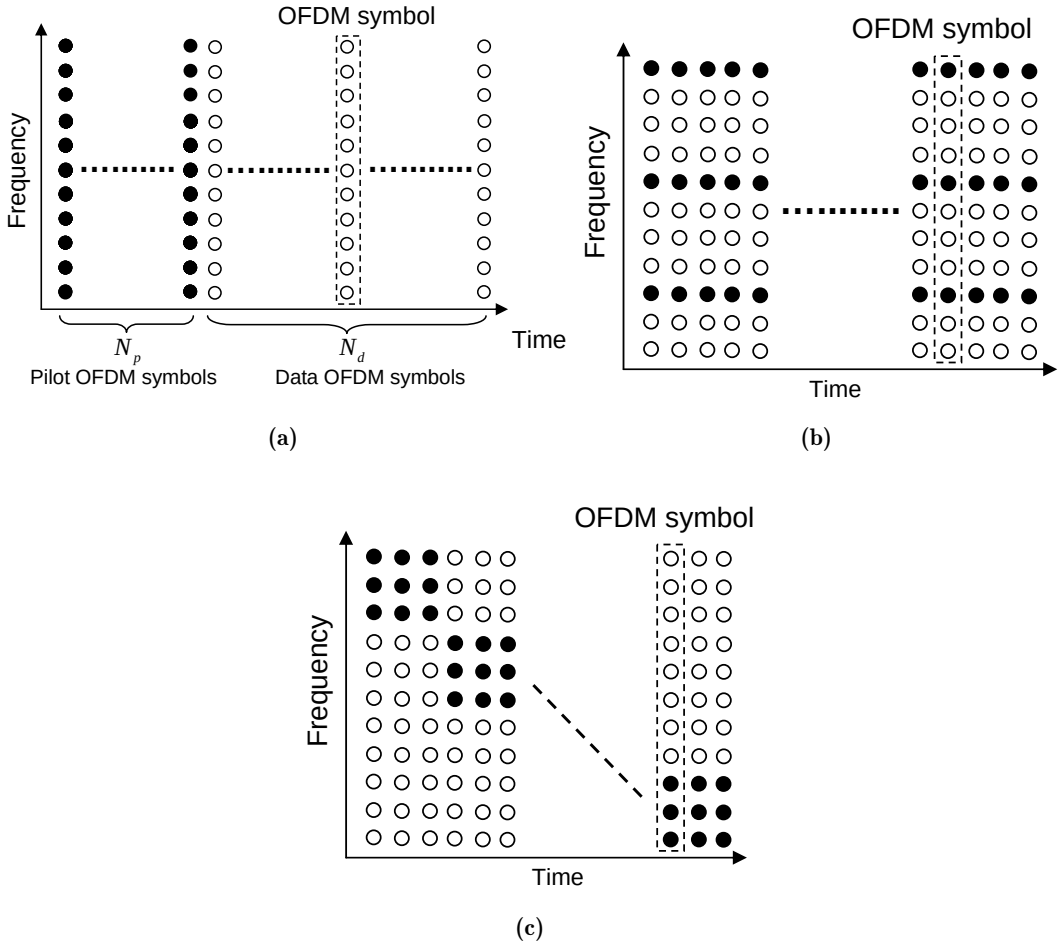

Figure 1.2: *Pilot arrangements: (a) Block-type with N_p pilot OFDM symbols and N_d data OFDM symbols; (b) Comb-type with K_p pilot sub-carriers and K_d data sub-carriers; and (c) Lattice-type with K_p pilot sub-carriers and K_d data sub-carriers with time varying positions.*

of the Fisher Information Matrix (FIM) denoted $\mathbf{J}^{p}_{\boldsymbol{\theta\theta}}$ where $\boldsymbol{\theta}$ is the unknown parameter vector to be estimated corresponding in this case to the channel vector[4] i.e. $\boldsymbol{\theta} = \mathbf{h}$.

Since the noise is an independent identically distributed (i.i.d.) random process, the FIM for $\boldsymbol{\theta}$, when N_p pilot OFDM symbols of power σ_p^2 are used, can be expressed as follows:

$$\mathbf{J}^{p}_{\boldsymbol{\theta\theta}} = \sum_{i=1}^{N_p} \mathbf{J}^{p_i}_{\boldsymbol{\theta\theta}}, \tag{1.7}$$

where $\mathbf{J}^{p_i}_{\boldsymbol{\theta\theta}}$ is the FIM associated with the i-th pilot OFDM symbol given by [36, 35]:

$$\mathbf{J}^{p_i}_{\boldsymbol{\theta\theta}} = \mathrm{E}\left\{ \left(\frac{\partial \ln \mathrm{p}(\mathbf{y}(\mathrm{i}), \mathbf{h})}{\partial \boldsymbol{\theta}^*} \right) \left(\frac{\partial \ln \mathrm{p}(\mathbf{y}(\mathrm{i}), \mathbf{h})}{\partial \boldsymbol{\theta}^*} \right)^{\mathrm{H}} \right\}, \tag{1.8}$$

[4]We ignored here the unknown noise power parameter $\sigma^2_{\mathbf{v}}$ since its estimation error does not affect the desired channel parameter estimation.

where E(.) is the expectation operator; and $p(\mathbf{y}(i),\mathbf{h})$ is the probability density function of the received signal given $\mathbf{h}$.

According to the complex derivation $\frac{\partial}{\partial\theta^*}=\frac{1}{2}\left(\frac{\partial}{\partial\alpha}+j\frac{\partial}{\partial\beta}\right)$ for $\theta=\alpha+j\beta$, the derivation of equation (1.8) is then expressed by:

$$\mathbf{J}_{\boldsymbol{\theta\theta}}^{p_i}=\frac{\tilde{\mathbf{X}}(i)^H\tilde{\mathbf{X}}(i)}{\sigma_{\mathbf{v}}^2}. \tag{1.9}$$

Therefore the lower bound, denoted CRB_{OP} (OP stands for 'Only Pilot'), of the unbiased MSE (Mean Square Error) channel estimation when only pilots are exploited to estimate the channel is given by $\left(\tilde{\mathbf{X}}_p=\left[\tilde{\mathbf{X}}(1)^T\cdots\tilde{\mathbf{X}}(N_p)^T\right]^T\right)$:

$$CRB_{OP}=\sigma_{\mathbf{v}}^2 tr\left\{\left(\tilde{\mathbf{X}}_p^H\tilde{\mathbf{X}}_p\right)^{-1}\right\}. \tag{1.10}$$

The best performance is reached when the pilot sequences are orthogonal, as designed in [22, 37], in which case, $\tilde{\mathbf{X}}_p^H\tilde{\mathbf{X}}_p$ is simplified as follows $\tilde{\mathbf{X}}_p^H\tilde{\mathbf{X}}_p=N_p\sigma_p^2\mathbf{I}_{N_tN_rN}$.

1.4 CRB for semi-blind channel estimation with block-type pilot arrangement

This section addresses the derivation of the CRB analytical expression for semi-blind channel estimation when the pilot arrangement pattern is assumed to be a block-type one. In this context the CRB computation relies not only on the known transmitted pilot OFDM symbols (i.e. training sequences) but also on the unknown transmitted OFDM symbols.

To derive the CRB expression, three cases have been considered depending on whether the transmitted data is stochastic Circular Gaussian (CG)[5], stochastic Non-Circular Gaussian (NCG) or i.i.d. BPSK/QPSK signals. Data symbols and noise are assumed to be both i.i.d. and independent. Therefore the FIM, denoted $\mathbf{J}_{\boldsymbol{\theta\theta}}$, is divided into two parts:

$$\mathbf{J}_{\boldsymbol{\theta\theta}}=\mathbf{J}_{\boldsymbol{\theta\theta}}^{p}+\mathbf{J}_{\boldsymbol{\theta\theta}}^{d}, \tag{1.11}$$

where $\mathbf{J}_{\boldsymbol{\theta\theta}}^{p}$ is related to the FIM associated with known pilots (given by (1.7) and (1.9)), and $\mathbf{J}_{\boldsymbol{\theta\theta}}^{d}$ concerns the FIM dedicated to the unknown data. Depending on the data model, the vector of unknown parameters $\boldsymbol{\theta}$ is composed of complex and real parameters (i.e $\boldsymbol{\theta}_c$ and $\boldsymbol{\theta}_r$) as follows:

$$\boldsymbol{\theta}=\left[\boldsymbol{\theta}_c^T\ (\boldsymbol{\theta}_c^*)^T\ \boldsymbol{\theta}_r^T\right]^T, \tag{1.12}$$

[5] We adopt here the Gaussian CRB as it is the most tractable one as well as the least favorable distribution case [38].

where $\boldsymbol{\theta}_c$ represents the complex-valued[6] channel taps while $\boldsymbol{\theta}_r$ concerns the unknown data and noise parameters. The FIM for a complex parameter $\boldsymbol{\theta}$ is derived in [40, 39]. With respect to this new parameter vector, the previous pilot-based FIM matrix is expressed as:

$$\mathbf{J}^{p}_{\boldsymbol{\theta}\boldsymbol{\theta}} = \begin{bmatrix} \frac{\tilde{\mathbf{X}}_p^H \tilde{\mathbf{X}}_p}{\sigma^2_{\mathbf{v}}} & \mathbf{0} & \mathbf{0} \\ \mathbf{0} & \frac{\tilde{\mathbf{X}}_p^H \tilde{\mathbf{X}}_p}{\sigma^2_{\mathbf{v}}} & \mathbf{0} \\ \mathbf{0} & \mathbf{0} & \mathbf{J}^{p}_{\boldsymbol{\theta}_r\boldsymbol{\theta}_r} \end{bmatrix}, \tag{1.13}$$

where $\mathbf{J}^{p}_{\boldsymbol{\theta}_r\boldsymbol{\theta}_r}$ will be specified later for each considered data model.

Before proceeding further, let us introduce the following notation: Denote $\mathbf{x}$ the signal composed of known pilots $\mathbf{x}_p$ and unknown transmitted data $\mathbf{x}_d$: $\mathbf{x} = [\mathbf{x}_p^T \ \mathbf{x}_d^T]^T$. The unknown transmitted data $\mathbf{x}_d$ is composed of N_d OFDM symbols, i.e $\mathbf{x}_d = [\mathbf{x}_{s_1}^T \ \mathbf{x}_{s_2}^T \ \cdots \ \mathbf{x}_{s_{N_d}}^T]^T$.

1.4.1 Circular Gaussian data model

In this section, the N_d unknown data OFDM symbols are assumed to be stochastic CG and i.i.d. with zero mean and a covariance matrix $\mathbf{C}_{\mathbf{x}} = \mathrm{diag}\,(\boldsymbol{\sigma}^2_{\mathbf{x}})$ with $\boldsymbol{\sigma}^2_{\mathbf{x}} \overset{\text{def}}{=} \left[\sigma^2_{\mathbf{x}_1} \cdots \sigma^2_{\mathbf{x}_{N_t}}\right]^T$ where $\sigma^2_{\mathbf{x}_i}$ denotes the transmit power of the i-th user. The data FIM is equal to the FIM of the first data OFDM symbol multiplied by the number of symbols N_d. The observed OFDM symbol is CG, i.e $\mathbf{y} \sim NC(0, \mathbf{C}_{\mathbf{y}})$, where the output auto-covariance matrix is given by:

$$\mathbf{C}_{\mathbf{y}} = \sum_{i=1}^{N_t} \sigma^2_{\mathbf{x}_i} \boldsymbol{\lambda}_i \boldsymbol{\lambda}_i^H + \sigma^2_{\mathbf{v}} \mathbf{I}_{KN_r}. \tag{1.14}$$

The unknown parameters $\boldsymbol{\theta}_c$ and $\boldsymbol{\theta}_r$ of the vector $\boldsymbol{\theta}$ in equation (1.12) are given by:

$$\boldsymbol{\theta}_c = \mathbf{h}\,; \qquad \boldsymbol{\theta}_r = \left[\boldsymbol{\sigma}^{2\,T}_{\mathbf{x}} \ \sigma^2_{\mathbf{v}}\right]^T. \tag{1.15}$$

For the pilot-based FIM, the sub-matrix $\mathbf{J}^{p}_{\boldsymbol{\theta}_r\boldsymbol{\theta}_r}$ is provided by:

$$\mathbf{J}^{p}_{\boldsymbol{\theta}_r\boldsymbol{\theta}_r} = \begin{bmatrix} \mathbf{0}_{N_t \times N_t} & \mathbf{0}_{N_t \times 1} \\ \mathbf{0}_{1 \times N_t} & \frac{N_r K}{2\sigma^4_{\mathbf{v}}} \end{bmatrix} \tag{1.16}$$

The data-based FIM of this model is given by [36]:

$$\mathbf{J}^{d}_{\boldsymbol{\theta}\boldsymbol{\theta}} = tr\left\{ \mathbf{C}^{-1}_{\mathbf{y}} \frac{\partial \mathbf{C}_{\mathbf{y}}}{\partial \boldsymbol{\theta}^*} \mathbf{C}^{-1}_{\mathbf{y}} \left(\frac{\partial \mathbf{C}_{\mathbf{y}}}{\partial \boldsymbol{\theta}^*} \right)^H \right\}. \tag{1.17}$$

[6] A complex parameter represents two real valued parameters. So, one can use either the real and imaginary parts or equivalently, the complex parameter and its conjugate (see [39] for more details).

The derivation of the FIM is related to the following equations: $\frac{\partial \mathbf{C_y}}{\partial \sigma^2_{\mathbf{x}_i}} = \frac{1}{2}\boldsymbol{\lambda}_i\boldsymbol{\lambda}_i^H$; $\frac{\partial \mathbf{C_y}}{\partial \sigma^2_{\mathbf{v}}} = \frac{1}{2}\mathbf{I}_{KN_r}$; and $\frac{\partial \mathbf{C_y}}{\partial h_i^*} = \boldsymbol{\lambda}\mathbf{C_x}\frac{\partial \boldsymbol{\lambda}^H}{\partial h_i^*}$. To simplify the latter, for each $i = 1, \cdots, NN_rN_t$, the corresponding indices $i_{N_t} = 1, \cdots, N_t$; $i_{N_r} = 1, \cdots, N_r$; and $i_N = 1, \cdots, N$ are calculated. Therefore after some simplifications, we obtain $\frac{\partial \mathbf{C_y}}{\partial h_i^*} = \sigma^2_{\mathbf{x}_{i_{N_t}}}\boldsymbol{\lambda}_{i_{N_t}}\frac{\partial \boldsymbol{\lambda}^H_{i_{N_t}}}{\partial h_i^*}$. The FIM $\mathbf{J}^d_{\boldsymbol{\theta\theta}}$ has the following form:

$$\mathbf{J}^d_{\boldsymbol{\theta\theta}} = N_d \begin{bmatrix} \mathbf{J_{hh}} & \mathbf{J_{hh^*}} & \mathbf{J_{h\sigma^2_x}} & \mathbf{J_{h\sigma^2_v}} \\ \mathbf{J_{h^*h}} & \mathbf{J_{h^*h^*}} & \mathbf{J_{h^*\sigma^2_x}} & \mathbf{J_{h^*\sigma^2_v}} \\ \mathbf{J_{\sigma^2_x h}} & \mathbf{J_{\sigma^2_x h^*}} & \mathbf{J_{\sigma^2_x\sigma^2_x}} & \mathbf{J_{\sigma^2_x\sigma^2_v}} \\ \mathbf{J_{\sigma^2_v h}} & \mathbf{J_{\sigma^2_v h^*}} & \mathbf{J_{\sigma^2_v\sigma^2_x}} & \mathbf{J_{\sigma^2_v\sigma^2_v}} \end{bmatrix}, \tag{1.18}$$

where

$$[\mathbf{J_{hh}}]_{i,j} = [\mathbf{J_{h^*h^*}}]^H_{i,j} = tr\left\{\mathbf{C_y}^{-1}\sigma^2_{\mathbf{x}_{i_{N_t}}}\boldsymbol{\lambda}_{i_{N_t}}\frac{\partial \boldsymbol{\lambda}^H_{i_{N_t}}}{\partial h_i^*}\mathbf{C_y}^{-1}\sigma^2_{\mathbf{x}_{j_{N_t}}}\frac{\partial \boldsymbol{\lambda}_{j_{N_t}}}{\partial h_j}\boldsymbol{\lambda}^H_{j_{N_t}}\right\}, 1 \le i,j \le N_tN_rN \tag{1.19}$$

$$[\mathbf{J_{hh^*}}]_{i,j} = [\mathbf{J_{h^*h}}]^H_{i,j} = tr\left\{\mathbf{C_y}^{-1}\sigma^2_{\mathbf{x}_{i_{N_t}}}\boldsymbol{\lambda}_{i_{N_t}}\frac{\partial \boldsymbol{\lambda}^H_{i_{N_t}}}{\partial h_i^*}\mathbf{C_y}^{-1}\sigma^2_{\mathbf{x}_{j_{N_t}}}\boldsymbol{\lambda}_{j_{N_t}}\frac{\partial \boldsymbol{\lambda}^H_{j_{N_t}}}{\partial h_j^*}\right\}, \tag{1.20}$$

$$\left[\mathbf{J_{\sigma^2_x\sigma^2_x}}\right]_{i,j} = \frac{1}{4}tr\left\{\mathbf{C_y}^{-1}\boldsymbol{\lambda}_i\boldsymbol{\lambda}_i^H\mathbf{C_y}^{-1}\boldsymbol{\lambda}_j\boldsymbol{\lambda}_j^H\right\}, 1 \le i,j \le N_t \tag{1.21}$$

$$\mathbf{J}_{\sigma^2_v\sigma^2_v} = \frac{1}{4}tr\left\{\mathbf{C_y}^{-1}\mathbf{C_y}^{-1}\right\}, \tag{1.22}$$

$$\left[\mathbf{J_{h\sigma^2_x}}\right]_{i,j} = \left[\mathbf{J_{h^*\sigma^2_x}}\right]^H_{i,j} = \frac{1}{2}tr\left\{\mathbf{C_y}^{-1}\sigma^2_{\mathbf{x}_{i_{N_t}}}\boldsymbol{\lambda}_{i_{N_t}}\frac{\partial \boldsymbol{\lambda}^H_{i_{N_t}}}{\partial h_i^*}\mathbf{C_y}^{-1}\boldsymbol{\lambda}_j\boldsymbol{\lambda}_j^H\right\}, \begin{array}{l} 1 \le i \le N_tN_rN \\ 1 \le j \le N_t \end{array} \tag{1.23}$$

$$\left[\mathbf{J_{h\sigma^2_v}}\right]_i = \left[\mathbf{J_{hh^*\sigma^2_v}}\right]^H_i = \frac{1}{2}tr\left\{\mathbf{C_y}^{-1}\sigma^2_{\mathbf{x}_{i_{N_t}}}\boldsymbol{\lambda}_{i_{N_t}}\frac{\partial \boldsymbol{\lambda}^H_{i_{N_t}}}{\partial h_i^*}\mathbf{C_y}^{-1}\right\}, 1 \le i \le N_tN_rN \tag{1.24}$$

$$\left[\mathbf{J_{\sigma^2_x\sigma^2_v}}\right]_i = \frac{1}{4}tr\left\{\mathbf{C_y}^{-1}\boldsymbol{\lambda}_i\boldsymbol{\lambda}_i^H\mathbf{C_y}^{-1}\right\}, 1 \le i \le N_t. \tag{1.25}$$

Once the total FIM $\mathbf{J}_{\boldsymbol{\theta\theta}}$ is obtained by the summation of the two FIMs given by equations (1.13) and (1.18) it is inverted to obtain the CRB matrix. Then, the top-left $NN_tN_r \times NN_tN_r$ subblock of the CRB matrix (referred to as h-block) is extracted to deduce the CRB, denoted CRB^{CG}_{SB}, for the channel parameter vector.

1.4.2 Non-Circular Gaussian data model

In this section, the unknown data OFDM symbols are assumed to be NCG with:

$$\begin{aligned}\mathbf{C}_{\mathbf{x}} &= E\left[\mathbf{x}\mathbf{x}^H\right] = \mathrm{diag}\left\{\boldsymbol{\sigma}_{\mathbf{x}}^2\right\},\\ \mathbf{C'}_{\mathbf{x}} &= E\left[\mathbf{x}\mathbf{x}^T\right] = \rho_c \mathrm{diag}\left\{e^{j\phi_1}\cdots e^{j\phi_{N_t}}\right\}\mathbf{C}_x,\end{aligned} \tag{1.26}$$

where $0 < \rho_c \leq 1$ is the non-circularity rate (for simplicity, we consider here a common non-circularity coefficient for all users); and $\boldsymbol{\phi} = [\phi_1 \cdots \phi_{N_t}]^T$ the non-circularity phases.

The vectors $\boldsymbol{\theta}_c$ and $\boldsymbol{\theta}_r$ are given by :

$$\boldsymbol{\theta}_c = \mathbf{h}\,; \qquad \boldsymbol{\theta}_r = \left[\boldsymbol{\sigma}_{\mathbf{x}}^{2\,T}\ \boldsymbol{\phi}^T\ \rho_c\ \sigma_{\mathbf{v}}^2\right]^T. \tag{1.27}$$

For the pilot based FIM, $\mathbf{J}^p_{\boldsymbol{\theta}_r\boldsymbol{\theta}_r}$ is still equal to zero except for its lower-right entry corresponding to $\mathbf{J}^p_{\sigma_{\mathbf{v}}^2\sigma_{\mathbf{v}}^2}$ which is equal to $\frac{N_r K}{2\sigma_{\mathbf{v}}^4}$. The data-based FIM of this model is given by the following expression [39, 41]:

$$\left[\mathbf{J}^d_{\boldsymbol{\theta}\boldsymbol{\theta}}\right]_{i,j} = \frac{1}{2} tr\left\{\tilde{\mathbf{C}}_{\mathbf{y}}^{-1}\frac{\partial\tilde{\mathbf{C}}_{\mathbf{y}}}{\partial\boldsymbol{\theta}^*}\tilde{\mathbf{C}}_{\mathbf{y}}^{-1}\left(\frac{\partial\tilde{\mathbf{C}}_{\mathbf{y}}}{\partial\boldsymbol{\theta}^*}\right)^H\right\}, \tag{1.28}$$

where

$$\tilde{\mathbf{C}}_{\mathbf{y}} = \begin{bmatrix}\mathbf{C}_{\mathbf{y}} & \mathbf{C'}_{\mathbf{y}}\\ \mathbf{C'}^*_{\mathbf{y}} & \mathbf{C}^*_{\mathbf{y}}\end{bmatrix}, \tag{1.29}$$

$$\mathbf{C'}_{\mathbf{y}} = E\left[\mathbf{y}\mathbf{y}^T\right] = \sum_{i=1}^{N_t}\rho_c e^{j\phi_i}\sigma_{\mathbf{x}_i}^2\boldsymbol{\lambda}_i{\boldsymbol{\lambda}_i}^T. \tag{1.30}$$

The FIM $\mathbf{J}^d_{\boldsymbol{\theta}\boldsymbol{\theta}}$ has the following form:

$$\mathbf{J}^d_{\boldsymbol{\theta}\boldsymbol{\theta}} = N_d\begin{bmatrix}
\mathbf{J}_{\mathbf{h}\mathbf{h}} & \mathbf{J}_{\mathbf{h}\mathbf{h}^*} & \mathbf{J}_{\mathbf{h}\boldsymbol{\sigma}_{\mathbf{x}}^2} & \mathbf{J}_{\mathbf{h}\boldsymbol{\phi}} & \mathbf{J}_{\mathbf{h}\rho_c} & \mathbf{J}_{\mathbf{h}\sigma_{\mathbf{v}}^2}\\
\mathbf{J}_{\mathbf{h}^*\mathbf{h}} & \mathbf{J}_{\mathbf{h}^*\mathbf{h}^*} & \mathbf{J}_{\mathbf{h}^*\boldsymbol{\sigma}_{\mathbf{x}}^2} & \mathbf{J}_{\mathbf{h}^*\boldsymbol{\phi}} & \mathbf{J}_{\mathbf{h}^*\rho_c} & \mathbf{J}_{\mathbf{h}^*\sigma_{\mathbf{v}}^2}\\
\mathbf{J}_{\boldsymbol{\sigma}_{\mathbf{x}}^2\mathbf{h}} & \mathbf{J}_{\boldsymbol{\sigma}_{\mathbf{x}}^2\mathbf{h}^*} & \mathbf{J}_{\boldsymbol{\sigma}_{\mathbf{x}}^2\boldsymbol{\sigma}_{\mathbf{x}}^2} & \mathbf{J}_{\boldsymbol{\sigma}_{\mathbf{x}}^2\boldsymbol{\phi}} & \mathbf{J}_{\boldsymbol{\sigma}_{\mathbf{x}}^2\rho_c} & \mathbf{J}_{\boldsymbol{\sigma}_{\mathbf{x}}^2\sigma_{\mathbf{v}}^2}\\
\mathbf{J}_{\boldsymbol{\phi}\mathbf{h}} & \mathbf{J}_{\boldsymbol{\phi}\mathbf{h}^*} & \mathbf{J}_{\boldsymbol{\phi}\boldsymbol{\sigma}_{\mathbf{x}}^2} & \mathbf{J}_{\boldsymbol{\phi}\boldsymbol{\phi}} & \mathbf{J}_{\boldsymbol{\phi}\rho_c} & \mathbf{J}_{\boldsymbol{\phi}\sigma_{\mathbf{v}}^2}\\
\mathbf{J}_{\rho_c\mathbf{h}} & \mathbf{J}_{\rho_c\mathbf{h}^*} & \mathbf{J}_{\rho_c\boldsymbol{\sigma}_{\mathbf{x}}^2} & \mathbf{J}_{\rho_c\boldsymbol{\phi}} & \mathbf{J}_{\rho_c\rho_c} & \mathbf{J}_{\rho_c\sigma_{\mathbf{v}}^2}\\
\mathbf{J}_{\sigma_{\mathbf{v}}^2\mathbf{h}} & \mathbf{J}_{\sigma_{\mathbf{v}}^2\mathbf{h}^*} & \mathbf{J}_{\sigma_{\mathbf{v}}^2\boldsymbol{\sigma}_{\mathbf{x}}^2} & \mathbf{J}_{\sigma_{\mathbf{v}}^2\boldsymbol{\phi}} & \mathbf{J}_{\sigma_{\mathbf{v}}^2\rho_c} & \mathbf{J}_{\sigma_{\mathbf{v}}^2\sigma_{\mathbf{v}}^2}
\end{bmatrix}, \tag{1.31}$$

To derive the FIMs $\left[\mathbf{J}^d_{\boldsymbol{\theta}\boldsymbol{\theta}}\right]_{i,j}$, the following computational details are required:

$$\frac{\partial\tilde{\mathbf{C}}_{\mathbf{y}}}{\partial\sigma_{\mathbf{x}_i}^2} = \frac{1}{2}\begin{bmatrix}\boldsymbol{\lambda}_i{\boldsymbol{\lambda}_i}^H & \rho_c e^{j\phi_i}\boldsymbol{\lambda}_i{\boldsymbol{\lambda}_i}^T\\ \rho_c e^{-j\phi_i}\boldsymbol{\lambda}_i^*{\boldsymbol{\lambda}_i}^H & \boldsymbol{\lambda}_i^*{\boldsymbol{\lambda}_i}^T\end{bmatrix}, \quad 1 \leq i \leq N_t, \tag{1.32}$$

$$\frac{\partial\tilde{\mathbf{C}}_{\mathbf{y}}}{\partial\phi_i} = \frac{1}{2}\sigma_{\mathbf{x}_i}^2\rho_c\begin{bmatrix}\mathbf{0} & je^{j\phi_i}\boldsymbol{\lambda}_i{\boldsymbol{\lambda}_i}^T\\ -je^{-j\phi_i}\boldsymbol{\lambda}_i^*{\boldsymbol{\lambda}_i}^H & \mathbf{0}\end{bmatrix}, \quad 1 \leq i \leq N_t, \tag{1.33}$$

$$\frac{\partial \tilde{\mathbf{C}}_{\mathbf{y}}}{\partial \rho_c} = \frac{1}{2\rho_c}\begin{bmatrix} \mathbf{0} & \mathbf{C'}_{\mathbf{y}} \\ \mathbf{C'}^{*}_{\mathbf{y}} & \mathbf{0} \end{bmatrix}, \qquad \frac{\partial \tilde{\mathbf{C}}_{\mathbf{y}}}{\partial \sigma^2_{\mathbf{v}}} = \frac{1}{2}\mathbf{I}_{2KN_r}. \tag{1.34}$$

The computation of $\frac{\partial \tilde{\mathbf{C}}_{\mathbf{y}}}{\partial h_i^*}$ for each $i = 1, \cdots, NN_rN_t$ corresponds to:

$$\frac{\partial \tilde{\mathbf{C}}_{\mathbf{y}}}{\partial h_i^*} = \begin{bmatrix} \mathbf{D}_1 & \mathbf{0} \\ \mathbf{D}_2 + \mathbf{D}_2^T & \mathbf{D}_1^T \end{bmatrix}, \tag{1.35}$$

where, for $i_{N_t} = 1, \cdots, N_t$; $i_{N_r} = 1, \cdots, N_r$; and $i_N = 1, \cdots, N$.

$$\mathbf{D}_1 = \sigma^2_{\mathbf{x}_{i_{N_t}}} \boldsymbol{\lambda}_{i_{N_t}} \frac{\partial \boldsymbol{\lambda}^H_{i_{N_t}}}{\partial h_i^*}, \qquad \mathbf{D}_2 = \rho_c e^{j\phi_{i_{N_t}}} \sigma^2_{\mathbf{x}_{i_{N_t}}} \boldsymbol{\lambda}^*_{i_{N_t}} \frac{\partial \boldsymbol{\lambda}^H_{i_{N_t}}}{\partial h_i^*}. \tag{1.36}$$

Once the total FIM $\mathbf{J}_{\boldsymbol{\theta}\boldsymbol{\theta}}$ is obtained, it is inverted to get the global CRB, then the $\mathbf{h}$-block of the CRB is extracted to calculate the CRB denoted CRB_{SB}^{NCG}.

1.4.3 BPSK and QPSK data model

This section addresses the computation of the CRB according to BPSK and QPSK data model denoted CRB_{SB}^{BPSK} and CRB_{SB}^{QPSK}. The SIMO-OFDM system is first considered. The MIMO-OFDM system, under the assumption of high SNR, is then discussed.

1.4.3.1 SIMO-OFDM system

The received signal at the k-th sub-carrier, is provided by:

$$\mathbf{y}_{(k)} = [y_{1,k} \cdots y_{N_r,k}]^T = \boldsymbol{\lambda}_{(k)} \sigma_{\mathbf{x}} x_{(k)} + \mathbf{v}_{(k)} \qquad \text{for} \quad k = 1, \ldots, K. \tag{1.37}$$

where $x_{(k)}, k = 1, \ldots, K$ are independent identically distributed (i.i.d.) random symbols taking values ± 1 (respectively, $\pm\sqrt{2}/2 \pm i\sqrt{2}/2$) with equal probabilities for BPSK (respectively QPSK) modulations. $\boldsymbol{\lambda}_{(k)}$ is the k-th component of the FFT of $\mathbf{h}$ given in equation (1.4), i.e. $\boldsymbol{\lambda}_{(k)} = \left[(\mathbf{W}\mathbf{h}_{1,1})_k, \cdots, (\mathbf{W}\mathbf{h}_{1,N_r})_k\right]^T$. The likelihood function is given as a mixture of Q Circular Gaussian as follows:

$$p(\mathbf{y}_{(k)}, \boldsymbol{\theta}) = \frac{1}{Q(\pi\sigma^2_{\mathbf{v}})^{N_r}} \sum_{q=1}^{Q} e^{-\left\|\mathbf{y}_{(k)} - \boldsymbol{\lambda}_{(k)}\sigma_{\mathbf{x}} x_q\right\|^2 / \sigma^2_{\mathbf{v}}}, \tag{1.38}$$

with $Q = 2$ and $x_q = \pm 1$ (respectively $Q = 4$ and $x_q = \pm\sqrt{2}/2 \pm i\sqrt{2}/2$) for BPSK (respectively QPSK) modulation and $\boldsymbol{\theta}$ is given by (1.12) with $\boldsymbol{\theta}_c = \mathbf{h}$ and $\boldsymbol{\theta}_r = [\sigma_{\mathbf{x}}, \sigma_{\mathbf{v}}]^T$.

Equation (1.38) is then rewritten as:

$$p_{BPSK}(\mathbf{y}_{(k)}, \boldsymbol{\theta}) = \frac{1}{(\pi\sigma^2_{\mathbf{v}})^{N_r}} e^{-\left(\|\mathbf{y}_{(k)}\|^2 + \sigma^2_{\mathbf{x}}\|\boldsymbol{\lambda}_{(k)}\|^2\right)/\sigma^2_{\mathbf{v}}} \cosh\left(\frac{\sigma_{\mathbf{x}}}{\sigma^2_{\mathbf{v}}} g_1\left(\mathbf{y}_{(k)}\right)\right), \tag{1.39}$$

$$p_{QPSK}(\mathbf{y}_{(k)},\boldsymbol{\theta}) = \frac{1}{(\pi\sigma_{\mathbf{v}}^2)^{N_r}} e^{-\left(\|\mathbf{y}_{(k)}\|^2+\sigma_{\mathbf{v}}^2\|\boldsymbol{\lambda}_{(k)}\|^2\right)/\sigma_{\mathbf{v}}^2} \cosh\left(\frac{\sigma_{\mathbf{x}}}{\sqrt{2}\sigma_{\mathbf{v}}^2} g_1\left(\mathbf{y}_{(k)}\right)\right) \cosh\left(\frac{\sigma_{\mathbf{x}}}{\sqrt{2}\sigma_{\mathbf{v}}^2} g_2\left(\mathbf{y}_{(k)}\right)\right), \tag{1.40}$$

where $g_1\left(\mathbf{y}_{(k)}\right) = 2\Re\left(\mathbf{y}_{(k)}^H \boldsymbol{\lambda}_{(k)}\right)$ and $g_2\left(\mathbf{y}_{(k)}\right) = 2\Im\left(\mathbf{y}_{(k)}^H \boldsymbol{\lambda}_{(k)}\right)$ ($\Re(.)$ and $\Im(.)$ being the real and imaginary parts). To calculate the FIM in (1.18), the following second derivatives are first computed:

$$\frac{\partial^2 \ln p_{BPSK}(\mathbf{y}_{(k)},\boldsymbol{\theta})}{\partial h_i^* \partial h_j^*} = -\frac{\sigma_{\mathbf{x}}^2}{\sigma_{\mathbf{v}}^2} \frac{\partial \boldsymbol{\lambda}_{(k)}^H}{\partial h_i^*} \frac{\partial \boldsymbol{\lambda}_{(k)}}{\partial h_j} + \frac{\sigma_{\mathbf{x}}^2}{\sigma_{\mathbf{v}}^4} {g_1}''\left(\mathbf{y}_{(k)}\right)_{ij} f, \tag{1.41}$$

$$\frac{\partial^2 \ln p_{BPSK}(\mathbf{y}_{(k)},\boldsymbol{\theta})}{\partial \sigma_{\mathbf{x}} \partial \sigma_{\mathbf{x}}} = -\frac{\left\|\boldsymbol{\lambda}_{(k)}\right\|^2}{2\sigma_{\mathbf{v}}^2} + \frac{{g_1}^2\left(\mathbf{y}_{(k)}\right)}{4\sigma_{\mathbf{v}}^4} f, \tag{1.42}$$

$$\frac{\partial^2 \ln p_{BPSK}(\mathbf{y}_{(k)},\boldsymbol{\theta})}{\partial \sigma_{\mathbf{v}} \partial \sigma_{\mathbf{v}}} = \frac{1}{4}\left(\frac{2N_r}{\sigma_{\mathbf{v}}^2} - \frac{6\left(\|\mathbf{y}_{(k)}\|^2+\sigma_{\mathbf{x}}^2\|\boldsymbol{\lambda}_{(k)}\|^2\right)}{\sigma_{\mathbf{v}}^4} + \frac{6\sigma_{\mathbf{x}} g_1\left(\mathbf{y}_{(k)}\right)}{\sigma_{\mathbf{v}}^4} \tanh\left(\frac{\sigma_{\mathbf{x}}}{\sigma_{\mathbf{v}}^2} g_1\left(\mathbf{y}_{(k)}\right)\right) + \frac{\sigma_{\mathbf{x}}^2 {g_1}^2\left(\mathbf{y}_{(k)}\right)}{4\sigma_{\mathbf{v}}^6} f\right), \tag{1.43}$$

$$\frac{\partial^2 \ln p_{BPSK}(\mathbf{y}_{(k)},\boldsymbol{\theta})}{\partial h_i^* \partial \sigma_{\mathbf{x}}} = \frac{1}{2}\left(-\frac{2\sigma_{\mathbf{x}}}{\sigma_{\mathbf{v}}^2} \frac{\partial \boldsymbol{\lambda}_{(k)}^H}{\partial h_i^*} \boldsymbol{\lambda}_{(k)} + \frac{\sigma_{\mathbf{x}}}{\sigma_{\mathbf{v}}^4} g_1\left(\mathbf{y}_{(k)}\right) {g_1}'\left(\mathbf{y}_{(k)}\right)_i f + \frac{1}{4\sigma_{\mathbf{v}}^2} {g_1}'\left(\mathbf{y}_{(k)}\right)_i \tanh\left(\frac{\sigma_{\mathbf{x}}}{\sigma_{\mathbf{v}}^2} g_1\left(\mathbf{y}_{(k)}\right)\right)\right), \tag{1.44}$$

$$\frac{\partial^2 \ln p_{BPSK}(\mathbf{y}_{(k)},\boldsymbol{\theta})}{\partial h_i^* \partial \sigma_{\mathbf{v}}} = \frac{1}{2}\left(\frac{2\sigma_{\mathbf{x}}^2}{\sigma_{\mathbf{v}}^3} \frac{\partial \boldsymbol{\lambda}_{(k)}^H}{\partial h_i^*} \boldsymbol{\lambda}_{(k)} - \frac{2\sigma_{\mathbf{x}}^2}{\sigma_{\mathbf{v}}^5} g_1\left(\mathbf{y}_{(k)}\right) {g_1}'\left(\mathbf{y}_{(k)}\right)_i f - \frac{\sigma_{\mathbf{x}}}{2\sigma_{\mathbf{v}}^3} {g_1}'\left(\mathbf{y}_{(k)}\right)_i \tanh\left(\frac{\sigma_{\mathbf{x}}}{\sigma_{\mathbf{v}}^2} g_1\left(\mathbf{y}_{(k)}\right)\right)\right), \tag{1.45}$$

$$\frac{\partial^2 \ln p_{BPSK}(\mathbf{y}_{(k)},\boldsymbol{\theta})}{\partial \sigma_{\mathbf{x}} \partial \sigma_{\mathbf{v}}} = \frac{1}{4}\left(\frac{4\sigma_{\mathbf{x}}}{\sigma_{\mathbf{v}}^3}\left\|\boldsymbol{\lambda}_{(k)}\right\|^2 - \frac{2\sigma_{\mathbf{x}}}{\sigma_{\mathbf{v}}^5} {g_1}^2\left(\mathbf{y}_{(k)}\right) f - \frac{2g_1\left(\mathbf{y}_{(k)}\right)}{2\sigma_{\mathbf{v}}^3} \tanh\left(\frac{\sigma_{\mathbf{x}}}{\sigma_{\mathbf{v}}^2} g_1\left(\mathbf{y}_{(k)}\right)\right)\right), \tag{1.46}$$

where ${g_1}'$, ${g_1}''$ and f are given by: ${g_1}'\left(\mathbf{y}_{(k)}\right)_i \overset{\text{def}}{=} \frac{\partial \boldsymbol{\lambda}_{(k)}^H}{\partial h_i^*}\mathbf{y}_{(k)}$, ${g_1}''\left(\mathbf{y}_{(k)}\right)_{i,j} \overset{\text{def}}{=} \mathbf{y}_{(k)}^H \frac{\partial \boldsymbol{\lambda}_{(k)}}{\partial h_j} \frac{\partial \boldsymbol{\lambda}_{(k)}^H}{\partial h_i^*}\mathbf{y}_{(k)}$ and $f \overset{\text{def}}{=} \frac{1}{\cosh^2\left(\frac{\sigma_{\mathbf{x}}}{\sigma_{\mathbf{v}}^2} g_1\left(\mathbf{y}_{(k)}\right)\right)}$. Using the regularity condition, we obtain:

$$E\left[\frac{\partial \ln p_{BPSK}(\mathbf{y}_{(k)},\boldsymbol{\theta})}{\partial \sigma_{\mathbf{x}}}\right] = 0 \Rightarrow E\left[g_1\left(\mathbf{y}_{(k)}\right) \tanh\left(\frac{\sigma_{\mathbf{x}}}{\sigma_{\mathbf{v}}^2} g_1\left(\mathbf{y}_{(k)}\right)\right)\right] = 2\sigma_{\mathbf{x}}\left\|\boldsymbol{\lambda}_{(k)}\right\|^2, \tag{1.47}$$

$$E\left[\frac{\partial \ln p_{BPSK}(\mathbf{y}_{(k)},\boldsymbol{\theta})}{\partial h_i^*}\right] = 0 \Rightarrow E\left[{g_1}'\left(\mathbf{y}_{(k)}\right) \tanh\left(\frac{\sigma_{\mathbf{x}}}{\sigma_{\mathbf{v}}^2} g_1\left(\mathbf{y}_{(k)}\right)\right)\right] = \sigma_{\mathbf{x}} \frac{\partial \boldsymbol{\lambda}_{(k)}^H}{\partial h_i^*}\boldsymbol{\lambda}_{(k)}. \tag{1.48}$$

To compute the FIM entries, equations (1.47) and (1.48) of the regularity conditions are used together with the fact that f vanishes to 0 when SNR>0 as shown in Figure 1.3a. This approximation is exploited to neglect all integration terms[7] involving function f.

[7]Note that this approximation takes into account the fact that all the terms multiplying function f are also bounded and vanish rapidly to 0 for large values of their arguments.

Therefore, the total FIM $\mathbf{J}^d_{\boldsymbol{\theta\theta}}$ is expressed as follows:

$$\mathbf{J}^d_{\boldsymbol{\theta\theta}} = N_d \sum_{k=1}^{K} \mathbf{J}^d_{\boldsymbol{\theta\theta}}(k), \tag{1.49}$$

where the entries of $\mathbf{J}^d_{\boldsymbol{\theta\theta}}(k)$ are given by:

$$[\mathbf{J}_{\mathbf{hh}}]_{i,j} = [\mathbf{J}_{\mathbf{h}^*\mathbf{h}^*}]^H_{i,j} = \frac{\sigma^2_{\mathbf{x}}}{\sigma^2_{\mathbf{v}}} \frac{\partial \boldsymbol{\lambda}^H_{(k)}}{\partial h^*_i} \frac{\partial \boldsymbol{\lambda}_{(k)}}{\partial h_j}, \qquad [\mathbf{J}_{\mathbf{hh}^*}]_{i,j} = [\mathbf{J}_{\mathbf{h}^*\mathbf{h}}]_{i,j} = 0, \tag{1.50}$$

$$[\mathbf{J}_{\sigma_{\mathbf{x}}\sigma_{\mathbf{x}}}] = \frac{\left\|\boldsymbol{\lambda}_{(k)}\right\|^2}{2\sigma^2_{\mathbf{v}}}, \qquad [\mathbf{J}_{\sigma_{\mathbf{v}}\sigma_{\mathbf{v}}}] = \frac{N_r}{\sigma^2_{\mathbf{v}}}, \tag{1.51}$$

$$[\mathbf{J}_{\mathbf{h}\sigma_{\mathbf{x}}}]_i = [\mathbf{J}_{\mathbf{h}^*\sigma_{\mathbf{x}}}]^H_i = \frac{\sigma_{\mathbf{x}}}{2\sigma^2_{\mathbf{v}}} \frac{\partial \boldsymbol{\lambda}^H_{(k)}}{\partial h^*_i} \boldsymbol{\lambda}_{(k)}, \tag{1.52}$$

$$[\mathbf{J}_{\mathbf{h}\sigma_{\mathbf{v}}}]_i = [\mathbf{J}_{\mathbf{h}^*\sigma_{\mathbf{v}}}]^H_i = [\mathbf{J}_{\sigma_{\mathbf{x}}\sigma_{\mathbf{v}}}] = 0. \tag{1.53}$$

Remark: The high SNR approximation can be explained by the fact that the integral evaluation

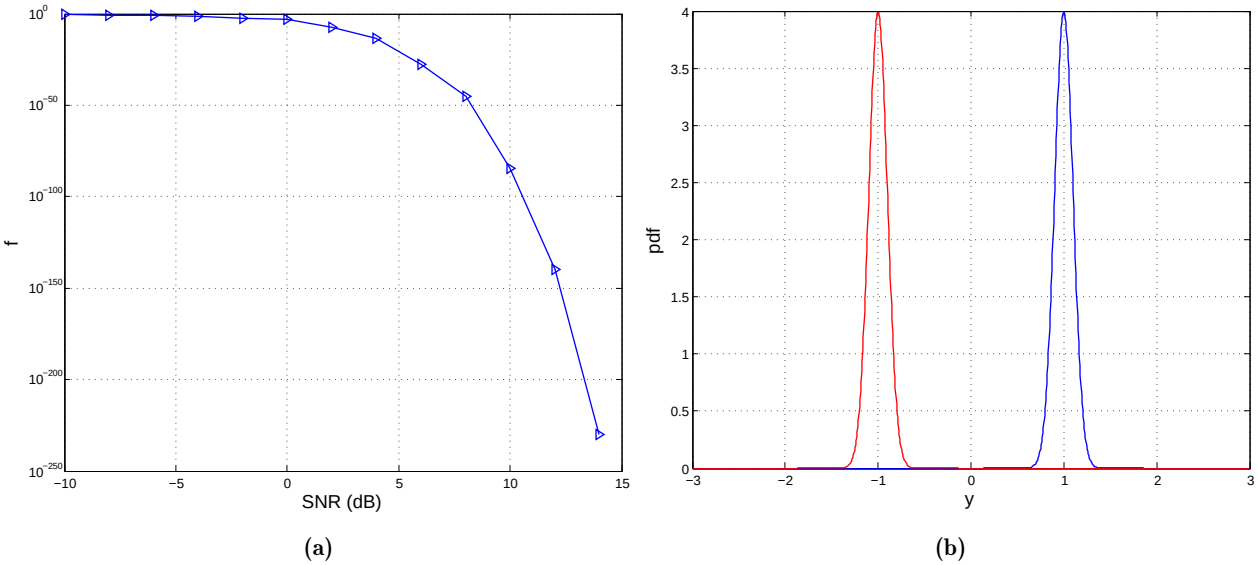

(a) **(b)**

Figure 1.3: *(a) Representation of function f w.r.t. the SNR, (b) BPSK Probability density function*

can be approximated by a sum of two integrals corresponding to the two pdf terms (peaks) illustrated in Figure 1.3b. In other words the FIM of the BPSK case can be approximated as a weighted sum of gaussian FIMs.

In QPSK modulation, since high SNR (i.e. SNR>0) is assumed, the two functions: $f_1 \overset{\text{def}}{=} \frac{1}{\cosh^2\left(\frac{\sigma_{\mathbf{x}}}{\sqrt{2}\sigma^2_{\mathbf{v}}} g_1\left(\mathbf{y}_{(k)}\right)\right)}$ and $f_2 \overset{\text{def}}{=} \frac{1}{\cosh^2\left(\frac{\sigma_{\mathbf{x}}}{\sqrt{2}\sigma^2_{\mathbf{v}}} g_2\left(\mathbf{y}_{(k)}\right)\right)}$ vanish to 0. Similar approximations are

then used and lead to the same FIM expression as for the BPSK case $\left(\text{i.e.} CRB_{SB}^{BPSK} = CRB_{SB}^{QPSK}\right)$.

1.4.3.2 MIMO-OFDM system

In the case of $(N_t \times N_r)$ MIMO-OFDM system, the likelihood function given by equation (1.38) is nothing else than a mixture of Q^{N_t} Gaussian pdfs:

$$p(\mathbf{y}_{(k)}, \boldsymbol{\theta}) = \frac{1}{Q^{N_t}} \sum_{q=1}^{Q^{N_t}} \frac{1}{(\pi\sigma_{\mathbf{v}}^2)^{N_r}} e^{-\left\|\mathbf{y}_{(k)} - \boldsymbol{\lambda}_{(k)} \mathbf{C}_{\mathbf{x}}^{\frac{1}{2}} \mathbf{x}_q\right\|^2 \Big/ \sigma_{\mathbf{v}}^2}, \tag{1.54}$$

with $\boldsymbol{\lambda}_{(k)} = \left[\boldsymbol{\lambda}_{(k),1}, \cdots, \boldsymbol{\lambda}_{(k),N_t}\right]$ where $\boldsymbol{\lambda}_{(k),i} = \left[\left(\mathbf{W}\mathbf{h}_{i,1}\right)_k, \cdots, \left(\mathbf{W}\mathbf{h}_{i,N_r}\right)_k\right]^T$.

Consequently, the computation of the FIM appears to be prohibitive. This CRB is computed under high SNR assumption as a weighted sum of Gaussian FIMs as explained previously.

$$\mathbf{J}_{\boldsymbol{\theta}\boldsymbol{\theta}}^d(k) = \frac{1}{\sigma_{\mathbf{v}}^2 Q^{N_t}} \sum_{q=1}^{Q^{N_t}} \left(\frac{\partial \boldsymbol{\lambda}_{(k)} \mathbf{C}_{\mathbf{x}}^{\frac{1}{2}} \mathbf{x}_q}{\partial \boldsymbol{\theta}^*}\right)^H \left(\frac{\partial \boldsymbol{\lambda}_{(k)} \mathbf{C}_{\mathbf{x}}^{\frac{1}{2}} \mathbf{x}_q}{\partial \boldsymbol{\theta}^*}\right) \tag{1.55}$$

$$\begin{aligned} \left[\mathbf{J}_{\boldsymbol{\theta}\boldsymbol{\theta}}^d(k)\right]_{i,j} &= \tfrac{1}{\sigma_{\mathbf{v}}^2 Q^{N_t}} \sum_{q=1}^{Q^{N_t}} \mathbf{x}_q^H \left(\tfrac{\partial \boldsymbol{\lambda}_{(k)} \mathbf{C}_{\mathbf{x}}^{\frac{1}{2}}}{\partial \theta_i^*}\right)^H \left(\tfrac{\partial \boldsymbol{\lambda}_{(k)} \mathbf{C}_{\mathbf{x}}^{\frac{1}{2}}}{\partial \theta_j^*}\right) \mathbf{x}_q \\ \left[\mathbf{J}_{\boldsymbol{\theta}\boldsymbol{\theta}}^d(k)\right]_{i,j} &= \tfrac{1}{\sigma_{\mathbf{v}}^2 Q^{N_t}} \sum_{q,m,l} x_q^*(m)\, x_q(l)\, \boldsymbol{\Gamma}_{m,l}^{i,j} \quad 1 \le m,\ l \le N_t \end{aligned} \tag{1.56}$$

Where $\boldsymbol{\Gamma}^{i,j} = \left(\frac{\partial \boldsymbol{\lambda}_{(k)} \mathbf{C}_{\mathbf{x}}^{\frac{1}{2}}}{\partial \theta_i^*}\right)^H \left(\frac{\partial \boldsymbol{\lambda}_{(k)} \mathbf{C}_{\mathbf{x}}^{\frac{1}{2}}}{\partial \theta_j^*}\right)$ and $\boldsymbol{\Gamma}_{m,l}^{i,j}$ refers to its (m,l)-th element.

Note that QAM constellations being symmetric around zero, we have:

$$\begin{aligned} \tfrac{1}{Q^{N_t}} \sum_{q=1}^{Q^{N_t}} x_q^*(m)\, x_q(l) &= 0, \ \text{for } m \neq l, \\ \tfrac{1}{Q^{N_t}} \sum_{q=1}^{Q^{N_t}} x_q^*(m)\, x_q(m) &= 1, \ \text{for } m = l, \end{aligned} \tag{1.57}$$

The latter equality is due to the chosen normalization while the former equality is due to the symmetry (around zero) of the constellation. Therefore:

$$\left[\mathbf{J}_{\boldsymbol{\theta}\boldsymbol{\theta}}^d(k)\right]_{i,j} = \frac{1}{\sigma_{\mathbf{v}}^2} tr\left\{\boldsymbol{\Gamma}^{i,j}\right\} \tag{1.58}$$

The sub-blocks of the FIM given in equation (1.18) have the form shown in (1.58) with:

$$[\mathbf{J}_{\mathbf{h}\mathbf{h}}]_{i,j} = [\mathbf{J}_{\mathbf{h}^*\mathbf{h}^*}]_{i,j}^H = \frac{1}{\sigma_{\mathbf{v}}^2} tr\left\{\mathbf{C}_{\mathbf{x}} \frac{\partial \boldsymbol{\lambda}_{(k)}^H}{\partial h_i^*} \frac{\partial \boldsymbol{\lambda}_{(k)}}{\partial h_j^*}\right\}; \quad [\mathbf{J}_{\boldsymbol{\sigma}_{\mathbf{x}}\boldsymbol{\sigma}_{\mathbf{x}}}] = \frac{\boldsymbol{\lambda}_{(k)}^H \boldsymbol{\lambda}_{(k)}}{2\sigma_{\mathbf{v}}^2} \tag{1.59}$$

$$[\mathbf{J}_{\mathbf{h}\sigma_{\mathbf{x}}}]_{i,j} = [\mathbf{J}_{\mathbf{h}^*\sigma_{\mathbf{x}}}]_{i,j}^H = \frac{1}{\sigma_{\mathbf{v}}^2} tr\left\{\frac{\partial \boldsymbol{\lambda}_{(k)}^H}{\partial h_i^*} \boldsymbol{\lambda}_{(k)} \frac{\partial \mathbf{C}_{\mathbf{x}}^{\frac{1}{2}}}{\partial \sigma_{x_j}} \mathbf{C}_{\mathbf{x}}^{\frac{1}{2}}\right\}; \quad [\mathbf{J}_{\sigma_{\mathbf{v}}\sigma_{\mathbf{v}}}] = \frac{N_r}{\sigma_{\mathbf{v}}^2}. \tag{1.60}$$

And the other block terms appearing in matrix (1.18) are zeros. Note that this approximate FIM is common to all symmetric constellations including the considered BPSK and QPSK signals.

1.5 CRB for semi-blind channel estimation with comb-type and lattice-type pilot arrangements

This section deals with the derivation of the CRB when the arrangement of the known pilots is assumed to be a comb or a lattice type structure[8]. As in the previous section, the CRB computation exploits both known and unknown transmitted OFDM symbols.

As developed in section 1.3, the pilot-based FIM is given by equation (1.13), where the total number of transmitted OFDM symbols is $N_p = N_d = N_s$. The FIM associated to the K_p sub-carriers of the i-th OFDM symbol is then given by:

$$\mathbf{J}_{\mathbf{hh}}^{p_i} = \frac{\tilde{\mathbf{X}}_{p_i}^H \tilde{\mathbf{X}}_{p_i}}{\sigma_{\mathbf{v}}^2}, \qquad \mathbf{J}_{\sigma_{\mathbf{v}}^2\sigma_{\mathbf{v}}^2}^{p_i} = \frac{N_r K_p}{2\sigma_{\mathbf{v}}^4}. \tag{1.61}$$

As for the block pilot case, the best performance is obtained when the pilot sequences are orthogonal in which case the CRB matrix is equal to $\frac{\sigma_{\mathbf{v}}^2 K}{\sigma_p^2 N_p K_p}\mathbf{I}_{N_t N_r N}$.

To derive the semi-blind CRB in the comb-type pilot arrangement, the mean and covariance matrix of the likelihood function are required and are provided as follows:

$$\mu = \boldsymbol{\lambda}_p \mathbf{x}_p = \tilde{\mathbf{X}}_p \mathbf{h}, \qquad \mathbf{C}_{\mathbf{y}} = \sum_{i=1}^{N_t} \sigma_{\mathbf{x}_i}^2 \boldsymbol{\lambda}_{d_i} \boldsymbol{\lambda}_{d_i}^H + \sigma_{\mathbf{v}}^2 \mathbf{I}_{KN_r}. \tag{1.62}$$

1.5.1 Circular Gaussian data model

In this section, the unknown data OFDM symbols are assumed to be stochastic CG, the FIM of one OFDM symbol is provided by:

$$\mathbf{J}_{\boldsymbol{\theta\theta}} = \left(\frac{\partial \mu}{\partial \boldsymbol{\theta}^*}\right)^H \mathbf{C}_{\mathbf{y}}^{-1} \frac{\partial \mu}{\partial \boldsymbol{\theta}^*} + tr\left\{\mathbf{C}_{\mathbf{y}}^{-1} \frac{\partial \mathbf{C}_{\mathbf{y}}}{\partial \boldsymbol{\theta}^*} \mathbf{C}_{\mathbf{y}}^{-1} \left(\frac{\partial \mathbf{C}_{\mathbf{y}}}{\partial \boldsymbol{\theta}^*}\right)^H\right\}. \tag{1.63}$$

$$\mathbf{J}_{\boldsymbol{\theta\theta}^*} = tr\left\{\mathbf{C}_{\mathbf{y}}^{-1} \frac{\partial \mathbf{C}_{\mathbf{y}}}{\partial \boldsymbol{\theta}^*} \mathbf{C}_{\mathbf{y}}^{-1} \frac{\partial \mathbf{C}_{\mathbf{y}}}{\partial \boldsymbol{\theta}^*}\right\}. \tag{1.64}$$

Equation (1.15) provides the vector of unknown parameters; and the $\mathbf{h}$-block FIM is equal to:

$$\mathbf{J}_{\mathbf{hh}} = \sum_{i=1}^{N_s} \tilde{\mathbf{X}}_{p_i}^H \mathbf{C}_{\mathbf{y}}^{-1} \tilde{\mathbf{X}}_{p_i} + N_s tr\left\{\mathbf{C}_{\mathbf{y}}^{-1} \frac{\partial \mathbf{C}_{\mathbf{y}}}{\partial \mathbf{h}^*} \mathbf{C}_{\mathbf{y}}^{-1} \left(\frac{\partial \mathbf{C}_{\mathbf{y}}}{\partial \mathbf{h}^*}\right)^H\right\}. \tag{1.65}$$

[8]The lattice type structure is in fact a comb type structure with varying pilot positions along the OFDM symbols. Hence, the CRB derivation of the latter is similar to that of the comb-type case.

$$\mathbf{J}_{\mathbf{h}\mathbf{h}^*} = N_s tr\left\{\mathbf{C}_\mathbf{y}^{-1}\frac{\partial \mathbf{C}_\mathbf{y}}{\partial \mathbf{h}^*}\mathbf{C}_\mathbf{y}^{-1}\frac{\partial \mathbf{C}_\mathbf{y}}{\partial \mathbf{h}^*}\right\}. \tag{1.66}$$

The other entries of the FIM are obtained in a similar way as in section 1.4.1. Also, the derivative of $\mathbf{C}_\mathbf{y}$ w.r.t. the channel parameters is obtained as before after replacing $\boldsymbol{\lambda}_i$ by $\boldsymbol{\lambda}_{d_i}$.

1.5.2 Non-Circular Gaussian data model

In the NCG case, the FIM has the same form as the CG one described by equations (1.63) and (1.64). We just need to extend the parameter vector as in section 1.4.2 and to replace $\mathbf{C}_\mathbf{y}$ by $\tilde{\mathbf{C}}_\mathbf{y}$ provided in equation (1.29) and $\boldsymbol{\lambda}_i$ by $\boldsymbol{\lambda}_{d_i}$ corresponding to the K_d data sub-carriers.

1.5.3 BPSK and QPSK data model

According to the results in section 1.4.3, the FIM is expressed as follows:

$$\mathbf{J}_{\boldsymbol{\theta}\boldsymbol{\theta}} = \mathbf{J}^p_{\boldsymbol{\theta}\boldsymbol{\theta}} + N_S \sum_{k=K_p+1}^{K} \mathbf{J}^d_{\boldsymbol{\theta}\boldsymbol{\theta}}(k), \tag{1.67}$$

where $\mathbf{J}^p_{\boldsymbol{\theta}\boldsymbol{\theta}}$ is deduced from equation (1.61); and $\mathbf{J}^d_{\boldsymbol{\theta}\boldsymbol{\theta}}(k)_{k=K_p+1,\cdots,K}$ is given in section 1.4.3 by equations (1.49) and (1.58).

1.6 Computational issue in large MIMO-OFDM communications systems

The aim of this section is to study the semi-blind channel estimation performance in large MIMO-OFDM communications systems where the base station is assumed to be equipped with a relatively large number of antennas and serves a large number of users.

Depending on the data model (CG or NCG), the CRB are provided by equations (1.17), (1.28), (1.65) and (1.66) in the previous sections. For a large MIMO-OFDM system, the implementation of these equations consumes not only a huge memory space but also a high computational time. Indeed the CRB computation requires the manipulation of several large dimensional matrix operations such as inversion, Hermitian transpose, trace and product. To avoid these strong implementation constraints, a new efficient algorithm is proposed. It exploits the structure of the covariance matrix composed of diagonal blocks. Before describing the developed algorithm, the following subsection introduces the new organization of the diagonal blocks into a new structure called vector representation.

1.6.1 Vector representation of a block diagonal matrix

Consider $\mathbf{R}$ a block diagonal matrix containing $M_l \times M_c$ diagonal matrices, each one of size $K \times K$ (i.e. $\mathbf{R} : M_l K \times M_c K$). Denote $\mathbf{A}$ the efficient organization of $\mathbf{R}$ where only the diagonal vectors of each diagonal block matrix are kept so that its dimension is reduced (i.e. $\mathbf{A} : M_l K \times M_c$). This organization into a new vector is given by the following notation:

$$\mathbf{a}^{m_l,m_c} = \mathrm{diag}\left(\mathbf{R}^{m_l,m_c}\right), \tag{1.68}$$

where $\mathbf{a}^{m_l,m_c} = \begin{bmatrix} a^{m_l,m_c}(1) & \cdots & a^{m_l,m_c}(K) \end{bmatrix}^T$ is the m_c column and m_l block row vector of $\mathbf{A}$, $1 \leq m_l \leq M_l$ and $1 \leq m_c \leq M_c$. Figure 1.4 illustrates this organization for $M_l = 3$ and $M_c = 2$.

$$\mathbf{R}= \begin{pmatrix} \alpha_1^{1,1} & 0 & \cdots & 0 & \alpha_1^{1,2} & 0 & \cdots & 0 \\ 0 & \ddots & 0 & \vdots & 0 & \ddots & 0 & \vdots \\ \vdots & 0 & \ddots & 0 & \vdots & 0 & \ddots & 0 \\ 0 & \cdots & 0 & \alpha_K^{1,1} & 0 & \cdots & 0 & \alpha_K^{1,2} \\ \alpha_1^{2,1} & 0 & \cdots & 0 & \alpha_1^{2,2} & 0 & \cdots & 0 \\ 0 & \ddots & 0 & \vdots & 0 & \ddots & 0 & \vdots \\ \vdots & 0 & \ddots & 0 & \vdots & 0 & \ddots & 0 \\ 0 & \cdots & 0 & \alpha_K^{2,1} & 0 & \cdots & 0 & \alpha_K^{2,2} \\ \alpha_1^{3,1} & 0 & \cdots & 0 & \alpha_1^{3,2} & 0 & \cdots & 0 \\ 0 & \ddots & 0 & \vdots & 0 & \ddots & 0 & \vdots \\ \vdots & 0 & \ddots & 0 & \vdots & 0 & \ddots & 0 \\ 0 & \cdots & 0 & \alpha_K^{3,1} & 0 & \cdots & 0 & \alpha_K^{3,2} \end{pmatrix} \xrightarrow[\text{representation}]{\text{Vector}} \mathbf{A}= \begin{pmatrix} \alpha_1^{1,1} & \alpha_1^{1,2} \\ \vdots & \vdots \\ \vdots & \vdots \\ \alpha_K^{1,1} & \alpha_K^{1,2} \\ \alpha_1^{2,1} & \alpha_1^{2,2} \\ \vdots & \vdots \\ \vdots & \vdots \\ \alpha_K^{2,1} & \alpha_K^{2,2} \\ \alpha_1^{3,1} & \alpha_1^{3,3} \\ \vdots & \vdots \\ \vdots & \vdots \\ \alpha_K^{3,1} & \alpha_K^{3,3} \end{pmatrix}$$

Figure 1.4: *Vector representation of the block diagonal matrix* $\mathbf{R}$ *with* $M_l = 3$ *and* $M_c = 2$.

1.6.2 Fast computational matrix product

We propose a fast computation of the matrix product of two $\mathbf{R}$-type matrices (i.e. $\mathbf{R}_1 : M_l K \times M_c K$ and $\mathbf{R}_2 : M_c K \times M_x K$) using their corresponding $\mathbf{A}$-type matrices (i.e. $\mathbf{A}_1$ and $\mathbf{A}_2$):

$$\mathbf{A} = \mathbf{A}_1 \circledast \mathbf{A}_2 \tag{1.69}$$

where $\circledast$ denotes the equivalent product. The element at m_x column and m_l block row vector of $\mathbf{A}$ is given by: $\odot$ being the element-wise product.

$$\mathbf{a}^{m_l,m_x} = \sum_{m_c=1}^{M_c} {\mathbf{a}_1}^{m_l,m_c} \odot {\mathbf{a}_2}^{m_c,m_x}. \tag{1.70}$$

For example, the direct product of our $(N_r K \times N_r K)$ covariance matrices or their derivatives costs $N_r^3 K^3$ flops while the optimal product costs only $N_r^3 K$ (i.e. we reduce the costs by a factor

K^2). The trace of a square matrix $\mathbf{R}$ based on it's vector representation $\mathbf{A}$ is given by:

$$tr\{\mathbf{R}\} = \sum_{k=1}^{K} \sum_{m_l=1}^{M_l} \mathbf{a}^{m_l,m_l}(k). \tag{1.71}$$

1.6.3 Iterative matrix inversion algorithm

This subsection deals with the $\mathbf{R}$-type matrix inversion (i.e. $\mathbf{R}^{-1}$) using its vector representation $\mathbf{A}$ introduced previously. To do so, an iterative matrix inversion algorithm is proposed. It exploits the Schur's complement summarized as follows:

$$\begin{bmatrix} \mathbf{E} & \mathbf{F} \\ \mathbf{G} & \mathbf{H} \end{bmatrix}^{-1} = \begin{bmatrix} \mathbf{E}^{-1} + \mathbf{E}^{-1}\mathbf{F}\mathbf{H}^{-1}\mathbf{G}\mathbf{E}^{-1} & -\mathbf{E}^{-1}\mathbf{F}\mathbf{H}^{-1} \\ -\mathbf{H}^{-1}\mathbf{G}\mathbf{E}^{-1} & \mathbf{H}^{-1} \end{bmatrix}, \tag{1.72}$$

where $\mathbf{E}$ and $\mathbf{H}$ are assumed to be invertible matrices. The proposed iterative matrix inversion algorithm (starting from the top-left matrix sub-block) follows the steps described below:

- Initialization step:

  - Set $\mathbf{E}_0 = \mathbf{a}^{1,1}$. The inversion of $\mathbf{E}_0$, denoted $\mathbf{I}_1$, is given by $\mathbf{I}_1 = 1./\mathbf{E}_0$, where ./ denotes the element-wise division.

  - Set $\mathbf{E}_1 = \mathbf{a}^{1,1}$, $\mathbf{F}_1 = \mathbf{a}^{1,2}$, $\mathbf{G}_1 = \mathbf{a}^{2,1}$ and $\mathbf{H}_1 = \mathbf{a}^{2,2}$. The inversion of the matrix $\begin{bmatrix} \mathbf{E}_1 & \mathbf{F}_1 \\ \mathbf{G}_1 & \mathbf{H}_1 \end{bmatrix}$ of $\mathbf{A}$-type, denoted $\mathbf{I}_2$, is given by:

$$\mathbf{I}_2 = \begin{bmatrix} \mathbf{I}_2^{1,1} & \mathbf{I}_2^{1,2} \\ \mathbf{I}_2^{2,1} & \mathbf{I}_2^{2,2} \end{bmatrix}, \tag{1.73}$$

  where

$$\begin{aligned} \mathbf{I}_2^{2,2} &= 1./\mathbf{H}_1, \\ \mathbf{I}_2^{1,1} &= \mathbf{I}_1 + \mathbf{I}_1 \circledast \mathbf{F}_1 \circledast \mathbf{I}_2^{2,2} \circledast \mathbf{G}_1 \circledast \mathbf{I}_1, \\ \mathbf{I}_2^{1,2} &= -\mathbf{I}_1 \circledast \mathbf{F}_1 \circledast \mathbf{I}_2^{2,2}, \\ \mathbf{I}_2^{2,1} &= -\mathbf{I}_2^{2,2} \circledast \mathbf{G}_1 \circledast \mathbf{I}_1, \end{aligned} \tag{1.74}$$

  and $\circledast$ denotes the equivalent product as explained in section 1.6.2.

- The matrix inversion process is iterated. At the m-th iteration, the algorithm inverses the

matrix $\begin{bmatrix} \mathbf{E}_{m-1} & \mathbf{F}_{m-1} \\ \mathbf{G}_{m-1} & \mathbf{H}_{m-1} \end{bmatrix}$ of **A**-type, where:

$$\begin{aligned} \mathbf{E}_{m-1} &= \begin{bmatrix} \mathbf{a}^{1,1} & \cdots & \mathbf{a}^{1,m-1} \\ \vdots & \ddots & \vdots \\ \mathbf{a}^{m-1,1} & \cdots & \mathbf{a}^{m-1,m-1} \end{bmatrix}; \quad \mathbf{F}_{m-1} = \begin{bmatrix} \mathbf{a}^{1,m} \\ \vdots \\ \mathbf{a}^{m-1,m} \end{bmatrix}; \\ \mathbf{G}_{m-1} &= \begin{bmatrix} \mathbf{a}^{m,1} & \cdots & \mathbf{a}^{m,m-1} \end{bmatrix}; \qquad \mathbf{H}_{m-1} = \mathbf{a}^{m,m}. \end{aligned} \tag{1.75}$$

Based on the results of the previous iteration, i.e. $(m-1)$-th iteration and using the Schur's complement formula, the inverse matrix $\mathbf{I}_m$:

$$\mathbf{I}_m = \begin{bmatrix} \mathbf{I}_m^{1,1} & \mathbf{I}_m^{1,2} \\ \mathbf{I}_m^{2,1} & \mathbf{I}_m^{2,2} \end{bmatrix}, \tag{1.76}$$

is given by the following expressions:

$$\begin{aligned} \mathbf{I}_m^{2,2} &= 1./\mathbf{H}_{m-1}, \\ \mathbf{I}_m^{1,1} &= \mathbf{I}_{m-1} + \mathbf{I}_{m-1} \circledast \mathbf{F}_{m-1} \circledast \mathbf{I}_m^{2,2} \circledast \mathbf{G}_{m-1} \circledast \mathbf{I}_{m-1}, \\ \mathbf{I}_m^{1,2} &= -\mathbf{I}_{m-1} \circledast \mathbf{F}_{m-1} \circledast \mathbf{I}_m^{2,2}, \\ \mathbf{I}_m^{2,1} &= -\mathbf{I}_m^{2,2} \circledast \mathbf{G}_{m-1} \circledast \mathbf{I}_{m-1}. \end{aligned} \tag{1.77}$$

- The inversion process is iterated until the M_l-th iteration. The **A**-type matrix inversion is then deduced as follows: $\mathbf{A}^{(-1)} = \mathbf{I}_{M_l}$.

The previous matrix inversion procedure as well as the proposed matrix product, based on the vector representation, lead to an overall CRB computational cost saving of order $\mathcal{O}(K^2)$ (i.e. we reduce the cost from $\mathcal{O}(K^3 N_r^3)$ to $\mathcal{O}(K N_r^3)$).

1.7 Semi-blind channel estimation performance bounds analysis

The objectives of this section is to discuss the semi-blind channel estimation performance bounds through the derived CRB and to show the impact of the pilot reduction on the channel estimation quality. Block-type, comb-type and lattice-type pilot arrangements are considered for (4×4) and large MIMO-OFDM wireless systems. Note that all the CRB plots given in the sequel correspond to the analytical expressions derived in this chapter.

1.7.1 (4×4) MIMO-OFDM system

This section deals with IEEE 802.11n wireless communications systems (i.e. MIMO-OFDM systems) [22]. The training sequences correspond to those specified by the standard as shown

Parameters	Specifications
Channel model	IEEE 802.11n
Channel length	$N = 4$
Number of LTF pilot OFDM symbols	$N_p^{LTF} = 2$
Number of HT-LTF pilot OFDM symbols	$N_p^{HT-LTF} = 4$
Number of data OFDM symbols	$N_d = 40$
Pilot signal power	$\sigma_p^2 = 23$ dBm
Data signal power	$\boldsymbol{\sigma}_{\mathbf{x}}^2 = [20\ 21\ 18\ 19]$ dBm
Number of sub-carriers	$K = 64$
Signal to Noise Ratio	SNR_p = [-5:20] dB
Non-circularity rate	$\rho_c = 0.9$
Non-circularity phases	$\boldsymbol{\phi} = \left[\frac{\pi}{4}\ \frac{\pi}{2}\ \frac{\pi}{6}\ \frac{\pi}{3}\right]$

Table 1.1: *MIMO-OFDM simulation parameters.*

in Figure 1.5. In the legacy preamble (i.e. 802.11a), two identical fields named Long Training Field (LTF) are dedicated to channel estimation. Each field (or pilot) is represented by one OFDM symbol ($K = 64$ samples) where a CP ($L = 16$ samples) is added at its front. In the High Throughput preamble, a set of identical fields named High Throughput Long Training fields (HT-LTF) are specified and each field is represented by one OFDM symbol ($K = 64$ samples) with a CP (16 samples). These fields (or pilots) are dedicated to MIMO channel estimation. Their number depends on the number of transmit antennas (N_t). Therefore the training sequence length is equal to $N_p = N_p^{LTF} + N_p^{HT-LTF}$. The data field is represented by a set of OFDM symbols depending on the length of the transmitted packet.

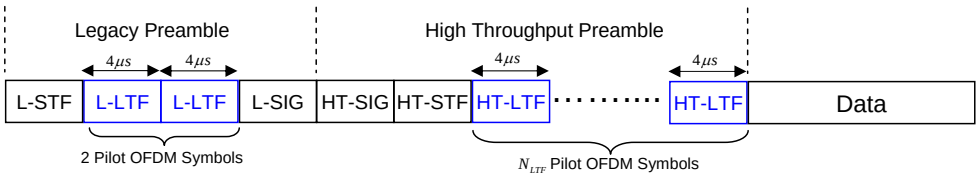

Figure 1.5: *Physical frame HT-mixed format in the IEEE 802.11n standard for 20 MHz bandwith.*

Simulation parameters are summarized in Table 1.1, where the used IEEE 802.11n channel model is of type B with path delay [0 10 20 30] μs and an average path gains of [0 -4 -8 -12] dB. The Signal to Noise Ratio associated with pilots at the reception is defined as $SNR_p = \frac{\|\boldsymbol{\lambda}\mathbf{x}_p\|^2}{N_r K \sigma_{\mathbf{v}}^2}$. The

signal to noise ratio SNR_d associated with data is given in a similar way by $SNR_d = \frac{E\left[\|\boldsymbol{\lambda}\mathbf{x}_d\|^2\right]}{N_r K \sigma_{\mathbf{v}}^2}$.

1.7.1.1 Block-type pilot arrangement

Figure 1.7 compares the normalized CRB $\left(\frac{tr\{CRB\}}{\|\mathbf{h}\|^2}\right)$ versus SNR_p. The CRB curves confirm that the CRBs of semi-blind channel estimation are lower than the CRB when only pilots are exploited (CRB_{OP}). Note that, CRB_{SB}^{NCG} gives better results than the CRB_{SB}^{CG} while the $BPSK$ and $QPSK$ cases provide the best CRB results.

Semi-blind channel estimation approach is traditionally used to improve the channel identification accuracy. However this chapter shows that semi-blind approach can be exploited to increase the throughput in MIMO-OFDM wireless system while maintaining the same achieved channel estimation quality when using only pilots samples. For this, to reach the CRB_{OP}, the proposed strategy consists of decreasing the number of pilot samples and increasing accordingly the number of data samples for the semi-blind case, until we reach the same estimation performance (i.e. at the crossing point of the two CRB plots). This strategy, when preserving the orthogonality of the pilot matrix, may lead to a hybrid OFDM symbol containing both pilot samples and data samples as shown in Figure 1.6. Note that this new pilot arrangement yields to N_d block-type data and N_p comb-type pilot arrangement. The total FIM is then the sum of the two FIMs as derived in sections 1.4 and 1.5.

Figure 1.8 shows the influence of increasing the number of data OFDM symbols (N_d) on the CRB_{SB} for a given $SNR_p = 10$ dB around the IEEE 802.11n operating mode. Obviously, the larger the data size is, the higher gain is obtained in favor of the semi-blind method under the assumption of quasi-static channel. For fast varying channels, we need to consider moderate or short packet sizes (N_d), however, we observe that the obtained performance gain remains significant even for that case, i.e. for $N_d < 40$.

Figure 1.9 illustrates the CRB of semi-blind channel estimation versus the number of samples removed from the pilot OFDM symbol for $SNR_p = 10$ dB. The proposed strategy replaces these removed samples by data samples leading therefore to a comb-type OFDM symbol (see Figure 1.6). The horizontal line provides the CRB for pilot-based channel estimation and is considered as the reference to be reached. For CRB_{SB}^{CG}, 840 samples are removed from pilot OFDM symbols i.e. 55%, and for CRB_{SB}^{NCG} 1280 (83%) samples[9] are removed from pilot OFDM symbols. For CRB_{SB}^{BPSK} and CRB_{SB}^{QPSK} more samples are removed. Indeed only 5% are

[9] In this example, we have 4 transmitters each having 6 pilot symbols of size 64 so that the total number of pilot samples is $6 \times 4 \times 64 = 1536$. Hence, removing 1280 pilot samples corresponds to an approximate reduction percentage of 83%.

retained. These results show clearly that semi-blind estimation in MIMO-OFDM wireless system brings a significant gain in terms of throughput.

Figure 1.10 shows the impact of the number of data OFDM symbols on the number of the deleted pilot samples for $SNR_p = 10$ dB. When the number of data OFDM symbols increases, the number of samples of the pilot OFDM symbol to remove increases too. Note that the results observed in Figure 1.9 can be deduced from Figure 1.10 for $N_d = 40$.

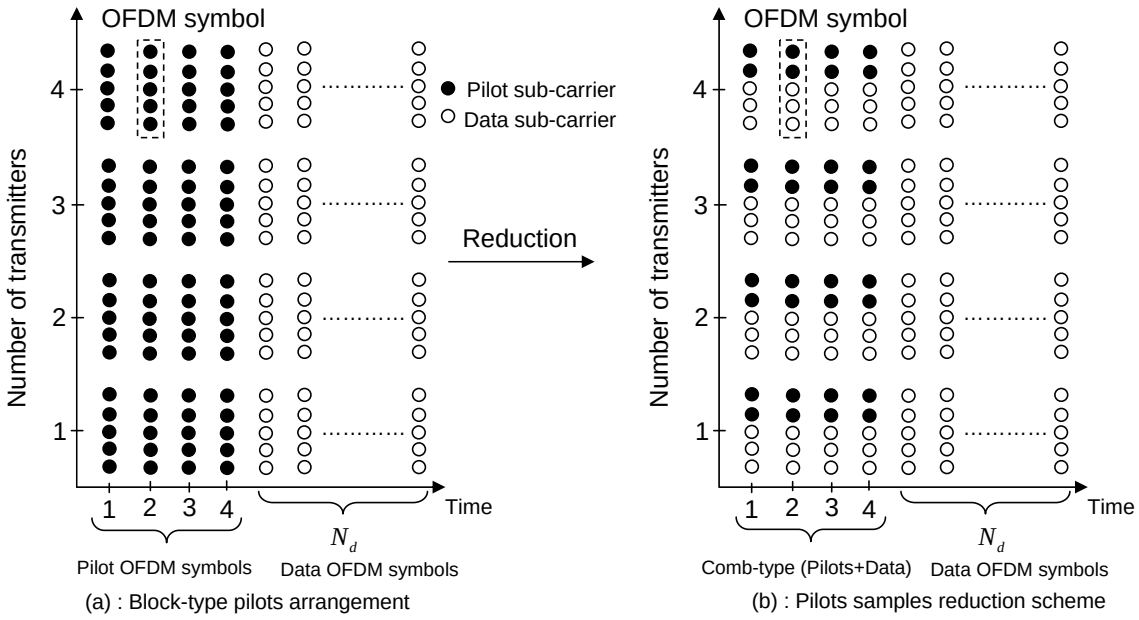

Figure 1.6: *Pilot samples reduction scheme for block-type pilot arrangement.*

1.7.1.2 Comb-type and lattice pilot arrangement

This section analyzes the limit bounds of the channel estimation performance when comb-type pilots arrangement is used. The number of pilot samples per OFDM symbol is $K_p = 8$, $K_d = 56$ for data, $N_s = 40$, while the other simulation parameters (i.e. N, $\boldsymbol{\sigma}_{\mathbf{x}}^2$, σ_p^2, SNR_p, $\boldsymbol{\phi}$, ρ, K and the channel model) are given in Table 1.1.

Both comb and lattice arrangements depend on the position of pilot sub-carriers in the OFDM symbol as shown in Figure 1.2b and Figure 1.2c. Figure 1.12, shows the normalized CRB versus SNR_p. Note that the two configurations provide approximately the same results in our context.

Figure 1.13 and Figure 1.14 illustrate the CRB of semi-blind channel estimation versus the number of samples removed from the pilots for $SNR_p = 10$ dB. The difference between the two figures is the way that is adopted to reduce the pilot samples: in serial or parallel way as presented in Figure 1.11. Serial reduction procedure is done in Figure 1.13 where we remove

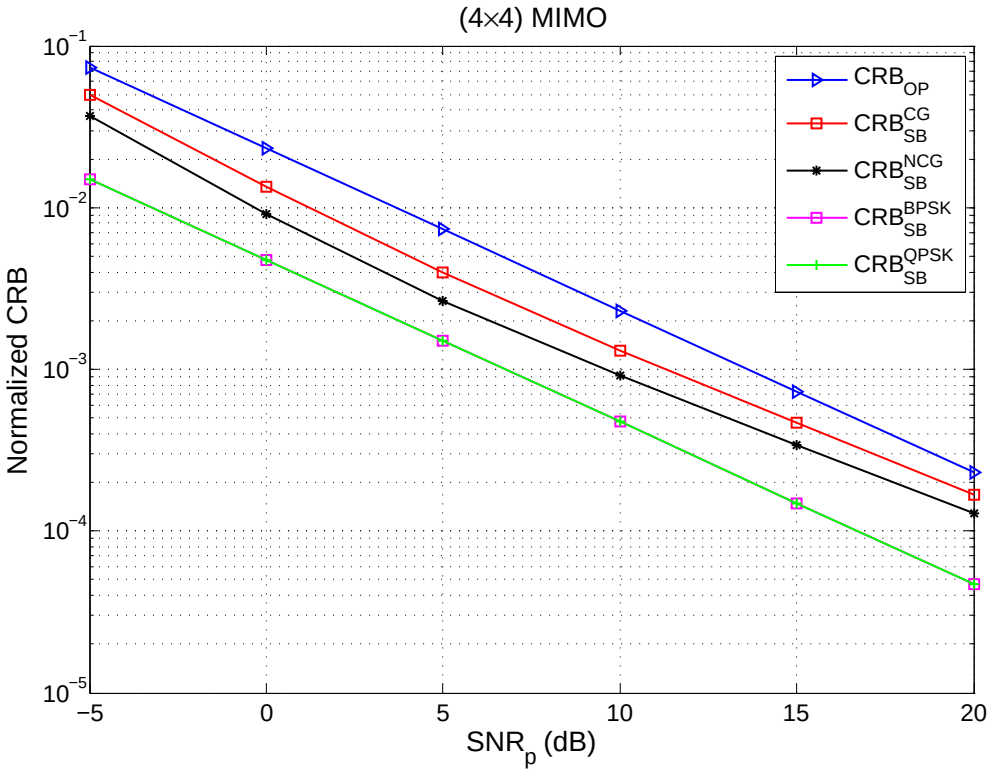

Figure 1.7: *Normalized CRB for the block-type pilot arrangement versus $SNR_p(dB)$*

K_p pilot samples from each OFDM symbol in a serial way. As a result, we obtain a frame that contains both comb and block type pilot arrangements. Figure 1.14 shows the result of parallel reduction, i.e. we reduce the number of pilot's sub-carriers in all OFDM symbols simultaneously (i.e. each time, one removes N_s pilot samples that are replaced by data samples). The advantage of the parallel reduction is that we preserve the frame structure (i.e. Comb-type).

Note that with the 'parallel' approach, 50% of pilot samples are removed against only 40% in a serial way in the case of CG signal model. For the NCG signal model, 81% of pilot samples are removed with the parallel scheme and 70% with serial scheme. When BPSK/QPSK model signals are used, the same amount of pilot samples reduction is reached(90%).

Table 1.2 summarized the obtained reduction rates with the block-type and the comb-type (with parallel and serial schemes), respectively. Note that the reduction rates are relatively close with a slight advantage in favour of the block-type pilot design.

1.7.2 Large MIMO-OFDM system

In this section, the MIMO-OFDM system is composed of 10 transmit antennas and 100 receive antennas involving the manipulation of huge matrices of size 6400×6400 exploiting therefore the

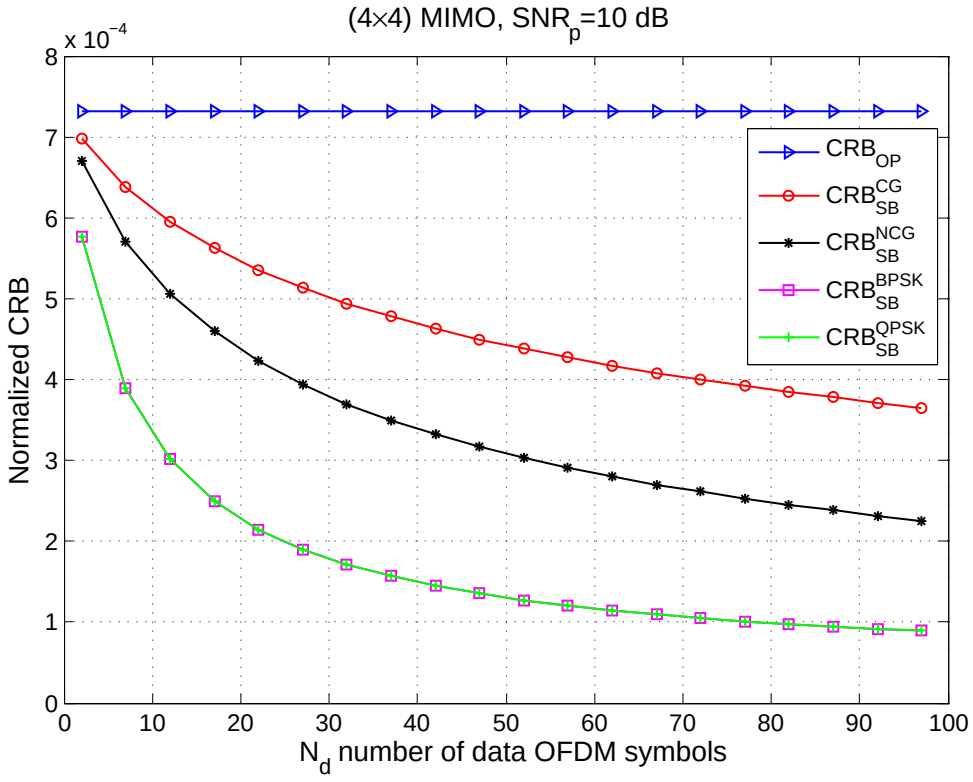

Figure 1.8: *Normalized CRB for the block-type pilot arrangement versus N_d*

	CG	NCG	BPSK/QPSK
block-type	55%	83%	95%
Comb-type (in parallel)	50%	81%	90%
Comb-type (in serial)	40%	70%	90%

Table 1.2: *Block-type and Comb-type comparisons.*

fast computational algorithms developed in section 1.6. To the best of our knowledge, until now no standard has been dedicated to such MIMO-OFDM system. So, Zadoff-Chu (ZC) sequences, used in the LTE standard [4], are adopted in this chapter as pilot training sequences. ZC sequence is defined by the following equation:

$$x_u(k) = e^{-\frac{j\pi uk^2}{K}}, \tag{1.78}$$

when the sequence length, denoted K, is even and $u \in \{1,3,5\cdots K-1\}$ being the sequence index [42]. For the channel model, the specular model proposed in [43] is used, where we assume a uniform linear array antenna with antenna spacing equals to half wavelength. We consider channels having $N = 4$ i.i.d. paths with: an average path gains of [0 -2 -6 -10] dB, Directions Of Arrivals of $[\frac{\pi}{5}\ \frac{\pi}{10}\ \frac{\pi}{7}\ \frac{\pi}{3}]$ and Directions Of Departures of $[\frac{\pi}{4}\ \frac{\pi}{6}\ \frac{\pi}{10}\ \frac{\pi}{3}]$.

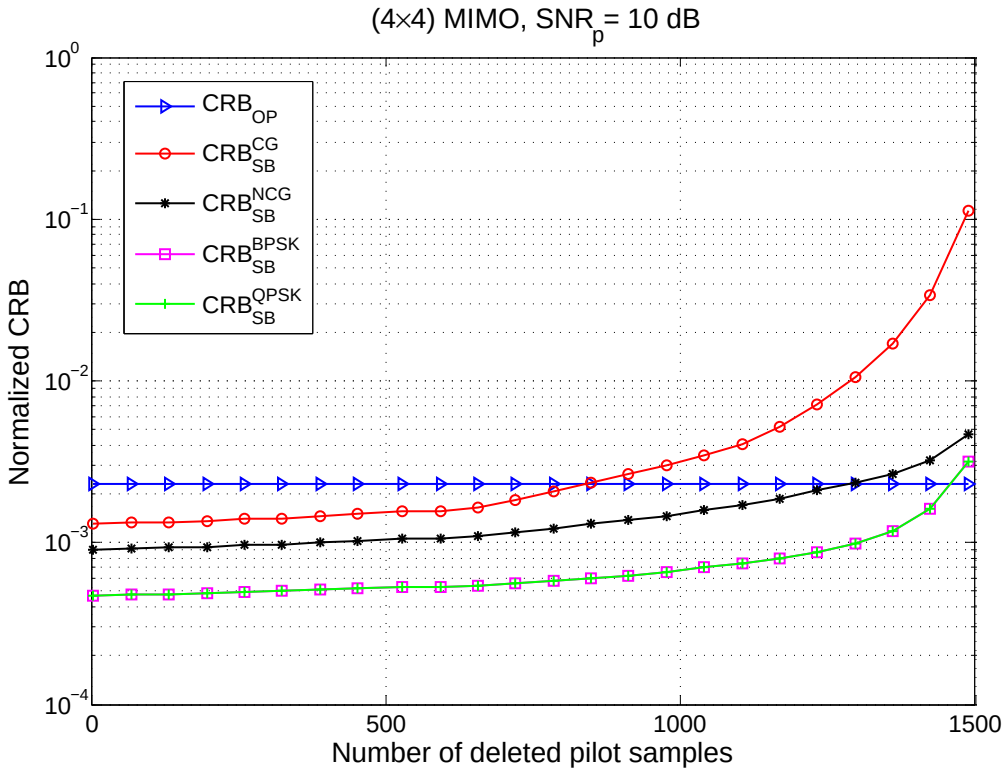

Figure 1.9: *Normalized CRB versus the number of deleted pilot samples for the block-type pilot arrangement*

Figure 1.15 compares the normalized CRB versus SNR_p. The CRB curves show clearly that the CRB_{SB} of semi-blind channel estimation are lower than the CRB of the only pilots case (CRB_{OP}).

Figure 1.16 illustrates the CRB of semi-blind channel estimation versus the number of samples removed from the pilot OFDM symbols using a block-type pilot arrangement and for $SNR_p = 10$ dB. The horizontal line provides the CRB for full pilot-based channel estimation and is considered as the reference to be reached. For CRB_{SB}^{CG}, 54% samples are removed from the pilot OFDM symbol, and for CRB_{SB}^{NCG} 87% samples are removed from the pilot OFDM symbol. These results show clearly that semi-blind channel estimation in large MIMO-OFDM wireless system brings a significant gain in terms of throughput.

1.8 Discussions and concluding remarks

This chapter has focused on the theoretical performance limit of the semi-blind channel estimation in MIMO-OFDM and large MIMO-OFDM systems. Analytical derivations of the channel estimation CRBs have been provided for different data models and for different pilot design patterns (i.e. block-type, lattice-type and comb-type pilot arrangement). In particular, the

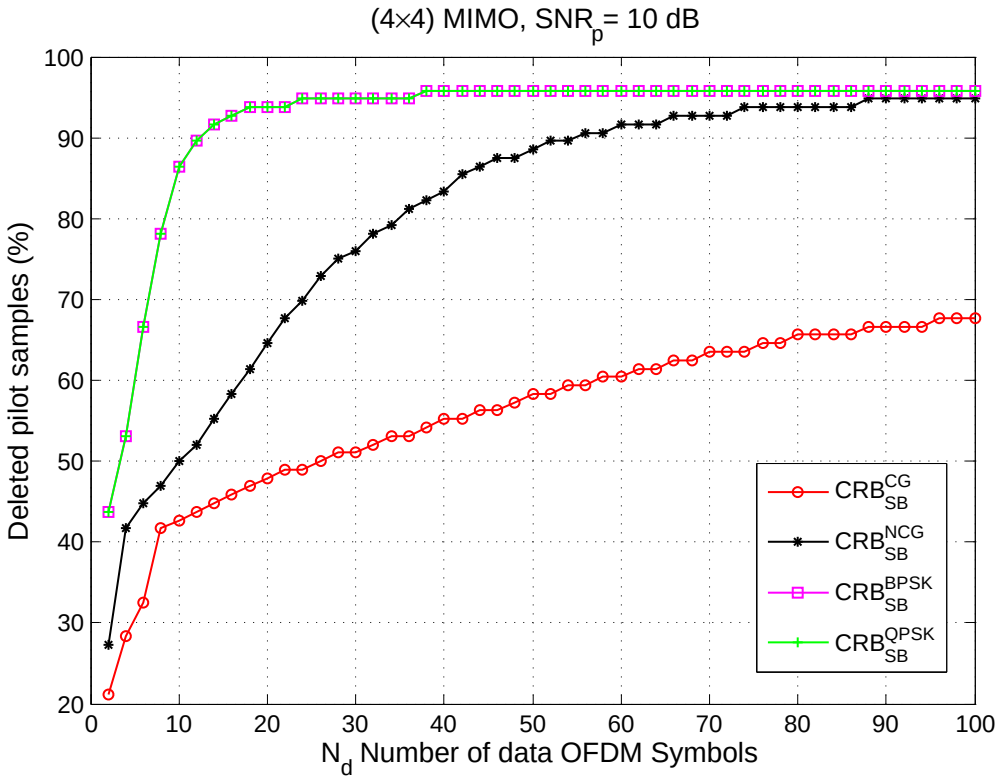

Figure 1.10: *Number of deleted pilot samples versus N_d for the block-type pilot arrangement.*

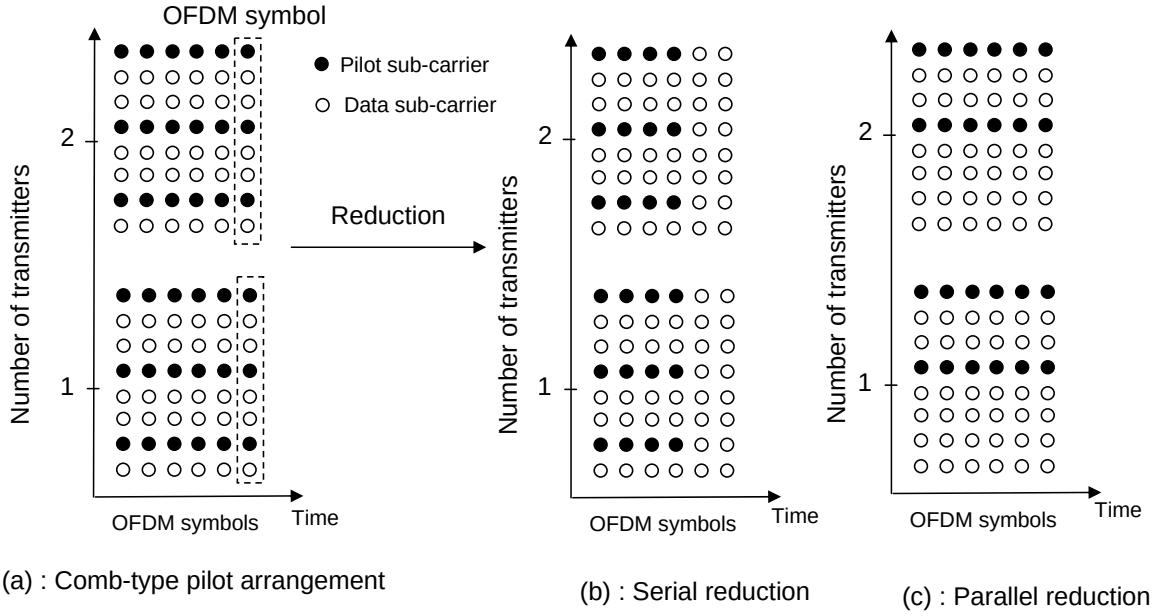

Figure 1.11: *Pilot samples reduction scheme for comb-type and lattice-type pilot arrangements.*

previous analytical study includes new CRB derivations for the Non-Circular Gaussian and the BPSK/QPSK data model cases. For the latter, a realistic CRB approximation has been given to bypass the high complexity of the exact BPSK/QPSK CRB computation. Another

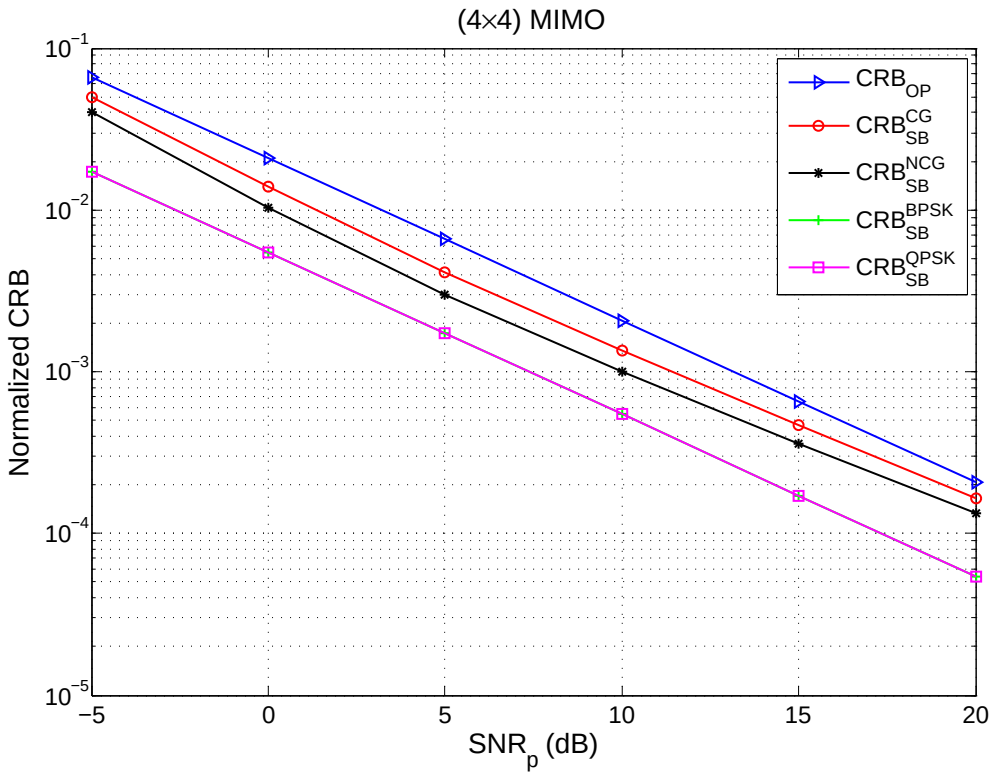

Figure 1.12: *Normalized CRB versus SNR_p for the comb-type pilot arrangement*

contribution of this chapter consists of an effective computational technique to deal with the huge-size matrix manipulation needed for the CRB calculation in the large size MIMO scenario. Finally, based on the previous CRB derivation, through investigations of the pilot reduction potential of the semi-blind channel method has been conducted in the contexts of IEEE 802.11n MIMO-OFDM and large MIMO-OFDM, respectively. The main outcomes of this work consist of the key observations made out of the previous investigation which can be summarized as follows:

- The most important observation is the huge pilot samples reduction (in the considered examples, one can reach more than 95% reduction of the pilot size) and consequently the throughput gain obtained thanks to the semi-blind channel estimation while maintaining the same pilot-based channel estimation quality. Note that, this pilot size reduction is an important research topic that has been considered by several authors including [44] where a semi-orthogonal pilot design is introduced allowing for a savings of the overhead size of approximately 50% of the overhead size. Herein, we show that, thanks to the semi-blind approach, the attainable reduction is much higher as it can exceed 95% of the original size.

- For the BPSK/QPSK case, we have observed that the pilot reduction is maximal in that the left pilot samples are necessary to remove the inherent ambiguity of the blind identification

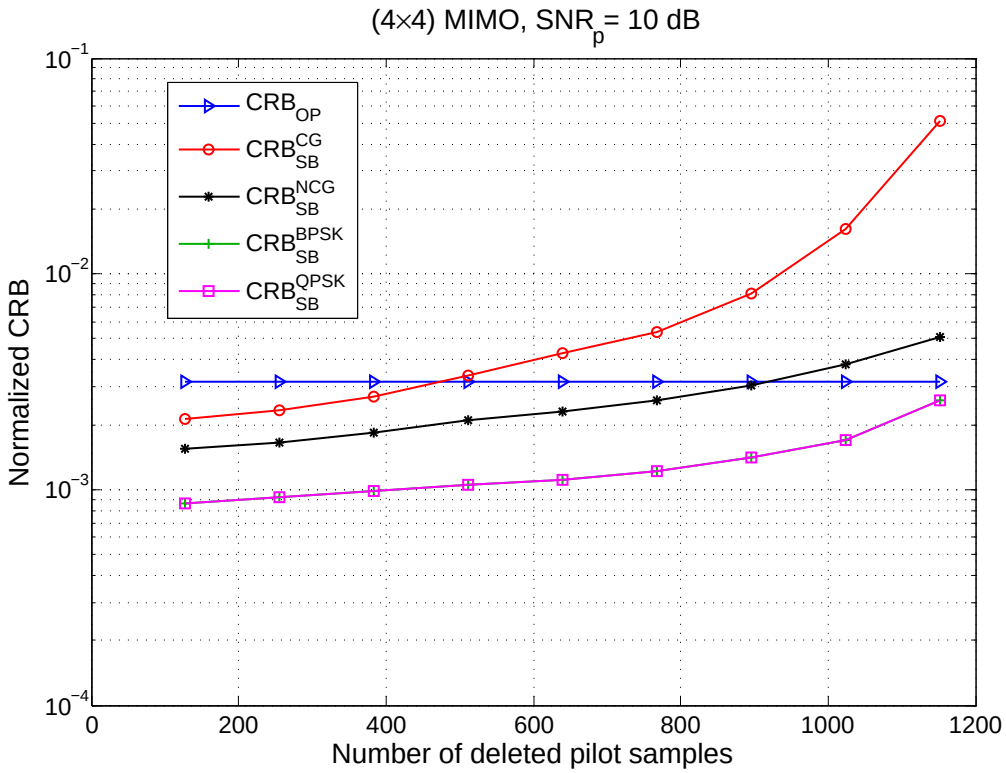

Figure 1.13: *Normalized CRB versus the number of deleted pilot samples for the comb-type pilot arrangement (serial reduction)*

techniques. One can even suggest completely removing the pilot for channel estimation and use the synchronization sequence to get rid of the blind identification indeterminacies.

- For large dimensional systems, the design of a large number of semi-orthogonal sequences is a challenging problem [44]. As we have shown that only small size pilot sequences are needed for the semi-blind channel estimation, the design of such semi-orthogonal pilots becomes much easier.

- The non-circularity property is shown to provide an additional gain of about 30% in terms of pilot size reduction as compared to the circular case. In addition when considering the finite alphabet nature of the transmit signal (BPSK/QPSK), one can almost double the reduction rate obtained for the Gaussian circular signals.

- For quasi-static channels, we observed that the block-type pilot design is slightly preferable to the comb-type one. Also, in our investigation we considered two types of comb structures (Figure 1.2b and Figure 1.2c) but both lead to approximately the same performance limit.

- The performance gains observed in the context of large MIMO-OFDM are slightly higher

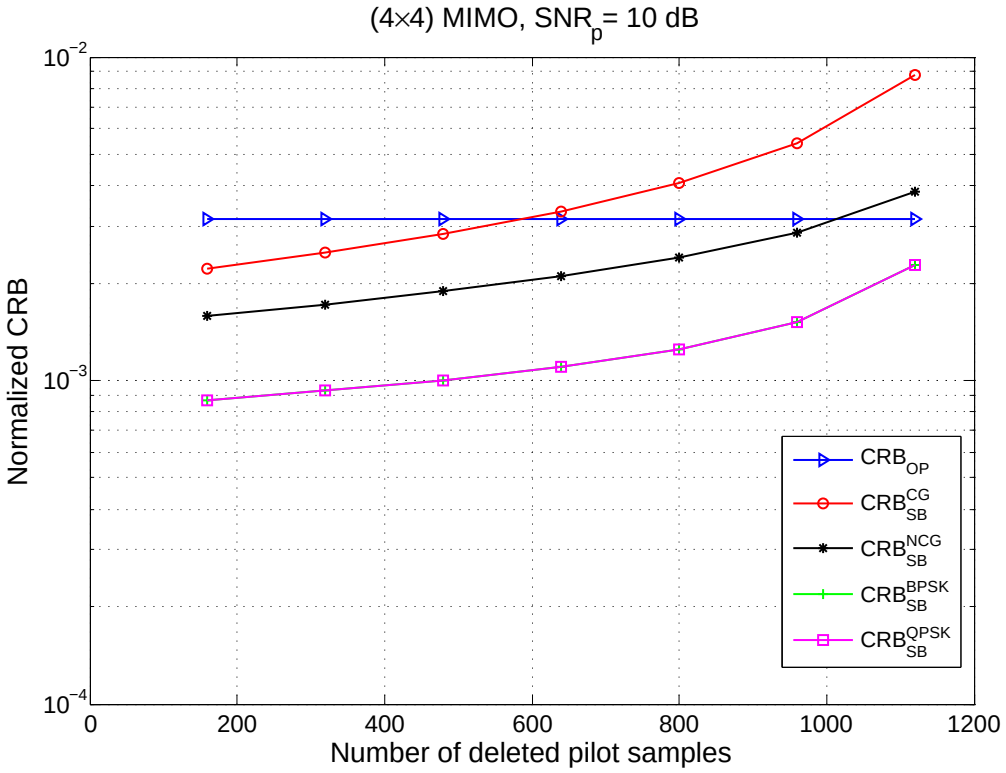

Figure 1.14: *Normalized CRB versus the number of deleted pilot samples for the comb-type pilot arrangement (parallel reduction)*

than those observed for IEEE 802.11n MIMO-OFDM systems. In fact, the additional gain is due to the large number of receive antennas as compared to the number of transmit antennas (100 receive antennas and 10 transmit antennas in the considered example) which represents a typical configuration in large MIMO systems [14].

- In this chapter, we have chosen to exploit the semi-blind strategy to gain in terms of data throughput while preserving the channel estimation quality, however other ways exist to take advantage of the SB scheme. For instance, one can use the SB methods to improve the channel estimation and consequently the symbol detection quality as shown in [26, 27]. Or otherwise, one can use the pilot size shortening to achieve a non negligible transmit power reduction as shown in [33], an objective aligned with the current trends for a green communications systems.

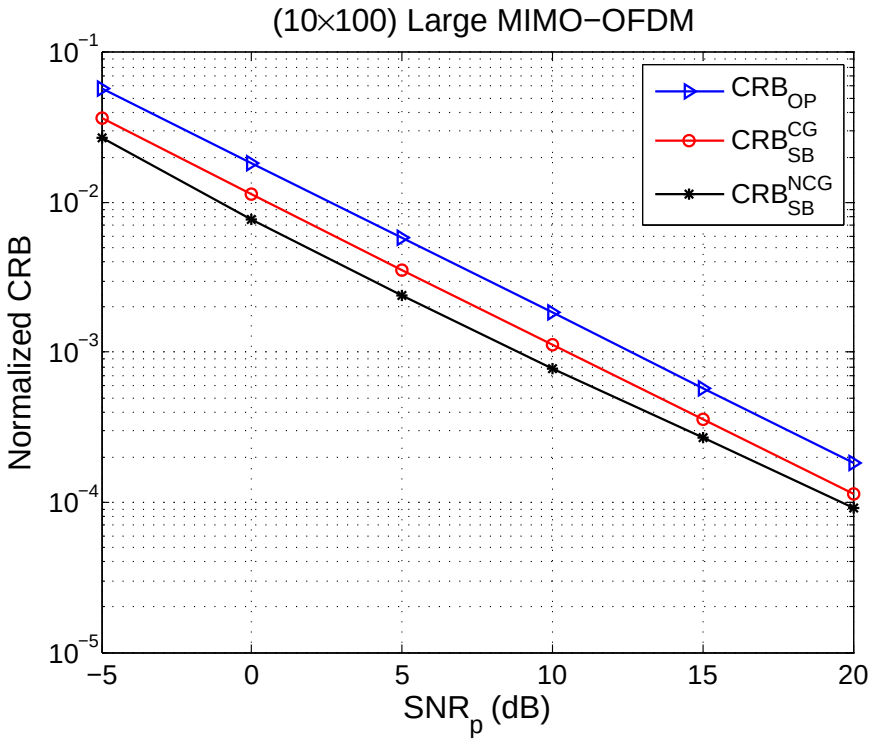

Figure 1.15: *Normalized CRB in* 10×100 *large MIMO-OFDM system versus* SNR_p *(dB)*

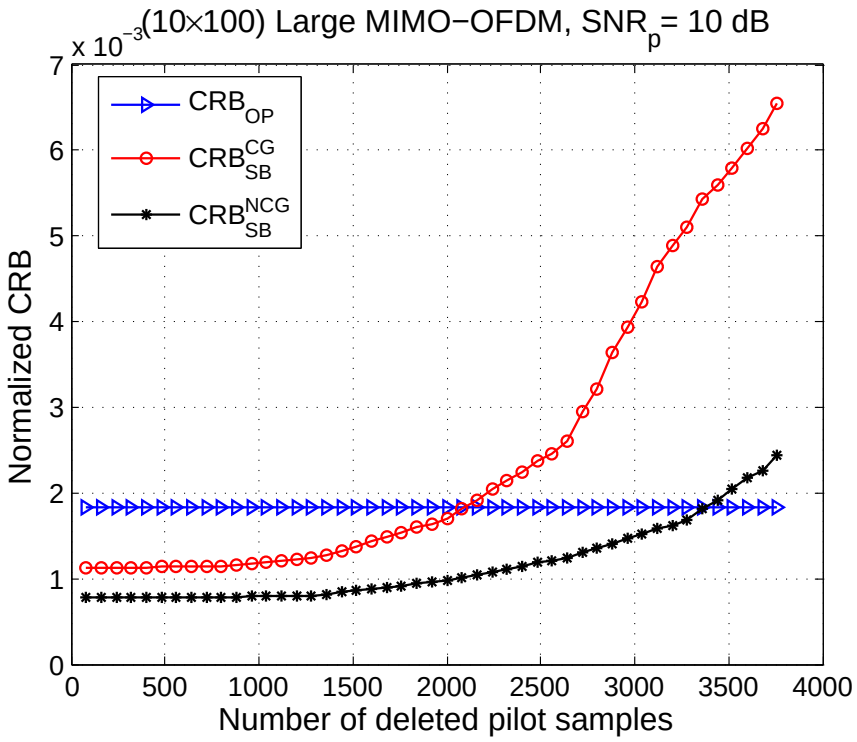

Figure 1.16: *Normalized CRB in* 10×100 *large MIMO-OFDM system versus the number of deleted pilot samples*

CHAPTER 2

Massive MIMO-OFDM semi-blind channel estimation performance analysis

In order to succeed,
we must first believe that we can.

Nikos Kazantzakis.

This work has been done in collaboration with Ouahbi REKIK. It has been published in EUSIPCO 2018 conference[1].

Abstract

Channel estimation is a critical process in a massive MIMO-OFDM system. However, pilot contamination, an undeniable challenging issue, severely affects the performance of the system and hence the aim of this chapter is to investigate the effectiveness of semi-blind channel estimation approaches, using the Cramér Rao Bound (CRB) tool. This analysis demonstrates in particular that when considering the finite alphabet signals, it is possible to efficiently solve the pilot contamination problem with semi-blind channel estimation approach.

[1] [45] O. Rekik, A. Ladaycia, K. Abed-Meraim, and A. Mokraoui, "Performance Bounds Analysis for Semi-Blind Channel Estimation with Pilot Contamination in Massive MIMO-OFDM Systems," in 2018 26th EUSIPCO, Sep. 2018, Rome, Italy.

Chapter content

2.1 Introduction

Massive Multiple-Input Multiple-Output (MIMO) is a promising technology for the next generation cellular networks [17]. With a higher number of Base Station (BS) antennas (beyond 100 antennas), compared to the classical MIMO systems, massive MIMO technology has proven its ability to improve the spectral and power efficiency [18]. So that, both throughput and system capacity will be highly enhanced in order to satisfy the increasing amount of data exchange and demand for quality of service for the future cellular networks [46].

In order to fully exploit all of the potentials offered by a massive MIMO system, accurate Channel State Information (CSI) is necessary. It is obtained only during the uplink transmission, thanks to the channel reciprocity property and according to the widely accepted Time Division Duplexing (TDD) protocol [30], [31]. In that case, all users in all cells send their uplink training sequences synchronously which are used, by the BS, to estimate the uplink channels. The traditional methods used to get the CSI rely on the pilot-based channel estimation (e.g. [17]). However, due to the non-orthogonality of the pilot sequences, these methods are severely affected by what is called *pilot contamination* [47], as depicted in Figure 2.1. It is one of the major issues of massive MIMO systems that must be addressed because its effect cannot be reduced by increasing the number of BS antennas.

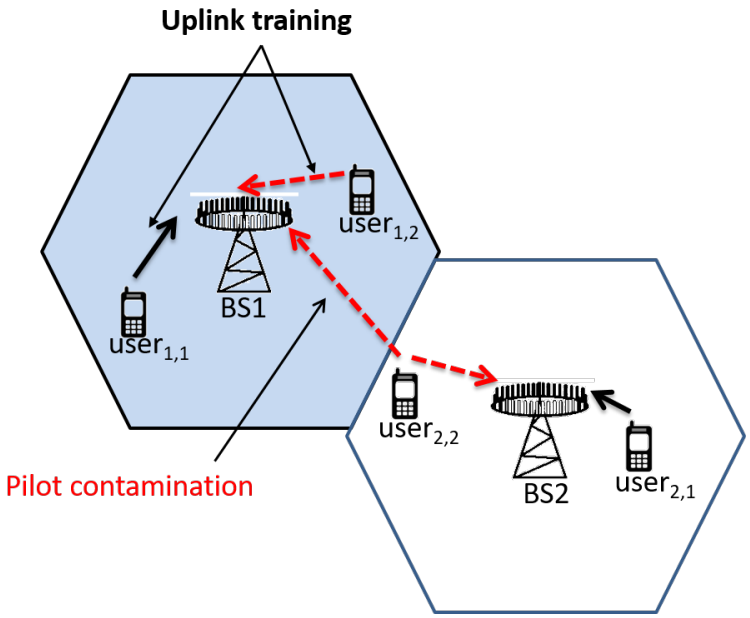

Figure 2.1: *Illustration of pilot contamination in massive MIMO-OFDM systems where* $user_{1,2}$ *and* $user_{2,2}$ *(resp.* $user_{1,1}$ *and* $user_{2,1}$*) share the same training sequence.*

Many pilot contamination mitigation strategies have been proposed. Some of them propose

to create more orthogonal pilots by slicing the time and frequency resources [48], however such a choice will lead to a system capacity decrease. Other approaches are based on suppressing the inter-cell interference by appropriate signal processing techniques, based on statistical information of channel matrices [49], [50]. In such approaches, only a small portion of spatial dimensions is used for data transmission, whereas the unemployed dimensions will be used for suppressing noise and interference. However, many assumptions have to be considered to get statistical information of channel matrices. Instead of depending only on pilot sequences, a data-aided channel estimation has been considered (e.g. [51]). Thus, besides pilots, the decoded data is used for channel estimation. Nonetheless, It is strongly assumed to have the ability to recover most of data for accurate channel estimation. Some approaches have focused on designing appropriate inter-cell communications protocols and resource allocation [52, 53, 54] in order to allow reusing pilots without inter-cell interference. The counterpart is that the information exchange among cells will add more complexity to the cellular networks.

In recent works, a particular attention has been drawn to blind (e.g. [55, 56]), and semi-blind (e.g [57, 58, 59]) methods. The former is fully based on the statistical properties of the transmitted data, whereas the latter depends on the joint use of pilots and data.

The focus of this study falls into the scope of performance analysis of semi-blind channel estimation with pilot contamination in the context of multi-cell massive MIMO-OFDM systems. For an estimator-independent performance analysis, the Cramér Rao Bound (CRB) is derived for both pilot-based and semi-blind channel estimation by taking into account a perfect synchronisation between the BS of the cell of interest and the neighboring cells BSs. This study is an extension of the MIMO-OFDM case, done in chapter 1, to a massive MIMO-OFDM system, by taking into account the multi-cell context and the phenomenon of pilot contamination in the case of synchronized BSs transmissions.

It is worth to note that semi-blind techniques allow to retain the advantages of pilot-based and blind-based approaches; i.e. more channel estimation accuracy and more robustness against pilot contamination, while reducing their drawbacks; i.e. pilot contamination and inherent ambiguity with high computational complexity.

2.2 Massive MIMO-OFDM system model

This section presents the massive MIMO-OFDM wireless system model adopted in this thesis. An uplink transmission is considered. The system is composed of N_c cells each one having one BS with N_r antennas and N_t randomly located users using each a single antenna.

Let us ignore at first the received signals from the adjacent cells. Therefore the received signal, after cyclic prefix removal and FFT, at the r-th BS antenna of the l-th cell, assumed to be a K sub-carriers OFDM signal, is given by (see chapter 1):

$$\mathbf{y}_{l,r} = \sum_{i=1}^{N_t} \mathbf{F}\, \boldsymbol{\mathcal{T}}(\mathbf{h}_{l,i,r}) \frac{\mathbf{F}^H}{K} \mathbf{x}_{l,i} + \mathbf{v}_{l,r}, \tag{2.1}$$

where K is the OFDM symbol length; $\mathbf{F}$ represents a K-point Fourier matrix; $\mathbf{h}_{l,i,r}$ is a $N \times 1$ vector representing the channel taps between the i-th user, of the l-th cell, and the r-th receive antenna; $\boldsymbol{\mathcal{T}}(\mathbf{h}_{l,i,r})$ is a circulant matrix; $\mathbf{x}_{l,i}$ is the i-th user OFDM symbol of cell l. $\mathbf{v}_{l,r}$ is assumed to be an additive white Circulant Gaussian (CG) noise so that $E[\mathbf{v}_{l,r}(k)\mathbf{v}_{l,r}(i)^H] = \sigma^2_{\mathbf{v}_l}\mathbf{I}_K\delta_{ki}$ where $\sigma^2_{\mathbf{v}_l}$ is the noise variance at the l-th cell; δ_{ki} being the Kronecker delta operator.

Using the eigenvalue decomposition of the circulant matrix $\boldsymbol{\mathcal{T}}(\mathbf{h}_{l,i,r})$ given by:

$$\boldsymbol{\mathcal{T}}(\mathbf{h}_{l,i,r}) = \frac{\mathbf{F}^H}{K} \mathbf{diag}\left\{\mathbf{W}\mathbf{h}_{l,i,r}\right\} \mathbf{F}, \tag{2.2}$$

the received signal, of dimension $N_r K \times 1$, at the l-th BS can be re-expressed as follows:

$$\mathbf{y}_l = \boldsymbol{\lambda}_l \mathbf{x}_l + \mathbf{v}_l, \tag{2.3}$$

where $\mathbf{y}_l = [\mathbf{y}^T_{l,1} ... \mathbf{y}^T_{l,N_r}]^T$; $\mathbf{x}_l = [\mathbf{x}^T_{l,1} ... \mathbf{x}^T_{l,N_t}]^T$; $\mathbf{v}_l = [\mathbf{v}^T_{l,1} ... \mathbf{v}^T_{l,N_r}]^T$; $\boldsymbol{\lambda}_l = [\boldsymbol{\lambda}_{l,1} ... \boldsymbol{\lambda}_{l,N_t}]$ with $\boldsymbol{\lambda}_{l,i} = [\boldsymbol{\lambda}_{l,i,1} ... \boldsymbol{\lambda}_{l,i,N_r}]^T$ where $\boldsymbol{\lambda}_{l,i,r} = \mathbf{diag}\{\mathbf{W}\mathbf{h}_{l,i,r}\}$ and $\mathbf{W}$ is formed by the N first columns of $\mathbf{F}$.

In order to facilitate the derivation of the CRB w.r.t. $\mathbf{h}_1$, equation (2.3) is rewritten as follows:

$$\mathbf{y}_l = \tilde{\mathbf{X}}_l \mathbf{h}_l + \mathbf{v}_l, \tag{2.4}$$

where $\mathbf{h}_l = [\mathbf{h}^T_{l,1,1} ... \mathbf{h}^T_{l,N_t,1} ..... \mathbf{h}^T_{l,1,N_r} ... \mathbf{h}^T_{l,N_t,N_r}]^T$ is a $N_r N_t N \times 1$ vector; $\tilde{\mathbf{X}}_l = \mathbf{I}_{N_r} \otimes \mathbf{X}_l$ is a $N_r K \times N_r N_t N$ dimensional matrix with $\mathbf{X}_l = [\mathbf{X}_{l,D_1}\mathbf{W} ... \mathbf{X}_{l,D_{N_t}}\mathbf{W}]$ of size $K \times N_t N$, and $\mathbf{X}_{l,D_i}$ is a $K \times K$ diagonal matrix containing the i-th user symbols, i.e. $\mathbf{X}_{l,D_i} = \mathbf{diag}(\mathbf{x}_{l,i})$, and $\otimes$ refers to the Kronecker product.

Now, let us take into account the effect of the neighboring cells on the first one, considered without loss of generality as the interest cell. With the assumption of perfect synchronization between the N_c cells, equation (2.3) becomes:

$$\mathbf{y}_1 = \sum_{l=1}^{N_c} \boldsymbol{\lambda}_l \mathbf{x}_l + \mathbf{v}_1 = \boldsymbol{\lambda}_{tot} \mathbf{x}_{tot} + \mathbf{v}_1, \tag{2.5}$$

where $\boldsymbol{\lambda}_{tot} = [\boldsymbol{\lambda}_1 \dots \boldsymbol{\lambda}_{N_c}]$ and $\mathbf{x}_{tot} = [\mathbf{x}^T_1 \dots \mathbf{x}^T_{Nc}]^T$.

Similarly to (2.4), equation (2.5) can be rewritten as follows:

$$\mathbf{y}_1 = \sum_{l=1}^{N_c} \tilde{\mathbf{X}}_l \mathbf{h}_l + \mathbf{v}_1 = \tilde{\mathbf{X}}_{tot} \mathbf{h}_{tot} + \mathbf{v}_1, \tag{2.6}$$

where $\tilde{\mathbf{X}}_{tot} = [\tilde{\mathbf{X}}_1 \dots \tilde{\mathbf{X}}_{N_c}]$ and $\mathbf{h}_{tot} = [\mathbf{h}_1^T \dots \mathbf{h}_{N_c}^T]^T$.

2.3 Pilot contamination effect

Herein, the effect of pilot contamination on the performance of semi-blind channel estimation approaches is investigated, under the assumption of perfectly synchronized BSs in the different N_c cells in a massive MIMO-OFDM system. In such a case, and with same pilots in all cells, the worst case of pilot contamination occurs as explained next.

During the uplink data transmission, the BS has to learn the transmission channel by exploiting the known symbols (i.e. pilots) at the uplink. To adopt this strategy the pilots used within the same cell and in the neighboring cells should be mutually orthogonal. However this necessitates a complex cell synchronization and cooperation scheme. In addition, the channel time coherence [60], [61] limits the total number of orthogonal pilots leading to the reuse of the same pilots in many neighboring cells. The worst case occurs when the same set of pilots is reused in all N_c adjacent cells. In this situation, equation (2.6) becomes:

$$\mathbf{y}_1 = \sum_{l=1}^{N_c} \tilde{\mathbf{X}}_{1_P} \mathbf{h}_l + \mathbf{v}_1 = \tilde{\mathbf{X}}_{1_P} \sum_{l=1}^{N_c} \mathbf{h}_l + \mathbf{v}_1, \tag{2.7}$$

where $\tilde{\mathbf{X}}_{1_P}$ corresponds to the pilot symbols of the first cell.

To illustrate the pilot contamination effect in that case, the Least Squares (LS) estimate of the first cell channel vector, i.e. $\mathbf{h}_1$, is given by:

$$\hat{\mathbf{h}}_1^{LS} = \tilde{\mathbf{X}}_{1_P}^{\#} \mathbf{y}_1 = \mathbf{h}_1 + \sum_{l=1, l\neq 1}^{N_c} \mathbf{h}_l + \tilde{\mathbf{X}}_{1_P}^{\#} \mathbf{v}_1, \tag{2.8}$$

with $\tilde{\mathbf{X}}_{1_P}^{\#} = (\tilde{\mathbf{X}}_{1_P}^H \tilde{\mathbf{X}}_{1_P})^{-1} \tilde{\mathbf{X}}_{1_P}^H$ is the pseudo inverse of $\tilde{\mathbf{X}}_{1_P}$.

This equation clearly shows that the channel estimate $\hat{\mathbf{h}}_1^{LS}$ is affected by an additional bias corresponding to the sum of channel components of the users sharing the same pilot sequences in different cells. This phenomenon, referred to as pilot contamination, severely degrades the channel estimation performance. To overcome this problem, an alternative solution consists of using semi-blind channel estimation approach. In the sequel, the potential of this approach is analyzed and discussed through the use of the CRB tool.

2.4 Cramér Rao Bound derivation

Here we derive the CRB for pilot-based and semi-blind channel estimation. For the complex valued channel taps, the parameters vector $\boldsymbol{\theta}$ is defined, in our case, as follows:

$$\boldsymbol{\theta} = [\mathbf{h}_{tot}^T \ (\mathbf{h}_{tot}^*)^T]^T, \tag{2.9}$$

where, for simplicity, the signal and noise powers are assumed to be known.

Under the assumption that pilots and data (corresponding to block-type arrangement) are statistically independent, as in chapter 1 the FIM is given by equation (1.11).

2.4.1 CRB for pilot-based channel estimation

The noise components are assumed to be independent identically distributed (i.i.d.), and only N_p pilots are used for channel estimation. Based on the data model, the pilot-based FIM can be expressed by:

$$\mathbf{J}_{\boldsymbol{\theta\theta}}^{p} = \sum_{i=1}^{N_p} \mathbf{J}_{\boldsymbol{\theta\theta}}^{p_i}, \tag{2.10}$$

with $\mathbf{J}_{\boldsymbol{\theta\theta}}^{p_i}$ is the FIM associated to the p_i-th pilot symbol given by:

$$\mathbf{J}_{\boldsymbol{\theta\theta}}^{p_i} = \begin{pmatrix} \mathbf{J}_{\mathbf{h}_{tot}\mathbf{h}_{tot}}^{p_i} & \mathbf{0} \\ \mathbf{0} & \mathbf{J}_{\mathbf{h}_{tot}^*\mathbf{h}_{tot}^*}^{p_i} \end{pmatrix}, \tag{2.11}$$

where $\mathbf{J}_{\mathbf{h}_{tot}^*\mathbf{h}_{tot}^*}^{p_i} = (\mathbf{J}_{\mathbf{h}_{tot}\mathbf{h}_{tot}}^{p_i})^*$.

By considering a massive MIMO-OFDM system with N_c cells, the pilot-based FIM associated to the channel vector $\mathbf{h}_{tot}$ is then expressed as follows:

$$\mathbf{J}_{\mathbf{h}_{tot}\mathbf{h}_{tot}}^{p_i} = \frac{\tilde{\mathbf{X}}_{tot,p_i}^H \tilde{\mathbf{X}}_{tot,p_i}}{\sigma_{\mathbf{v}_1}^2}, \tag{2.12}$$

which can also be written in a more detailed form:

$$\mathbf{J}_{\mathbf{h}_{tot}\mathbf{h}_{tot}}^{p_i} = \frac{1}{\sigma_{\mathbf{v}_1}^2} \begin{pmatrix} \tilde{\mathbf{X}}_{1_{p_i}}^H \tilde{\mathbf{X}}_{1_{p_i}} & \dots & \tilde{\mathbf{X}}_{1_{p_i}}^H \tilde{\mathbf{X}}_{N_{cp_i}} \\ \vdots & \ddots & \vdots \\ \tilde{\mathbf{X}}_{N_{cp_i}}^H \tilde{\mathbf{X}}_{1_{p_i}} & \dots & \tilde{\mathbf{X}}_{N_{cp_i}}^H \tilde{\mathbf{X}}_{N_{cp_i}} \end{pmatrix}. \tag{2.13}$$

Ideally, if the pilots of the cells are mutually orthogonal, i.e. $\tilde{\mathbf{X}}_{i,p_i}^H \tilde{\mathbf{X}}_{j,p_i} = \mathbf{0} \ \forall \ i \neq j$, then the FIM becomes a bloc diagonal matrix which is the most favorable case. On the other hand, if the cells share the same set of pilots, i.e. the worst case of pilot contamination, the FIM is then

equivalent to:

$$\mathbf{J}^{p_i}_{\mathbf{h}_{tot}\mathbf{h}_{tot}} = \frac{1}{\sigma^2_{\mathbf{v}_1}} \begin{pmatrix} \tilde{\mathbf{X}}^H_{1_{p_i}} \tilde{\mathbf{X}}_{1_{p_i}} & \dots & \tilde{\mathbf{X}}^H_{1_{p_i}} \tilde{\mathbf{X}}_{1_{p_i}} \\ \vdots & \ddots & \\ \tilde{\mathbf{X}}^H_{1_{p_i}} \tilde{\mathbf{X}}_{1_{p_i}} & \dots & \tilde{\mathbf{X}}^H_{1_{p_i}} \tilde{\mathbf{X}}_{1_{p_i}} \end{pmatrix}. \tag{2.14}$$

To compute the CRB, the FIM has to be inverted. However, according to this last equation, $\mathbf{J}^{p_i}_{\boldsymbol{h}_{tot}\boldsymbol{h}_{tot}}$, and consequently $\mathbf{J}_{\boldsymbol{h}_{tot}\boldsymbol{h}_{tot}}$, is not a full rank matrix. In fact, according to proposition 2.1, the kernel of this FIM is of dimension $2(N_c-1)N_tN_rN$, corresponding to the number of indeterminacies we need to get rid of. In other words, this translates the *non-identifiability* of the channel vector of the interest cell when pilot contamination occurs.

Proposition 2.1. *The FIM in (2.14) is a singular matrix and its kernel dimension is* $2(N_c-1)N_tN_rN$ *which corresponds to the number of indeterminacies of the problem (i.e. the number of unknown real channel parameters for the* N_c-1 *neighboring cells).*

Proof: See appendix 2.A.

2.4.2 CRB for semi-blind channel estimation

In this section we derive the CRB for the semi-blind channel estimation for a multi-cell massive MIMO-OFDM system with pilot contamination. Both pilots and data are taken into account in the derivation of the FIM as shown in equation (1.11). At first, we investigate the performance bounds of the semi-blind scheme when only the Second Order Statistics (SOS) are considered. For that, we use a Circular Gaussian data model as developed in chapter 1. Latter on, we extend this analysis to the case where information based on Higher Order Statistics is available. This will be illustrated using a finite alphabet source signal.

2.4.2.1 Gaussian source signal

As mentioned previously, we consider here only the SOS corresponding to the Gaussian CRB. Hence, we assume that the data symbols are i.i.d. Circular Gaussian distributed with zero mean and a diagonal covariance matrix composed of the users' transmit powers i.e. $\mathbf{C}_{\mathbf{x_l}} = \mathbf{diag}(\sigma^2_{x_{l,i}})$ with $l = 1...N_c$ and $i = 1...N_t$. Under this assumption, the received signal $\mathbf{y}_1$ is Circular Gaussian with covariance matrix:

$$\mathbf{C}_{\mathbf{y}_1} = \sum_{l=1}^{N_c} \boldsymbol{\lambda}_l \mathbf{C}_{\mathbf{x}_l} \boldsymbol{\lambda}_l^H + \sigma^2_{\mathbf{v}_1} \mathbf{I}_{KN_r}. \tag{2.15}$$

The data-based FIM can be expressed as follows (e.g.[62], [35]):

$$\mathbf{J}^d_{\mathbf{h}_{tot}\mathbf{h}_{tot}} = \begin{pmatrix} \mathbf{J}^d_{\mathbf{h}_{tot}\mathbf{h}_{tot}} & \mathbf{J}^d_{\mathbf{h}_{tot}\mathbf{h}^*_{tot}} \\ \mathbf{J}^d_{\mathbf{h}^*_{tot}\mathbf{h}_{tot}} & \mathbf{J}^d_{\mathbf{h}^*_{tot}\mathbf{h}^*_{tot}} \end{pmatrix}, \tag{2.16}$$

where $\mathbf{J}^d_{\mathbf{h}_{tot}\mathbf{h}_{tot}}$ is a $(N_cN_rN_tN)$-dimensional matrix with elements $J^d_{h_ih_j}$ given by:

$$J^d_{h_ih_j} = tr\left\{\mathbf{C}^{-1}_{\mathbf{y}_1}\frac{\partial\mathbf{C}_{\mathbf{y}_1}}{\partial h_i^*}\mathbf{C}^{-1}_{\mathbf{y}_1}\left(\frac{\partial\mathbf{C}_{\mathbf{y}_1}}{\partial h_j^*}\right)^H\right\}. \tag{2.17}$$

The i-th component of the vector $\mathbf{h}_{tot}$ corresponds to the channel tap of indices $\{i_{N_c}, i_{N_t}, i_{N_r}, i_N\}$ associated to the cell, the user, the BS antenna and the time lag of h_i. Based on the results provided in chapter 1, $J^d_{h_ih_j}$ is given by:

$$J^d_{h_ih_j} = \left(J^d_{h_i^*h_j^*}\right)^* = tr\left\{\mathbf{C}^{-1}_{\mathbf{y}_1}\sigma^2_{i_{N_c},i_{N_t}}\boldsymbol{\lambda}_{i_{N_c},i_{N_t}}\frac{\partial\boldsymbol{\lambda}^H_{i_{N_c},i_{N_t}}}{\partial h_i^*}\mathbf{C}^{-1}_{\mathbf{y}_1}\sigma^2_{j_{N_c},j_{N_t}}\frac{\partial\boldsymbol{\lambda}_{j_{N_c},j_{N_t}}}{\partial h_j}\boldsymbol{\lambda}^H_{j_{N_c},j_{N_t}}\right\} \tag{2.18}$$

and

$$J^d_{h_ih_j^*} = \left(J^d_{h_i^*h_j}\right)^* = tr\left\{\mathbf{C}^{-1}_{\mathbf{y}_1}\sigma^2_{i_{N_c},i_{N_t}}\boldsymbol{\lambda}_{i_{N_c},i_{N_t}}\frac{\partial\boldsymbol{\lambda}^H_{i_{N_c},i_{N_t}}}{\partial h_i^*}\mathbf{C}^{-1}_{\mathbf{y}_1}\sigma^2_{j_{N_c},j_{N_t}}\boldsymbol{\lambda}_{j_{N_c},j_{N_t}}\frac{\partial\boldsymbol{\lambda}^H_{j_{N_c},j_{N_t}}}{\partial h_j^*}\right\} \tag{2.19}$$

It is important to notice that using a semi-blind estimation method with only the SOS of the received data is not sufficient to alleviate the pilot contamination problem. Indeed, the SOS-SB scheme reduces the number of indeterminacies but does not get rid of all of them. More precisely, we have the following proposition:

Proposition 2.2. *The FIM in (2.17) is a singular matrix and, in the case $N_r > N_cN_t$, its kernel dimension is $(N_cN_t)^2$ correponding to the number of indeterminacies in the blind channel estimation case. When considering the SOS-based semi-blind channel estimation, the kernel dimension of the FIM in (1.11) becomes $((N_c-1)N_t)^2$.*

Proof: See Appendix 2.B.

2.4.2.2 Finite alphabet source signal

Here we consider the non Gaussian nature of communications signals through the use of a finite alphabet (BPSK) data model. The observed signal at the k-th sub-carrier is given by [32]:

$$\mathbf{y}_{1(k)} = \boldsymbol{\lambda}_{tot_{(k)}}\mathbf{C}_{\mathbf{x}}{}^{\frac{1}{2}}\mathbf{x}_{(k)} + \mathbf{v}_{1(k)} \quad \text{for} \quad k = 1, ..., K, \tag{2.20}$$

where $\boldsymbol{\lambda}_{tot_{(k)}}$ is the k-th Fourier component of $\mathbf{h}_{tot}$; $\mathbf{C}_{\mathbf{x}}$ is a block diagonal matrix formed by users' transmit powers of each cell; $\mathbf{x}_{(k)} = [\mathbf{x}^T_{1,(k)}...\mathbf{x}^T_{N_c,(k)}]^T$ with $\mathbf{x}_{l,(k)} = [x_{l,1,(k)}...x_{l,N_t,(k)}]^T$ so that $x_{l,i,(k)}$ for $k = 1...K$ are i.i.d. BPSK symbols taking values ± 1 with equal probabilities.

In this case, the likelihood function is a sum of $2^{N_cN_t}$ Gaussian pdfs given by:

$$p(\mathbf{y}_{1(k)}, \boldsymbol{\theta}) = \frac{1}{2^{N_cN_t}}\sum_{q=1}^{2^{N_cN_t}}\frac{1}{(\pi\sigma^2_{\mathbf{v}_1})^{N_r}}e^{-\left\|\frac{\mathbf{y}_{1(k)}-\boldsymbol{\lambda}_{tot_{(k)}}\mathbf{C}_{\mathbf{x}}{}^{\frac{1}{2}}\mathbf{x}_q}{\sigma^2_{\mathbf{v}_1}}\right\|}, \tag{2.21}$$

where $\mathbf{x}_q$ is the q-th realization of $\mathbf{x}_{(k)}$.

To obtain a tractable FIM expression, a realistic approximation is proposed in [32] leading to the data-based FIM, at the k-th sub-carrier, given by:

$$\mathbf{J}^{d}_{\mathbf{h}_{tot}\mathbf{h}_{tot}}(k) = \frac{1}{\sigma^2_{\mathbf{v}_1} 2^{N_c N_t}} \sum_{q=1}^{2^{N_c N_t}} \left(\frac{\partial \boldsymbol{\lambda}_{tot_{(k)}} \mathbf{C}_{\mathbf{x}}^{\frac{1}{2}} \mathbf{x}_q}{\partial \mathbf{h}^*_{tot}} \right)^H \left(\frac{\partial \boldsymbol{\lambda}_{tot_{(k)}} \mathbf{C}_{\mathbf{x}}^{\frac{1}{2}} \mathbf{x}_q}{\partial \mathbf{h}^*_{tot}} \right). \tag{2.22}$$

The total data-based FIM is then obtained as follows:

$$\mathbf{J}^{d}_{\mathbf{h}_{tot}\mathbf{h}_{tot}} = N_d \sum_{k=1}^{K} \mathbf{J}^{d}_{\mathbf{h}_{tot}\mathbf{h}_{tot}}(k), \tag{2.23}$$

where N_d is the total number of data symbols.

Thanks to the implicit higher order statistics information available in this non-Gaussian case, the semi-blind based channel estimation is able to alleviate completely the pilot contamination problem according to the following proposition:

Proposition 2.3. *The non Gaussian semi-blind FIM as given in (2.17) is non singular meaning that all indeterminacies have been removed.*

Proof: See Appendix 2.C.

In this case, the top-left $(N_r N_t N) \times (N_r N_t N)$ block of the FIM inverse is considered as the CRB for the semi-blind estimation of the first cell channel vector.

2.5 Performance analysis and discussions

In the following section, numerical experiments will be performed to highlight the different results given in the previous sections for a massive MIMO-OFDM system. The pilots are generated according to Zadoff-Chu sequences [4], whereas the simulation parameters are summarized in Table 2.1, unless otherwise mentioned.

***Experiment 1*:** Figure 2.2 illustrates the normalized CRB for the channel parameters vector $\mathbf{h}_1$, given by $\frac{tr\{\text{CRB}\}}{\|\mathbf{h}_1\|^2}$, for semi-blind channel estimation (SB) with respect to the SNR for BPSK model as well as the Gaussian (G) data model using orthogonal pilots. A comparison is made with respect to the pilot-based $\text{CRB}^{\text{O}}_{\text{OP}}$ case using orthogonal (O) intra and inter-cell pilots. Note that $\text{CRB}^{\text{NO}}_{\text{OP}}$ and $\text{CRB}^{\text{G-NO}}_{\text{SB}}$ for the non orthogonal case (when the adjacent cells use the same pilots) are not considered since, as mentioned in sections 2.4.1 and 2.4.2.1, the channel parameters vector of the interest cell cannot be identified in that cases. However, such an ambiguity is removed by semi-blind techniques for finite alphabet source signals as illustrated by the plot of $\text{CRB}^{\text{BPSK-NO}}_{\text{SB}}$, which stands for the semi-blind CRB of a BPSK signal for the worst case of non

Parameters	Specifications
Number of cells	$N_c = 3$
Number of receive antennas	$N_r = 100$
Number of users per cell	$N_t = 2$
Channel taps	$N = 4$
Number of OFDM sub-carriers	$K = 64$
Number of OFDM pilot symbols	$N_p = 4$
Number of OFDM data symbols	$N_d = 40$
N_c pilot signal powers (dBm)	$P_{x_p} = [23\ 18\ 15]$
$(N_t) \times N_c$ data signal powers (dBm)	$P_{x_d} = [(20\ 18.8431), (15.7062\ 13.3648), (11.2\ 9.01)]$

Table 2.1: *Massive MIMO-OFDM simulation parameters.*

orthogonal (NO) pilots (i.e. adjacent cells using the same pilots). As can be seen, $\mathrm{CRB}_{\mathrm{SB}}^{\mathrm{BPSK-NO}}$ is almost superposed with $\mathrm{CRB}_{\mathrm{SB}}^{\mathrm{BPSK-O}}$, which denotes the case of orthogonal pilots.

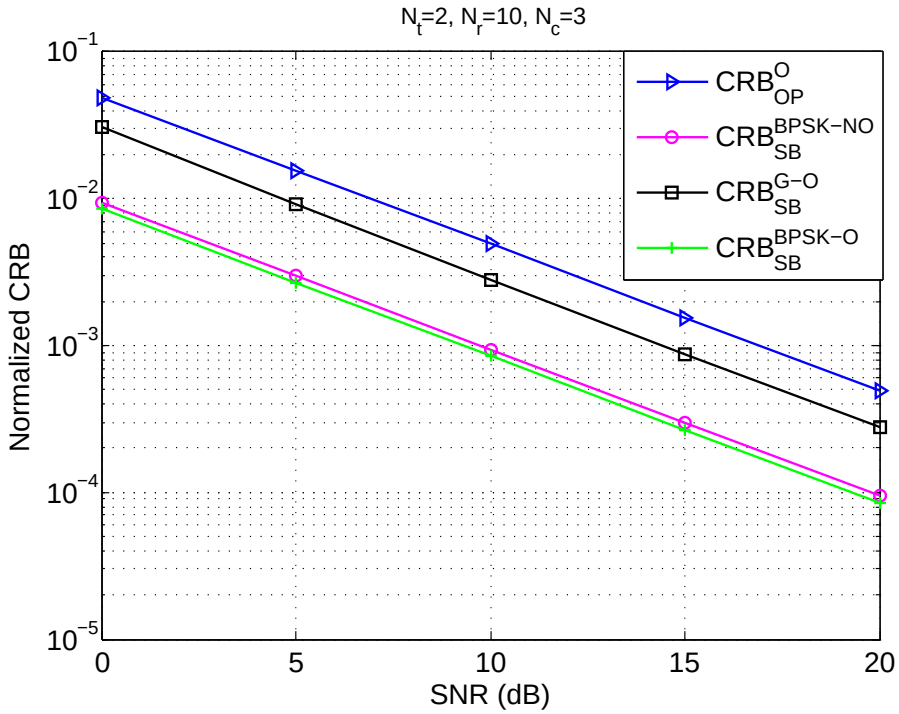

Figure 2.2: *Normalized CRB versus SNR.*

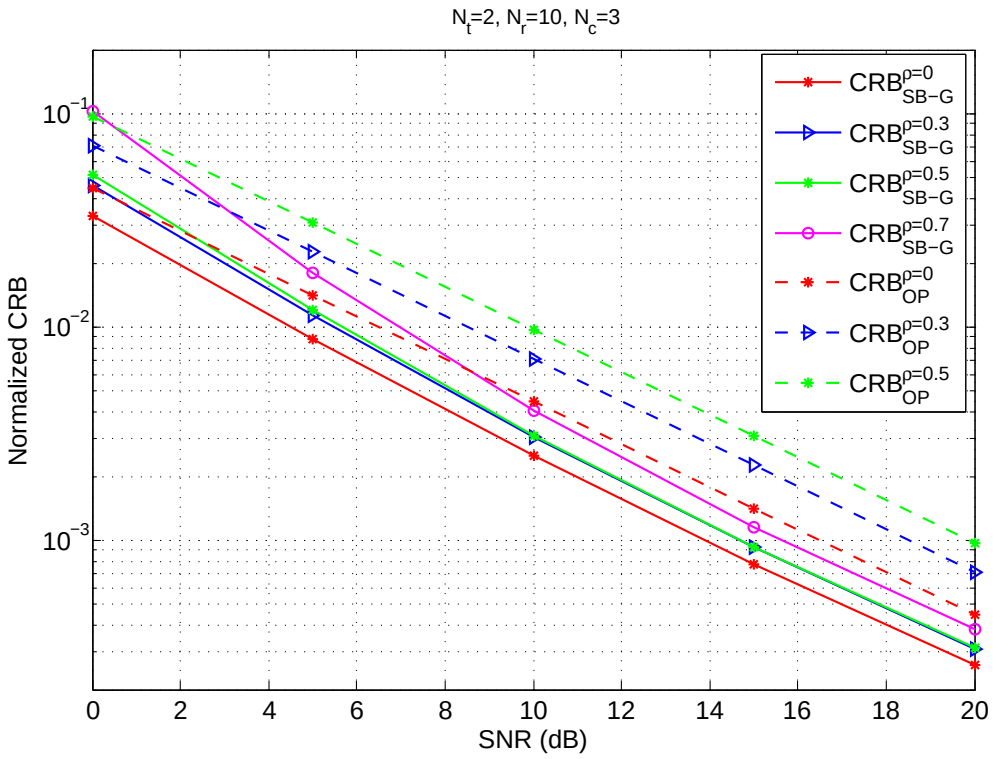

Figure 2.3: *Gaussian CRB versus SNR with different orthogonality levels.*

***Experiment 2*:** We investigate now the impact of pilots orthogonality level through the following metric:

$$\rho = \frac{\left\| \tilde{\mathbf{X}}_{i_P}^H \tilde{\mathbf{X}}_{j_P} \right\|}{\left\| \tilde{\mathbf{X}}_{i_P} \right\| \left\| \tilde{\mathbf{X}}_{j_P} \right\|}, \tag{2.24}$$

where $\|.\|$ is the 2-norm.

Note that $0 \leq \rho \leq 1$, so that $\rho = 0$ corresponds to the perfect orthogonality, whereas $\rho = 1$ stands for the worst case of pilot contamination, i.e. same synchronized pilots.

As can be expected, in the case of non-perfectly orthogonal pilots, the channel vector estimation is slightly degraded but even with a high level of non orthogonality ($\rho = 70\%$ for the SB case and $\rho = 50\%$ for the OP case), the channel estimation for the OP and the Gaussian cases remains possible with relatively good estimation accuracy for moderate and high SNRs as illustrated in Figure 2.3.

***Experiment 3*:** By considering the worst scenario of pilot contamination, the effect of the number of OFDM data symbols, i.e. N_d, on the $\mathrm{CRB}_{\mathrm{SB}}^{\mathrm{BPSK-NO}}$, for a given SNR$= 10dB$, is illustrated in Figure 2.4. It can be observed that, starting by one OFDM data symbol, the BS can successfully identify and estimate the channel components of the interest cell. Moreover,

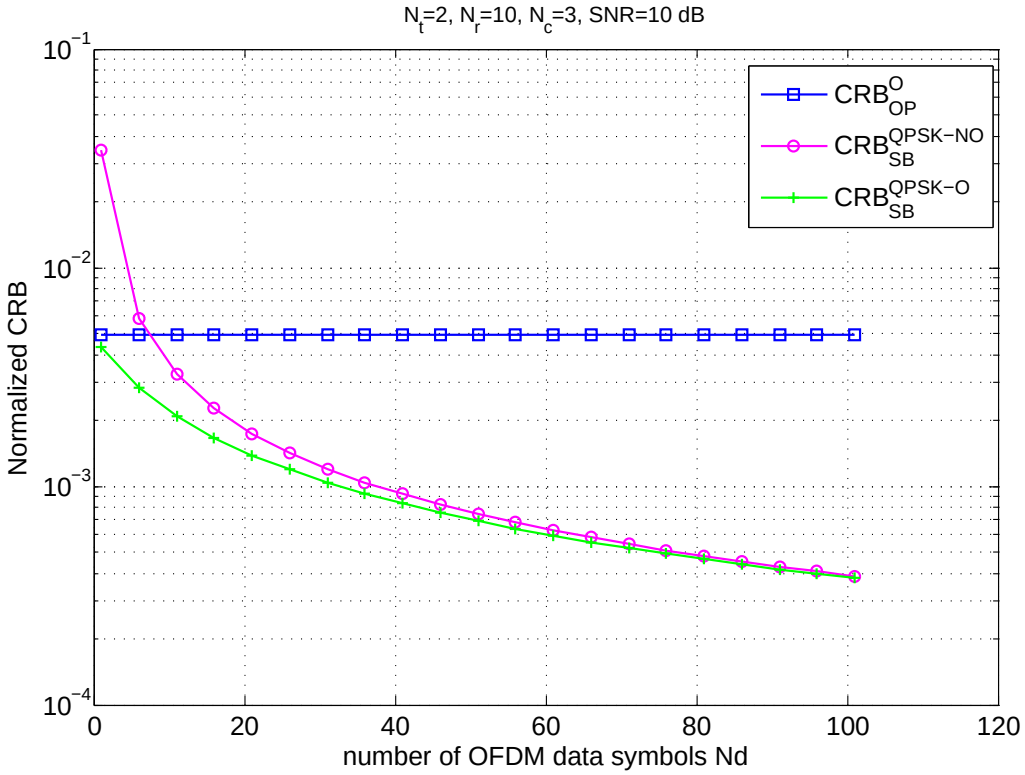

Figure 2.4: *Normalized CRB versus number of OFDM data symbols N_d.*

the CRB is significantly lowered with just few tens of OFDM data symbols and almost reaches the performance of the orthogonal case, i.e. $\mathrm{CRB}_{\mathrm{SB}}^{\mathrm{BPSK-O}}$. Such a result matches perfectly with the limited coherence time constraint of massive MIMO systems and helps to reduce the computational cost. As compared to $\mathrm{CRB}_{\mathrm{OP}}^{\mathrm{O}}$ we can see a significant performance gain in favor of the semi-blind method.

***Experiment 4*:** By considering again the worst case of pilot contamination, the behavior of the CRBs considered in Figure 2.2, with respect to the number of BS antennas, i.e. N_r, is investigated in Figure 2.5. It is easily observed that when N_r increases, which leads also to the increase of the number of channel components to be estimated, the $\mathrm{CRB}_{\mathrm{SB}}^{\mathrm{BPSK}}$ is significantly lowered thanks to the increased receive diversity. Such a result supports the effectiveness of semi-blind techniques for pilot contamination mitigation in the context of massive MIMO-OFDM systems.

***Experiment 5*:** The channel order is often not known with accuracy and needs extra processing for its estimation. Thus, in Figure 2.6 we investigate the behavior of the aforementioned performance when the number of the channel taps is overestimated, i.e. considered equal to its maximum value corresponding to the cyclic prefix size ($N = L$). For illustration purpose, we

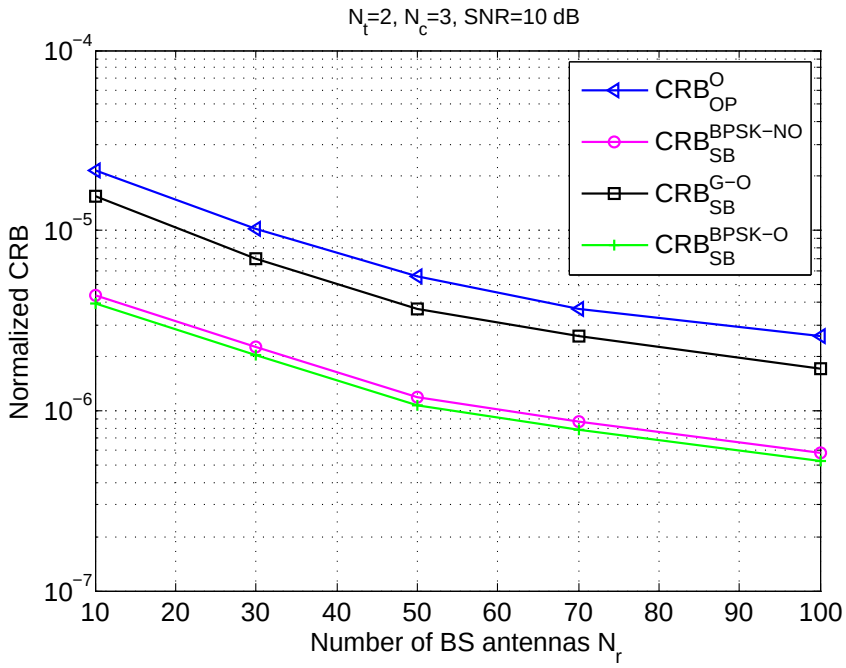

Figure 2.5: *Normalized CRB versus number of BS antennas N_r.*

have considered two cells, each with one user and a BS with $N_r = 10$ antennas. As can be seen from Figure 2.6, the channel order overestimation leads to a performance loss of approximately 6 dB which corresponds to the ratio (in dB) between the overestimated and the exact channel orders.

2.6 Conclusion

The focus of this chapter is on the performance analysis of semi-blind channel estimation approaches, under the effect of pilot contamination. A multi-cell massive MIMO-OFDM system has been considered with perfectly synchronized BSs. An estimator-independent analysis has been conducted on the basis of the CRB. More precisely, analytical CRB expressions have been derived by considering, the worst case of pilot contamination for different data models. For the case of pilot-based channel estimation, pilot contamination introduces a non-identifiability of the channel vector of the interest cell. A $2(N_c-1)N_tN_rN$-dimensional kernel of the FIM corresponds to such an ambiguity.

For the case of semi-blind channel estimation, it is possible to solve efficiently the pilot contamination problem when considering finite alphabet communications signals. However, the issue of channel identifiability is not fully solved when considering only the second order statistics.

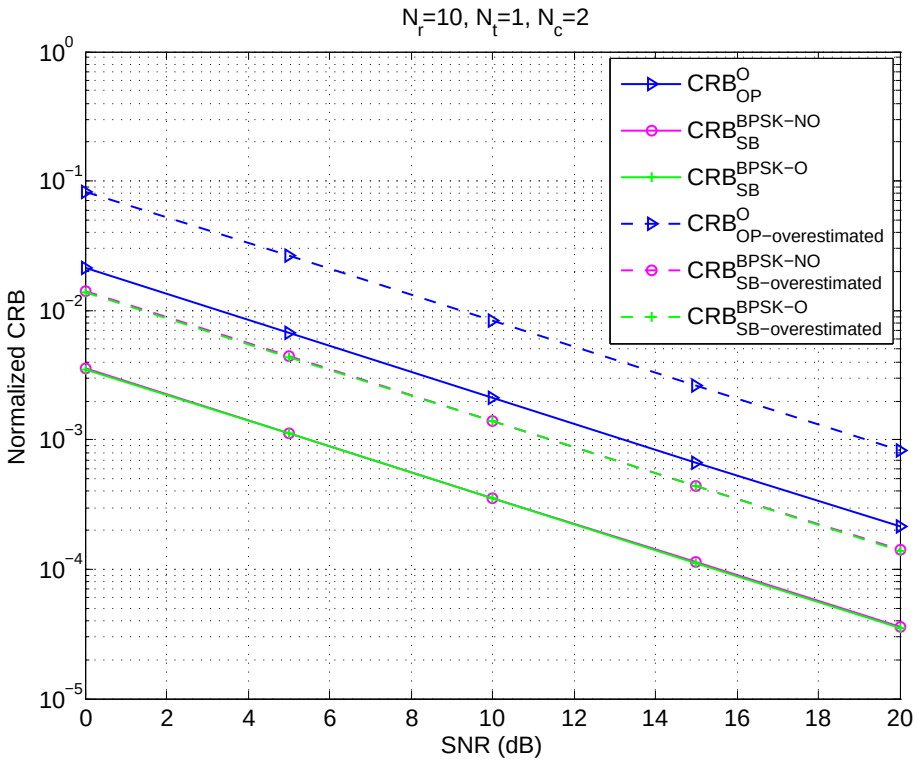

Figure 2.6: *Normalized CRB versus SNR with channel order overestimation*

2.A Proof of proposition 2.1

Proof. The FIM kernel dimension corresponds to the number of indeterminacies we need to remove (or equivalently the number of constraints we need to consider) to achieve full identifiability.

In the case of only pilots channel estimation in the presence of pilot contamination, the only parameters vector that can be estimated without bias is $\mathbf{h}_{tot} = \sum_{i=1}^{N_c} \mathbf{h}_i$.

Now, from $\mathbf{h}_{tot}$ one is able to determine every single channel $\mathbf{h}_i, i = 1, ...N_c$ iff $(N_c - 1)$ channel vectors are known (besides $\mathbf{h}_{tot}$). Since each channel vector is complex valued and of size $N_t N_r N$, this corresponds to $2(N_c - 1)N_t N_r N$ unknown real-valued parameters needed for full identifiability. □

2.B Proof of proposition 2.2

Proof. Considering the data only first (i.e. blind context), it is known that if the $N_r \times (N_c N_t)$ channel transfer function is irreductible, then one can estimate the channel parameters using the SOS up to an $(N_c N_t) \times (N_c N_t)$ unknown constant matrix [63],[64].

Now, since we assumed the source power known, the latter indeterminacy reduces to an unknown $(N_c N_t) \times (N_c N_t)$ unitary matrix, which can be modeled by $(N_c N_t)^2$ free real angle

parameters.

Somehow, the data SOS allows us to reduce the convolution model into an instantaneous $(N_c N_t)$ dimensional linear mixture model.

Finally, as in the only pilots case, due to the pilot contamination, the only way to complete the channel identification via the pilot use, is to have (know) the space directions of the interfering users of the neighboring cells corresponding to $((N_c - 1)N_t)^2$ real parameters to determine. □

2.C Proof of proposition 2.3

Proof. For non-Gaussian (communications) signals, the information provided by the Second Order Statistics as well as Higher Order Statistics of the data allows us to identify the channels up to an unknown $(N_c N_t) \times (N_c N_t)$ diagonal unitary matrix(see for example identifiability results in [65]). This corresponds to $N_c N_t$ unknown real parameters that can be easily estimated through the use of the pilots. □

CHAPTER 3

SIMO-OFDM system CRB derivation and application

Our greatest weakness lies in giving up. The most certain way to succeed is always to try just one more time.

Thomas A. Edison.

Abstract

This chapter focuses on SIMO-OFDM communications system, which is a particular case of the MIMO-OFDM case derived in chapter 1. Unlike in chapter 1, where the CRB derivations have been done in the frequency domain, the performances limits are derived in time domain. By using the CRB tool, before performing Fourier transform (i.e. in time domain), we compare the estimation error variance of the pilot-based and semi-blind based techniques for different data models[1](deterministic and stochastic models). A practical application of the derived CRB is proposed in this chapter, which consists on the protection of the exchanged data between a drone and mobile stations against blind interceptions[2].

[1] [66] A. Ladaycia, A. Mokraoui, K. Abed-Meraim, and A. Belouchrani, "What semi-blind channel estimation brings in terms of throughput gain?" in 2016 10th ICSPCS, Dec. 2016, pp. 1-6, Gold Coast, Australia.

[2] [67] A. Ladaycia, A. Belouchrani, K. Abed-Meraim, and A. Mokraoui, "Parameter optimization for defeating blind interception in drone protection," in 2017 Seminar on Detection Systems Architectures and Technologies (DAT), Feb. 2017, pp. 1-6, Alger, Algeria.

Chapter content

3.1 Introduction

Channel estimation in SIMO-OFDM communications systems can be done in time domain (i.e. before applying Fourier transform to the received signal) or in the frequency domain as developed in chapter 1. This chapter focuses on the channel estimation performance of a SIMO-OFDM wireless communications system. The objective is to show that a semi-blind channel estimation approach based on a compromise between the inserted block-type arrangement pilots and the transmitted symbols can preserve the SIMO-OFDM performance system while increasing significantly the information throughput. In order to analyze the theoretical performance limit of the different considered channel estimation approaches, CRB is derived. The CRB bounds, in a IEEE 802.11n wireless context, are then analyzed and discussed.

A practical application of the derived CRBs consists of protecting the exchanged data between a drone and mobile stations against blind interceptions. The developed strategy for a SIMO-OFDM communications system consists to prevent the interceptors to achieve a good blind channel estimation while allowing an accurate channel identification by the drone in the same wireless transmission conditions. To do so, a relevant selection of the communication parameters such as an appropriate data model with a specific data power is proposed. Simulations show that, under the same wireless transmission conditions, the blind channel estimation approach achieves the worst performance ensuring therefore the protection of the transmitted data.

3.2 SIMO-OFDM wireless communications system

Before deriving the CRB to analyze the performance of the channel estimation approaches, this section introduces the mathematical representation, in time domain, of the SIMO-OFDM wireless communications system.

Consider a SIMO-OFDM wireless system using N_r receive antennas, as shown in Figure 3.1, receiving the signal $\mathbf{y}(k)$ given by:

$$\mathbf{y}(k) = \sum_{i=0}^{N-1} \mathbf{h}(i)x(k-i) + \mathbf{v}(k), \tag{3.1}$$

where $\mathbf{h}(i) = [h_1(i) \cdots h_{N_r}(i)]^T$; $\mathbf{y}(k) = [y_1(k) \cdots y_{N_r}(k)]^T$; and $\mathbf{v}(k) = [v_1(k) \cdots v_{N_r}(k)]^T$ is an additive independent white Complex-Gaussian circular noise with $E\left[\mathbf{v}(k)\mathbf{v}(i)^H\right] = \sigma^2_{\mathbf{v}}\mathbf{I}_{N_r}\delta_{ki}$. The received signal is assumed to be an OFDM one where a Cyclic CP is introduced in each front of an OFDM symbol. The signal $\mathbf{x}$ is composed of K samples and a CP of L samples. Under the

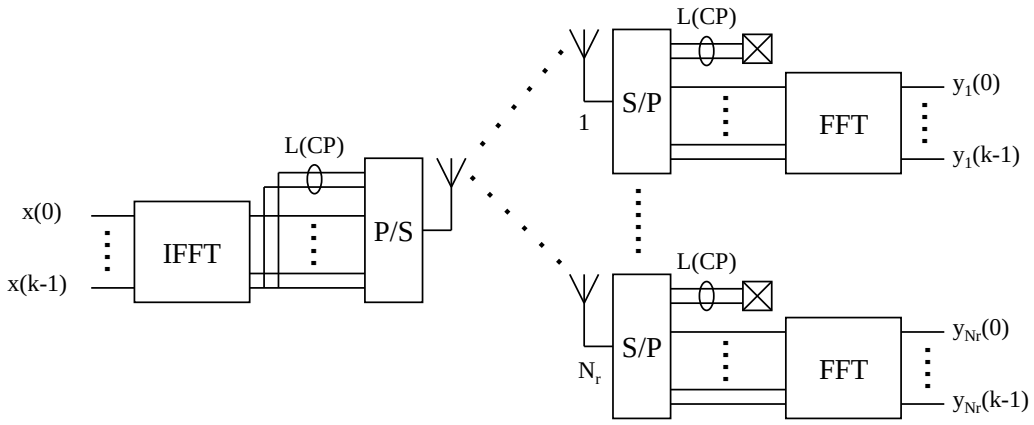

Figure 3.1: *SIMO-OFDM wireless communications system.*

assumption that $N \leq L$, the received signal is expressed as:

$$\mathbf{y} = \mathbf{T}(\mathbf{h})\mathbf{x} + \mathbf{v}, \tag{3.2}$$

where $\mathbf{x} = [x(0)\cdots x(K-1)]^T$; $\mathbf{y} = \left[\mathbf{y}_1^T \cdots \mathbf{y}_{N_r}^T\right]^T$ with $\mathbf{y}_i = [y_i(0)\cdots y_i(K-1)]^T$; and $\mathbf{h} = \left[\mathbf{h}_1^T \cdots \mathbf{h}_{N_r}^T\right]^T$ with $\mathbf{h}_i = [h_i(0)\cdots h_i(N-1)]^T$. $\mathbf{T}(\mathbf{h})$ is a matrix containing N_r circulant $K \times K$ Toeplitz blocks:

$$\mathbf{T}(\mathbf{h}) = \begin{bmatrix} \mathbf{T}(\mathbf{h}_1) \\ \vdots \\ \mathbf{T}(\mathbf{h}_{N_r}) \end{bmatrix}. \tag{3.3}$$

The first row of the i-th block (with $i = 1, \cdots, N_r$) is
$\begin{bmatrix} h_i(0) & \mathbf{0}_{1\times(K-N)} & h_i(N-1) \cdots h_i(1) \end{bmatrix}$, while the others are deduced by a simple cyclic shift to the right of the previous row.

In order to simplify the CRB calculations (i.e. derivative with respect to $\mathbf{h}$) in the next sections, equation (3.2) is rewritten as follows:

$$\mathbf{y} = \tilde{\mathbf{X}}\mathbf{h} + \mathbf{v}. \tag{3.4}$$

$$\tilde{\mathbf{X}} = \mathbf{I}_{N_r} \otimes \mathbf{X}, \tag{3.5}$$

where $\mathbf{X}$, given in the next equation, is a circulant matrix of size $K \times N$. Each column is obtained

by a simple down cyclic shift of the previous one with the first column being $\mathbf{x}$.

$$\mathbf{X} = \begin{bmatrix} x(0) & x(K-1) & \cdots & x(K-(N-1)) \\ x(1) & x(0) & \cdots & x(K-(N-2)) \\ \vdots & \ddots & \ddots & \ddots \\ x(K-1) & x(K-2) & \cdots & x(K-N) \end{bmatrix}. \tag{3.6}$$

3.3 CRB for SIMO-OFDM pilot-based channel estimation

The objective of this section is to derive an explicit expression of the CRB for radio-mobile channels in terms of MSE when only pilots are used by the receiver to estimate the SIMO-OFDM channels. In what follows, OFDM block-type arrangement pilots are considered as Figure 1.2a.

The CRB is computed as the inverse of the FIM denoted $\mathbf{J}_{\theta\theta}$ where θ is the unknown parameter vector to be estimated:

$$\theta = \left[\mathbf{h}^T \; {\sigma_{\mathbf{v}}}^2\right]^T. \tag{3.7}$$

The noise being i.i.d., the FIM for θ can be written as follows:

$$\mathbf{J}_{\theta\theta} = \sum_{i=1}^{N_p} \mathbf{J}_{\theta\theta i} = N_p \begin{bmatrix} \frac{\tilde{\mathbf{X}}_p^H \tilde{\mathbf{X}}_p}{\sigma_{\mathbf{v}}^2} & 0 \\ 0 & \frac{N_r K}{2\sigma_{\mathbf{v}}^4} \end{bmatrix}, \tag{3.8}$$

where, for simplicity, we assumed that the same OFDM symbol is repeated N_p times as it is the case in many communications standards (see [22]). The lower bound of unbiased channel MSE (Mean Square Error) estimation, when only pilots are used, is CRB_{OP} provided by:

$$CRB_{OP} = \frac{\sigma_{\mathbf{v}}^2}{N_p} \left(\tilde{\mathbf{X}}_p^H \tilde{\mathbf{X}}_p\right)^{-1}. \tag{3.9}$$

3.4 CRB for SIMO-OFDM semi-blind channel estimation

For semi-blind channel estimation in the SIMO-OFDM communications system context, the computation of the CRB relies on the transmitted frame composed of known pilot OFDM symbols (preamble or training sequence) and unknown transmitted data. To derive the explicit expression of the CRB, two cases have been distinguished depending on whether the transmitted data is deterministic or stochastic Gaussian[3] $\mathbf{x}_d \sim NC(0, \sigma_{\mathbf{x}}^2)$.

In this context and under the assumptions that the data symbols and noise signal are both i.i.d., the FIM can be divided into two parts: one part is dedicated to pilots and denoted $\mathbf{J}_p$ (given by equation (3.8)); and the second part concerns the unknown data $\mathbf{J}_d$, i.e. $\mathbf{J} = \mathbf{J}_p + \mathbf{J}_d$.

[3] We adopt here the Gaussian CRB as it is the most tractable one and also because it represents the least favorable distribution case [38].

We assume that the unknown transmitted data, denoted $\mathbf{x}_d$, is composed of N_d OFDM symbols, i.e $\mathbf{x}_d = [\mathbf{x}_{s_1}^T\ \mathbf{x}_{s_2}^T\ \cdots\ \mathbf{x}_{s_{N_d}}^T]^T$. Denote $\mathbf{x}$ the signal composed of known pilots and transmitted data: $\mathbf{x} = [\mathbf{x}_p^T\ \mathbf{x}_d^T\ ]^T$. The received signal, denoted $\mathbf{y}$, corresponding to the transmitted unknown data $\mathbf{x_d}$ is expressed as follows:

$$\mathbf{y} = \mathbf{T}_d(\mathbf{h})\mathbf{x}_d + \mathbf{v} = \tilde{\mathbf{X}}_d\mathbf{h} + \mathbf{v}, \tag{3.10}$$

where $\tilde{\mathbf{X}}_d$ has the following form:

$$\tilde{\mathbf{X}}_d = \left[\tilde{\mathbf{X}}_{s_1}^T\ \tilde{\mathbf{X}}_{s_2}^T\ \cdots\ \tilde{\mathbf{X}}_{s_{N_d}}^T\right]^T, \tag{3.11}$$

with $\tilde{\mathbf{X}}_{s_i}$ the matrix given by equation (3.5) and filled with the elements of the i-th data OFDM symbol $\mathbf{x}_{s_i}$. Matrix $\mathbf{T}_d(\mathbf{h})$ is given by:

$$\mathbf{T}_d(\mathbf{h}) = \mathbf{I}_{N_d} \otimes \mathbf{T}(\mathbf{h}). \tag{3.12}$$

3.4.1 Deterministic Gaussian data model

Here the unknown data OFDM symbols are assumed to be deterministic so that the unknown parameter vector θ becomes:

$$\theta = \left[\mathbf{h^T}\ \mathbf{x_d^T}\ \boldsymbol{\sigma_v^2}\right]^T. \tag{3.13}$$

The corresponding FIM expression is given in [39, 68, 36]:

$$\mathbf{J}_d = \begin{bmatrix} \frac{\tilde{\mathbf{X}}_d^H\tilde{\mathbf{X}}_d}{{\sigma_\mathbf{v}}^2} & \frac{\tilde{\mathbf{X}}_d^H\mathbf{T}_d(\mathbf{h})}{{\sigma_\mathbf{v}}^2} & 0 \\ \frac{\mathbf{T}_d(\mathbf{h})^H\tilde{\mathbf{X}}_d}{{\sigma_\mathbf{v}}^2} & \frac{\mathbf{T}_d(\mathbf{h})^H\mathbf{T}_d(\mathbf{h})}{{\sigma_\mathbf{v}}^2} & 0 \\ 0 & 0 & \frac{N_r M_d}{2\sigma_\mathbf{v}^4} \end{bmatrix}. \tag{3.14}$$

The global FIM when taking into account the FIM of the pilots becomes:

$$\mathbf{J} = \begin{bmatrix} \frac{\tilde{\mathbf{X}}_d^H\tilde{\mathbf{X}}_d + N_p\left(\tilde{\mathbf{X}}_p^H\tilde{\mathbf{X}}_p\right)}{\sigma_\mathbf{v}^2} & \frac{\tilde{\mathbf{X}}_d^H\mathbf{T}_d(\mathbf{h})}{\sigma_\mathbf{v}^2} & 0 \\ \frac{\mathbf{T}_d(\mathbf{h})^H\tilde{\mathbf{X}}_d}{\sigma_\mathbf{v}^2} & \frac{\mathbf{T}_d(\mathbf{h})^H\mathbf{T}_d(\mathbf{h})}{\sigma_\mathbf{v}^2} & 0 \\ 0 & 0 & \frac{N_r(M_d+M_p)}{2{\sigma_\mathbf{v}}^4} \end{bmatrix}. \tag{3.15}$$

Therefore the CRB explicit expression for semi-blind channel estimation is given as follows:

$$CRB_{SB}^{Det} = \sigma_\mathbf{v}^2\left(\mathbf{A} - \mathbf{B}\mathbf{D}^{-1}\mathbf{C}\right)^{-1} \tag{3.16}$$

where $\mathbf{A} = \tilde{\mathbf{X}}_d^H\tilde{\mathbf{X}}_d + N_p\left(\tilde{\mathbf{X}}_p^H\tilde{\mathbf{X}}_p\right)$; $\mathbf{B} = \mathbf{C}^H = \tilde{\mathbf{X}}_d^H\mathbf{T}_d(\mathbf{h})$; and $\mathbf{D} = \mathbf{T}_d(\mathbf{h})^H\mathbf{T}_d(\mathbf{h})$. To avoid the inversion of the very large matrix, we use the Schur's complement as well as the properties of circulant matrices to compute the CRB denoted CRB_{SB}^{Det} in a relatively simple way.

3.4.1.1 Special-case: Hybrid pilot in semi-blind channel estimation with deterministic Gaussian data model

This section derives the CRB_{SB}^{Det} when an OFDM symbol may be considered as a hybrid OFDM symbol containing both pilot samples and data samples, i.e. $\mathbf{x}_{hyb} = \begin{bmatrix} \mathbf{x}_{hyb_p}^T & \mathbf{x}_{hyb_d}^T \end{bmatrix}^T$. The received hybrid symbol has then the following form:

$$\mathbf{y}_{hyb} = \begin{bmatrix} \mathbf{T}_{hyb_p}(\mathbf{h}) & \mathbf{T}_{hyb_d}(\mathbf{h}) \end{bmatrix} \begin{bmatrix} \mathbf{x}_{hyb_p} \\ \mathbf{x}_{hyb_d} \end{bmatrix} + \mathbf{v}. \tag{3.17}$$

Finally CRB_{SB}^{Det} is given as in equation (3.16) where matrix $\mathbf{A}$ corresponds to:

$$\begin{aligned} \mathbf{A} &= \tilde{\mathbf{X}}_d^H \tilde{\mathbf{X}}_d + N_p \left(\tilde{\mathbf{X}}_p^H \tilde{\mathbf{X}}_p \right) + \tilde{\mathbf{X}}_{hyb}^H \tilde{\mathbf{X}}_{hyb} \\ &- \tilde{\mathbf{X}}_{hyb}^H \mathbf{T}_{hyb_d}(\mathbf{h}) \left(\mathbf{T}_{hyb_d}^H(\mathbf{h}) \mathbf{T}_{hyb_d}(\mathbf{h}) \right)^{-1} \mathbf{T}_{hyb_d}(\mathbf{h})^H \tilde{\mathbf{X}}_{hyb}. \end{aligned} \tag{3.18}$$

3.4.2 Stochastic Gaussian data model (CRB_{SB}^{Stoch})

This section addresses the case where the unknown data is assumed to be stochastic Gaussian and i.i.d. with zero mean and variance $\sigma_{\mathbf{x}}^2$. Hence, the FIM is equal to the FIM of the first data OFDM symbol multiplied by the number of symbols N_d. The vector of the unknown parameters θ is:

$$\theta = \left[\mathbf{h}^T \; {\sigma_s}^2 \; {\sigma_{\mathbf{v}}}^2 \right]^T. \tag{3.19}$$

The FIM of this model is therefore given by [36]:

$$[\mathbf{J}_{\theta\theta}]_{i,j} = tr \left\{ \mathbf{C}_{YY}^{-1} \frac{\partial \mathbf{C}_{YY}}{\partial \theta_i^*} \mathbf{C}_{YY}^{-1} \left(\frac{\partial \mathbf{C}_{YY}}{\partial \theta_j^*} \right)^H \right\}, \tag{3.20}$$

where

$$\mathbf{C}_{YY} = \sigma_s^2 \mathbf{T}(\mathbf{h}) \mathbf{T}(\mathbf{h})^H + \sigma_{\mathbf{v}}^2 \mathbf{I}_{N_r K}. \tag{3.21}$$

To derive the FIM we used the following information:
$\frac{\partial \mathbf{C}_{YY}}{\partial h_i^*} = \sigma_s^2 \mathbf{T}(\mathbf{h}) \mathbf{T}\left(\frac{\partial \mathbf{h}}{\partial h_i^*} \right)^H$, $\frac{\partial \mathbf{C}_{YY}}{\partial \sigma_s^2} = \frac{1}{2} \mathbf{T}(\mathbf{h}) \mathbf{T}(\mathbf{h})^H$, and $\frac{\partial \mathbf{C}_{YY}}{\partial \sigma_{\mathbf{v}}^2} = \frac{1}{2} \mathbf{I}_{N_r K}$.

The FIM $\mathbf{J}_d$ has the following form:

$$\mathbf{J}_d = N_d \begin{bmatrix} \mathbf{J}_{hh} & \mathbf{J}_{h\sigma_s^2} & \mathbf{J}_{h\sigma_{\mathbf{v}}^2} \\ \mathbf{J}_{{\sigma_s}^2 h} & \mathbf{J}_{{\sigma_s}^2 {\sigma_s}^2} & \mathbf{J}_{{\sigma_s}^2 {\sigma_{\mathbf{v}}}^2} \\ \mathbf{J}_{{\sigma_{\mathbf{v}}}^2 h} & \mathbf{J}_{{\sigma_{\mathbf{v}}}^2 {\sigma_s}^2} & \mathbf{J}_{{\sigma_{\mathbf{v}}}^2 {\sigma_{\mathbf{v}}}^2} \end{bmatrix}, \tag{3.22}$$

where

$$\begin{aligned} [\mathbf{J}_{hh}]_{i,j} = \\ tr \left\{ \mathbf{C}_{YY}^{-1} {\sigma_s}^2 \mathbf{T}(\mathbf{h}) \mathbf{T}\left(\frac{\partial \mathbf{h}}{\partial h_i^*} \right)^H \mathbf{C}_{YY}^{-1} {\sigma_s}^2 \mathbf{T} \left(\frac{\partial \mathbf{h}}{\partial h_j^*} \right) \mathbf{T}(\mathbf{h})^H \right\}, \end{aligned} \tag{3.23}$$

$$\mathbf{J}_{{\sigma_s}^2{\sigma_s}^2} = \frac{1}{4} tr\left\{\mathbf{C}_{YY}^{-1}\mathbf{T}(\mathbf{h})\mathbf{T}(\mathbf{h})^H\mathbf{C}_{YY}^{-1}\mathbf{T}(\mathbf{h})\mathbf{T}(\mathbf{h})^H\right\}, \tag{3.24}$$

$$\mathbf{J}_{{\sigma_\mathbf{v}}^2{\sigma_\mathbf{v}}^2} = \frac{1}{4} tr\left\{\mathbf{C}_{YY}^{-1}\mathbf{C}_{YY}^{-1}\right\}, \tag{3.25}$$

$$\left[\mathbf{J}_{h{\sigma_s}^2}\right]_i = \frac{1}{2} tr\left\{\mathbf{C}_{YY}^{-1}{\sigma_s}^2\mathbf{T}(\mathbf{h})\mathbf{T}\left(\frac{\partial \mathbf{h}}{\partial h_i^*}\right)^H\mathbf{C}_{YY}^{-1}\mathbf{T}(\mathbf{h})\mathbf{T}(\mathbf{h})^H\right\}, \tag{3.26}$$

$$\left[\mathbf{J}_{h{\sigma_\mathbf{v}}^2}\right]_i = \frac{1}{2} tr\left\{\mathbf{C}_{YY}^{-1}{\sigma_s}^2\mathbf{T}(\mathbf{h})\mathrm{T}\left(\frac{\partial \mathbf{h}}{\partial h_i^*}\right)^H\mathbf{C}_{YY}^{-1}\right\}, \tag{3.27}$$

$$\left[\mathbf{J}_{{\sigma_s}^2{\sigma_\mathbf{v}}^2}\right] = \frac{1}{4} tr\left\{\mathbf{C}_{YY}^{-1}\mathbf{T}(\mathbf{h})\mathbf{T}(\mathbf{h})^H\mathbf{C}_{YY}^{-1}\right\}. \tag{3.28}$$

For the blind case, as well known, the blind estimation techniques through second order statistics (i.e. using only the data FIM $\mathbf{J}_d$ given by equation (3.22)), channel impulse response can be determined up to a complex unknown factor. Therefore, the FIM is rank deficient.

In order to avoid the ambiguity of the unknown factor and obtain the CRB, one can fix one non-zero complex channel parameter, $\mathbf{h}_n$ to its largest energy $\|\mathbf{h}_n\|^2$. Which is equivalent to delete the rows and columns corresponding to $\mathbf{h}_n$ in the FIM [69, 70]. Then the CRB denoted by CRB_{Blind}^{CG} is given by the $\mathbf{h}$-bloc of the inverse of FIM.

3.4.2.1 Special-case: Hybrid pilot in semi-blind channel estimation with stochastic Gaussian model

This section modifies the CRB_{SB}^{Stoch} expression when a hybrid OFDM symbol is considered according to:

$$\mathbf{C}_{YY_{hyb}} = {\sigma_s}^2\mathbf{T}_{hyb_d}(\mathbf{h})\mathbf{T}_{hyb_d}(\mathbf{h})^H + \sigma_\mathbf{v}^2. \tag{3.29}$$

$$\mu(\mathbf{h}) = \mathbf{x}_{hyb_p}\mathbf{T}_{hyb_p}(\mathbf{h}). \tag{3.30}$$

The final FIM under the previous assumptions is expressed as: $\mathbf{J} = \mathbf{J}_p + \mathbf{J}_{hyb} + \mathbf{J}_d$, where each element $\left[\mathbf{J}_{hyb}\right]_{i,j}$ has the following form:

$$\begin{aligned}\left[\mathbf{J}_{hyb}\right]_{i,j} = &\left(\frac{\partial \mu(\mathbf{h})}{\partial \theta_i^*}\right)^H\mathbf{C}_{YY_{hyb}}^{-1}\left(\frac{\partial \mu(\mathbf{h})}{\partial \theta_j^*}\right) \\ &+tr\left\{\mathbf{C}_{YY_{hyb}}^{-1}\left(\frac{\partial \mathbf{C}_{YY_{hyb}}}{\partial \theta_i^*}\right)\mathbf{C}_{YY_{hyb}}^{-1}\left(\frac{\partial \mathbf{C}_{YY_{hyb}}}{\partial \theta_j^*}\right)^H\right\}.\end{aligned} \tag{3.31}$$

3.4.2.2 Reduction of the FIM computational complexity

This section addresses the issue of reducing the computational complexity of the FIM. Note that each element $[\mathbf{J}_d]_{i,j}$ depends on $\mathbf{C}_{YY}^{-1}$. Therefore it is important to reduce its computational complexity.

To calculate $\mathbf{C}_{YY}^{-1}$, we propose to exploit the circular structure of $\mathbf{T}(\mathbf{h})$. Moreover, we exploit the sparsity structure of $\mathbf{T}(\mathbf{h})$ and $\mathbf{T}\left(\frac{\partial \mathbf{h}}{\partial h_i^*}\right)$ to reduce the matrix products that increase dramatically with the number of antenna (N_r), OFDM symbol samples (K) and the channel length (N).

Thereby $\mathbf{T}(\mathbf{h})$ can be written as:

$$\mathbf{T}(\mathbf{h}) = (\mathbf{I}_{N_r} \otimes \mathbf{F})\mathbf{D}\mathbf{F}^H, \tag{3.32}$$

where $\mathbf{D} = \begin{bmatrix} \mathbf{D}_1{}^T & \cdots & \mathbf{D}_{N_r}{}^T \end{bmatrix}^T$ with $\mathbf{D}_i$ a diagonal matrix containing the Fourier transform of $\mathbf{h}_i$ and $\mathbf{F}$ the Fourier matrix operator. Equations (3.21) and (3.32) yield to:

$$\mathbf{C}_{YY} = (\mathbf{I}_{N_r} \otimes \mathbf{F})\left({\sigma_s}^2\mathbf{D}\mathbf{D}^H + {\sigma_\mathbf{v}}^2\mathbf{I}_{N_rK}\right)\left(\mathbf{I}_{N_r} \otimes \mathbf{F}^\mathbf{H}\right). \tag{3.33}$$

Therefore to compute $\mathbf{C}_{YY}^{-1}$, the inverse of $\left({\sigma_s}^2\mathbf{D}\mathbf{D}^H + {\sigma_\mathbf{v}}^2\mathbf{I}_{N_rK}\right)$ is calculated using the Woodbury matrix identity leading to this simplified expression: $\left({\sigma_s}^2\mathbf{D}\mathbf{D}^H + {\sigma_\mathbf{v}}^2\mathbf{I}_{N_rK}\right)^{-1} =$

$$\frac{1}{{\sigma_\mathbf{v}}^2}\mathbf{I}_{N_rK} - \frac{{\sigma_s}^2}{{\sigma_\mathbf{v}}^4}\mathbf{D}\left(\mathbf{I}_K + \frac{{\sigma_s}^2}{{\sigma_\mathbf{v}}^2}\sum_{i=1}^{N_r}\mathbf{D}_i^H\mathbf{D}_i\right)^{-1}\mathbf{D}^H. \tag{3.34}$$

To compute $\mathrm{T}\left(\frac{\partial \mathbf{h}}{\partial h_i^*}\right)$ with $i = 1, \cdots, NN_r$, we start by calculating indices i_{N_r} and i_N corresponding to the i_{N_r}-th antenna and the i_N-th tap of the channel function ($i_{N_r} = 1, \cdots, N_r$, $i_N = 1, \cdots, N$) respectively. The fact that $\mathbf{T}(\mathbf{h})$ is block circular, so $\mathbf{T}\left(\frac{\partial \mathbf{h}}{\partial h_i^*}\right)$ contains $N_r - 1$ zero blocks and its i_{N_r}-th block is equal to the $\mathbf{I}_K$ circularly shifted to the left by i_N steps.

Finally, $\mathbf{C}_{YY}^{-1}\frac{\partial \mathbf{C}_{YY}}{\partial \mathbf{h}_i^*}$ is simplified as follows:

$$\mathbf{C}_{YY}^{-1}\frac{\partial \mathbf{C}_{YY}}{\partial \mathbf{h}_i^*} =$$

$$\begin{bmatrix} \mathbf{0} & \cdots & \mathbf{0} & {\sigma_s}^2\mathbf{C}_{YY}^{-1}\mathbf{T}_{shift}(\mathbf{h}_1) & \mathbf{0} & \cdots & \mathbf{0} \\ \vdots & \vdots & \vdots & \vdots & \vdots & \vdots & \vdots \\ \mathbf{0} & \cdots & \mathbf{0} & {\sigma_s}^2\mathbf{C}_{YY}^{-1}\mathbf{T}_{shift}(\mathbf{h}_{N_r}) & \mathbf{0} & \cdots & \mathbf{0} \end{bmatrix}, \tag{3.35}$$

where $\mathbf{T}_{shift}(\mathbf{h}_i)$ is equal to $\mathbf{T}(\mathbf{h}_i)$ circularly shifted to the left by i_N steps.

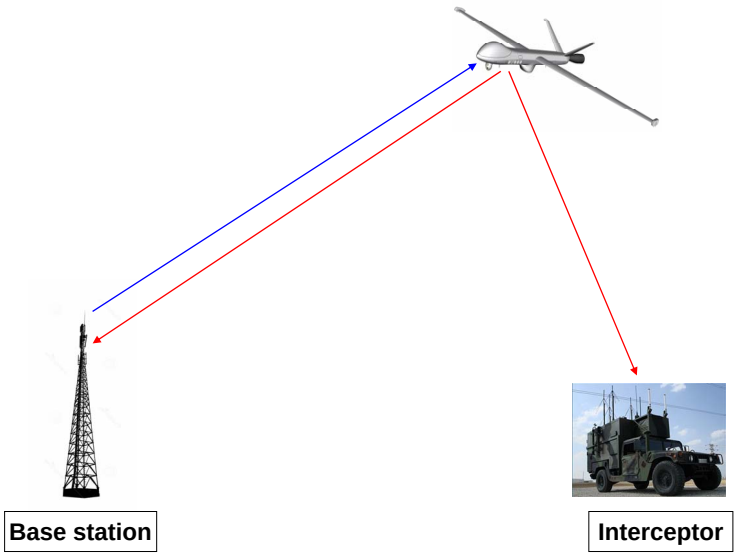

Figure 3.2: *Interception of signals.*

3.5 CRB analysis for defeating blind interception

While exchanging data between drones and base stations, one can intercept this data by the deployment of interceptor at the area of interest (as illustrated in Figure 3.2) and then applying blind identification methods, the interceptor can then exploit the data and even uses spoofing.

The system drone-base station is considered as a SIMO-OFDM communications system, as illustrated in Figure 3.1. The channel estimation is done by the base station, which exploits the pilot OFDM symbols send by the drone as illustrated in Figure 3.3. The interceptor does not know the training sequences dedicated to the channel estimation, so it considers the transmitted signal as data to blindly estimate the propagation channel between drone and interceptor. This section analyzes the parameters to be used by the drone communications system. A relevant selection of the parameters, in terms of the CRB, is then provided in such a way that any blind channel estimation method is not able to correctly recover the transmission channel making then the interception of the transmitted data difficult while improving the performance of data-aided channel estimation approaches.

The CRB tool (derived in section 3.3 and in section 3.4) allows to find the waveform model providing the worst blind channel estimation CRB. The reduction of the number of data symbols also contributes to the degradation of the blind channel estimation. However this reduction affects the transmission rate between the drone and the base stations. To solve this problem, a large number of data symbols can be subdivided into sub-sequences and transmitted to multiple frequency channels making then difficult the blind channel estimation since a large number of

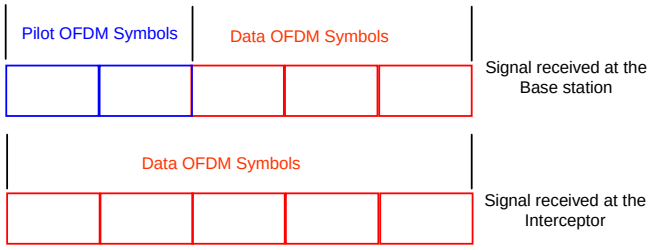

Figure 3.3: *Received OFDM symbols as considered by the stations and the interceptor.*

sub-channels should be estimated using at each time only a small number of data symbols.

3.6 Simulation results and discussions

The objectives of this section is to discuss the blind and semi-blind channel estimation performance bounds using the derived CRBs to show: (i): the impact of the pilot reduction on the channel estimation and to quantify the reduced pilots; (ii): the parameters of the transmitted signal to avoid the blind interception.

3.6.1 Throughput gain analysis of SIMO-OFDM semi-blind channel estimation

Herein we analyze the limit bounds of the channel estimation performance in the IEEE 802.11n SIMO-OFDM wireless system [22]. The test training sequence corresponds to that specified by the standard. Figure 1.5 represents the IEEE 802.11n physical frame HT-Mixed format. In the legacy preamble (i.e. 802.11a) two identical fields named LTF are dedicated to channel estimation. Each field (or pilot) is represented by one OFDM symbol ($K = 64$ samples) where a CP ($L = 16$ samples) is added at its front. In the High Throughput preamble, a set of identical fields named HT-LTF are specified and represented by one OFDM symbol ($K = 64$ samples) with a CP (16 samples). These fields (or pilots) are specified to MIMO channel estimation. Their number depends on the number of transmit antennas (N_t). Since in this chapter $N_t = 1$, only one HT-LTF pilot OFDM symbol is used (see [22]). Therefore the training sequence length is equal to $N_p = N_p^{LTF} + N_p^{HT-LTF}$. The data field is represented by a set of OFDM symbols depending on the length of the transmitted packet. Simulation parameters are summarized in Table 3.1.

The Signal to Noise Ratio associated with pilots at the reception is defined as $SNR_p = \frac{\|\mathbf{T}(\mathbf{h})\mathbf{x}_p\|^2}{N_r M_p \sigma_{\mathbf{v}}^2}$. The signal to noise ratio SNR_d associated with data is given (in dB) by: $SNR_d = SNR_p - (Px_p - Px_d)$ where Px_p (respectively Px_d) is the power of pilots (respectively data) (both in dB).

Parameters	Specifications
Channel model	Cost 207
Number of transmit antennas	$N_t = 1$
Number of receive antennas	$N_r = 3$
Channel length	N = 4
Number of LTF pilot OFDM symbols	$N_p^{LTF} = 2$
Number of HT-LTF pilot OFDM symbols	$N_p^{HT-LTF} = 1$
Number of data OFDM symbols	$N_d = 40$
Pilot signal power	$P_{x_p} = 23$ dBm
Data signal power	$P_{x_d} = 20$ dBm
Number of sub-carriers	$K = 64$
Signal to Noise Ratio	SNR_p = [-5:20] dB

Table 3.1: *SIMO-OFDM simulation parameters.*

Figure 3.4 compares the normalized CRB ($\frac{tr\{CRB\}}{\|\mathbf{h}\|^2}$) versus SNR_p. The CRB curves show clearly that semi-blind channel estimation CRB_{SB} (in deterministic and Stochastic) are lower than the CRB (CRB_{OP}) when only pilots are exploited. Note that, as expected, stochastic case (CRB_{SB}^{Stoch}) gives better results than the deterministic case (CRB_{SB}^{Det}).

Traditionally semi-blind channel estimation approach is used to improve the channel identification accuracy. However, in this chapter the semi-blind approach is considered in order to increase the throughput in SIMO-OFDM wireless system while maintaining the same channel estimation quality that is achieved when using pilots only. For this, in order to reach the CRB_{OP}, we propose to decrease the number of pilot samples and increase the number of data samples. This strategy may lead to a hybrid OFDM symbol containing both pilot samples and data samples. .

Figure 3.5 shows the influence of increasing the number of data OFDM symbols (N_d) on the CRB_{SB} deterministic and stochastic for a given $SNR_p = 6$ dB corresponding to the IEEE 802.11n operating mode. Obviously, the larger the data size is the higher gain we obtain in favor of the semi-blind method.

Figure 3.6 illustrates the CRB of semi-blind channel estimation versus the number of samples removed from the pilot OFDM symbol for a given $SNR_p = 6$ dB. The proposed strategy is to replace these removed samples by data samples leading therefore to a hybrid OFDM symbol.

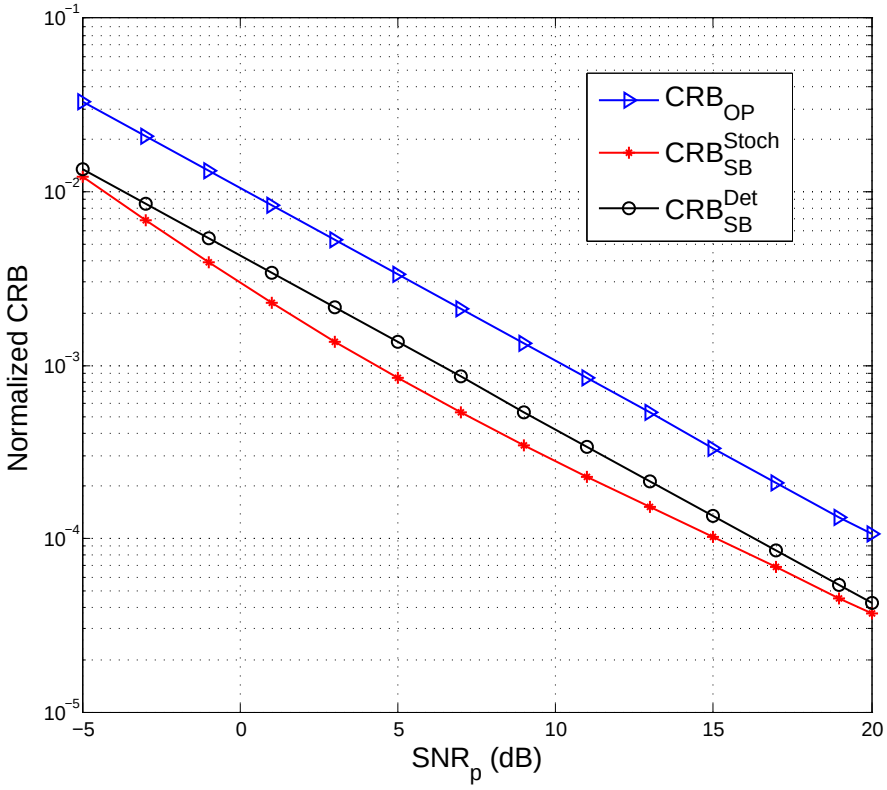

Figure 3.4: *Normalized CRB versus SNR_p.*

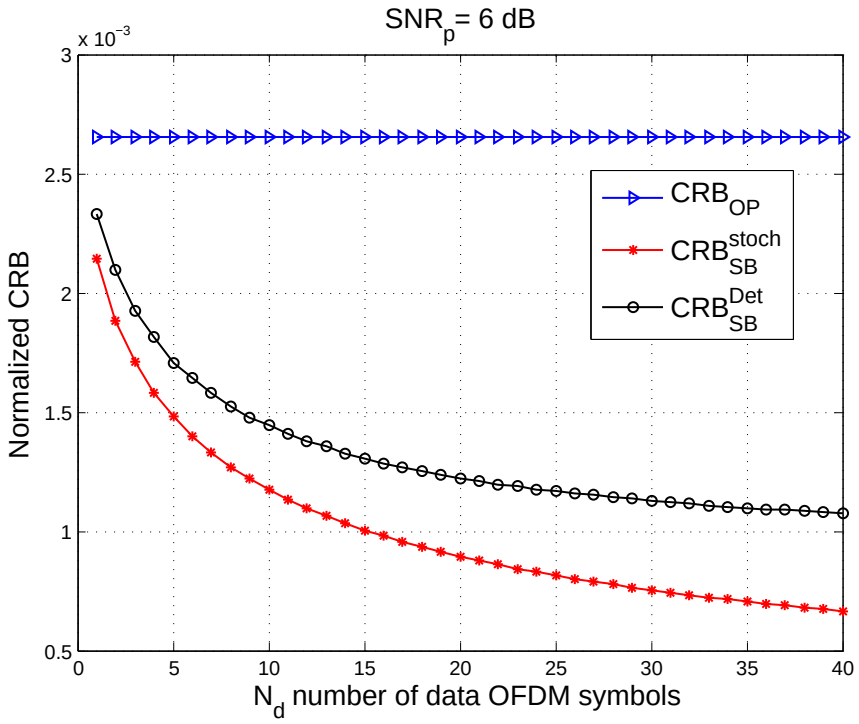

Figure 3.5: *Normalized CRB versus N_d ($SNR_p = 6$ dB).*

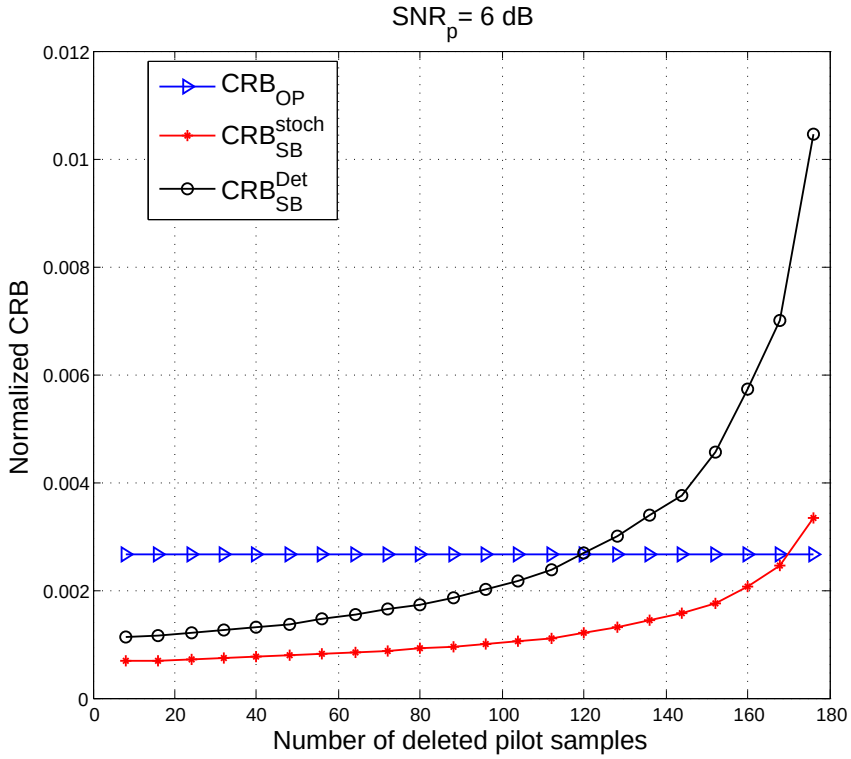

Figure 3.6: *Normalized CRB versus the number of deleted pilot samples ($SNR_p = 6$ dB).*

The horizontal line provides the CRB for pilot-based channel estimation and is considered as the reference to be reached. For CRB_{SB}^{Det}, 119 samples are removed from pilot OFDM symbol i.e. only 73 samples (38%) are retained as pilot samples. For CRB_{SB}^{Stoch} more samples are removed. Indeed only 23 samples (i.e. 11%) are retained. These results show clearly that semi-blind estimation in SIMO-OFDM wireless system brings a significant gain in terms of throughput.

Figure 3.7 shows the impact of the number of data OFDM symbols on the number of the deleted pilot samples for a given $SNR_p = 6$ dB and a normalized $CRB_{SB}^{Stoch} = 2.652 \times 10^{-3}$. When the number of data OFDM symbols increases, the number of samples of the pilot OFDM symbol to remove increases too. Note that the results observed in Figure 3.6 can be deduced from Figure 3.7 when the number of data OFDM symbol is equal to 40.

Figure 3.8 illustrates the number of deleted pilot samples versus the number of receive antennas (N_r) of the SIMO-OFDM system in semi-blind channel estimation. The larger the number of receive antennas is, the higher is the number of removed pilot symbols. Note that, in the SISO case and for the deterministic CRB, the data symbols do not help reducing the pilot size since each new observation brings as many unknowns as equations.

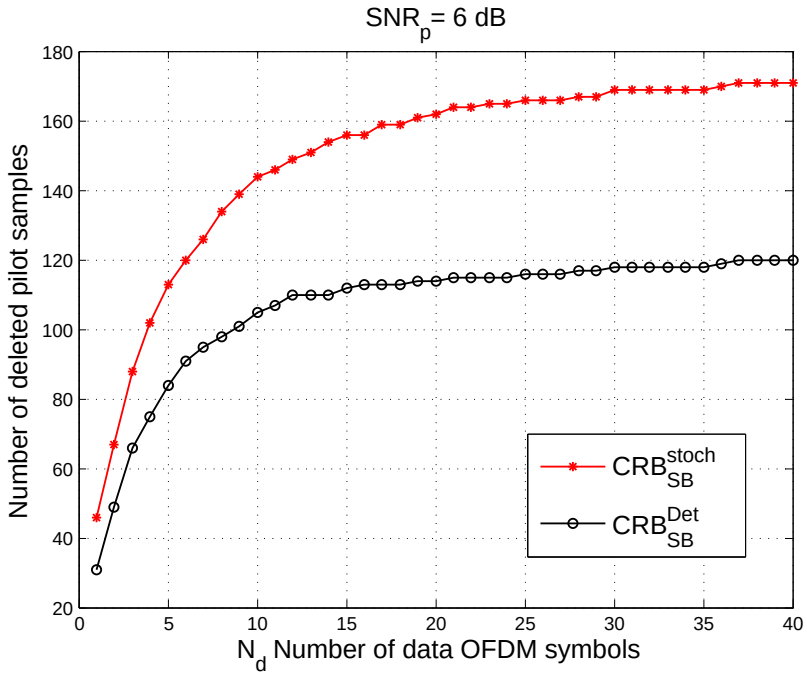

Figure 3.7: *Number of deleted pilot samples versus N_d ($SNR_p = 6$ dB; and $CRB_{SB}^{Stoch} = 2.652 \times 10^{-3}$).*

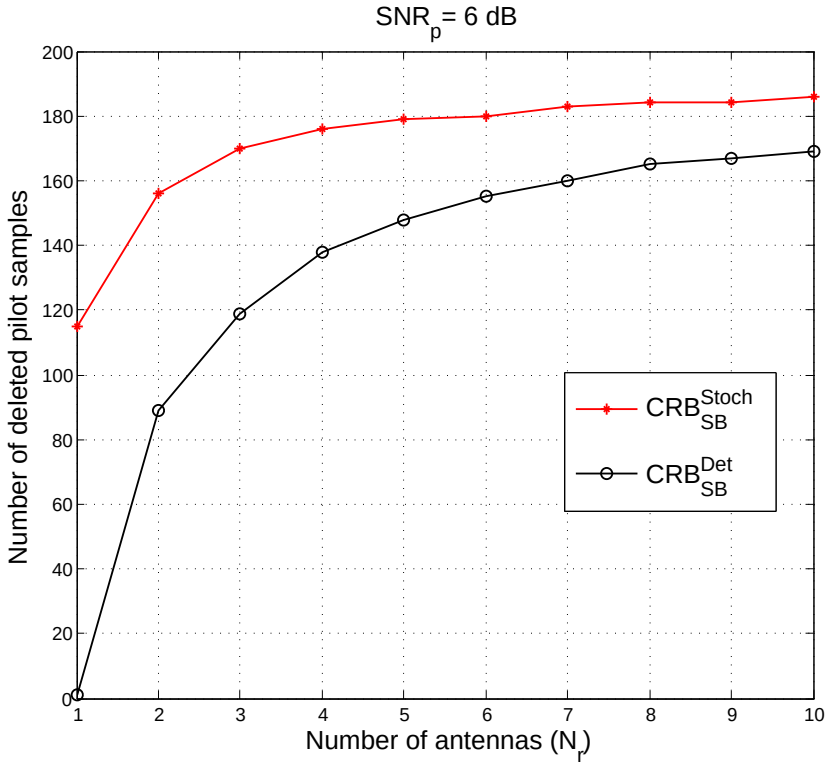

Figure 3.8: *Number of deleted pilot samples versus the number N_r of receive antennas ($SNR_p = 6$ dB).*

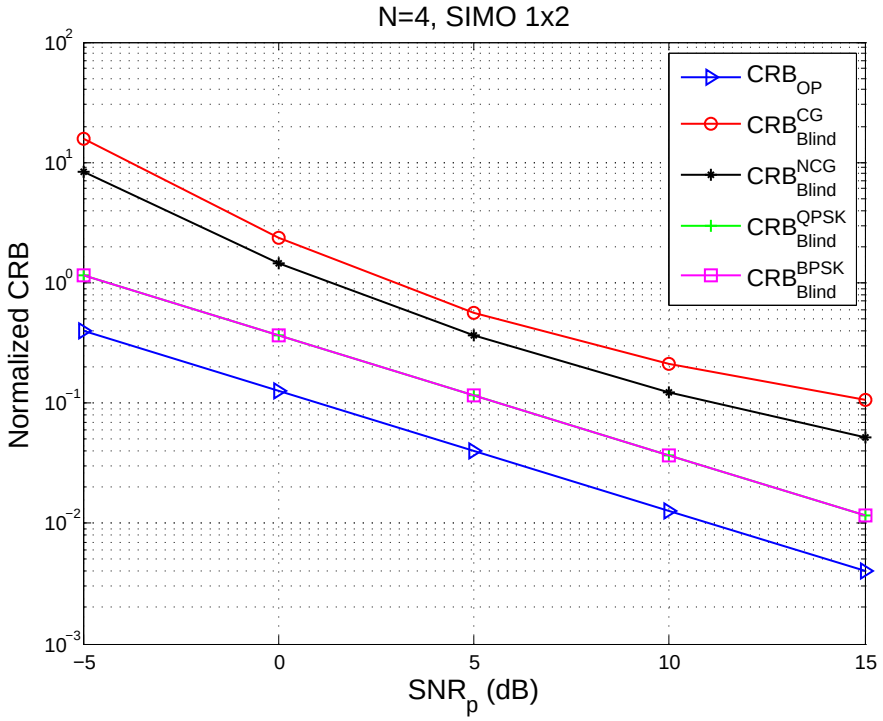

Figure 3.9: *Normalized CRB versus SNR_p.*

3.6.2 Blind interception analysis

In this subsection, the blind interception is investigated using CRBs in order to protect the exchanged data between drone and BS. Simulations are conducted using two receivers ($N_r = 2$), two training sequences ($N_p = 2$) and two data OFDM symbols ($N_d = 2$). The rest of simulation parameters are given in Table 3.1

Figure 3.9 compares the normalized CRB ($\frac{tr\{CRB\}}{\|\mathbf{h}\|^2}$) versus SNR_p. The CRB curves show clearly that the blind channel estimation CRB_{Blind} in CG, NCG and BPSK/QPSK data models are higher than the CRB when only pilots are exploited (CRB_{OP}). Note that BPSK/QPSK case ($CRB^{BPSK}_{Blind} CRB^{QPSK}_{Blind}$) gives better results than other data models and the CG data model (CRB^{CG}_{Blind}) provides the worst blind channel estimation performance. These results remain valid even if the number of receive antennas increases.

In accordance with these results and in order to protect the transmitted information by the drone, we propose to tune some parameters of the SIMO-OFDM system. We first impose to the SIMO-OFDM system to operate at 0 dB (by adjusting the data power) and to process on a signal modelled as a CG data. Indeed with these working conditions, the stations are able to estimate the channel taps with an acceptable performance (see in Figure 3.9, $CRB_{OP} = 0.12$) compared to the interceptor (see Figure 3.9, $CRB^{CG}_{Blind} = 2.38$) which is not able to recover the

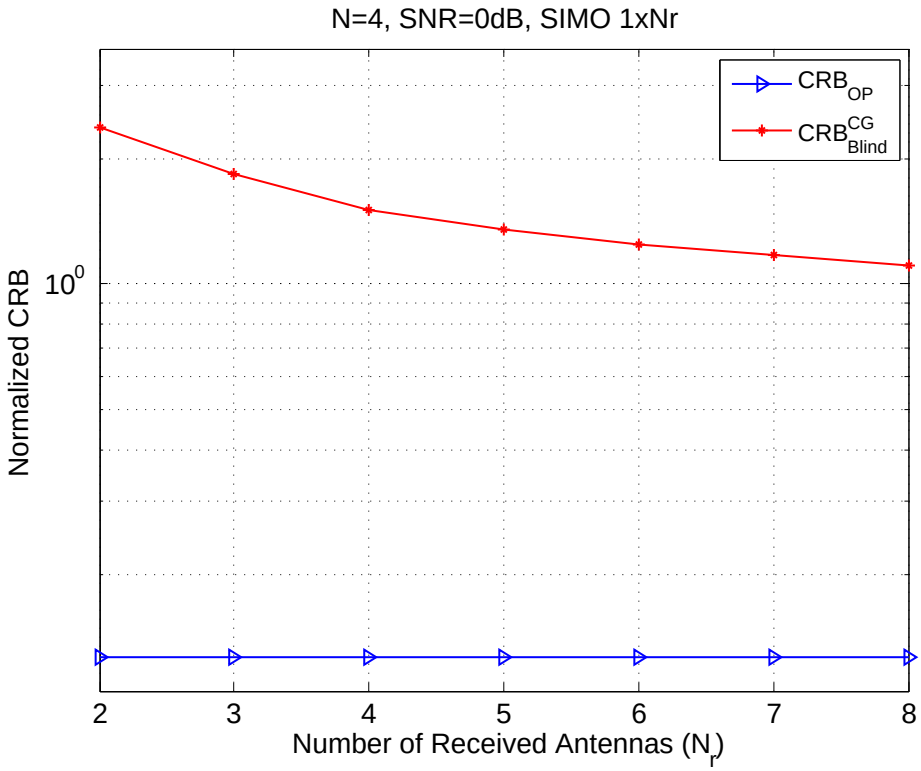

Figure 3.10: *Normalized CRB versus N_r ($SNR = 0$ dB).*

transmitted information between the drone and the mobile stations.

Figure 3.10, Figure 3.11 and Figure 3.12 show the impact of the number of the receive antennas on the blind channel estimation performance limits for three SIMO-OFDM system operating modes i.e. $SNR = 0$ dB, $SNR = +5$ dB and $SNR = -5$ dB (with the worst previous case i.e CG data model). Increasing the number of the receive antennas improves the blind channel estimation performance, but remains greater than the identification threshold ($CRB = 1$) in Figure 3.10 and Figure 3.12. However in Figure 3.11, the interceptor can estimate the channel taps then extracts the transmitted data.

3.7 Conclusion

This chapter focused on the theoretical limit of channel estimation performance in SIMO-OFDM wireless system. Analytical derivation of CRBs have been provided for: (i) pilot-based channel estimation (CRB_{OP}); (ii) blind channel estimation when data is assumed to be CG (CRB^{CG}_{Blind}), NCG (CRB^{NCG}_{Blind}); and (iii) semi-blind channel estimation when data is assumed to be deterministic (CRB^{Det}_{SB}) and stochastic Gaussian (CRB^{Stoch}_{SB}), respectively. the main outcomes of this study are:

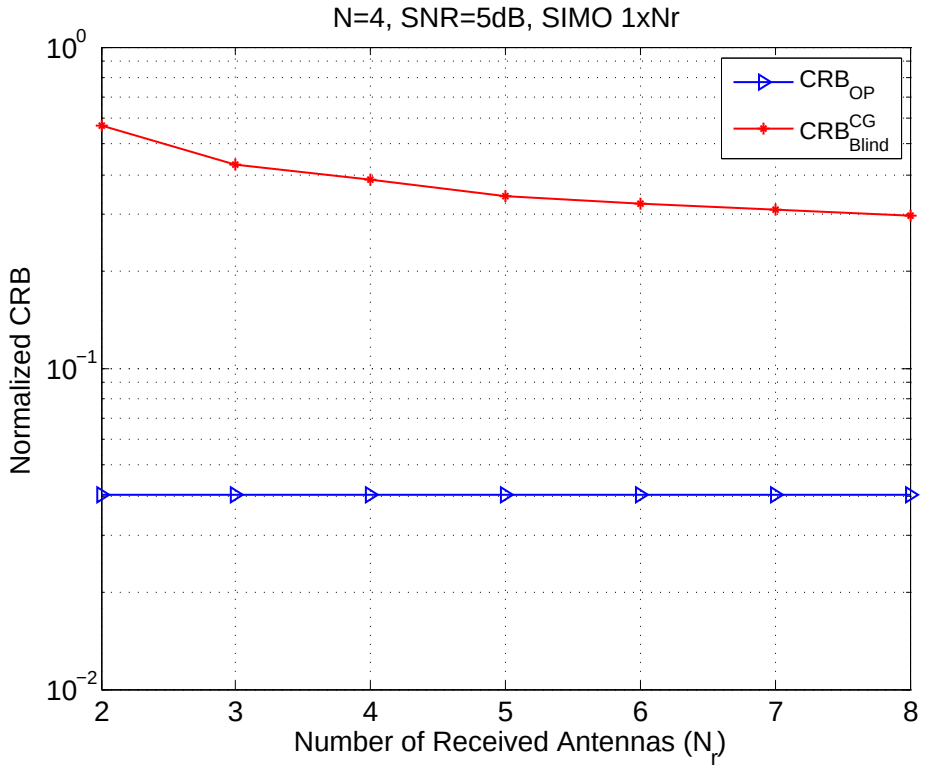

Figure 3.11: *Normalized CRB versus* N_r *(*$SNR = 5$ *dB).*

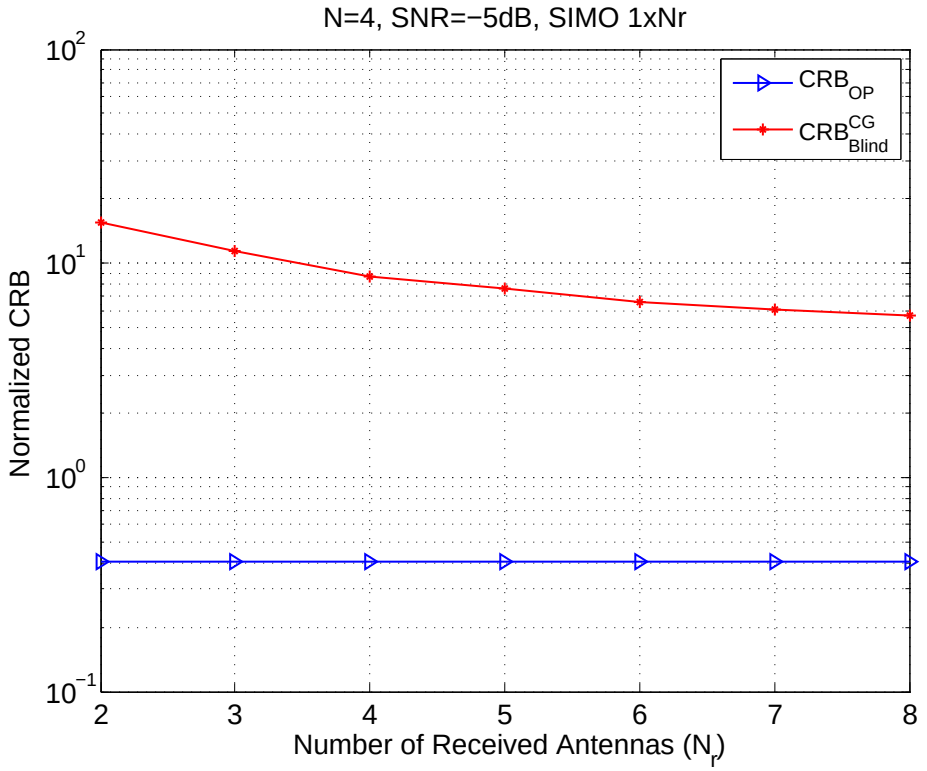

Figure 3.12: *Normalized CRB versus* N_r *(*$SNR = -5$ *dB).*

- In the context of IEEE 802.11n SIMO-OFDM system, the test results showed clearly the pilot samples reduction and consequently the throughput gain in SIMO-OFDM semi-blind channel estimation while maintaining the same pilot-based limit channel estimation quality.

- In the context of blind interception, the analysis of simulation results show that the worst blind channel estimation performance is obtained in the case of CG data model (CRB_{Blind}^{CG}) while an acceptable performance of pilot-based channel estimation is achieved. Therefore to avoid the interception of the information, the SIMO-OFDM communications system is tuned in such away to adjust the power of the CG data depending on the number of pilots and the length of the physical packet.

CHAPTER 4

Analysis of CFO and frequency domain channel estimation effects

In theory there is no difference between theory and practice. In practice there is.

Lawrence "Yogui" Berra,1925

Abstract

This study deals with semi-blind channel estimation CRB performance of MIMO-OFDM wireless communications system in the uplink transmission. The first contribution shows that the Carrier Frequency Offset (CFO) impacts advantageously the CRB of the semi-blind channel estimation mainly due to the CFO cyclostationarity propriety. The second contribution states that when the relation between the subcarrier channel coefficients is not taken into account, i.e. without resorting to the inherent OFDM 'channel structure' during the channel estimation, results in a loss of the estimation performance. An evaluation of the significant performance loss resulting from this approach is provided[1].

[1] [71] A. Ladaycia, A. Mokraoui, K. Abed-Meraim, and A. Belouchrani, "Further investigations on the performance bounds of MIMO-OFDM channel estimation," in The 13th International Wireless Communications and Mobile Computing Conference (IWCMC 2017), June 2017, pp. 223-228, Valance, Spain.

Chapter content

4.1 Introduction

MIMO-OFDM wireless communications system provides many advantages as the channel capacity enhancement and the improvement of the communications reliability. However to achieve good performance, the receiver should pay attention to compensate the time and frequency offsets before extracting the information from the transmitted physical packet. Indeed the Carrier Frequency Offset (CFO) affects the subcarriers orthogonality and degrades the OFDM system performance. A state of the art on this issue shows that the CFO estimation can be performed either on redundant information (Non-Data-Aided (NDA) approaches) or training sequences (Data-Aided (DA) approaches) included in the transmitted physical packet. DA approaches exploit training sequences either designed by authors or specified by some standards. In [72], the authors use null subcarriers and propose a suboptimal method to estimate the CFO. Pilot-based estimators have been discussed in [73], [74], [75] and [76] where the authors exploit cascaded orthogonal pilots to jointly estimate the CFO and CSI, which remains, in wireless communications system, a current concern since the overall system performance depends strongly on it.

This chapter studies the lower bounds performance of semi-blind channel estimation of a multiuser MIMO-OFDM wireless system in the uplink transmission for different receivers according to the strategies described below.

The objective of the first study is to show that, by exploiting the cyclostationarity introduced by the CFO to the NCG signals, the presence of Multiple CFO (MCFO), considered as a problem in MIMO-OFDM systems, improves the channel identification when semi-blind techniques using Zadoff Chu (ZC) training sequences are performed. To analyze the theoretical performance of this approach, the analytical CRB is derived. The CRBs, in the case of NCG signal with and without CFO, are then analyzed and discussed. To the best of our knowledge, despite the existing huge of literature on the considered topic, this analysis is the only one that investigates thoroughly how the CFO impacts the CRB of the semi-blind channel estimation advantageously.

The second study evaluates and compares the lower bounds performance for the estimation of the subcarrier channel coefficients with and without considering the OFDM structure (i.e. when taking into account the relation between these coefficients through the Fourier transform of the channel taps and when ignoring this relation in the estimation process). Indeed, for the sake of computational simplicity, many existing OFDM receivers estimate these channel coefficients as if they were 'independent' [77].

4.2 MIMO-OFDM communications system model in the presence of MCFO

Before describing the multiuser MIMO-OFDM wireless communications system adopted in this chapter, this section introduces some notations and assumptions.

The communications system is considered in the uplink transmission. It is composed of N_t transmit antennas associated with users sharing the same radio ressources and N_r receive antennas (see Figure 1.1) deployed on the same device (i.e. on a single transmitting base station). In this context, the receiver has a single local oscillator and each transmitter has its own local oscillator. Therefore the received signal may be affected by Multiple independent CFO (MCFO) introduced by the difference in local oscillator frequencies at the transmitters and receiver. Denote ν_i the normalized CFO occurred between the i-th transmitter local oscillator and the r-th user of the receiver local oscillator.

Each OFDM symbol is composed of K samples (i.e K subcarriers). A Cyclic Prefix (CP) of L samples (with $L \geq N$; N being the maximum delay of the channel) is inserted between consecutive OFDM symbols to prevent against Inter-Symbol Interference. These samples are chosen as the L last samples of the OFDM symbol preceding the CP.

The transmitted signal $\mathbf{x}$ is assumed to be independent Non-Circular complex-Gaussian (NCG). It is represented by the vector $\mathbf{x}$ of size $N_tK \times 1$ and is given by $\mathbf{x} = \left[\mathbf{x}_1^T \cdots \mathbf{x}_{N_t}^T\right]^T$ where $\mathbf{x}_i$ is the OFDM symbol transmitted by the i-th antenna; and $(.)^T$ represents the transpose operator. The covariance matrices for the transmitted signal $\mathbf{x}$ are expressed by:

$$\begin{aligned} \mathbf{C}_{\mathbf{x}} &= E\left[\mathbf{x}\mathbf{x}^H\right] = \text{diag}\left\{\sigma_{\mathbf{x}_1}^2 \cdots \sigma_{\mathbf{x}_{N_t}}^2\right\} \\ \mathbf{C'}_{\mathbf{x}} &= E\left[\mathbf{x}\mathbf{x}^T\right] = \rho_c \text{diag}\left\{e^{j\phi_1} \cdots e^{j\phi_{N_t}}\right\} \mathbf{C}_{\mathbf{x}}, \end{aligned} \tag{4.1}$$

where ρ_c is the non-circularity rate (with $0 < \rho_c < 1$); ϕ_i (with $i = 1, \cdots, N_t$) the non-circularity phases; $\sigma_{\mathbf{x}_i}^2$ the variance of the $\mathbf{x}_i$ OFDM symbol.

Denote $\mathbf{h}_{i,r}$ the vector Channel Impulse Response of size $N \times 1$ between the i-th transmitter and r-th receiver. The vector $\mathbf{v}$ of size $N_rK \times 1$ ($\mathbf{v} = \left[\mathbf{v}_1^T \cdots \mathbf{v}_{N_r}^T\right]^T$) is considered as an additive channel noise assumed to be independent white Complex-Gaussian Circular of zero-mean and variance $\sigma_{\mathbf{v}}^2$.

After removing the CP, the received discrete baseband signal $\mathbf{y}$ associated with the n_s-th OFDM symbol ($\mathbf{y} = \left[\mathbf{y}_1^T \cdots \mathbf{y}_{N_r}^T\right]^T$ of size $N_rK \times 1$), in time domain, is given in a matrix form as:

$$\mathbf{y} = \bar{\mathbf{\Lambda}}_{n_s}\mathbf{x} + \mathbf{v}, \tag{4.2}$$

where the matrix $\bar{\mathbf{\Lambda}}_{n_s}$ of size $N_rK \times N_tK$ is defined as:

$$\begin{aligned}
\bar{\mathbf{\Lambda}}_{n_s} &= \left[\bar{\mathbf{\Lambda}}_{n_s}^{1} \cdots \bar{\mathbf{\Lambda}}_{n_s}^{N_t}\right] \text{ with} \\
\bar{\mathbf{\Lambda}}_{n_s}^{i} &= \left(I_{N_r} \otimes \mathbf{\Gamma}_{n_s}(\nu_i)\right) \left[\mathbf{\Lambda}_{i,1}^{T} \cdots \mathbf{\Lambda}_{i,N_r}^{T}\right]^{T} \text{ and} \\
\mathbf{\Lambda}_{i,r} &= \frac{\mathbf{F}^H}{\sqrt{K}} \mathrm{diag}\left\{\mathbf{W}\mathbf{h}_{i,r}\right\},
\end{aligned} \tag{4.3}$$

where $\mathbf{\Lambda}_{i,r}$, $\bar{\mathbf{\Lambda}}_{n_s}^{i}$ are matrices of size $K \times K$ and $N_rK \times K$ respectively ; $\mathbf{F}$ the Discrete Fourier Transform matrix; $\mathbf{W}$ the N first columns of $\mathbf{F}$; and $\mathbf{\Gamma}_{n_s}(\nu_i)$ the normalized CFO matrix of size $K \times K$ at the n_s-th OFDM symbol given by:

$$\begin{aligned}
\mathbf{\Gamma}_{n_s}(\nu_i) = e^{j2\pi\nu_i(n_s-1)(K+L)/K} \times \\
\mathrm{diag}\left\{1, e^{j2\pi\nu_i/K}, \cdots, e^{j2\pi\nu_i(K-1)/K}\right\}.
\end{aligned} \tag{4.4}$$

To facilitate the CRB derivation for channel estimation in the next sections, equation (4.2) is rewritten in this form:

$$\mathbf{y} = \tilde{\mathbf{X}}\mathbf{h} + \mathbf{v}, \tag{4.5}$$

where $\mathbf{h}$ is the MIMO channel vector $\mathbf{h} = \left[\mathbf{h}_1^T \cdots \mathbf{h}_{N_r}^T\right]^T$ of size $NN_tN_r \times 1$ with $\mathbf{h}_r = \left[\mathbf{h}_{1,r}^T \cdots \mathbf{h}_{N_t,r}^T\right]^T$; and $\tilde{\mathbf{X}} = \mathbf{I}_{N_r} \otimes \mathbf{X}$ where the matrix $\mathbf{X}$ of size $K \times NN_t$ is defined by:

$$\begin{aligned}
\mathbf{X} = \Big[\mathbf{\Gamma}_{n_s}(\nu_1) \frac{\mathbf{F}^H}{\sqrt{K}} \mathrm{diag}\left\{\mathbf{x}_1\right\} \mathbf{W} \cdots \\
\mathbf{\Gamma}_{n_s}(\nu_{N_t}) \frac{\mathbf{F}^H}{\sqrt{K}} \mathrm{diag}\left\{\mathbf{x}_{N_t}\right\} \mathbf{W}\Big].
\end{aligned} \tag{4.6}$$

4.3 CRB for channel coefficients estimation in presence of MCFO

The aim of this section is to derive, in the presence of MCFO, the lower bound on the semi-blind channel estimator's variance (of unbiased estimators) using not only the known pilot OFDM symbols (i.e. training sequence) but also the encapsulated unknown data OFDM symbols in the physical packet. Figure 1.2a illustrates the block-type arrangement OFDM pilots in a physical packet adopted in this chapter.

The CRB for semi-blind channel estimation is deduced from the inverse of the complex FIM denoted $\mathbf{J}_{\boldsymbol{\theta\theta}}$ which is composed of the FIMs associated to pilots and data, derived as follows.

4.3.1 FIM for known pilot OFDM symbols

This section, based on equations (4.2) and (4.5), focuses on the derivation of the FIM $\mathbf{J}_{\boldsymbol{\theta\theta}}^{p}$ when only N_p received pilot OFDM symbols are used to estimate the MIMO channel. The vector of parameters is then defined as:

$$\boldsymbol{\theta} = \left[\mathbf{h}^T \ \mathbf{h}^{*T} \ \boldsymbol{\nu}^T \ {\sigma_{\mathbf{v}}}^2\right]^T, \tag{4.7}$$

where $\boldsymbol{\nu}$ is the MCFO vector given by $[\nu_1 \cdots \nu_{N_t}]^T$.

Since the channel noise is assumed to be i.i.d., the FIM for $\boldsymbol{\theta}$ when N_p pilot OFDM symbols are used is deduced as:

$$\mathbf{J}^{p}_{\boldsymbol{\theta\theta}} = \sum_{i=1}^{N_p} \mathbf{J}^{p_i}_{\boldsymbol{\theta\theta}}, \tag{4.8}$$

where $\mathbf{J}^{p_i}_{\boldsymbol{\theta\theta}}$ is the FIM associated with the i-th pilot OFDM symbol defined as:

$$\mathbf{J}^{p_i}_{\boldsymbol{\theta\theta}} = \begin{bmatrix} \mathbf{J_{hh}} & \mathbf{J_{hh^*}} & \mathbf{J_{h\nu}} & \mathbf{J_{h\sigma_v^2}} \\ \mathbf{J_{h^*h}} & \mathbf{J_{h^*h^*}} & \mathbf{J_{h^*\nu}} & \mathbf{J_{h^*\sigma_v^2}} \\ \mathbf{J_{\nu h}} & \mathbf{J_{\nu h^*}} & \mathbf{J_{\nu\nu}} & \mathbf{J_{\nu\sigma_v^2}} \\ \mathbf{J_{\sigma_v^2 h}} & \mathbf{J_{\sigma_v^2 h^*}} & \mathbf{J_{\sigma_v^2\nu}} & \mathbf{J_{\sigma_v^2\sigma_v^2}} \end{bmatrix}. \tag{4.9}$$

Each sub-matrix, $\mathbf{J}_{\theta_i\theta_j}$ (with θ_i, $\theta_j \in \boldsymbol{\Theta}$), is deduced according to:

$$\mathbf{J_{\theta_i\theta_j}} = \mathrm{E}\left\{ \left(\frac{\partial \ln p(\mathbf{y}(i), \boldsymbol{\theta})}{\partial \theta_{\mathbf{i}}^*} \right) \left(\frac{\partial \ln p(\mathbf{y}(i), \boldsymbol{\theta})}{\partial \theta_{\mathbf{j}}^*} \right)^H \right\} \tag{4.10}$$

where E(.) is the expectation operator; and $p(\mathbf{y}(i), \boldsymbol{\theta})$ the probability density function of the received baseband signal given $\boldsymbol{\theta}$.

Based on the complex derivative ($\frac{\partial}{\partial \theta^*} = \frac{1}{2}\left(\frac{\partial}{\partial \alpha} + j\frac{\partial}{\partial \beta}\right)$ for $\theta = \alpha + j\beta$), the derivation of equation (4.10) leads to:

$$\mathbf{J}_{\theta_i\theta_j} = \frac{1}{\sigma_v^2} \left(\frac{\partial \left(\tilde{\mathbf{X}}\mathbf{h} \right)}{\partial \theta_i^*} \right)^H \left(\frac{\partial \left(\tilde{\mathbf{X}}\mathbf{h} \right)}{\partial \theta_j^*} \right) \text{ with } \theta_i,\, \theta_j \in \boldsymbol{\Theta}. \tag{4.11}$$

4.3.2 FIM for unknown data OFDM symbols

This section, based on equations (4.2) and (4.5), deals with the derivation of the FIM $\mathbf{J}^{d}_{\boldsymbol{\theta\theta}}$ when N_d unknown transmitted OFDM data symbols are used to estimate the MIMO channel. The vector of parameters is defined as:

$$\boldsymbol{\theta} = \left[\mathbf{h^T}\ \mathbf{h^{*T}}\ \boldsymbol{\Sigma}_{\mathbf{x}}^{\mathbf{T}}\ \boldsymbol{\Phi}^{\mathbf{T}}\ \boldsymbol{\nu}^{\mathbf{T}}\ \rho_{\mathbf{c}}\ \sigma_{\mathbf{v}}^{\mathbf{2}} \right]^T, \tag{4.12}$$

where $\boldsymbol{\Sigma}_{\mathbf{x}} = \left[\sigma^2_{\mathbf{x}_1} \cdots \sigma^2_{\mathbf{x}_{N_t}} \right]^T$ and $\boldsymbol{\Phi} = [\phi_1 \cdots \phi_{N_t}]^T$.

Since the channel noise is assumed to be i.i.d., the FIM for N_d unknown OFDM symbols is then expressed as:

$$\mathbf{J}^{d}_{\boldsymbol{\theta\theta}} = \sum_{n_s=1}^{N_d} \mathbf{J}^{d_{n_s}}_{\boldsymbol{\theta\theta}}, \tag{4.13}$$

where $\mathbf{J}_{\boldsymbol{\theta\theta}}^{d_{n_s}}$ is the FIM of the n_s-th data OFDM symbol defined as:

$$\mathbf{J}_{\boldsymbol{\theta\theta}}^{d_{n_s}} = \begin{bmatrix} \mathbf{J_{hh}} & \mathbf{J_{hh^*}} & \mathbf{J_{h\Sigma_x}} & \mathbf{J_{h\Phi}} & \mathbf{J_{h\nu}} & \mathbf{J_{h\rho_c}} & \mathbf{J_{h\sigma_v^2}} \\ \mathbf{J_{h^*h}} & \mathbf{J_{h^*h^*}} & \mathbf{J_{h^*\Sigma_x}} & \mathbf{J_{h^*\Phi}} & \mathbf{J_{h^*\nu}} & \mathbf{J_{h^*\rho_c}} & \mathbf{J_{h^*\sigma_v^2}} \\ \mathbf{J_{\Sigma_x h}} & \mathbf{J_{\Sigma_x h^*}} & \mathbf{J_{\Sigma_x\Sigma_x}} & \mathbf{J_{\Sigma_x\Phi}} & \mathbf{J_{\Sigma_x\nu}} & \mathbf{J_{\Sigma_x\rho_c}} & \mathbf{J_{\Sigma_x\sigma_v^2}} \\ \mathbf{J_{\Phi h}} & \mathbf{J_{\Phi h^*}} & \mathbf{J_{\Phi\Sigma_x}} & \mathbf{J_{\Phi\Phi}} & \mathbf{J_{\Phi\nu}} & \mathbf{J_{\Phi\rho_c}} & \mathbf{J_{\Phi\sigma_v^2}} \\ \mathbf{J_{\nu h}} & \mathbf{J_{\nu h^*}} & \mathbf{J_{\nu\Sigma_x}} & \mathbf{J_{\nu\Phi}} & \mathbf{J_{\nu\nu}} & \mathbf{J_{\nu\rho_c}} & \mathbf{J_{\nu\sigma_v^2}} \\ \mathbf{J_{\rho_c h}} & \mathbf{J_{\rho_c h^*}} & \mathbf{J_{\rho_c\Sigma_x}} & \mathbf{J_{\rho_c\Phi}} & \mathbf{J_{\rho_c\nu}} & \mathbf{J_{\rho_c\rho_c}} & \mathbf{J_{\rho_c\sigma_v^2}} \\ \mathbf{J_{\sigma_v^2 h}} & \mathbf{J_{\sigma_v^2 h^*}} & \mathbf{J_{\sigma_v^2\Sigma_x}} & \mathbf{J_{\sigma_v^2\Phi}} & \mathbf{J_{\sigma_v^2\nu}} & \mathbf{J_{\sigma_v^2\rho_c}} & \mathbf{J_{\sigma_v^2\sigma_v^2}} \end{bmatrix}. \tag{4.14}$$

The FIM, $\mathbf{J}_{\theta_i\theta_j}$ (with θ_i, $\theta_j \in \boldsymbol{\Theta}$), has been derived in [36], [40], [39] and is expressed as:

$$\mathbf{J}_{\theta_i\theta_j} = \frac{1}{2} tr\left\{ \tilde{\mathbf{C}}_{YY}^{-1} \frac{\partial \tilde{\mathbf{C}}_{YY}}{\partial \boldsymbol{\theta}_i^*} \tilde{\mathbf{C}}_{YY}^{-1} \left(\frac{\partial \tilde{\mathbf{C}}_{YY}}{\partial \boldsymbol{\theta}_j^*} \right)^H \right\}, \tag{4.15}$$

where

$$\tilde{\mathbf{C}}_{YY} = \begin{bmatrix} \mathbf{C}_{YY} & \mathbf{C'}_{YY} \\ \mathbf{C'}^*_{YY} & \mathbf{C}^*_{YY} \end{bmatrix}, \tag{4.16}$$

with

$$\mathbf{C}_{YY} = \sum_{i=1}^{N_t} \sigma_{\mathbf{x}_i}^2 \bar{\mathbf{\Lambda}}_{n_s}^i \left(\bar{\mathbf{\Lambda}}_{n_s}^i \right)^H + {\sigma_{\mathbf{v}}}^2 \mathbf{I}_{KN_r}, \tag{4.17}$$

$$\mathbf{C'}_{YY} = \sum_{i=1}^{N_t} \rho_c e^{j\phi_i} \sigma_{\mathbf{x}_i}^2 \bar{\mathbf{\Lambda}}_{n_s}^i \left(\bar{\mathbf{\Lambda}}_{n_s}^i \right)^T. \tag{4.18}$$

The FIM $\mathbf{J}_{\theta_i\theta_j}$ also requires the following information:

$$\frac{\partial \tilde{\mathbf{C}}_{YY}}{\partial \sigma_{\mathbf{x}_i}^2} = \frac{1}{2} \begin{bmatrix} \bar{\mathbf{\Lambda}}_{n_s}^i \left(\bar{\mathbf{\Lambda}}_{n_s}^i \right)^H & \rho_c e^{j\phi_i} \bar{\mathbf{\Lambda}}_{n_s}^i \left(\bar{\mathbf{\Lambda}}_{n_s}^i \right)^T \\ \rho_c e^{-j\phi_i} \left(\bar{\mathbf{\Lambda}}_{n_s}^i \right)^* \left(\bar{\mathbf{\Lambda}}_{n_s}^i \right)^H & \left(\bar{\mathbf{\Lambda}}_{n_s}^i \right)^* \left(\bar{\mathbf{\Lambda}}_{n_s}^i \right)^T \end{bmatrix}, \tag{4.19}$$

$$\frac{\partial \tilde{\mathbf{C}}_{YY}}{\partial \phi_i} = \frac{1}{2} \left(j\phi_i \rho_c \sigma_{\mathbf{x}_i}^2 \right) \times \begin{bmatrix} 0 & e^{j\phi_i} \bar{\mathbf{\Lambda}}_{n_s}^i \left(\bar{\mathbf{\Lambda}}_{n_s}^i \right)^T \\ -e^{-j\phi_i} \left(\bar{\mathbf{\Lambda}}_{n_s}^i \right)^* \left(\bar{\mathbf{\Lambda}}_{n_s}^i \right)^H & 0 \end{bmatrix}, \tag{4.20}$$

$$\frac{\partial \tilde{\mathbf{C}}_{YY}}{\partial \rho_c} = \frac{1}{2\rho_c} \begin{bmatrix} 0 & \mathbf{C'}_{YY} \\ \mathbf{C'}^*_{YY} & 0 \end{bmatrix}, \tag{4.21}$$

$$\frac{\partial \tilde{\mathbf{C}}_{YY}}{\partial \sigma_{\mathbf{v}}^2} = \frac{1}{2} \mathbf{I}_{2KN_r}. \tag{4.22}$$

The computation of $\frac{\partial \tilde{\mathbf{C}}_{YY}}{\partial h_i^*}$ for each $i = 1, \cdots, NN_rN_t$ provides:

$$\frac{\partial \tilde{\mathbf{C}}_{YY}}{\partial h_i^*} = \begin{bmatrix} \mathbf{D}_1 & 0 \\ \mathbf{D}_2 + \mathbf{D}_2^T & \mathbf{D}_1^T \end{bmatrix}, \tag{4.23}$$

where

$$\begin{aligned}\mathbf{D}_1 &= \sigma^2_{\mathbf{x}_{i_{N_t}}} \bar{\mathbf{\Lambda}}^{i_{N_t}}_{n_s} \frac{\partial\left(\bar{\mathbf{\Lambda}}^{i_{N_t}}_{n_s}\right)^H}{\partial h_i^*} \\ \mathbf{D}_2 &= \rho_c e^{j\phi_{i_{N_t}}} \sigma^2_{\mathbf{x}_{i_{N_t}}} \left(\bar{\mathbf{\Lambda}}^{i_{N_t}}_{n_s}\right)^* \frac{\partial\left(\bar{\mathbf{\Lambda}}^{i_{N_t}}_{n_s}\right)^H}{\partial h_i^*}.\end{aligned} \tag{4.24}$$

for $i_{N_t} = 1, \cdots, N_t$; $i_{N_r} = 1, \cdots, N_r$; and $i_N = 1, \cdots, N$.

Once the FIM $\mathbf{J}_{\boldsymbol{\theta\theta}}$ deduced as described above (from equations (4.8) and (4.13)), the CRB for semi-blind channel estimation in the presence of MCFO, denoted $CRB^{MCFO}_{NCG}(\mathbf{h})$, is extracted from the $\mathbf{h}$-block of the computed CRB.

4.4 CRB for subcarrier channel coefficient estimation

This section assumes that the mobile stations of the previous communications system are perfectly synchronized (i.e. $\nu_i = 0$). In this context, the DFT applied to equation (4.3) results in:

$$\begin{aligned}\bar{\mathbf{\Lambda}}_{n_s} &= \left[\bar{\mathbf{\Lambda}}^1_{n_s} \cdots \bar{\mathbf{\Lambda}}^{N_t}_{n_s}\right] \text{ with} \\ \bar{\mathbf{\Lambda}}^i_{n_s} &= \left[\underline{\mathbf{\Lambda}}^T_{i,1} \cdots \underline{\mathbf{\Lambda}}^T_{i,N_r}\right]^T \text{ and} \\ \underline{\mathbf{\Lambda}}_{i,r} &= \mathrm{diag}\left\{\boldsymbol{\lambda}_{i,r}\right\}, \text{ where} \\ \boldsymbol{\lambda}_{i,r} &= \mathbf{W}\mathbf{h}_{i,r}.\end{aligned} \tag{4.25}$$

For the sake of computational simplicity, instead of estimating the channel taps, many existing OFDM receivers estimate the subcarrier channel coefficients (i.e. the vector $\boldsymbol{\lambda}_{i,r}$) as if they were 'independent' (see e.g. [77]). The aim of this section is to derive the CRB for these subcarrier channel coefficients estimation without considering the OFDM structure (i.e. ignoring the relation between these coefficients through the Fourier transform of the channel taps).

The CRB, denoted $CRB_{NCG}(\boldsymbol{\lambda})$, requires the computation of the FIM where the complex parameter $\mathbf{\Theta_c}$ of the unknown vector parameters $\mathbf{\Theta}$ is:

$$\mathbf{\Theta}_c = \left[\boldsymbol{\lambda}^T_{i,r} \cdots \boldsymbol{\lambda}^T_{N_t,N_r}\right]^T. \tag{4.26}$$

The vector of the unknown real parameters $\boldsymbol{\theta}_r$ of the unknown vector parameters $\mathbf{\Theta}$ corresponds to:

$$\boldsymbol{\theta}_r = \left[\mathbf{\Sigma_x^T}\ \mathbf{\Phi^T}\ \rho_\mathbf{c}\ \sigma_\mathbf{v}^\mathbf{2}\right]^T. \tag{4.27}$$

Since the stations are synchronized (i.e. $\nu_i = 0$), the FIM $\mathbf{J}_{\boldsymbol{\theta\theta}}$ for the vector $\boldsymbol{\theta}$, compared to the previous section, is deduced from the FIM of one data (i.e $\mathbf{J}^{n_s=n_1}_{\boldsymbol{\theta\theta}}$) or pilot (i.e. $\mathbf{J}^{p_i=p_1}_{\boldsymbol{\theta\theta}}$) OFDM symbol using equations from (4.15) to (4.24). $\mathbf{J}^{n_1}_{\boldsymbol{\theta\theta}}$ (respectively $\mathbf{J}^{p_1}_{\boldsymbol{\theta\theta}}$) is then multiplied by the number of data i.e. N_d (respectively N_p) OFDM symbols as follows: $\mathbf{J}_{\boldsymbol{\theta\theta}} = N_p\mathbf{J}^{p_1}_{\boldsymbol{\theta\theta}} + N_d\mathbf{J}^{d_{n_1}}_{\boldsymbol{\theta\theta}}$.

Note that $\mathbf{J}_{\theta_i\theta_j}$ for the channel taps, given in the previous section, is replaced by the FIM computed for the subcarrier coefficients.

As in Section 4.3, the CRB for the subcarrier channel coefficients, denoted $CRB_{NCG}(\boldsymbol{\lambda})$, is then extracted from the $\boldsymbol{\lambda}$-block of the computed CRB. The lower bounds performance of the semi-blind channel estimation using both strategies (i.e. $CRB_{NCG}(\boldsymbol{\lambda})$, $CRB_{NCG}^{MCFO=0}(\mathbf{h})$) will be discussed in the following section.

4.5 Simulation results

This section analyzes the lower bounds performance of the semi-blind channel estimators (i.e. $CRB_{OP}^{MCFO}(\mathbf{h})$, $CRB_{NCG}^{MCFO}(\mathbf{h})$, $CRB_{NCG}(\mathbf{h})$ (without MCFO) and $CRB_{NCG}(\boldsymbol{\lambda})$) derived in the previous section.

4.5.1 Experimental settings

Zadoff-Chu (ZC) sequences, used in the LTE standard [4], are adopted as pilot training sequences. ZC sequence is given by the following equation:

$$x_u(k) = e^{-\frac{j\pi uk^2}{K}}, \tag{4.28}$$

when the sequence length, denoted K, is even and $u \in \{1,3,5\cdots K-1\}$ being the sequence index [42].

The simulation parameters being as follows: $N=4$ (channel length); $N_p=1$ (number of pilot OFDM symbols); $N_d=40$ (number of data OFDM symbols); $K=64$ (number of sib-carriers); $L=16$ (length of CP); $P_{x_p}=10$dBm (power of the pilot signal); $P_{x_d}=90$dBm (power of the data signal); ρ_c =0.9 (non-circularity rate); $\phi=[\frac{\pi}{4},\frac{\pi}{2},\frac{\pi}{3},\frac{\pi}{6}]$ (Non-circularity phase); and $\nu=[0.015,0.5,0.4,0.025]$ (Normalized CFO).

4.5.2 Channel estimation performance analysis

Figure 4.1 and Figure 4.2 illustrate the normalized $CRB\left(\frac{tr\{CRB\}}{\|\mathbf{h}\|^2}\right)$ versus SNR when: (i) only pilots are exploited to estimate the channel in presence of MCFO (i.e. $CRB_{OP}^{MCFO}(\mathbf{h})$); (ii) semi-blind channel estimation in presence of MCFO (i.e. $CRB_{NCG}^{MCFO}(\mathbf{h})$); and (iii) semi-blind channel estimation when the stations are perfectly synchronized (i.e. $CRB_{NCG}(\mathbf{h})$).

Figure 4.1 considers (2×2) MIMO-OFDM system using the following parameters: $N_p=1$; $N_d=40$; two normalized CFOs equal to 0.015 and 0.5. The CRB curves show clearly that the CRB of semi-blind channel estimation, in the presence or absence of MCFO, are lower than the

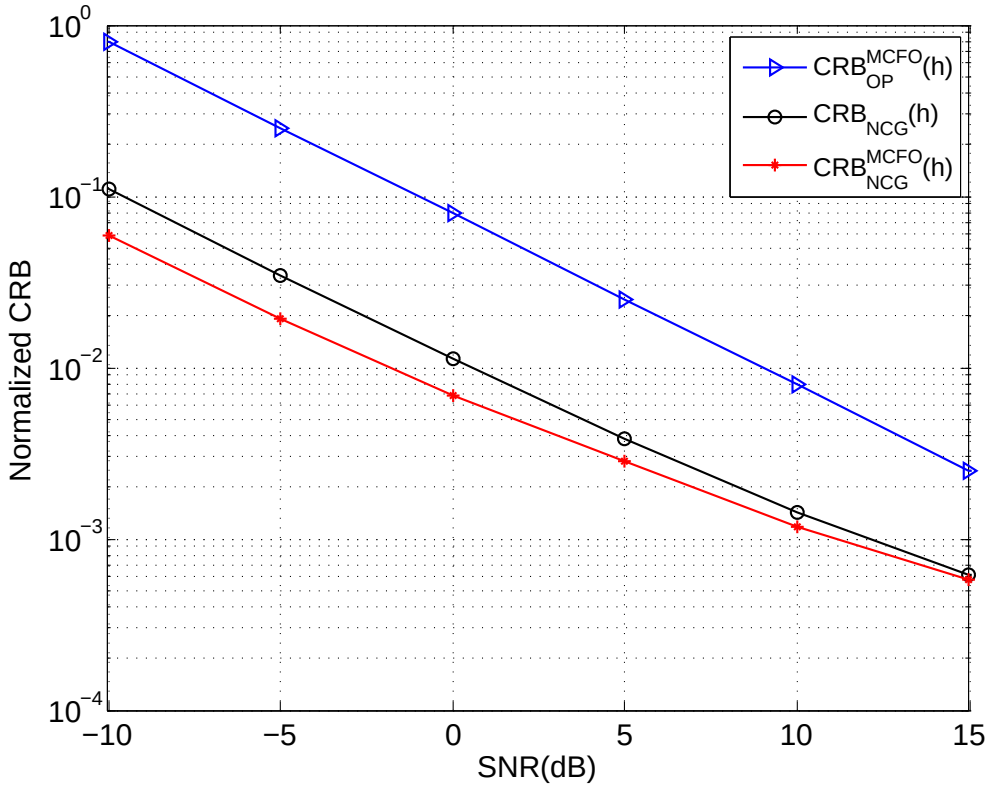

Figure 4.1: *Normalized CRB versus SNR (with and without MCFO).*

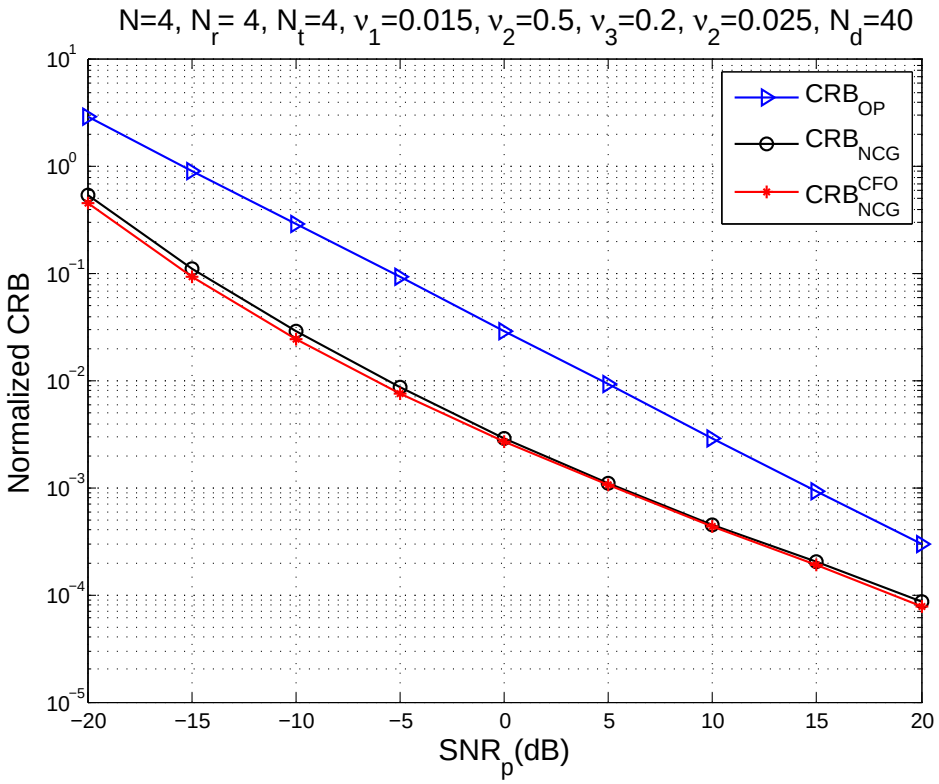

Figure 4.2: *Normalized CRB versus SNR (with* (4×4) *MIMO-OFDM).*

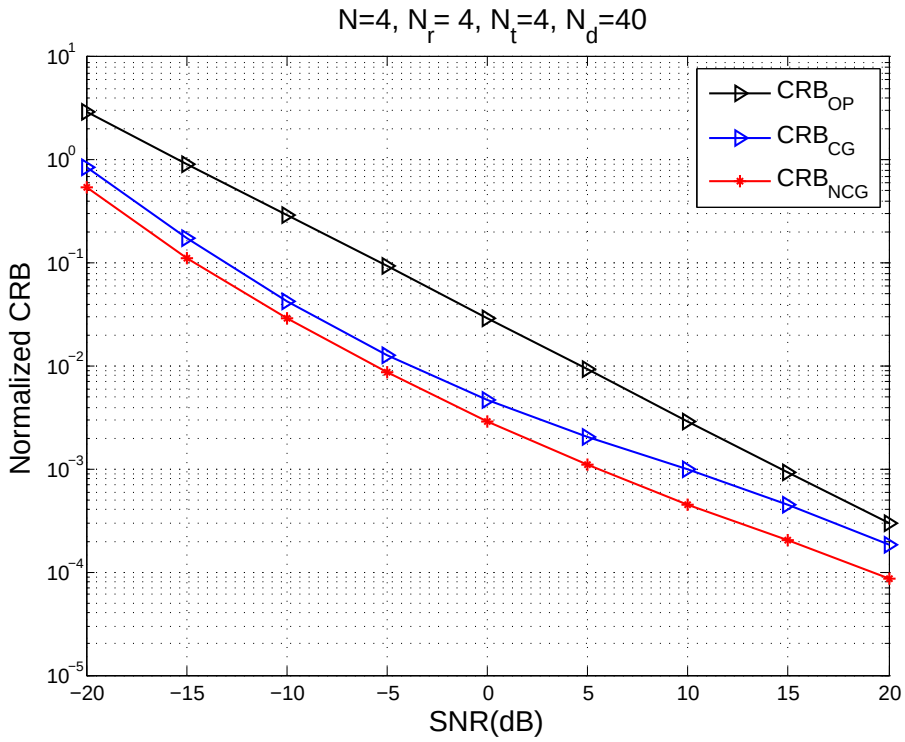

Figure 4.3: *Normalized CRB versus SNR with circular Gaussian and non-circular Gaussian signals (with* (4×4) *MIMO-OFDM).*

CRB when only pilots are used. Moreover the CRB in the presence of MCFO (CRB_{NCG}^{MCFO}) is about 3 dB lower than the CRB when the transmitters and receiver are perfectly synchronized ($CRB_{NCG}(\mathbf{h})$). Although the CFO being a traditional problem when only pilots are used to estimate the channel, the gain of 3 dB proves however to be an advantage in semi-blind channel identification. Figure 4.2 provides additional results in (4×4) MIMO-OFDM system and confirm our analysis.

Figure 4.3 provides the Circular and Non-circular Gaussian CRBs if (4×4) MIMO-OFDM system. Even thought the vector of the unknown parameters θ is larger, the CRB corresponding to NCG data signal is lower than the CRB corresponding to the CG signal.

For a given $SNR = 6$ dB (around the operating mode of the IEEE 802.11n), Figure 4.4 presents the normalized CRB of the semi-blind channel estimation in the presence and absence of MCFO (i.e. $CRB_{NCG}(\mathbf{h})$ and $CRB_{NCG}^{MCFO}(\mathbf{h})$) versus the number of data OFDM symbols (N_d). The analysis of the curves confirms the traditional result which states that when the number of symbols to estimate the channel increases, the estimation performance is better. Moreover, this analysis clearly shows the contribution of MCFO on the performance improvement of the channel estimation.

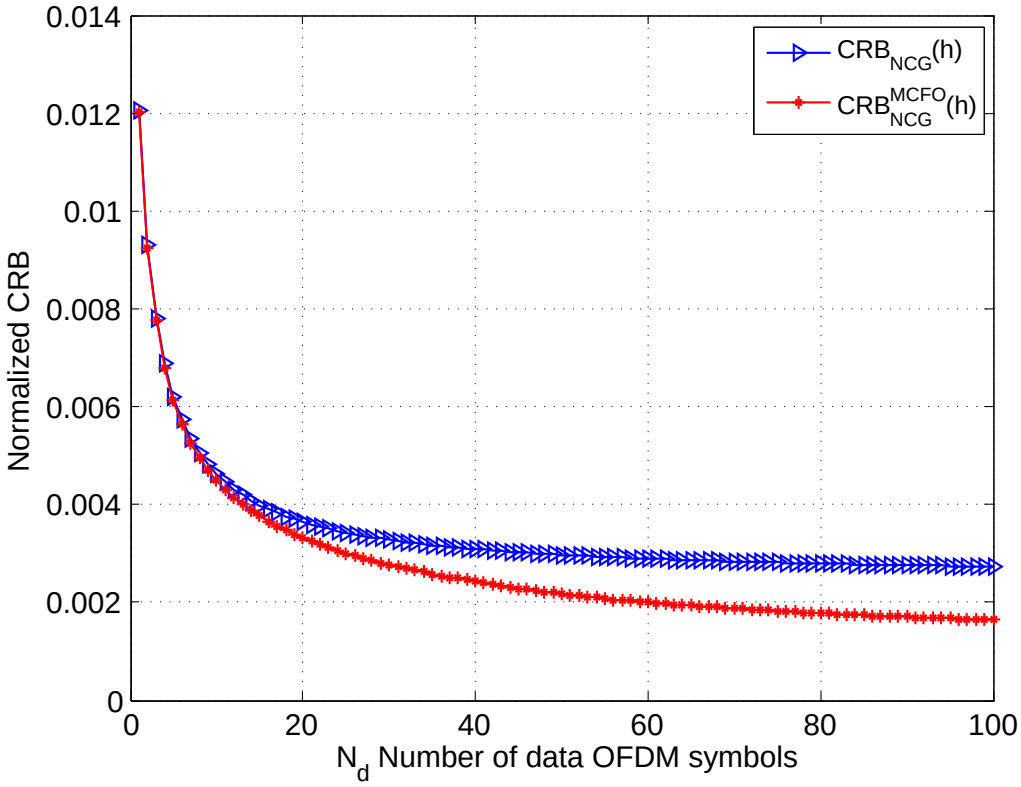

Figure 4.4: *Normalized CRB versus N_d (with $SNR = 6$ dB).*

Figure 4.5 compares the $CRB_{NCG}(\boldsymbol{\lambda})$ of the subcarrier channel coefficient estimation to the $CRB_{NCG}(\mathbf{h})$ of the channel taps estimation. A large gain (larger than 15 dB) is observed in favor of the situation where the channel structure (given by (4.3)) is taken into account in the estimation process. This study shows that the price paid for this simplicity is 'too high' as the performance loss (in terms of estimation accuracy) might be quite significant as illustrated by the simulation example. Moreover, note that when the CBR of $\boldsymbol{\lambda}$ is derived directly from the CRB of $\mathbf{h}$, the limit performance bound achieved by the CRB of $\mathbf{h}$ is recovered. This discussion remains valid when only pilots ($CRB_{OP}(\boldsymbol{\lambda})$, $CRB_{PO}(\mathbf{h})$) are exploited for the channel estimation. Figure 4.6 provides additional results in (4×4) MIMO-OFDM system and confirm our results.

Note that when a comb-type pilot arrangement (see Figure 1.2b) is used, the performance bounds of a MIMO-OFDM channel estimation (after some changes in the developed equations) remain similar to those provided by Figure 4.1, Figure 4.4 and Figure 4.5.

4.6 Conclusion

This chapter focused on lower bounds performance of the semi-blind channel identification in a multiuser MIMO-OFDM wireless communications system, in the uplink transmission, considering

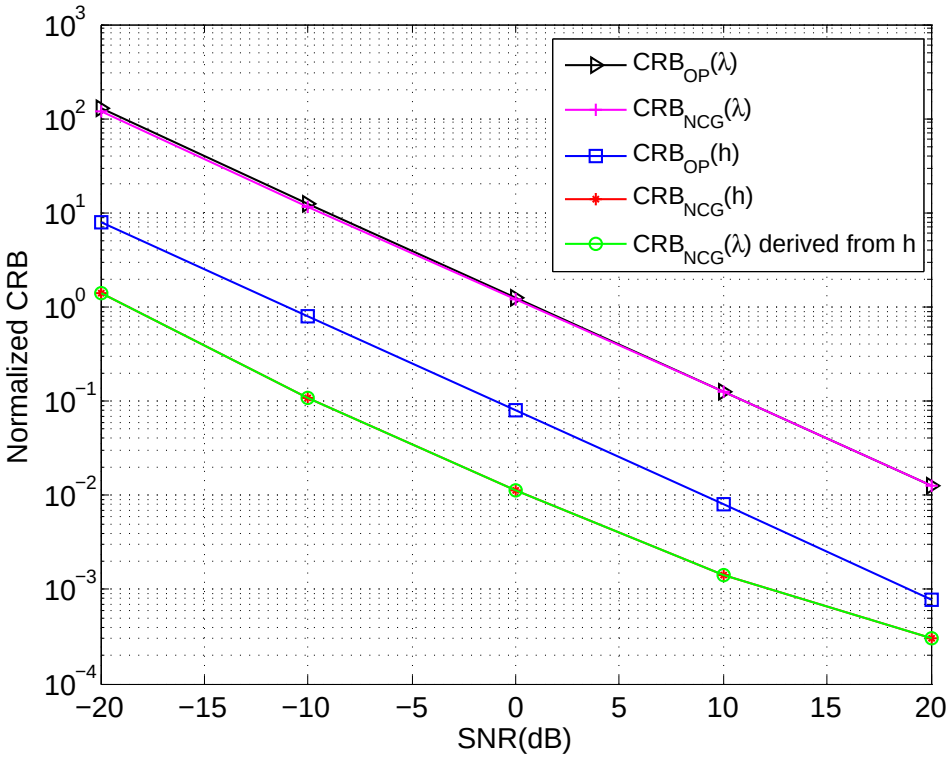

Figure 4.5: *Normalized CRB for the subcarrier channel coefficients estimation.*

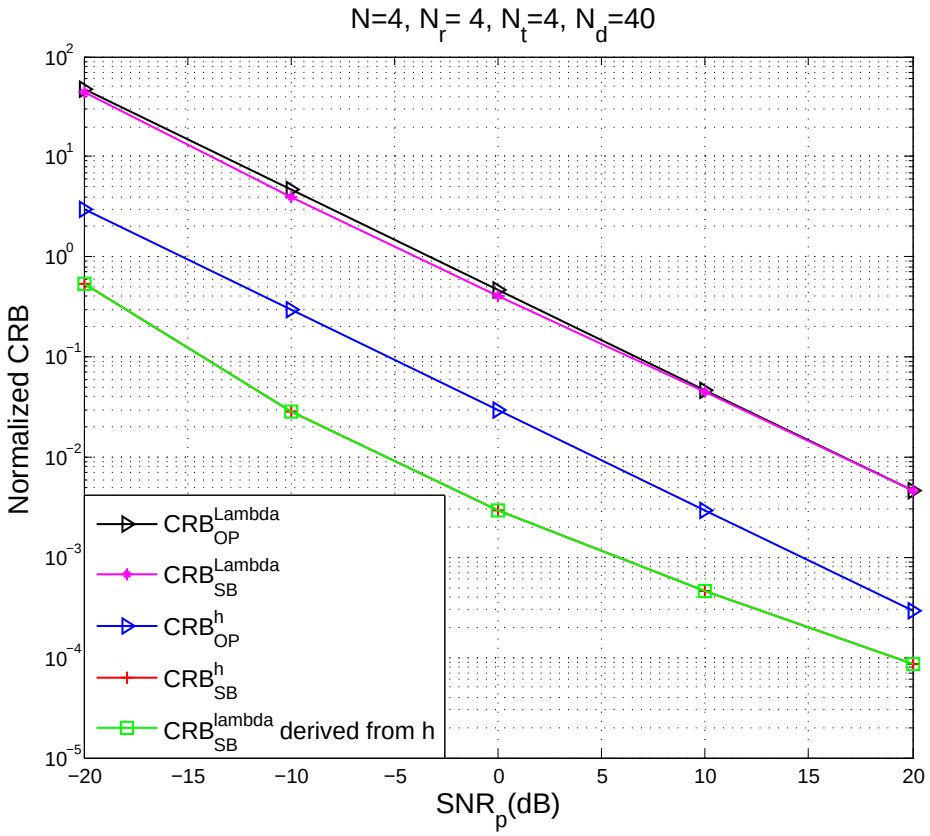

Figure 4.6: *Normalized CRB for the subcarriers channel coefficients estimation ((4×4) MIMO-OFDM).*

a NCG data model. Two important results have been derived as follow:

- The first one is related to the impact of the CFO on the improvement of the $CRB_{NCG}^{MCFO}(\mathbf{h})$ compared to the $CRB_{NCG}(\mathbf{h})$ without CFO.
- The second one, is based on the approach that estimates the subcarrier channel coefficients only for sake of simplicity. This strategy proved that the price paid for this simplicity is too high because the $CRB_{NCG}(\boldsymbol{\lambda})$ performance loss might be quite significant compared to the $CRB_{NCG}(\mathbf{h})$ of the channel taps estimation.

Part II

Proposed semi-blind channel estimation approaches

CHAPTER 5

Least Squares Decision Feedback (LS-DF) Semi-blind estimator

To get what you love, you must
first be patient with what you hate.

Al-Ghazali.

Abstract

This chapter proposes a Least Square Decision Feedback (LS-DF) semi-blind channel estimator showing that a reduction of 76% of the pilot's power is obtained compared to the LS pilot-based estimator for the same channel estimation performance. The LS-DF performance are compared then to the theoretical maximum power reduction of the transmitted pilots when semi-blind channel estimator is deployed while ensuring the same pilot-based channel estimation performance for BPSK/QPSK data models and a block-type pilot arrangement as specified in the IEEE 802.11n standard. The detailed description of our proposed algorithm has been published in the conference EUSIPCO 2017[1]

[1] [33] A. Ladaycia, A. Mokraoui, K. Abed-Meraim, and A. Belouchrani, "Toward green communications using semi-blind channel estimation," in 2017 25th European Signal Processing Conference (EUSIPCO), Aug. 2017, pp. 2254-2258, Kos, Greece.

Chapter content

5.1 Introduction

Channel estimation is of paramount importance to equalization and symbol detection problems in most wireless communications systems. This task is achieved using blind channel estimation methods (e.g. [24]), or based on pilots [20, 21]. However these pilots consume not only a large part of throughput but also significant power resources. This becomes even more important for future communications systems such as massive-MIMO systems. Indeed the explosive growth of high data rate applications where the corresponding energy consumption is also growing at a staggering rate has urged for an intensive research work on green communications to protect our environment and cope with global warming [78]. In [66], the throughput problem has been investigated for SIMO-OFDM systems. In [79], authors present the state-of-the-art of the green communications methods. Antenna selection using beamforming algorithm is proposed in [80].

This study suggests an unusual approach to reduce the consumed power making the most of the advantages of semi-blind channel estimation approaches. The underlying idea consists of removing pilot samples which are replaced by zero-samples while ensuring the same performance as pilot-based channel estimation approaches. The maximal reduction of the theoretical transmitted pilot's power is first addressed when semi-blind approaches are deployed instead of pilot-based approaches for the same estimation performance. To do so, the theoretical limit channel estimation performance, based on the analytical CRB, is considered. The real gain in terms of pilot's power reduction at the transmitter is then evaluated when Least Square Decision Feedback (LS-DF) semi-blind channel estimator is used. In addition, the overconsumption at the receiver is evaluated and discussed.

5.2 LS-DF semi-blind channel estimation algorithm

The MIMO-OFDM system model adopted in this study is given in chapter 1 as depicted in Figure 1.1. Moreover, the CRBs derived in chapter 1 (subsection 1.4.3 for alphabet finite (BPSK and QPSK) modulation), are used quantify the theoretical limit power reduction of the transmitted pilots without affecting the channel estimation quality. This will be used to compute the power saving due to this shortening at the transmitter side. For comparison fairness, we need to evaluate to power consumption increase at the receiver side due to the use of a more elaborate semi-blind estimation algorithm. For this reason, we introduce in this section a semi-blind estimation method that has the advantages of simplicity and effectiveness (i.e. it reaches the CRB for moderate and high SNRs).

5.2.1 Main steps of the LS-DF algorithm

The LS-DF channel estimation algorithm is considered as a LS estimator which incorporates the feedback equalizer. Traditionally the LS-DF algorithm re-injects the estimated signal as a feedback to the equalizer stage to enhance the estimation performance of the transmitted data. This process is iterated several times.

Instead of using the LS-DF algorithm in its original version, this study exploits this algorithm as a semi-blind channel estimator since the estimated data at the previous stage are now considered as "pilots" when the algorithm re-estimates the channel taps according to the LS channel estimation as illustrated in Figure 5.1.

According to the system model represented by equation (1.5), the conventional LS pilot-based channel estimation is expressed by (for more details see [21]):

$$\hat{\mathbf{h}}_{op} = \left(\tilde{\mathbf{X}}_p^H \tilde{\mathbf{X}}_p\right)^{-1} \tilde{\mathbf{X}}_p^H \mathbf{y}. \tag{5.1}$$

The LS channel estimation performance is widely discussed in literature. It has been shown that the MSE of this estimator reaches the CRB_{OP}. Therefore the MSE_{OP} is given by:

$$MSE_{OP} = \sigma_{\mathbf{v}}^2 tr\left\{\left(\tilde{\mathbf{X}}_p^H \tilde{\mathbf{X}}_p\right)^{-1}\right\}. \tag{5.2}$$

Moreover when the training sequences $\mathbf{x}_p$ are orthogonal, $\left(\tilde{\mathbf{X}}_p^H \tilde{\mathbf{X}}_p\right)$ is equal to $\sigma_p^2 \mathbf{I}_{NN_tN_r}$ and the MSE is minimal. After estimating the channel (i.e. $\hat{\mathbf{h}}_{op}$), the Zero-Forcing (ZF) equalizer is

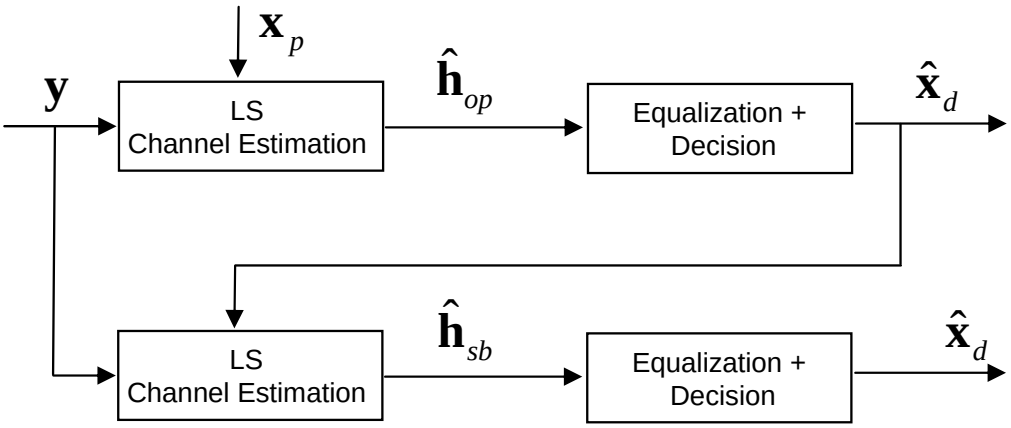

Figure 5.1: *LS-DF semi-blind channel estimation approach.*

adopted to estimate the transmitted signal. It refers to a form of linear equalization algorithm often used in communications systems. It applies the inverse of the channel frequency response $\hat{\boldsymbol{\lambda}}^{\#}$ to the received signal where $^{\#}$ denotes the pseudo inverse matrix, and $\hat{\boldsymbol{\lambda}}$ is the channel

frequency response of $\hat{\mathbf{h}}_{op}$ calculated as in subsection 1.2.1. The equalized signal, denoted $\mathbf{x}_{zf}$, is then deduced:

$$\mathbf{x}_{zf} = \hat{\boldsymbol{\lambda}}^{\#}\mathbf{y} = \hat{\boldsymbol{\lambda}}^{\#}\hat{\boldsymbol{\lambda}}\mathbf{x} + \hat{\boldsymbol{\lambda}}^{\#}\mathbf{v}. \tag{5.3}$$

After that, a hard decision is taken on the equalized signal to estimate the transmitted signal $\hat{\mathbf{x}}_d$. The new training sequences become:

$$\mathbf{x}_p = [\mathbf{x}_p{}^T\ \hat{\mathbf{x}}_d^T]^T. \tag{5.4}$$

Based on equation (5.1), the channel taps are then estimated ($\hat{\mathbf{h}}_{sb}$ in Figure 5.1). The ZF equalizer, given by equation (5.3), estimates the signal $\mathbf{x}_{zf}$ on which a hard decision is taken to estimate the transmitted data $\hat{\mathbf{x}}_d$.

5.2.2 Computational cost comparison of LS and LS-DF algorithms

This section compares the computational cost of the LS-DF semi-blind channel estimator to the LS pilot-based channel estimation. The computational cost is evaluated in terms of real number of flops (i.e. number of multiplications plus number of additions).

At the receiver, the number of flops consumed by LS pilot-based channel estimation algorithm is deduced from equation (5.1) where $\tilde{\mathbf{X}}_p$ and $\mathbf{y}$ are of size $N_pN_rK \times N_tN_rN$ and $N_pN_rK \times 1$ respectively. The details of the number of flops required to estimate $\hat{\mathbf{h}}_{op}$ are listed in Table 5.1.

At the receiver, the flops consumed by the LS-DF algorithm are equal to the flops due to the equalizer/decision stage added to the flops required to estimate $\hat{\mathbf{h}}_{sb}$ and $\hat{\mathbf{h}}_{op}$ (see Table 5.1). Note that the flops required for the equalizer/decision stage can be easily compensated by the reduction of the flops due to the removed pilots from the initial training sequence, this will be discussed in simulation results (90% samples of the initial training sequence are removed). Therefore the LS-DF semi-blind channel estimator consumes Δ_{Flops} more flops than the LS pilot-based channel estimator:

$$\begin{aligned}\Delta_{flops} &= 2(N_tN_rN)^3 + 4(N_tN_rN)^2(N_dN_rK) \\ &+ (N_tN_rN)(N_dN_rK) - (N_tN_rN)^2 - (N_tN_rN).\end{aligned} \tag{5.5}$$

In [81], the authors investigate the relationship between the flops number and the corresponding consumed power denoted Flops per Watt ($Flops/Watt$). It is then possible to measure the equivalent consumed power in Watts. Depending on the functional characteristics of the processor, the consumed power per Watt is between 5 and 100 $GFlops/Watt$. If P is the consumed power, given in $GFlops/Watt$, the consumed power associated to Δ_{Flops} can be deduced as follows:

$$\Delta_{Power} = \frac{\Delta_{flops}}{P} 10^{-6}\ \text{mWatt} \tag{5.6}$$

Operation	Number of flops
$\tilde{\mathbf{X}}_p^H \tilde{\mathbf{X}}_p$	$2(N_t N_r N)^2 N_p N_r K - (N_t N_r N)^2$
$\left(\tilde{\mathbf{X}}_p^H \tilde{\mathbf{X}}_p\right)^{-1}$	$2(N_t N_r N)^3$
$\left(\tilde{\mathbf{X}}_p^H \tilde{\mathbf{X}}_p\right)^{-1} \tilde{\mathbf{X}}_p^H$	$2(N_t N_r N)^2 N_p N_r K - (N_t N_r N) N_p N_r K$
$\left(\tilde{\mathbf{X}}_p^H \tilde{\mathbf{X}}_p\right)^{-1} \tilde{\mathbf{X}}_p^H \mathbf{y}$	$2(N_t N_r N) N_p N_r K - (N_t N_r N)$
$\hat{\mathbf{h}}_{op}$	$2(N_t N_r N)^3 + 4(N_t N_r N)^2 N_p N_r K$ $+ (N_t N_r N) N_p N_r K - (N_t N_r N)^2$ $- (N_t N_r N)$
$\hat{\mathbf{h}}_{sb}$	$4(N_t N_r N)^2 ((N_p + N_d) N_r K) +$ $(N_t N_r N) ((N_p + N_d) N_r K) +$ $2(N_t N_r N)^3 - (N_t N_r N)^2 - (N_t N_r N)$
$Flops_{Eq}$	$2N_t N_r N_d K^2 + 2(N_r K)^2 N_t K +$ $2(N_t K)^3 - (N_r K)^2$ $-N_t N_r K^2 - N_t N_d K$

Table 5.1: *Flops number.*

5.3 Performance analysis and discussions

This section analyzes and quantifies the transmitted power that can be reduced when semi-blind channel estimation approach is deployed while maintaining the same performance as LS pilot-based channel estimation approach.

The considered MIMO-OFDM wireless system is related to the IEEE 802.11n standard [22]. The training sequences correspond to those specified by the standard. In the legay preamble (i.e. 802.11a) two identical fields named LTF (Long Training Field) are dedicated to channel estimation. Each field (or pilot) is represented by one OFDM symbol ($K = 64$ samples) where a CP ($L = 16$ samples) is added at its front. In the High Throughput preamble, a set of identical fields named High Throughput Long Training fields (HT-LTF) are specified and represented by one OFDM symbol ($K = 64$ samples) with a CP (16 samples). These fields (or pilots) are specified to MIMO channel estimation. Their number depends on the number of transmit antennas (N_t). Since in this chapter $N_t = 3$, four ($N_p^{HT-LTF} = 4$) HT-LTF pilot OFDM symbols are used (see [22] for details). Therefore the training sequence length is equal to $N_p = N_p^{LTF} + N_p^{HT-LTF}$. The data field is represented by a set of OFDM symbols depending on the length of the transmitted packet (N_d). Simulation parameters are summarized in Table 5.2.

Parameters	Specifications
Channel model	Cost 207
Number of transmit antennas	$N_t = 3$
Number of receive antennas	$N_r = 4$
Channel length	$N = 4$
Number of LTF pilot OFDM symbols	$N_p^{LTF} = 2$
Number of HT-LTF pilot OFDM symbols	$N_p^{HT-LTF} = 4$
Number of data OFDM symbols	$N_d = 40$
Pilot signal power	$P_{x_p} = 23$ dBm
Data signal power	$P_{x_d} = 20$ dBm
Number of subcarriers	$K = 64$
Consumed power $(GFlops/Watt)$	$P = 5$

Table 5.2: *Simulation parameters.*

The Signal to Noise Ratio associated with pilots at the reception is defined as $SNR_p = \frac{\|\boldsymbol{\lambda}_p\|^2}{N_r N_p K \sigma_{\mathbf{v}}^2}$. The signal to noise ratio SNR_d associated with data is given (in dB) by: $SNR_d = SNR_p - (Px_p - Px_d)$ where Px_p (respectively Px_d) is the power of pilots (respectively data) (both in dB).

5.3.1 Theoretical limit pilot's power reduction

This section analyzes the maximum pilot's power reduction evaluated from the theoretical limit bound performance of the semi-blind channel estimation approach.

The transmitted pilot's power is reduced in such a way that semi-blind approach achieves the same performance as pilot-based channel estimation approach (i.e. CRB_{OP}). To do so, the proposed strategy replaces the removed pilot samples by zero-samples leading therefore to a reduction of the average pilot's transmitted power or equivalently to the transmitted energy).

Figure 5.2 provides the CRB for semi-blind channel estimation versus the reduced pilot's power for a given $SNR_p = 12$ dB. The horizontal line represents the CRB for pilot-based channel estimation and is considered as the reference to be reached. Only 8% of pilot's power is retained (i.e. 185 mW are reduced). These results show clearly that semi-blind estimation in MIMO-OFDM system brings a significant gain in terms of the transmitted pilot's energy reduction.

Figure 5.3 shows the impact of the number of data OFDM symbols on the pilot's transmitted

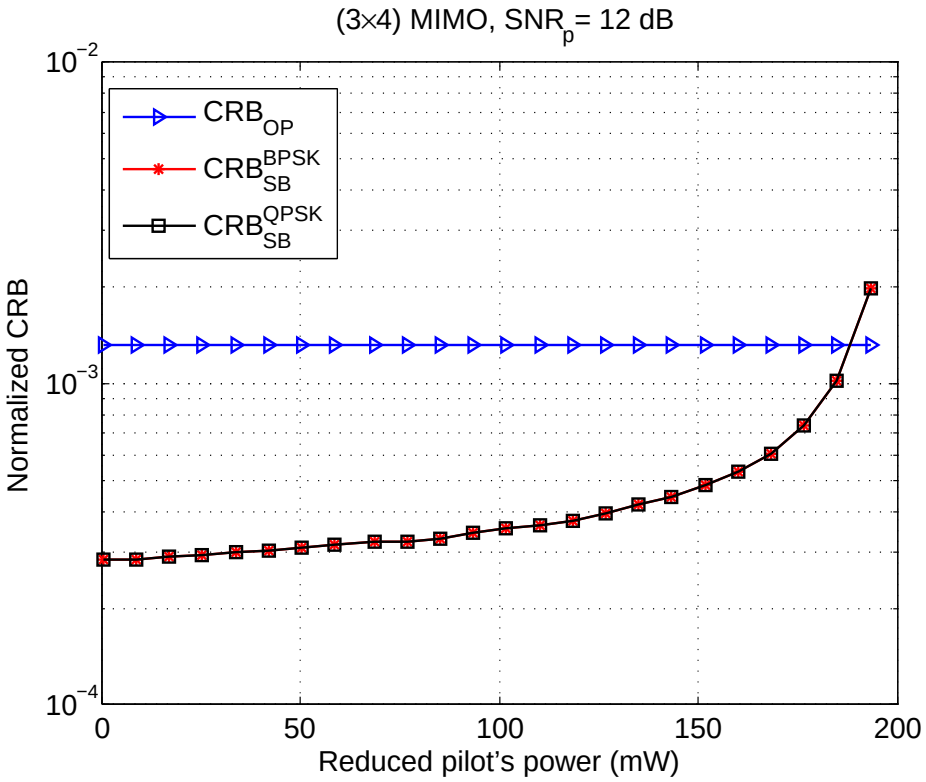

Figure 5.2: *Normalized CRB versus the reduced power ($SNR_p = 12$ dB).*

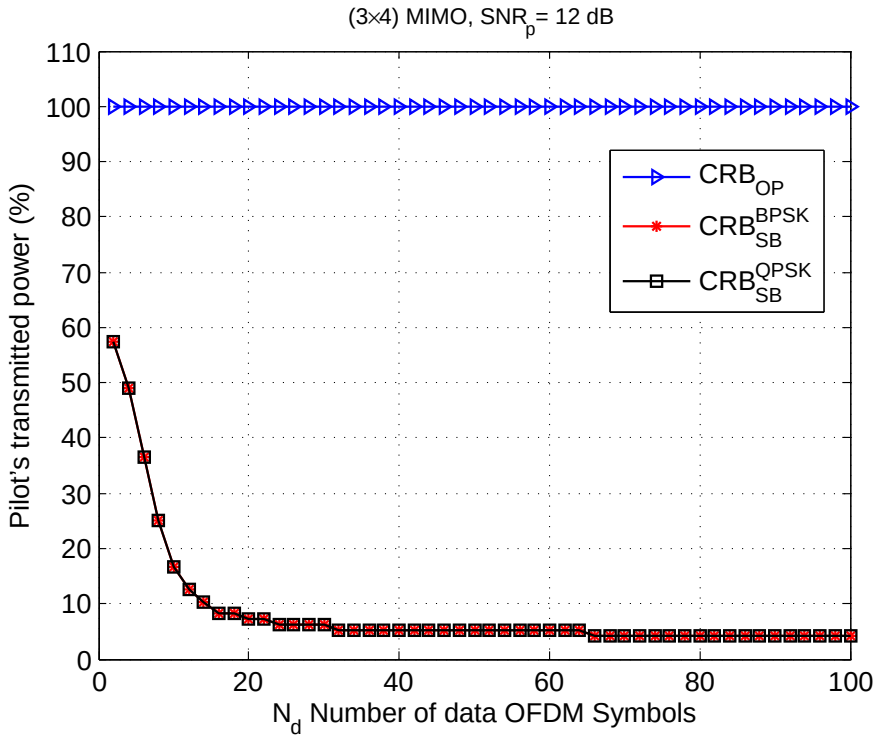

Figure 5.3: *Percentage of the transmitted pilot's power versus the number of data OFDM symbols N_d ($SNR_p = 12$ dB).*

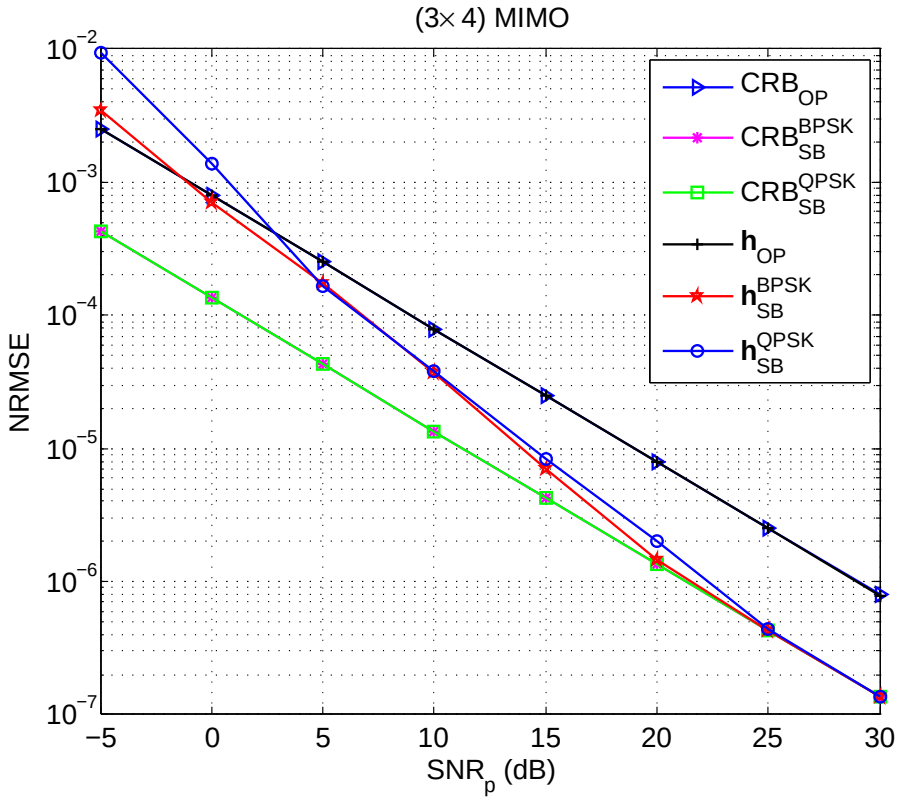

Figure 5.4: *NRMSE of LS and LS-DF estimators versus SNR_p.*

power (in percentage) for a given $SNR_p = 12$ dB. When the number of data OFDM symbols increases, the percentage of the reduced pilot's power becomes more significant. Note that the results observed in Figure 5.2 can be deduced from Figure 5.3 when the number of data OFDM symbols is equal to 40.

5.3.2 LS-DF performance in terms of power consumption

This section investigates the energy balance of the complete system (transmitter and receiver), namely the power deployed by the transmitter and that consumed by the receiver when the LS-DF algorithm is adopted.

The curves in Figure 5.4 present the Normalized Root Mean square Error (NRMSE) of LS and LS-DF estimators versus the SNR_p. Note that for the $\mathbf{h}_{SB}^{BPSK}$, $\mathbf{h}_{SB}^{QPSK}$ LS-DF reaches the CRB_{SB}^{BPSK}, CRB_{SB}^{QPSK} at height SNR, and gives better results compared to the LS pilot-based approach ($\mathbf{h}_{OP}$) from $SNR_p = 2$ dB.

Figure 5.5 presents the transmitted pilot's power versus the SNR_p. The higher the SNR_p is, the lower transmitted pilot's power is in favor of the LS-DF semi-blind estimator. The same results are obtained in Figure 5.6 which presents the reduced power versus SNR_p.

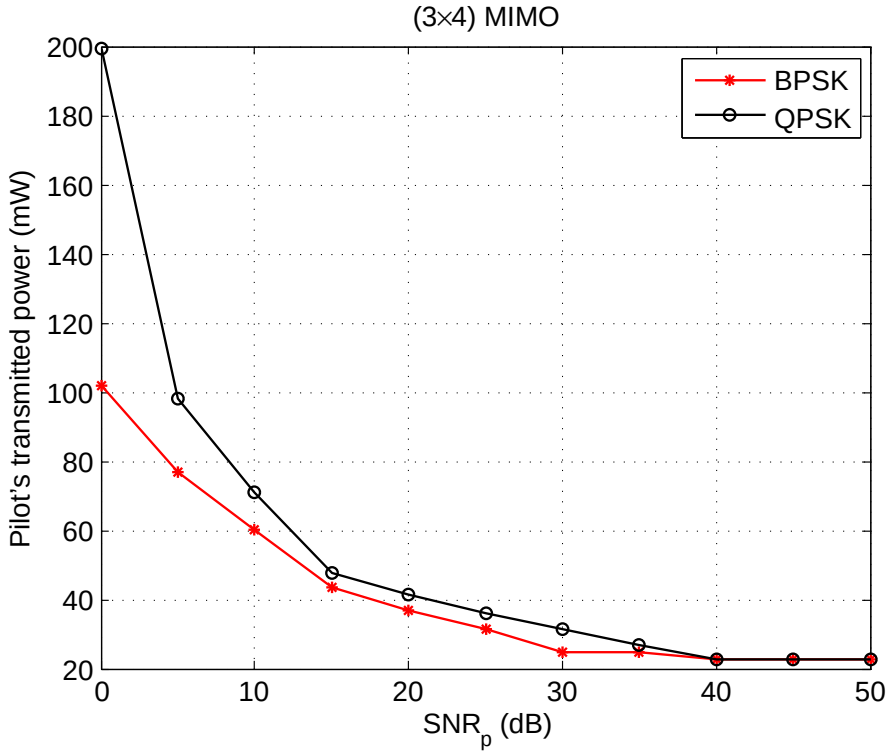

Figure 5.5: *Transmitted pilot's power versus SNR_p.*

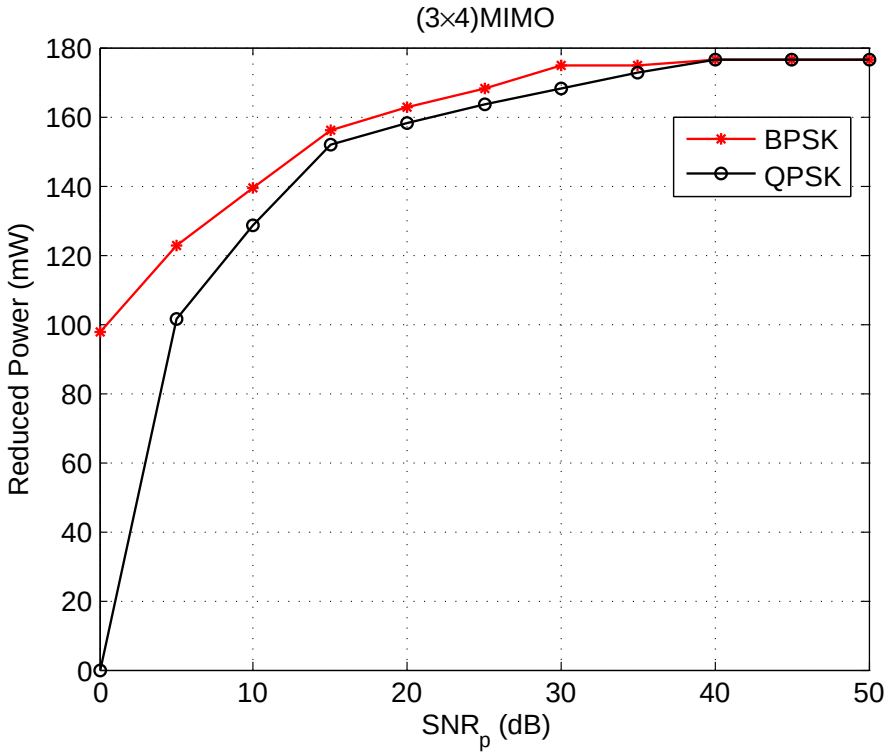

Figure 5.6: *Reduced pilot's power versus SNR_p.*

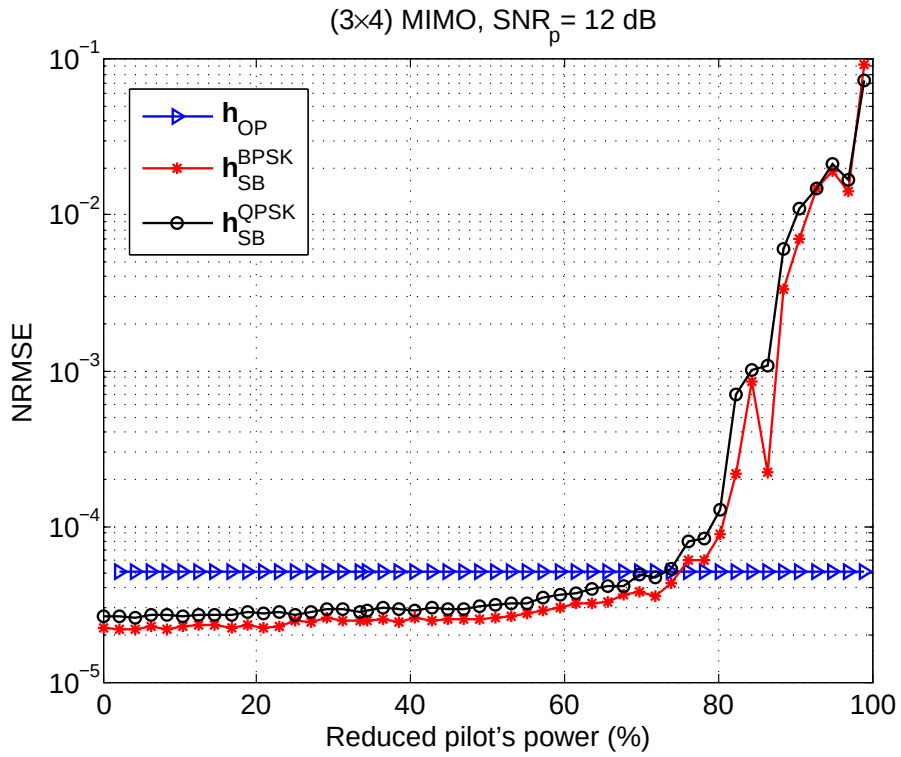

Figure 5.7: *NRMSE of the LS-DF channel estimator versus the percentage of the reduced pilot's power ($SNR_p = 12$ dB).*

Figure 5.7 provides the NRMSE of the LS-DF estimator versus the reduced pilot's power (in percentage) for a given $SNR_p = 12$ dB (with $N_d = 40$). The pilot's power is reduced in such a way that the LS-DF estimator performance ($\mathbf{h}_{SB}^{BPSK}$, $\mathbf{h}_{SB}^{QPSK}$) reaches the same performance as the LS pilot-based estimator. For BPSK data model, only 49 mW is required instead of 200 mW (100%) when pilot-based channel estimation is used (i.e. a reduction of 76%). For QPSK data model, 74% of the pilot's power is also reduced. Although the LS-DF algorithm leads to an overconsumption of the energy at the receiver side since more operations are required (see equation (5.5), $\Delta_{flops} = 94863360$ Flops, equivalent to $\Delta_{Power} = 19$ mW), the complete system (i.e. transmitter and receiver) saves 66% (i.e. 132 mW). The flops due to the equalization stage, assumed to compensate the flops associated to the removed pilots (assumption in section 5.2.2), are equivalent to $Flops_{eq} = 3233792$ *Flops*. While 2924976 *Flops* are due to the removed pilots. The flops difference is 308816 *Flops* and is in fact negligible ($308816 << \Delta_{flops}$ equivalent to 0.061 mW) confirming the assumption. Therefore the global MIMO-OFDM system (i.e. transmitter and receiver) saves 65,97% i.e. 131.94 mW of power consumption.

5.4 conclusion

This chapter focused on the power reduction problem in a MIMO-OFDM wireless system specifically during the channel estimation stage. The study proposed to deploy semi-blind channel estimation approach allowing the transmitter to reduce the number of samples in the training sequence while ensuring the same estimation performance as pilot-based channel estimation approach. The maximum theoretical reduction of the pilot's power consumption, based on the CRB for semi-blind channel estimation approach, is first investigated for the IEEE 802.11n MIMO-OFDM system with BPSK and QPSK data models. Simulation results, for the same channel estimation performance, show clearly a significant reduction of the pilot's power equivalent to 76% when LS-DF semi-blind channel estimation is deployed instead of the LS pilot-based channel estimation. A global power reduction of 65,97% is possible for the complete wireless MIMO-OFDM system.

CHAPTER 6

EM-based blind and semi-blind channel estimation

Problems are not stop signs, they are guidelines.

Robert H. Schuller.

Abstract

This chapter deals with semi-blind channel estimation of MIMO-OFDM system using Maximum Likelihood (ML) technique. For the ML cost optimization function, new Expectation Maximization (EM) algorithms for the channel taps estimation are introduced. Different approximation/simplification approaches are proposed for the algorithm's computational cost reduction. The first approach consists of decomposing the MIMO-OFDM system into parallel MISO-OFDM systems. The EM algorithm is then applied in order to estimate the MIMO channel in a parallel way. The second approach takes advantage of the semi-blind context to reduce the EM cost from exponential to linear complexity by reducing the size of the search space. Finally, the last proposed approach uses a parallel interference cancellation technique to decompose the MIMO-OFDM system into several SIMO-OFDM systems. The latter are identified in a parallel scheme and with a reduced complexity. These algorithms have been published in the conference ICASSP 2018[1] and submitted to IET communications[2]

[1] [82] A. Ladaycia, A. Belouchrani, K. Abed-Meraim, and A. Mokraoui, and, "EM-based semi-blind MIMO-OFDM channel estimation," in 2018 IEEE International Conference on Acoustics, Speech and Signal Processing (ICASSP2018), Apr. 2018, Alberta, Canada.

[2] [83] A. Ladaycia, A. Belouchrani, K. Abed-Meraim and A. Mokraoui, "Semi-Blind MIMO-OFDM Channel Estimation using EM-like Techniques," IET communications, Mai. 2019.(submitted)

Chapter content

6.1 Introduction

As shown in chapter 1, for a target estimation quality, the SB approach improves the throughput by reducing the training sequences up to 95%. In addition, SB methods can be used to reduce the transmitted power ('green communications'), e.g. [33] (chapter 5) or eventually to improve the estimation quality.

Among the channel estimation techniques, the Maximum Likelihood (ML) is one of the most efficient in terms of quality but at the cost of high computational complexity. To achieve the ML estimate at 'affordable' costs, the Expectation Maximization (EM) algorithm is considered for both channel and transmit data estimation (see e.g. [84]). In the case of a MIMO-OFDM system using TDD mode, the CSI is estimated at the base station (uplink) and then transmitted to the different users for channel equalization in the downlink.

The EM can be used blindly to estimate the channel or semi-blindly when training sequences are available. In [84], the authors used a precoder and employ data tones as virtual pilots for channel estimation. In [85] an alternative EM-based method is introduced for the estimation of the channel taps in the frequency domain. In [86], the authors proposed an EM algorithm by assuming a Gaussian distribution for the unknown data even when the data symbols are drawn from a finite constellation such as QPSK. Recently, this work has been extended in [87] by using a Gaussian mixture model, leading to improved estimation performance for high SNR (typically $SNR > 25dB$).

The objective of this chapter is to propose alternative EM-based solutions with improved efficiency as compared to similar existing methods[3]. First our EM-based algorithms are distinct from the previous ones ([85], [84]) in terms of the channel parameters to be estimated. Instead of estimating the channel coefficients in the frequency domain (i.e. subcarriers channel frequency gains), we estimate directly the channel taps in the time domain so one can obtain a significant gain as analyzed in chapter 1. Furthermore, in order to have parallelizable and/or reduced cost estimation methods, three approximate EM algorithms are proposed.

Before doing so, this chapter introduces first the exact version where the MIMO-OFDM system is treated as one block to estimate the overall channel vector through an iterative process. Afterward, three complementary approximate EM versions are proposed.

The first approximate EM algorithm, useful if parallel processing machins are available, decomposes the MIMO-OFDM system into parallel MISO-OFDM systems to estimate the vector channel taps independently for each receiver. In the case of underdetermined system (i.e. number

[3]Part of this work has been published in [82].

of transmitters greater than the receivers one), where the traditional methods could not estimate the transmit data, we succeed through the two proposed EM-based algorithms to estimate the channel taps and data properly.

The second method consists of a Simplified EM algorithm, denoted S-EM, that allows to reduce the computational heaviness based on an initial estimation of the channel and the data using the pilots. More specifically, this approximation consists of limiting the averaging in the expectation step to a neighborhood of the initial data vector estimate, hence reducing the complexity from an exponential to a linear cost in terms of the number of transmitters.

The last proposed approach, again takes advantage of the semi-blind context using an initial pilot-based estimation of the channel and the data together with a parallel interference cancellation technique to transform the original MIMO problem into parallel SIMO systems identification problems which can be solved in a parallel scheme and with reduced complexity.

6.2 System model

Consider a $(N_t \times N_r)$ MIMO-OFDM system composed of N_t transmit antennas and N_r receive antennas, as illustrated in Figure 1.1. The transmitted signal is an OFDM one, composed of K samples (subcarriers) and L Cyclic Prefix (CP) samples. The CP length is assumed to be greater or equal to the maximum multipath channel delay denoted N (i.e. $N \leq L$). The received signal at the k-th subcarrier by the r-th receive antenna, denoted $y_r(k)$, after removing the L CP samples and taking the K-point DFT, is given by:

$$y_r(k) = \sum_{i=1}^{N_t} \sum_{n=0}^{N-1} h_{ri}(n) w_K^{nk} d_i(k) + v_r(k) \quad 0 \leq k \leq K-1, \tag{6.1}$$

where $d_i(k)$ represents the transmitted data by the i-th transmitter at the k-th subcarrier. The noise v_r is assumed to be an additive white Circular Complex Gaussian (CCG) satisfying $E\left[\mathbf{v}(k)\mathbf{v}(i)^H\right] = \sigma_{\mathbf{v}}^2 \mathbf{I}_K \delta_{ki}$ where $(.)^H$ is the Hermitian operator; $\sigma_{\mathbf{v}}^2$ the noise variance; $\mathbf{I}_K$ the identity matrix of size $K \times K$ and δ_{ki} the Kronecker symbol. $h_{ri}(n)$ is the n-th channel taps coefficient between the i-th transmitter and the r-th receiver. w_K^{nk} (with $w_K = e^{-j2pi/K}$) represents the (n,k)-th coefficient of the K-DFT matrix. The matrix form of equation (6.1) can be given as:

$$y_r(k) = \mathbf{w}^T(k)\mathbf{H}_r\mathbf{d}(k) + v_r(k), \tag{6.2}$$

where the transmitted data $\mathbf{d}(k) = [d_1(k), \cdots, d_{N_t}(k)]^T$, and $\mathbf{w}(k) = \left[1 \quad w_K^k, \cdots, w_K^{(N-1)k}\right]^T$. The channel matrix taps $\mathbf{H}_r$ is given by:

$$\mathbf{H}_r = \begin{bmatrix} h_{r1}(0) & \cdots & h_{rN_t}(0) \\ \vdots & \ddots & \vdots \\ h_{r1}(N-1) & \cdots & h_{rN_t}(N-1) \end{bmatrix}. \tag{6.3}$$

The model equation (6.2), when considering all the received signal in a single vector $\mathbf{y}(k) = [y_1(k), \cdots, y_{N_r}(k)]^T$, can be rewritten in the following compact form:

$$\mathbf{y}(k) = \boldsymbol{\mathcal{W}}(k)\boldsymbol{\mathcal{H}}\mathbf{d}(k) + \mathbf{v}(k), \tag{6.4}$$

where $\boldsymbol{\mathcal{W}}(k) = \mathbf{I}_{N_r} \otimes \mathbf{w}^T(k)$ and $\boldsymbol{\mathcal{H}} = [\mathbf{H}_1^T, \cdots, \mathbf{H}_{N_r}^T]^T$.

In the following, the received OFDM symbols are assumed to be independent and identically distributed (i.i.d). The EM-algorithms are derived according to two different OFDM symbols arrangement: (i) the comb-type scheme (Figure 1.2b) with K_p pilot's subcarriers corresponding (after index permutation) to $k = 0, \cdots, K_p - 1$ and K_d subcarriers dedicated to data; (ii) the block-type pilot arrangement (Figure 1.2a) using N_p OFDM symbols for the pilot and N_d symbols for the data.

We assume the transmitted data to belong to a finite alphabet and we denote by D (respectively $|D|$) the finite set of all possible realizations of the data vector $\mathbf{d}$ (respectively its cardinal).

6.3 ML-based channel estimation

Our objective is to estimate the unknown channel parameters through a Maximum Likelihood (ML) criterion optimized by the EM technique, briefly reviewed in section (6.3.1). The unknown parameters are grouped in $\boldsymbol{\theta}$ containing the channel taps ($\text{vec}(\boldsymbol{\mathcal{H}})$ or $\text{vec}(\mathbf{H}_r)$) and the noise power ${\sigma_{\mathbf{v}}}^2$ (for simplicity, the signal power is assumed to be known). The ML estimation can be written as:

$$\boldsymbol{\theta}_{ML} = \arg\max_{\boldsymbol{\theta}} \log p(\mathbf{y}; \boldsymbol{\theta}), \tag{6.5}$$

where $p(\mathbf{y}; \boldsymbol{\theta})$ is the pdf of the observed vector $\mathbf{y}$ parameterized by $\boldsymbol{\theta}$.

6.3.1 EM algorithm

The EM algorithm is an iterative optimization technique that seeks for the ML estimate of the unknown parameters using the marginal likelihood of the observed data $\mathbf{y}$.

More precisely, the EM-algorithm is based on the two following steps:

- Expectation step (E-step): Computation of the auxiliary function as:

$$Q\left(\boldsymbol{\theta},\boldsymbol{\theta}^{[i]}\right)=E_{\mathbf{d}|\mathbf{y};\boldsymbol{\theta}^{[i]}}\left[\log p\left(\mathbf{y},\mathbf{d};\boldsymbol{\theta}\right)\right], \tag{6.6}$$

  Since $p\left(\mathbf{y},\mathbf{d};\boldsymbol{\theta}\right)=p\left(\mathbf{y}|\mathbf{d};\boldsymbol{\theta}\right)p\left(\mathbf{d}\right)$, equation (6.6) becomes (up to a constant independent of $\boldsymbol{\theta}$), equal:

$$Q\left(\boldsymbol{\theta},\boldsymbol{\theta}^{[i]}\right)=E_{\mathbf{d}|\mathbf{y};\boldsymbol{\theta}^{[i]}}\left[\log p\left(\mathbf{y}|\mathbf{d};\boldsymbol{\theta}\right)\right], \tag{6.7}$$

- Maximization step (M-step): Derivation of $\boldsymbol{\theta}^{[i+1]}$ which maximizes the auxiliary function $Q\left(\boldsymbol{\theta},\boldsymbol{\theta}^{[i]}\right)$ as:

$$\boldsymbol{\theta}^{[i+1]}=\arg\max_{\boldsymbol{\theta}} Q\left(\boldsymbol{\theta},\boldsymbol{\theta}^{[i]}\right) \tag{6.8}$$

This process is shown in [36], [88] to increase the likelihood value ($\mathcal{L}$), i.e $p\left(\mathbf{y}|\mathbf{d};\boldsymbol{\theta}\right)$, and consequently it leads to the algorithm's convergence to a local maximum point since:

$$\mathcal{L}\left(\mathbf{y},\boldsymbol{\theta}^{[i+1]}\right)\geq\mathcal{L}\left(\mathbf{y},\boldsymbol{\theta}^{[i]}\right) \tag{6.9}$$

6.3.2 MIMO-OFDM semi-blind channel estimation for comb-type pilot arrangement

This subsection addresses the derivation of the EM algorithm for semi-blind channel estimation when the pilot arrangement pattern is assumed to be a comb-type one (Figure 1.2b) or which each OFDM symbol consists of K_p pilots subcarriers and K_d data one. The total number of transmitted OFDM symbols is N_s.

The likelihood function, under the data model assumption, is expressed by:

$$p\left(\mathbf{y};\boldsymbol{\theta}\right)=\prod_{k=0}^{K_p-1}p\left(\mathbf{y}\left(k\right);\boldsymbol{\theta}\right)\prod_{k=K_p}^{K-1}p\left(\mathbf{y}\left(k\right);\boldsymbol{\theta}\right), \tag{6.10}$$

where $p\left(\mathbf{y}\left(k\right);\boldsymbol{\theta}\right)\sim\mathcal{N}\left(\boldsymbol{\mathcal{W}}(k)\boldsymbol{\mathcal{H}}\mathbf{d}_p(k),\sigma_{\mathbf{v}}^2\mathbf{I}\right)$, for $k=0,\cdots,K_p-1$, $\mathbf{d}_p(k)$ being the pilot vector at the k-th subcarrier, and for $k=K_p,\cdots K-1$

$$p\left(\mathbf{y}\left(k\right);\boldsymbol{\theta}\right)=\sum_{\xi=1}^{|D|}p\left(\mathbf{y}\left(k\right)|\mathbf{d}_\xi;\boldsymbol{\theta}\right)p\left(\mathbf{d}_\xi\right), \tag{6.11}$$

with $p\left(\mathbf{y}\left(k\right)|\mathbf{d}_\xi;\boldsymbol{\theta}\right)\sim\mathcal{N}\left(\boldsymbol{\mathcal{W}}(k)\boldsymbol{\mathcal{H}}\mathbf{d}_\xi,\sigma_{\mathbf{v}}^2\mathbf{I}\right)$.

The two steps of the EM algorithm are presented below.

6.3.2.1 E-step

After some straightforward derivations and simplifications (see Appendix 6.A), $Q\left(\boldsymbol{\theta},\boldsymbol{\theta}^{[i]}\right)$ can be given by:

$$Q\left(\boldsymbol{\theta},\boldsymbol{\theta}^{[i]}\right)=\sum_{k=0}^{K_p-1}\log p\left(\mathbf{y}(k)|\mathbf{d}_p(k);\boldsymbol{\theta}\right)+\sum_{k=K_p}^{K-1}\sum_{\xi=1}^{|D|}\alpha_{k,\xi}\left(\boldsymbol{\theta}^{[i]}\right)\log p\left(\mathbf{y}(k)|\mathbf{d}_\xi;\boldsymbol{\theta}\right), \tag{6.12}$$

where

$$\begin{aligned}\alpha_{k,\xi}\left(\boldsymbol{\theta}^{[i]}\right) &= p\left(\mathbf{d}_\xi|\mathbf{y};\boldsymbol{\theta}^{[i]}\right)\\ &= \frac{p\left(\mathbf{y}(k)|\mathbf{d}_\xi;\boldsymbol{\theta}^{[i]}\right)p(\mathbf{d}_\xi)}{p\left(\mathbf{y}(k);\boldsymbol{\theta}^{[i]}\right)}\\ &= \frac{p\left(\mathbf{y}(k)|\mathbf{d}_\xi;\boldsymbol{\theta}^{[i]}\right)p(\mathbf{d}_\xi)}{\sum_{\xi'=1}^{|D|} p\left(\mathbf{y}(k)|\mathbf{d}_{\xi'};\boldsymbol{\theta}^{[i]}\right)p\left(\mathbf{d}_{\xi'}\right)}.\end{aligned} \tag{6.13}$$

All the realizations $\mathbf{d}_\xi$ are assumed equiprobable and hence one can ignore the term $p(\mathbf{d}_\xi)$ in equation (6.13).

6.3.2.2 M-step

The objective of the M-step is to find $\boldsymbol{\theta}$, i.e. the channel matrix $\boldsymbol{\mathcal{H}}$ and the noise power $\sigma_{\mathbf{v}}^2$ maximizing the auxiliary function:

$$\boldsymbol{\theta}^{[i+1]} = \arg\max_{\boldsymbol{\theta}} Q\left(\boldsymbol{\theta},\boldsymbol{\theta}^{[i]}\right). \tag{6.14}$$

By zeroing the derivative of $Q\left(\boldsymbol{\theta},\boldsymbol{\theta}^{[i]}\right)$ in (6.12) w.r.t. $\boldsymbol{\mathcal{H}}$ and using the vec operator's properties $\left(\mathrm{vec}(\mathbf{ACB}) = \left(\mathbf{B}^T\otimes\mathbf{A}\right)\mathrm{vec}(\mathbf{C})\right)$, one obtains:

$$\begin{aligned}&\mathrm{vec}\left(\boldsymbol{\mathcal{H}}^{[i+1]}\right) =\\ &\left[\sum_{k=0}^{K_p-1}\left(\mathbf{d}_p(k)^*\mathbf{d}_p(k)^T\otimes\boldsymbol{\mathcal{W}}(k)^H\boldsymbol{\mathcal{W}}(k)\right) + \sum_{k=K_p}^{K-1}\sum_{\xi=1}^{|D|}\alpha_{k,\xi}\left(\boldsymbol{\theta}^{[i]}\right)\left(\mathbf{d}_\xi{}^*\mathbf{d}_\xi{}^T\otimes\boldsymbol{\mathcal{W}}(k)^H\boldsymbol{\mathcal{W}}(k)\right)\right]^{-1}\\ &\times\left[\sum_{k=0}^{K_p-1}\mathrm{vec}\left(\boldsymbol{\mathcal{W}}(k)^H\mathbf{y}_p(k)\,\mathbf{d}_p(k)^H\right) + \sum_{k=K_p}^{K-1}\sum_{\xi=1}^{|D|}\alpha_{k,\xi}\left(\boldsymbol{\theta}^{[i]}\right)\mathrm{vec}\left(\boldsymbol{\mathcal{W}}(k)^H\mathbf{y}(k)\,\mathbf{d}_\xi{}^H\right)\right].\end{aligned} \tag{6.15}$$

Similarly, setting to zero the derivative of $Q\left(\boldsymbol{\theta},\boldsymbol{\theta}^{[i]}\right)$ w.r.t. $\sigma_{\mathbf{v}}{}^2$ leads to:

$$\begin{aligned}&\{\sigma_{\mathbf{v}}{}^2\}^{[i+1]} =\\ &\frac{1}{K}\left(\sum_{k=0}^{K_p-1}\left\|\mathbf{y}_p(k)-\boldsymbol{\mathcal{W}}(k)\boldsymbol{\mathcal{H}}^{[i+1]}\mathbf{d}_p(k)\right\|^2 + \sum_{k=K_p}^{K-1}\sum_{\xi=1}^{|D|}\alpha_{k,\xi}\left(\boldsymbol{\theta}^{[i]}\right)\left\|\mathbf{y}(k)-\boldsymbol{\mathcal{W}}(k)\boldsymbol{\mathcal{H}}^{[i+1]}\mathbf{d}_\xi\right\|^2\right).\end{aligned} \tag{6.16}$$

The algorithm is summarized in **Algorithm 1** below.

6.3.3 MIMO-OFDM semi-blind channel estimation for block-type pilot arrangement

This subsection deals with EM algorithm for semi-blind channel estimation in the block-type pilot case (Figure 1.2a). In order to ease the derivation of the EM algorithm, in this context, the system model given in equation (6.4) can be rewritten as (1):

$$\mathbf{y} = \tilde{\mathbf{X}}\,\mathbf{P}\mathbf{h} + \mathbf{v}. \tag{6.17}$$

where, for simplicity, the time index corresponding to OFDM symbols is omitted. The data matrix is: $\tilde{\mathbf{X}} = \mathbf{I}_{N_r}\otimes\mathbf{X}$, where $\mathbf{X} = \left[\mathbf{X}_{D_1}\mathbf{W}\cdots\mathbf{X}_{D_{N_t}}\mathbf{W}\right]$ of size $K\times NN_t$ and $\mathbf{X}_{D_i} = \mathrm{diag}\{\mathbf{d}_i\}$

Algorithm 1 *SB-EM channel estimation algorithm*

Initialization:

1: $i = 0$;

2: $\boldsymbol{\theta}^{[0]} = \left[\text{vec}\left(\boldsymbol{\mathcal{H}}^{[0]}\right)^T, \{\sigma_{\mathbf{v}}^2\}^{[0]}\right]^T$ which represents the standard pilot-based channel and noise estimates;

Processing:

3: Estimate $\boldsymbol{\mathcal{H}}^{[i+1]}$ using $\boldsymbol{\mathcal{H}}^{[i]}$ and $\{\sigma_{\mathbf{v}}^2\}^{[i]}$ according to equation (6.15);

4: Estimate $\{\sigma_{\mathbf{v}}^2\}^{[i+1]}$ using $\boldsymbol{\mathcal{H}}^{[i+1]}$, $\boldsymbol{\mathcal{H}}^{[i]}$ and $\{\sigma_{\mathbf{v}}^2\}^{[i]}$ according to equation (6.16);

5: Set $\boldsymbol{\theta}^{[i]} = \boldsymbol{\theta}^{[i+1]}$;

6: While $\left(\|\boldsymbol{\mathcal{H}}^{[i+1]} - \boldsymbol{\mathcal{H}}^{[i]}\| > \epsilon\right)$ repeat from step 3;
Else: $\hat{\boldsymbol{\mathcal{H}}} = \boldsymbol{\mathcal{H}}^{[i+1]}$ and $\hat{\sigma}_{\mathbf{v}}^2 = \{\sigma_{\mathbf{v}}^2\}^{[i+1]}$;

is a diagonal matrix of size $K \times K$ corresponding to the OFDM symbol transmitted by the i-th transmitter. The channel vector taps is $\mathbf{h} = \text{vec}(\boldsymbol{\mathcal{H}})$ and $\mathbf{P}$ is a permutation matrix.

When Only Pilots (OP) are used to estimate the channel taps, the ML estimator coincides with the Least Squares (LS) estimator ([21]) given by:

$$\hat{\mathbf{h}}_{OP} = \left(\sum_{t=1}^{N_p} \mathbf{P}^H \tilde{\mathbf{X}}_{p_t}^H \tilde{\mathbf{X}}_{p_t} \mathbf{P}\right)^{-1} \sum_{t=1}^{N_p} \mathbf{P}^H \tilde{\mathbf{X}}_{p_t}^H \mathbf{y}_{p_t}, \tag{6.18}$$

where $\tilde{\mathbf{X}}_{p_t}$ refers to the t-th pilot OFDM matrix defined in (1.5).

The derivation is done in a similar way to the comb-type pilot (see Appendix 6.B), leading to the the EM semi-blind channel $\boldsymbol{\mathcal{H}}$ and ${\sigma_{\mathbf{v}}}^2$ noise power estimation given by:

$$\begin{aligned}\text{vec}\left(\boldsymbol{\mathcal{H}}^{[i+1]}\right) = &\left[\mathbf{P}^H \tilde{\mathbf{X}}_p^H \tilde{\mathbf{X}}_p \mathbf{P} + \sum_{k=0}^{K-1} \sum_{\xi=1}^{|D|} \alpha_{k,\xi}\left(\boldsymbol{\theta}^{[i]}\right)\left(\mathbf{d}_\xi{}^* \mathbf{d}_\xi{}^T \otimes \boldsymbol{\mathcal{W}}(k)^H \boldsymbol{\mathcal{W}}(k)\right)\right]^{-1} \\ &\times \left[\mathbf{P}^H \tilde{\mathbf{X}}_p^H \mathbf{Y}_p + \sum_{k=0}^{K-1} \sum_{\xi=1}^{|D|} \alpha_{k,\xi}\left(\boldsymbol{\theta}^{[i]}\right) \text{vec}\left(\boldsymbol{\mathcal{W}}(k)^H \mathbf{y}(k) \mathbf{d}_\xi{}^H\right)\right].\end{aligned} \tag{6.19}$$

$$\begin{aligned}&\{\sigma_{\mathbf{v}}{}^2\}^{[i+1]} = \\ &\frac{1}{K(N_p+N_d)}\left(\left\|\mathbf{Y}_p - \tilde{\mathbf{X}}_p \mathbf{P}\,\text{vec}\left(\boldsymbol{\mathcal{H}}^{[i+1]}\right)\right\|^2 + \sum_{k=0}^{K-1} \sum_{\xi=1}^{|D|} \alpha_{k,\xi}\left(\boldsymbol{\theta}^{[i]}\right)\left\|\mathbf{y}(k) - \boldsymbol{\mathcal{W}}(k)\boldsymbol{\mathcal{H}}^{[i+1]}\mathbf{d}_\xi\right\|^2\right).\end{aligned} \tag{6.20}$$

The algorithm, in the block-type pilot arrangement case, is the same as **Algorithm 1** using equations (6.19) and (6.20) in steps 3 and 4.

6.4 Approximate ML-estimation

Due to the heaviness of the EM-algorithm mainly due to the large number of channels (N_r) and the large value of $|D|$ which grows exponentially with the number of transmitters, herein we propose three simplified versions of the EM-algorithm to reduce the computational complexity while guaranteeing approximately the same estimation performance.

6.4.1 MISO-OFDM SB channel estimation

In this subsection, the MIMO-OFDM system is sub-divided into N_r parallel MISO systems, for which the EM is applied in a parallel scheme. By ignoring the common input data, one can see from equations (6.2) and (6.3) that the MIMO-OFDM system can be decomposed into N_r parallel MISO-OFDM systems, as illustrated in Figure 6.1. Besides allowing the parallel processing of the data, this approach is of practical interest when the noise is spatially colored since only the noise power at the considered receiver is estimated in this scheme.

The parameters of the r-th MISO-OFDM system are denoted as:

$$\boldsymbol{\theta}_r = \left[\text{vec}\left(\mathbf{H}_r\right)^T, \sigma^2_{\mathbf{v}_r}\right] \tag{6.21}$$

The estimation of $\mathbf{H}_r$ and $\sigma^2_{\mathbf{v}_r}$, using the EM algorithm, leads to the same expressions as in the MIMO case given in section (6.3) where $\boldsymbol{\mathcal{H}}$ and $\boldsymbol{\mathcal{W}}(k)$ are replaced by $\mathbf{H}_r$ and $\mathbf{w}(k)$, respectively.

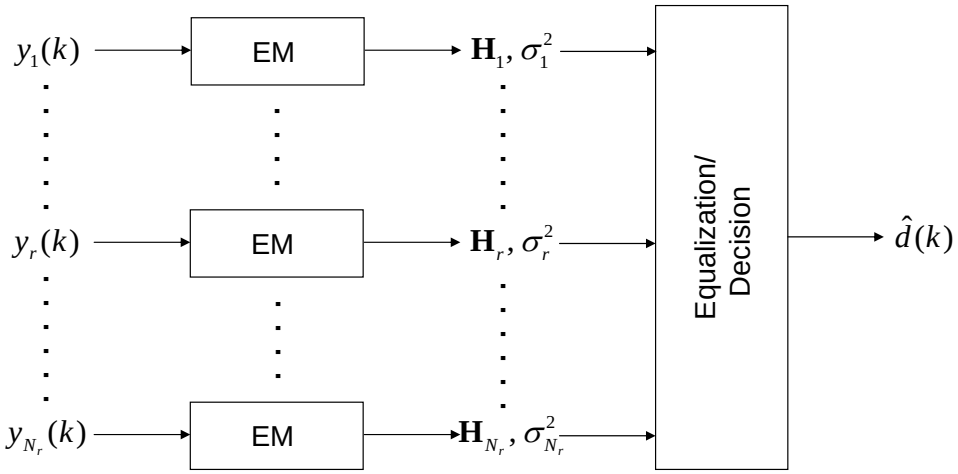

Figure 6.1: *MIMO-OFDM system model using N_r parallel MISO-OFDM systems.*

6.4.2 Simplified EM algorithm (S-EM)

The computational heaviness in equations (6.15) and (6.16) is due to the summation over all the possible realizations of the data vector $\mathbf{d}$ (i.e. $|D|$). In this subsection we propose a simplified method to reduce the summation set from $|D|$ (which growth exponentially with the number N_t) to another reduced summation set of size $|D'|$ proportional to N_t.

The proposed approach is summarized in Figure 6.2, where we use the Decision Feedback Equalizer technique (DFE) to re-estimate the channel using the EM-based algorithm. According to the system model comb-type equation (6.4) or block-type equation (6.17), the first step consists of estimating the channel taps based on equation (6.18) using only pilots.

After estimating the channel (i.e. $\hat{\mathbf{h}}_{op}$), a linear equalizer is adopted to have a first estimate of the transmitted signal applies the inverse of the channel frequency response to the received signal. After that, a hard decision is taken on the equalized signal to estimate the transmitted signal $\hat{\mathbf{d}}_d$ (for more detail see chapter 5). Using $\hat{\mathbf{d}}_d$, the summation in equations (6.15), (6.16), (6.19) and (6.20) is done on a reduced size set $|D'|$ corresponding to the neighborhood of $\hat{\mathbf{d}}_d$ defined here as the points differing from $\hat{\mathbf{d}}_d$ by at most one entry.

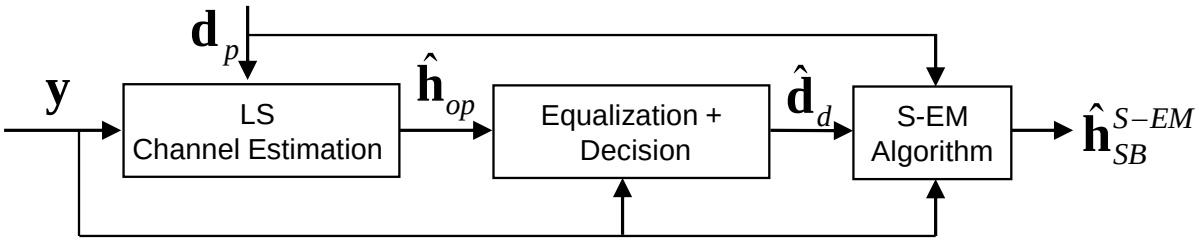

Figure 6.2: *Simplified EM algorithm.*

6.4.3 MIMO-OFDM SB-EM channel estimation algorithm based on N_t EM-SIMO

In this case, to avoid the summation through all the set of $|D|$, we propose in this subsection another simplified EM-algorithm, in which we decompose the MIMO-OFDM system into N_t SIMO-OFDM system. At each iteration, one can estimate the channel taps of the t-th transmitter after doing a DFE equalizer and eliminating the received signal from the other transmitters. As illustrated in Figure 6.3, we start by estimating the MIMO channel taps using the pilots with the LS estimator ($\hat{\mathbf{h}}_{op}$), then applying the ZF equalizer followed by a hard decision to estimate the transmitted data sent by each transmitter ($\hat{\mathbf{d}}_1 \cdots \hat{\mathbf{d}}_{N_t}$) . Once the transmitted data are estimated, one can consider it as interference and taking a SIMO-OFDM system. The data

model equation, given in equation (6.4), can be rewritten in this case as:

$$\mathbf{y}_u^{SIMO}(k) = \mathbf{y}(k) - \boldsymbol{\mathcal{W}}(k)\hat{\boldsymbol{\mathcal{H}}}_{\bar{u}}\hat{\mathbf{d}}_{\bar{u}}(k) = \boldsymbol{\mathcal{W}}(k)\boldsymbol{h}_u d_u(k) + \mathbf{z}_u(k), \tag{6.22}$$

where $\mathbf{y}_u^{SIMO}(k)$ is an estimate of the received signal from only the u-th user, $\boldsymbol{h}_u$ represents the u-th column of the channel matrix $\boldsymbol{\mathcal{H}}$ corresponding to the u-th SIMO-OFDM system channel taps. $\hat{\boldsymbol{\mathcal{H}}}_{\bar{u}}$ is the estimate of the channel matrix of the interfering users, i.e. $\hat{\boldsymbol{\mathcal{H}}}_{\bar{u}}$ is equal to $\hat{\boldsymbol{\mathcal{H}}}$ from which the u-th column is removed.

$\mathbf{z}_u(k)$ represents the noise and interference residual terms. Under the simplifying assumption $\mathbf{z}_u(k) \sim \mathcal{N}(0, \sigma^2_{\mathbf{z}_u}\mathbf{I})$, one can write:

$$p\left(\mathbf{y}_u^{SIMO}(k); \boldsymbol{\theta}_u\right) \sim \mathcal{N}\left(\boldsymbol{\mathcal{W}}(k)\boldsymbol{h}_u d_u(k), \sigma^2_{\mathbf{z}_u}\mathbf{I}\right), \tag{6.23}$$

where the vector of unknown parameters is: $\boldsymbol{\theta}_u = \left[\boldsymbol{h}_u^T, \sigma^2_{\mathbf{z}_u}\right]^T$.

By doing so, we obtain N_t SIMO-OFDM subsystems that can be processed 'independently' (possibly in parallel scheme) according to the following EM iterative algorithm: For $u = 1, \cdots, N_t$:

6.4.3.1 E-step

The auxiliary function $Q\left(\boldsymbol{\theta}_u, \boldsymbol{\theta}_u^{[i]}\right)$ can be written as:

$$Q\left(\boldsymbol{\theta}_u, \boldsymbol{\theta}_u^{[i]}\right) = \sum_{k=0}^{K_p-1} \log p\left(\mathbf{y}_{p,u}^{SIMO}(k) \,|d_{p,u}(k); \boldsymbol{\theta}_u\right) + \sum_{k=K_p}^{K-1} \sum_{\xi=1}^{|D_u|} \alpha_{k,\xi}\left(\boldsymbol{\theta}_u^{[i]}\right) \log p\left(\mathbf{y}_u^{SIMO}(k) \,|d_\xi; \boldsymbol{\theta}_u\right), \tag{6.24}$$

where $\{d_{p,u}(k)\}$ represent the pilot symbols and $|D_u|$ is the set of symbol values (alphabet) of the u-th user and:

$$p\left(\mathbf{y}_{p,u}^{SIMO}(k) \,|d_{p,u}(k); \boldsymbol{\theta}_u\right) \sim \mathcal{N}\left(\boldsymbol{\mathcal{W}}(k)\boldsymbol{h}_u d_{p,u}(k), \sigma^2_{\mathbf{z}_u}\mathbf{I}\right), \tag{6.25}$$

$$p\left(\mathbf{y}_u^{SIMO}(k) \,|d_\xi; \boldsymbol{\theta}_u\right) \sim \mathcal{N}\left(\boldsymbol{\mathcal{W}}(k)\boldsymbol{h}_u d_\xi, \sigma^2_{\mathbf{z}_u}\mathbf{I}\right), \tag{6.26}$$

$$\alpha_{k,\xi}\left(\boldsymbol{\theta}_u^{[i]}\right) = \frac{p\left(\mathbf{y}_u^{SIMO}(k) \,|d_\xi; \boldsymbol{\theta}_u^{[i]}\right) p(d_\xi)}{\sum_{\xi'=1}^{|D_u|} p\left(\mathbf{y}_u^{SIMO}(k) \,|d_{\xi'}; \boldsymbol{\theta}_u^{[i]}\right) p(d_{\xi'})}. \tag{6.27}$$

6.4.3.2 M-step

By zeroing the derivative of $Q\left(\boldsymbol{\theta}_u, \boldsymbol{\theta}_u^{[i]}\right)$ given in equation (6.24) w.r.t $\boldsymbol{h}_u$, we obtain:

$$\begin{aligned}\boldsymbol{h}_u^{[i+1]} = & \\ & \left[\sum_{t=1}^{N_s}\left(\sum_{k=0}^{K_p-1}\boldsymbol{\mathcal{W}}(k)^H\boldsymbol{\mathcal{W}}(k)d_{p_t,u}(k)d_{p_t,u}^*(k) + \sum_{k=K_p}^{K-1}\sum_{\xi=1}^{|D_u|}\alpha_{k,\xi,t}\left(\boldsymbol{\theta}_u^{[i]}\right)\boldsymbol{\mathcal{W}}(k)^H\boldsymbol{\mathcal{W}}(k)d_\xi d_\xi^*\right)\right]^{-1} \\ & \times \sum_{t=1}^{N_s}\left(\sum_{k=0}^{K_p-1}\boldsymbol{\mathcal{W}}(k)^H\mathbf{y}_{p_t,u}^{SIMO}(k)\,d_{p_t,u}^*(k) + \sum_{k=K_p}^{K-1}\sum_{\xi=1}^{|D_u|}\alpha_{k,\xi,t}\left(\boldsymbol{\theta}_u^{[i]}\right)\boldsymbol{\mathcal{W}}(k)^H\mathbf{y}_{u,t}^{SIMO}(k)\,d_\xi^*\right).\end{aligned} \tag{6.28}$$

Similarly, by zeroing the derivative of $Q\left(\boldsymbol{\theta}_u, \boldsymbol{\theta}_u^{[i]}\right)$ given in equation (6.24) w.r.t $\sigma^2_{\mathbf{z}_u}$, one can get:

$$\begin{aligned}\{\sigma_{\mathbf{z}_u}{}^2\}^{[i+1]} = \frac{1}{KN_s}\sum_{t=1}^{N_s}\Bigg(&\sum_{k=0}^{K_p-1}\left\|\mathbf{y}_{p_t,u}^{SIMO}(k) - \boldsymbol{\mathcal{W}}(k)\boldsymbol{h}_u^{[i+1]}d_{p_t,u}(k)\right\|^2 \\ &+ \sum_{k=K_p}^{K-1}\sum_{\xi=1}^{|D_u|}\alpha_{k,\xi,t}\left(\boldsymbol{\theta}_u^{[i]}\right)\left\|\mathbf{y}_{u,t}^{SIMO}(k) - \boldsymbol{\mathcal{W}}(k)\boldsymbol{h}_u^{[i+1]}d_\xi\right\|^2\Bigg).\end{aligned} \tag{6.29}$$

The EM-MIMO-OFDM SB channel estimation algorithm based on N_t EM-SIMO-OFDM is then summarized below in **Algorithm 2**.

Algorithm 2 *SB-EM channel estimation based on N_t EM-SIMO*

Initialization:

1: LS-channel estimation using pilots (i.e. $\hat{\boldsymbol{h}}_{OP}$);

2: Transmitted data estimation (i.e. $\hat{\mathbf{d}}$) using ZF (or other) equalizer followed by a hard decision;

3: Interference cancellation: Considering one SIMO system by eliminating the received signal from the other transmitted signals;

4: Initialization of $\boldsymbol{\theta}_u^{[0]} = \left[\boldsymbol{h}_u^{[0]T}, \{\sigma^2_{\mathbf{z}_u}\}^{[0]}\right]^T$, $u = 1, \cdots, N_t$ as the standard pilot-based channel and noise estimates;

Processing: : For $u = 1 : N_t$

5: Estimation of $\boldsymbol{h}_u^{[i+1]}$ using $\boldsymbol{h}_u^{[i]}$ and $\{\sigma^2_{\mathbf{z}_u}\}^{[i]}$ according to equation (6.28);

6: Estimation of $\{\sigma^2_{\mathbf{z}_u}\}^{[i+1]}$ using $\{\sigma^2_{\mathbf{z}_u}\}^{[i]}$, $\boldsymbol{h}_u^{[i]}$, and $\boldsymbol{h}_u^{[i+1]}$ according to equation (6.29);

7: Set $\boldsymbol{\theta}_u^{[i]} = \boldsymbol{\theta}_u^{[i+1]}$;

8: While $\left(\|\boldsymbol{h}_u^{[i+1]} - \boldsymbol{h}_u^{[i]}\| > \epsilon\right)$ repeat from step 5;

Else: $\hat{\boldsymbol{h}}_u = \boldsymbol{h}_u^{[i+1]}$ and $\hat{\sigma}^2_{\mathbf{z}_u} = \{\sigma^2_{\mathbf{z}_u}\}^{[i+1]}$; end For

6.5 Discussions

We provide here some insightful comments on the proposed EM-like algorithms.

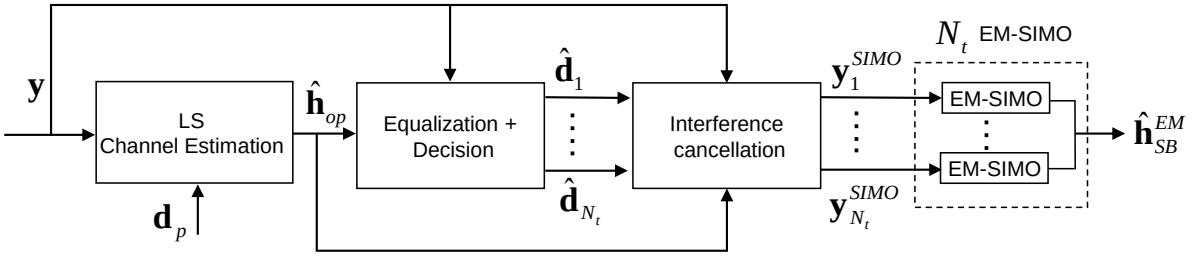

Figure 6.3: *N_t EM-SIMO SB channel estimation algorithm.*

- *Blind estimation*: For the blind channel estimation, one can ignore the pilot's terms in equations (6.15) and (6.16) and take into account only the data OFDM subcarriers as follows:

$$\begin{aligned}\text{vec}\left(\boldsymbol{\mathcal{H}}^{[i+1]}\right) = &\left[\sum_{t=1}^{N_s}\sum_{k=K_p}^{K-1}\sum_{\xi=1}^{|D|}\alpha_{k,\xi,t}\left(\boldsymbol{\theta}^{[i]}\right)\left(\mathbf{d}_\xi{}^{*}\mathbf{d}_\xi{}^{T}\otimes\boldsymbol{\mathcal{W}}(k)^{H}\boldsymbol{\mathcal{W}}(k)\right)\right]^{-1}\\ &\times\left[\sum_{t=1}^{N_s}\sum_{k=K_p}^{K-1}\sum_{\xi=1}^{|D|}\alpha_{k,\xi,t}\left(\boldsymbol{\theta}^{[i]}\right)\text{vec}\left(\boldsymbol{\mathcal{W}}(k)^{H}\mathbf{y}_t(k)\,\mathbf{d}_\xi{}^{H}\right)\right].\end{aligned} \tag{6.30}$$

$$\{\sigma_{\mathbf{v}}{}^{2}\}^{[i+1]} = \frac{1}{K_d N_s}\left(\sum_{t=1}^{N_s}\sum_{k=K_p}^{K-1}\sum_{\xi=1}^{|D|}\alpha_{k,\xi,t}\left(\boldsymbol{\theta}^{[i]}\right)\left\|\mathbf{y}_t(k)-\boldsymbol{\mathcal{W}}(k)\boldsymbol{\mathcal{H}}^{[i+1]}\mathbf{d}_\xi\right\|^2\right). \tag{6.31}$$

- *EM-MISO*: Besides allowing the parallel processing of the data, the proposed MISO-EM approach is of practical interest when the noise is spatially colored since only the noise power at the considered receiver is estimated in this scheme.

  On the other hand, since we deal with underdetermined system identification in this case, this approach cannot be considered for a large number of users. Indeed, it is known that the maximum number of sources allowed for system identifiability depends on the number of sensors, e.g. [89]. Hence, to deal with a large number of transmitters, we need to extend this approach by considering several blocks of receivers of size $1 < n_r < N_r$ each (i.e. each subsystem would be of size $N_t \times n_r$) that can be processed in parallel scheme.

- *Numerical cost*: If one considers a brute force implementation of the previous EM formulas, one can observe that for the standard EM-MIMO version, the cost is of order $O(N_s K M^{N_t}(N_t N_r N)^2)$ flops per iteration where M is the finite alphabet size. For the simplified EM version, the costs is reduced to $O(N_s K M N_t(N_t N_r N)^2)$ (i.e. the factor M^{N_t} becomes MN_t). For the EM-MISO, for each of the N_r subsystems (assumed to work in parallel scheme), we have a computational complexity of order $O(N_s K M^{N_t}(N_t N)^2)$. Finally, for the EM-SIMO version, the cost is $O(N_s N_t K M(N_r N)^2)$ flops per iteration.

- *Algorithm's convergence*: As mentioned in section III-A, the EM-MIMO algorithm converges to a local maximum point of the likelihood function [88]. This observation holds for the EM-MISO but since the latter is underdetermined, the algorithm's initialization is more difficult and the risk of local (instead of global) convergence is higher. Also, since the convergence rate of an EM algorithm is inversely related to the Fisher information of its complete-data space [88], the rate of convergence would be lower in that case as compared to the standard EM-MIMO algorithm. The EM-SIMO is somehow a specific version of the SAGE (Space-Alternating Generalized Expectation-Maximization) algorithm which is shown in [90] to lead to faster convergence under some mild assumptions. Finally, for the simplified EM version, the convergence is dependent of the quality of the first LS estimate. Indeed, since one restricts the search in (6.15), (6.16), (6.19) and (6.20) to the neighboring of the initially detected input vector (i.e. the set $|D'|$ instead of $|D|$), the estimation quality as well as the algorithm's convergence would depend strongly on this reduced size search space. In fact, if the exact input vector belongs to the set $|D'|$, then, the S-EM would have the same convergence properties as the standard EM-MIMO algorithm[4].

- *EM-SIMO*: In our work, we have chosen to use a parallel interference cancellation technique followed by an EM-based channel estimation for each SIMO subsystem. However, other possible implementations might be used (not considered here) including: (i) the use of sequential (instead of parallel) interference cancellation; (ii) the combination of the interference cancellation and the EM-based channel up-date in each iteration of our recursive EM algorithm.

6.6 Simulation results

This section analyzes the performance of the EM blind and semi-blind channel estimators in terms of the NRMSE evaluated as:

$$NRMSE = \sqrt{\frac{1}{N_{mc}} \sum_{i=1}^{N_{mc}} \frac{\left\|\hat{\mathbf{h}} - \mathbf{h}\right\|^2}{\|\mathbf{h}\|^2}}, \tag{6.32}$$

where $N_{mc} = 500$ represents the number of independent Monte Carlo realizations. The performance study is conducted for the three system configurations presented in this thesis i.e MIMO-OFDM system ($\mathbf{h}_{SB}^{EM-MIMO}$ and $\mathbf{h}_{B}^{EM-MIMO}$), parallel MISO-OFDM systems ($\mathbf{h}_{SB}^{EM-MISO}$ and

[4]Note that the error probability of the ZF equalizer is known in the literature, and hence, one can use this information to get an upper bound of the convergence probability of our S-EM algorithm.

Parameters	Specifications
Number of pilot subcarriers	$K_p = 8$
Number of data OFDM symbols	$N_s = 16$
Number of data subcarriers	$K_d = 56$
Pilot signal power	$\sigma_p^2 = 13$ dBm
Data signal power	$\boldsymbol{\sigma}_{\mathbf{d}}^2 = 10$ dBm
Number of subcarriers	$K = 64$

Table 6.1: *Simulation parameters.*

$\mathbf{h}_B^{EM-MISO}$), and SIMO-OFDM systems ($\mathbf{h}_{SB}^{EM-SIMO}$). Also, we have considered both comb-type and block-type pilots in our simulation and obtained the same kind of results. Therefore, for simplicity, we present next only those corresponding to the comb-type pilot design.

For simulations, the IEEE 802.11n training sequences are used as pilots and the channel model is assumed of type B with path delay [0 10 20 30] μs and an average path gains of [0 -4 -8 -12] dB [22]. Simulation parameters are summarized in Table 6.1.

6.6.1 EM-MIMO performance analysis

We analyse here the behavior of the EM-MIMO algorithm in terms of convergence rate and estimation accuracy. In the first experiment given in Figure 6.4, we can see that at $SNR = 10dB$, we have an algorithm's convergence in almost 1 iteration for a (2×2) MIMO system. In Figure 6.5, we illustrate the convergence rate for this same system but for different SNR values. Eventhough the number of iterations increases with the noise level, it remains relatively low and we reach the steady state regime in only few (less than 10) iterations.

Another way to exploit the SB scheme is to use it to reduce the pilot size while preserving the channel estimation quality similar to the one of the OP case [32]. Figure 6.6 presents the performance of the proposed EM-algorithm versus the number of samples removed from the pilot OFDM symbols for a given SNR equal to 10 dB (i.e. corresponding to the operating mode of the IEEE 802.11n). The black and magenta horizontal curves represent the full pilot-based channel estimation ($\mathbf{h}_{OP}$ where the pilot's size is constant) and 'EM-blind channel' ($\mathbf{h}_B^{EM}$) estimation[5], respectively. The SB channel estimation performance decreases when increasing the number of deleted pilot samples. However, it still gives better results than OP-channel estimation even though most of the pilot samples are removed.

[5]For the blind case, we have removed the indeterminacies, e.g., [64], in order to evaluate the NRMSE.

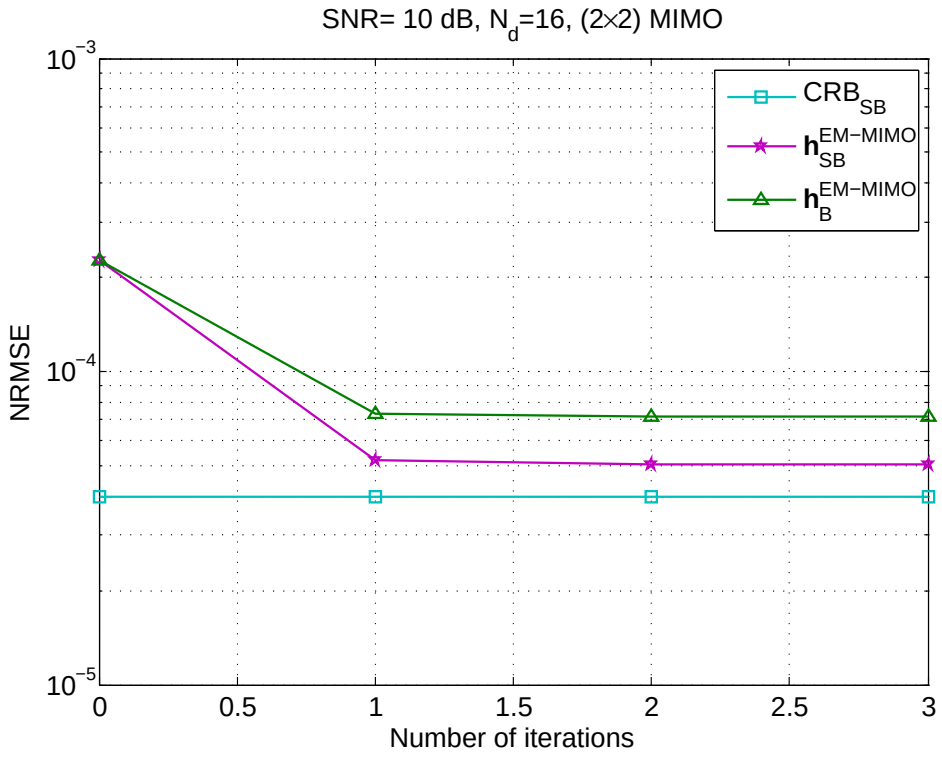

Figure 6.4: *EM-MIMO algorithm's convergence: Convergence at SNR= 10dB.*

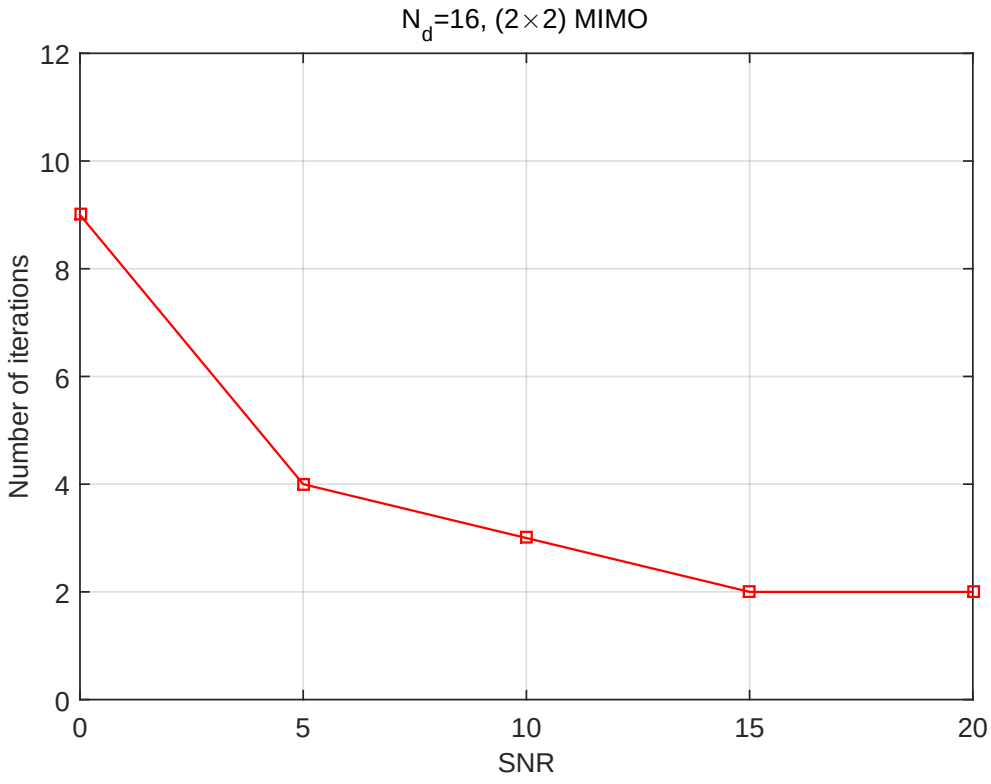

Figure 6.5: *SB EM-MIMO algorithm's convergence: Number of iterations to converge versus SNR.*

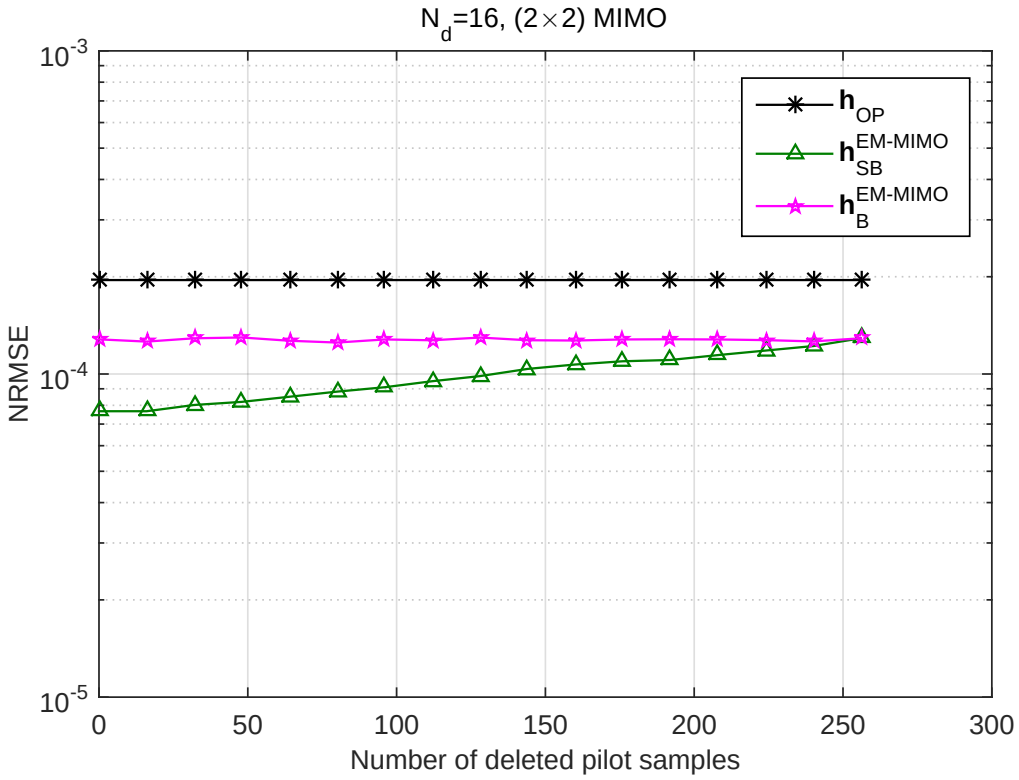

Figure 6.6: *Performance of the proposed EM algorithm versus the number of deleted pilot samples.*

Figure 6.7 compares the proposed EM-algorithm (i.e. EM-MIMO), its approximate version (S-EM) and the algorithm developed in [86] referred to as G-EM and denoted $\mathbf{h}_{SB}^{G-EM}$. The latter is based on a data Gaussian assumption. Note that, we have also compared our results with those of the GMM-based EM algorithm in [87] which shows improved performance only for quite high SNRs (starting from 25 dB in our context) as compared to the G-EM. Therefore, we choose here to keep only the comparative results with the latter algorithm. As shown in Figure 6.7, for (2×2) and (4×4) MIMO systems, we can see that the performance of the S-EM and the standard EM-MIMO are close but with a significant computational complexity gain in favor of the S-EM. Also our approximate EM algorithm outperforms the G-EM one. The significant gain can be partially explained by the fact that the authors of [86] estimate the channel coefficients in the frequency domain instead of estimating directly the channel taps $\mathbf{h}$ which leads to performance loss as shown in [71]. On the other hand, the G-EM has the advantage to not require the knowledge of the channel size N contrary to our methods.

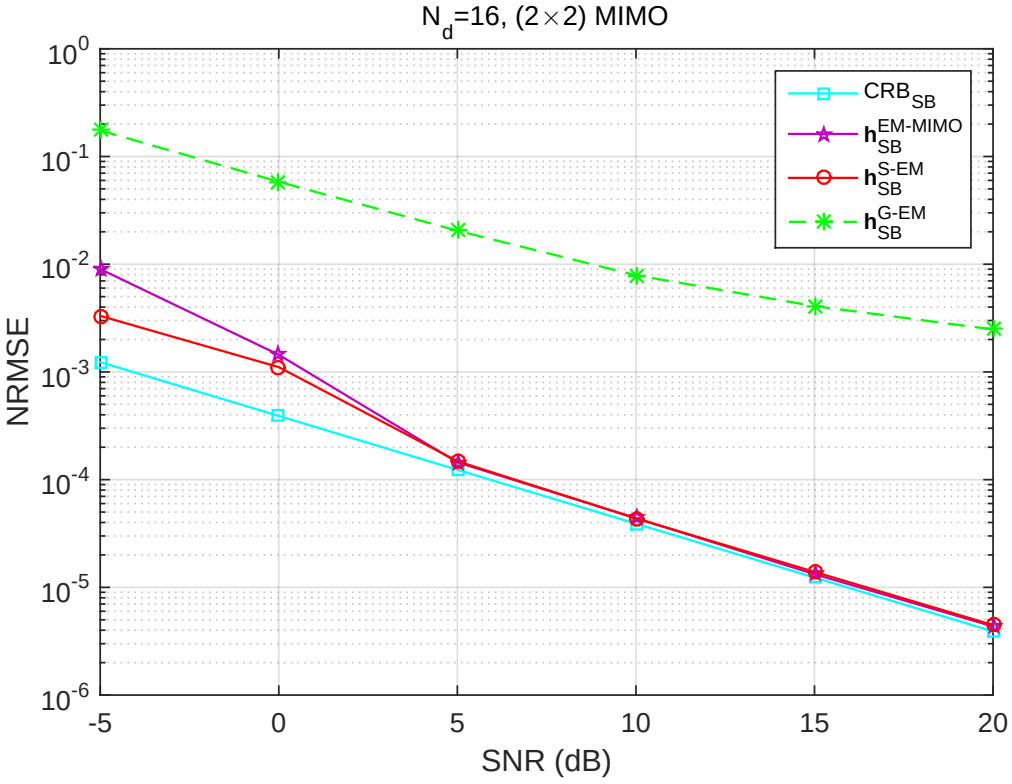

(a)

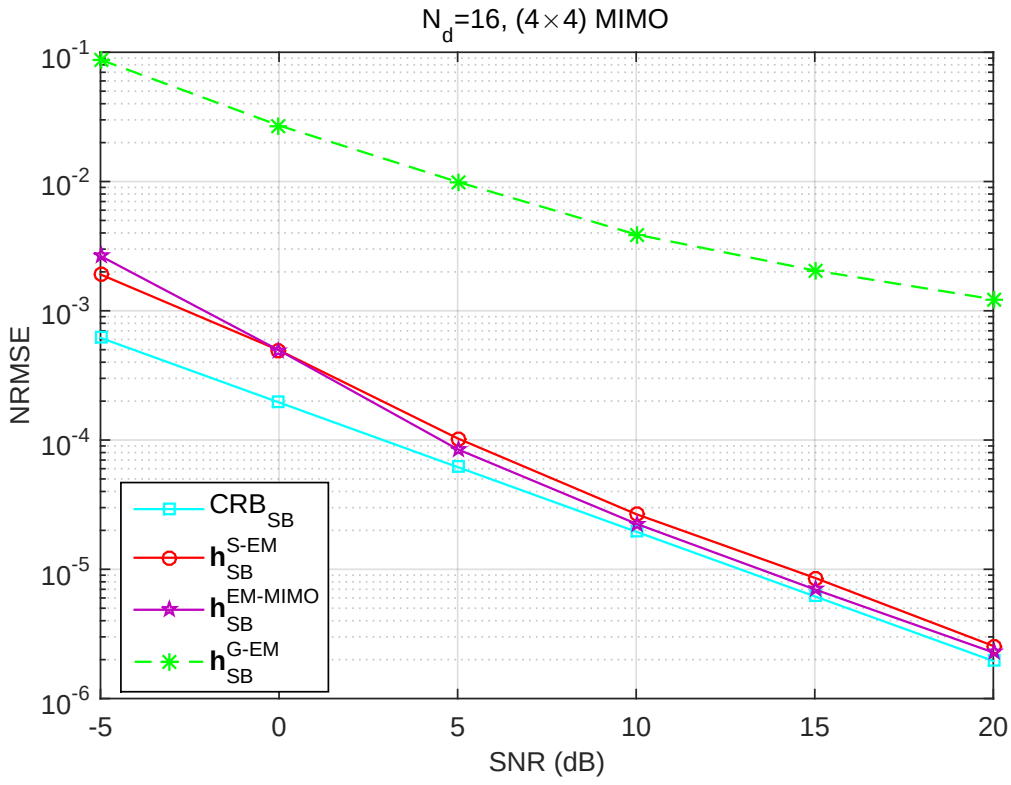

(b)

Figure 6.7: *EM-MIMO and S-EM algorithm's performance versus G-EM: (a)* 2×2 *MIMO-OFDM; (b)* 4×4 *MIMO-OFDM.*

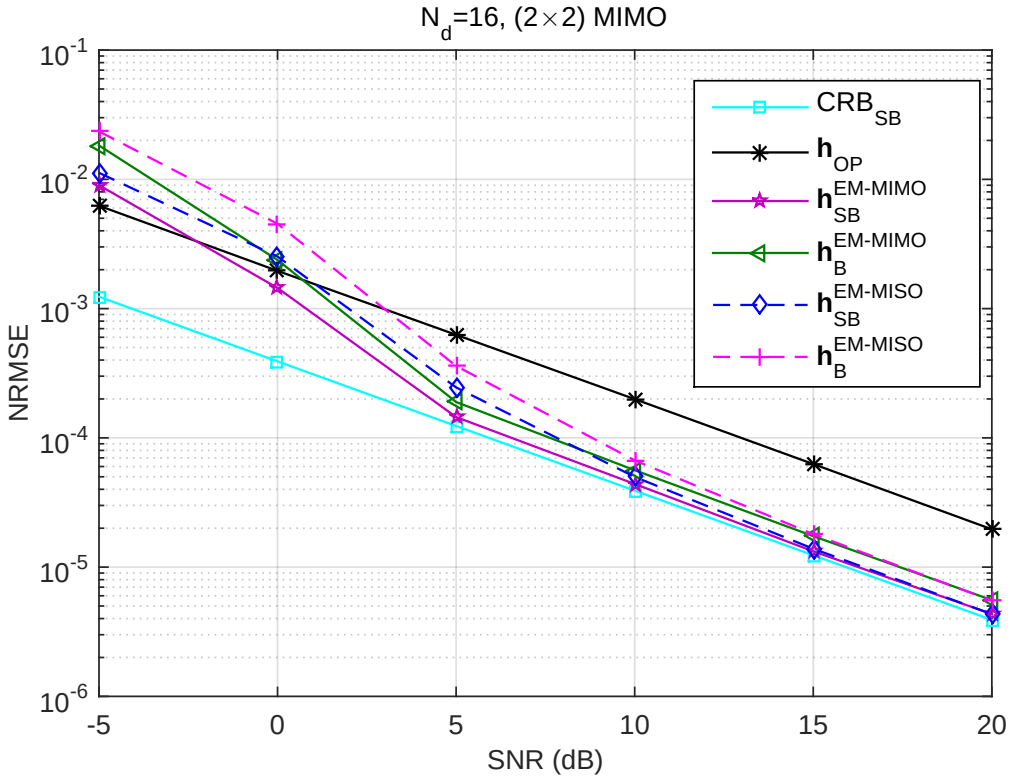

Figure 6.8: *NRMSE of the EM algorithms versus SNR:* 2×2 *MIMO.*

6.6.2 EM-MIMO versus EM-MISO

Here we compare the EM-MIMO performance and the performance of the proposed EM-MISO algorithm, where the MIMO-OFDM system is decomposed into N_r MISO-OFDM subsystems. Figures 6.8 and 6.9 provide the performance of the different channel estimation algorithms (i.e. $\mathbf{h}_{OP}$, $\mathbf{h}_{SB}^{EM-MIMO}$, $\mathbf{h}_{B}^{EM-MIMO}$, $\mathbf{h}_{SB}^{EM-MISO}$ and $\mathbf{h}_{B}^{EM-MISO}$) benchmarked by the performance limit defined by the Cramèr Rao bound CRB_{SB} detailed in [32]. The plots represent the NRMSE versus the SNR, in the case of (2×2) (Figure 6.8) and (4×4) (Figure 6.9) MIMO-OFDM systems. The curves show clearly that the SB EM-MISO behaves properly with a slight performance loss as compared to the SB EM-MIMO.

Now, we consider a (4×2) underdetermined MIMO system. Simulation results are provided in Figure 6.10 where we can see that even in this particular configuration the EM-based channel estimation algorithms perform very well. Figure 6.11 presents the behavior of the EM algorithms when increasing the number of data OFDM symbols (i.e. N_d) for a SNR set at 10 dB. The curve analysis confirms that when the number of data OFDM symbols increases, the performance of the EM algorithm in the blind and semi-blind approaches improvs significantly with only few tens of data OFDM symbols (which matches well with the limited coherence time of MIMO and

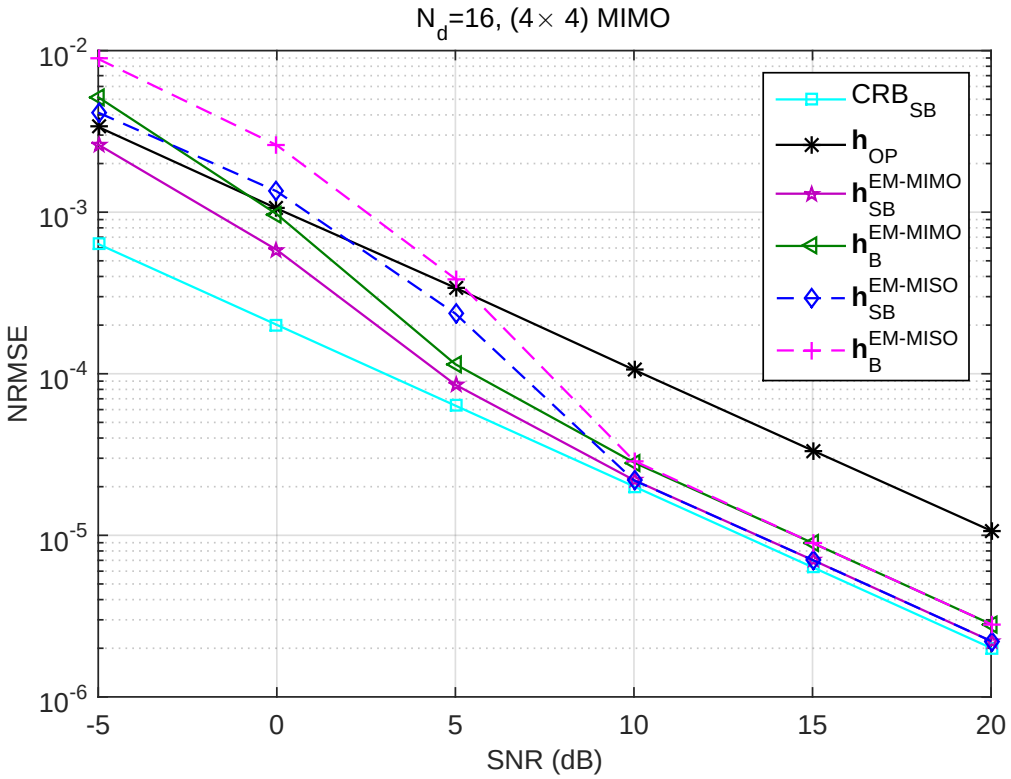

Figure 6.9: *NRMSE of the EM algorithms versus SNR:* 4×4 *MIMO.*

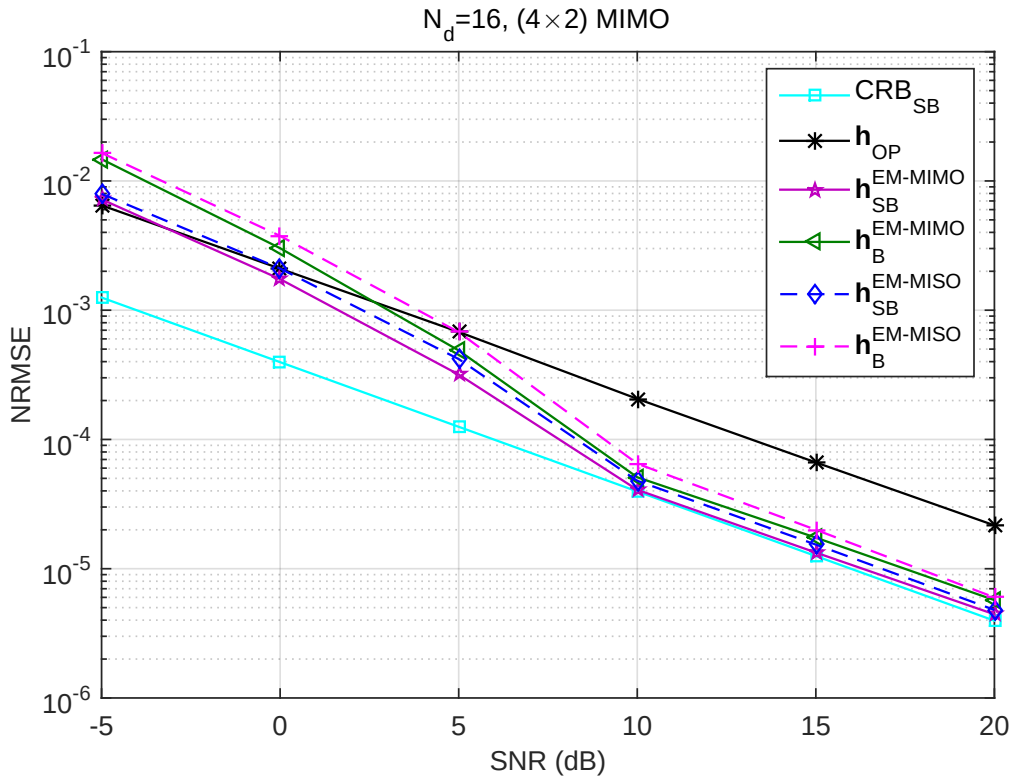

Figure 6.10: *NRMSE of the EM algorithms versus SNR in the underdetermined case* ($N_t > N_r$).

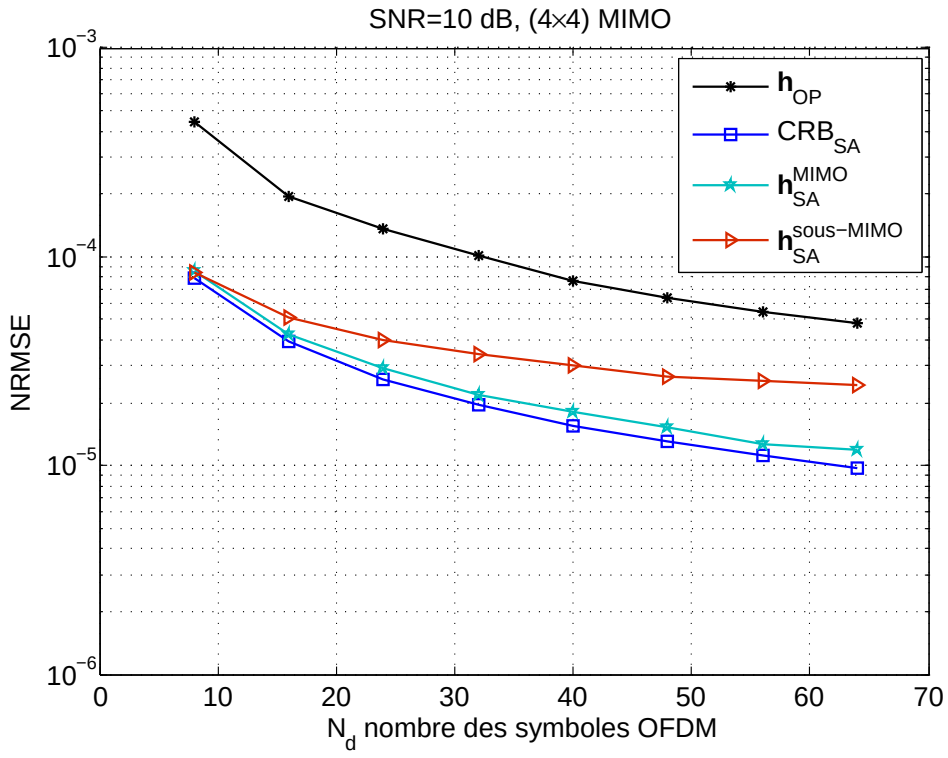

Figure 6.11: *NRMSE versus the number of OFDM symbols (N_d).*

massive MIMO systems).

6.6.3 EM-MIMO versus EM-SIMO

Figure 6.12 provides the performance versus the SNR of the proposed EM-SIMO algorithm in the case of (2×2) MIMO system decomposed into 2-SIMO subsystems (i.e. $\mathbf{h}_{SB}^{EM-SIMO}(ZF)$, where ZF refers here to the ZF equalizer used to initialize the algorithm). One observes that for a small number of users, the proposed algorithm provides good results with a significant reduction of the execution time.

Figure 6.13 illustrates the performance of the (4×4) MIMO system decomposed into 4-SIMO subsystems. We observe that when the number of users increases, the cumulative residual interference terms strongly affect the algorithm's performance (i.e. $\mathbf{h}_{SB}^{EM-SIMO}(ZF)$) if the latter uses a cheap equalizer, for instance the ZF, for its initialization. Hence, we present the EM-SIMO results for the case where the ZF equalizer is replaced by an ML-like detector based on Stack algorithm [91], [92] (i.e. $\mathbf{h}_{SB}^{EM-SIMO}$). As we can see, the performance improvement is significant as we almost reach the CRB even at low SNR values while $\mathbf{h}_{SB}^{EM-SIMO}(ZF)$ reaches the CRB only at 35 dB in that context. This highlights the importance of the initialization step

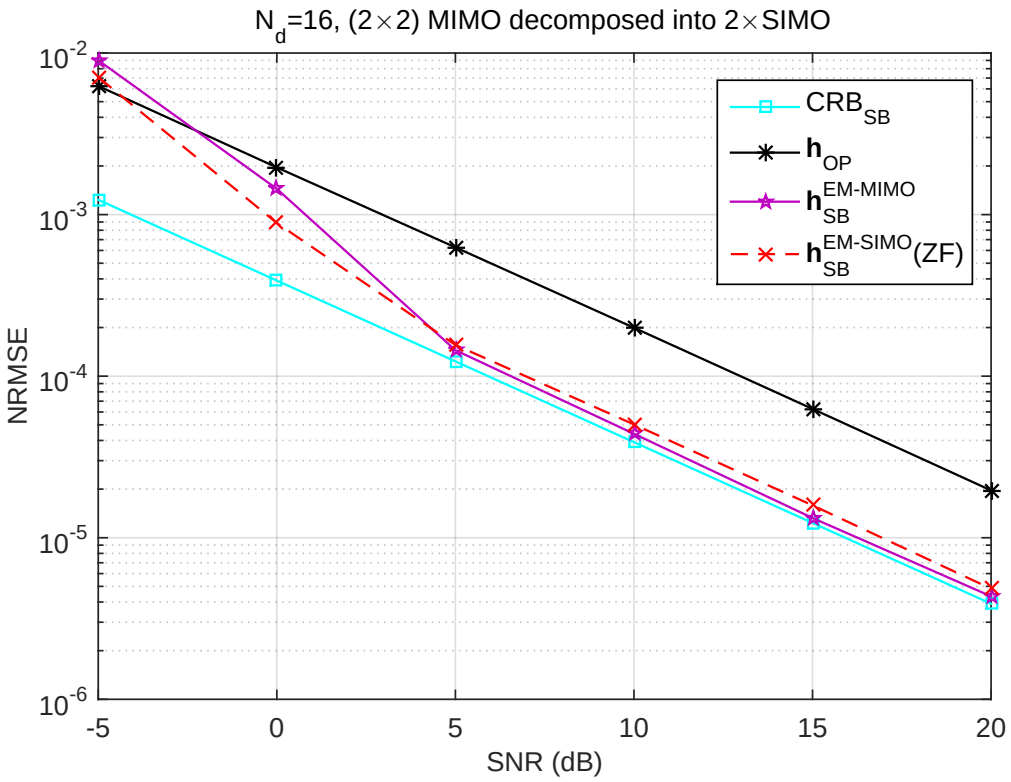

Figure 6.12: *Performance of EM-SIMO algorithm versus SNR:* 2×2 *MIMO.*

for the EM-SIMO especially for large dimensional systems.

6.7 Conclusion

This chapter introduces the EM based blind and semi-blind channel identification in MIMO-OFDM wireless communications systems. Since the EM-like algorithms are relatively expensive, a main focus of this work is the reduction of the numerical complexity while preserving at best the channel estimation quality. For that, we relied on three items:

(i) First, we took advantage of the semi-blind context which provides a good initial channel estimate (based on the available pilots) to achieve fast convergence rates (typically few iterations are sufficient to reach the steady state regime).

(ii) Since more and more systems use nowadays several computing units, we divided the overall estimation problem (MIMO) into several reduced size sub-problems (SIMO or MISO) to help reducing the cost and exploiting the parallel computational architectures.

(iii) Finally, we introduced an approximate EM algorithm (S-EM) which is shown to overcome other existing approximate EM solutions from the literature and more importantly it helps reducing the algorithm's complexity from exponential to polynomial one.

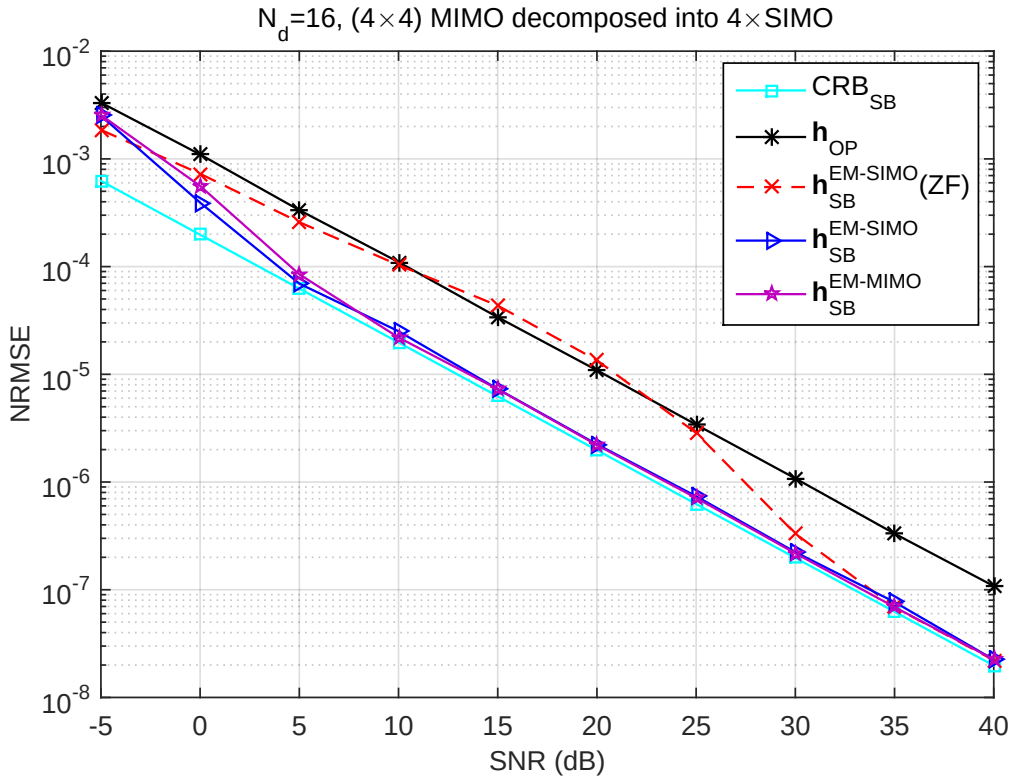

Figure 6.13: *Performance of EM-SIMO algorithm versus SNR:* 4×4 *MIMO.*

6.A Derivation of the EM algorithm for comb-type scheme

We assume that the OFDM symbols are i.i.d. and belong to a finite alphabet set of size $|D|$. The log-likelihood function is given by:

$$log\left(p\left(\mathbf{y};\boldsymbol{\theta}\right)\right) = \sum_{k=0}^{K_p-1} p\left(\mathbf{y}\left(k\right);\boldsymbol{\theta}\right) + \sum_{k=K_p}^{K-1} p\left(\mathbf{y}\left(k\right);\boldsymbol{\theta}\right), \tag{6.33}$$

- **E-step**

The auxiliary function $Q\left(\boldsymbol{\theta},\boldsymbol{\theta}^{[i]}\right)$, in the E-step of the EM-algorithm, can be derived as:

$$\begin{aligned} Q\left(\boldsymbol{\theta},\boldsymbol{\theta}^{[i]}\right) &= E_{\mathbf{d}|\mathbf{y};\theta^{[i]}}\left[\sum_{k=0}^{K_p-1} \log\left(p\left(\mathbf{y}(k)|\mathbf{d}_p(k);\boldsymbol{\theta}\right)\right) + \sum_{k=K_p}^{K-1} \log\left(p\left(\mathbf{y}(k)|\mathbf{d}_d(k);\boldsymbol{\theta}\right)\right)\right] \\ &= \sum_{k=0}^{K_p-1} \log\left(p\left(\mathbf{y}(k)|\mathbf{d}_p(k);\boldsymbol{\theta}\right)\right) + \sum_{k=K_p}^{K-1} E_{\mathbf{d}|\mathbf{y};\theta^{[i]}}\left[\log\left(p\left(\mathbf{y}(k)|\mathbf{d}_d(k);\boldsymbol{\theta}\right)\right)\right] \\ &= \sum_{k=0}^{K_p-1} \log\left(p\left(\mathbf{y}(k)|\mathbf{d}_p(k);\boldsymbol{\theta}\right)\right) + \sum_{k=K_p}^{K-1} \sum_{\xi=1}^{|D|} p\left(\mathbf{d}_\xi|\mathbf{y}(k);\boldsymbol{\theta}^{[i]}\right) \log\left(p\left(\mathbf{y}(k)|\mathbf{d}_\xi;\boldsymbol{\theta}\right)\right) \end{aligned} \tag{6.34}$$

where

$$\log\left(p\left(\mathbf{y}\left(k\right)|\mathbf{d}_\xi;\boldsymbol{\theta}\right)\right) = -\frac{1}{2}\log\left(2\pi\sigma_{\mathbf{v}}^2\right) - \frac{1}{2\sigma_{\mathbf{v}}^2}\left\|\mathbf{y}\left(k\right) - \boldsymbol{\mathcal{W}}(k)\boldsymbol{\mathcal{H}}\mathbf{d}_\xi\right\|^2 \tag{6.35}$$

$$\log\left(p\left(\mathbf{y}\left(k\right)|\mathbf{d}_p(k);\boldsymbol{\theta}\right)\right) = -\frac{1}{2}\log\left(2\pi\sigma_{\mathbf{v}}^2\right) - \frac{1}{2\sigma_{\mathbf{v}}^2}\|\mathbf{y}\left(k\right) - \boldsymbol{\mathcal{W}}(k)\boldsymbol{\mathcal{H}}\mathbf{d}_p(k)\|^2 \tag{6.36}$$

$$p\left(\mathbf{d}_\xi|\mathbf{y}(k);\boldsymbol{\theta}^{[i]}\right) = \alpha_{k,\xi}\left(\boldsymbol{\theta}^{[i]}\right) = \frac{p\left(\mathbf{y}\left(k\right)|\mathbf{d}_\xi;\boldsymbol{\theta}^{[i]}\right)p\left(\mathbf{d}_\xi\right)}{\sum\limits_{\xi'=1}^{|D|} p\left(\mathbf{y}\left(k\right)|\mathbf{d}_{\xi'};\boldsymbol{\theta}^{[i]}\right)p\left(\mathbf{d}_{\xi'}\right)} \tag{6.37}$$

By substituting equations (6.35) and (6.36) in equation (6.34), one can write the auxiliary function $Q\left(\boldsymbol{\theta},\boldsymbol{\theta}^{[i]}\right)$ as follow:

$$\begin{aligned} Q\left(\boldsymbol{\theta},\boldsymbol{\theta}^{[i]}\right) = g\left(\sigma_{\mathbf{v}}^2\right) &- \tfrac{1}{2\sigma_{\mathbf{v}}^2}\sum_{k=0}^{K_p-1}\|\mathbf{y}\left(k\right) - \boldsymbol{\mathcal{W}}(k)\boldsymbol{\mathcal{H}}\mathbf{d}_p(k)\|^2 \\ &- \tfrac{1}{2\sigma_{\mathbf{v}}^2}\sum_{k=K_p}^{K-1}\sum_{\xi=1}^{|D|}\alpha_{k,\xi}\left(\boldsymbol{\theta}^{[i]}\right)\|\mathbf{y}\left(k\right) - \boldsymbol{\mathcal{W}}(k)\boldsymbol{\mathcal{H}}\mathbf{d}_\xi\|^2 \end{aligned} \tag{6.38}$$

- **M-step**

The value of $\boldsymbol{\mathcal{H}}$ that maximize $Q\left(\boldsymbol{\theta},\boldsymbol{\theta}^{[i]}\right)$, can be calculated by setting the derivative of the latter w.r.t. $\boldsymbol{\mathcal{H}}$ to zero as next:

$$\begin{aligned} &\sum_{k=0}^{K_p-1}\boldsymbol{\mathcal{W}}(k)^H\boldsymbol{\mathcal{W}}(k)\boldsymbol{\mathcal{H}}\mathbf{d}_p(k)\mathbf{d}_p(k)^H + \sum_{k=K_p}^{K-1}\sum_{\xi=1}^{|D|}\alpha_{k,\xi}\left(\boldsymbol{\theta}^{[i]}\right)\left(\boldsymbol{\mathcal{W}}(k)^H\boldsymbol{\mathcal{W}}(k)\boldsymbol{\mathcal{H}}\mathbf{d}_\xi(k)\mathbf{d}_\xi(k)^H\right) \\ &- \sum_{k=0}^{K_p-1}\boldsymbol{\mathcal{W}}(k)^H\mathbf{y}_p\left(k\right)\mathbf{d}_p(k)^H - \sum_{k=K_p}^{K-1}\sum_{\xi=1}^{|D|}\alpha_{k,\xi}\left(\boldsymbol{\theta}^{[i]}\right)\boldsymbol{\mathcal{W}}(k)^H\mathbf{y}\left(k\right)\mathbf{d}_\xi{}^H = 0 \end{aligned} \tag{6.39}$$

Using the following vec operator property:

$$\mathrm{vec}\left(\boldsymbol{\mathcal{W}}(k)^H\boldsymbol{\mathcal{W}}(k)\boldsymbol{\mathcal{H}}\mathbf{d}_p(k)\mathbf{d}_p(k)^H\right) = \left(\mathbf{d}_p(k)^*\mathbf{d}_p(k)^T \otimes \boldsymbol{\mathcal{W}}(k)^H\boldsymbol{\mathcal{W}}(k)\right) \times \mathrm{vec}\left(\boldsymbol{\mathcal{H}}\right), \tag{6.40}$$

we obtain:

$$\begin{aligned} &\mathrm{vec}\left(\boldsymbol{\mathcal{H}}^{[i+1]}\right) = \\ &\left[\sum_{k=0}^{K_p-1}\left(\mathbf{d}_p(k)^*\mathbf{d}_p(k)^T \otimes \boldsymbol{\mathcal{W}}(k)^H\boldsymbol{\mathcal{W}}(k)\right) + \sum_{k=K_p}^{K-1}\sum_{\xi=1}^{|D|}\alpha_{k,\xi}\left(\boldsymbol{\theta}^{[i]}\right)\left(\mathbf{d}_\xi{}^*\mathbf{d}_\xi{}^T \otimes \boldsymbol{\mathcal{W}}(k)^H\boldsymbol{\mathcal{W}}(k)\right)\right]^{-1} \\ &\times\left[\sum_{k=0}^{K_p-1}\mathrm{vec}\left(\boldsymbol{\mathcal{W}}(k)^H\mathbf{y}_p\left(k\right)\mathbf{d}_p(k)^H\right) + \sum_{k=K_p}^{K-1}\sum_{\xi=1}^{|D|}\alpha_{k,\xi}\left(\boldsymbol{\theta}^{[i]}\right)\mathrm{vec}\left(\boldsymbol{\mathcal{W}}(k)^H\mathbf{y}\left(k\right)\mathbf{d}_\xi{}^H\right)\right]. \end{aligned} \tag{6.41}$$

6.B Derivation of the EM algorithm for block-type scheme

In the case of block-type pilot arrangement, we combine the two data models given in equations (6.17), for pilot OFDM symbols transmission, and (6.4) for data transmission.

- **E-step**

As developed in Appendix 6.A, the auxiliary function, in this case, is given by:

$$Q\left(\boldsymbol{\theta},\boldsymbol{\theta}^{[i]}\right)=\log\left(p\left(\mathbf{y}|\mathbf{d}_p;\boldsymbol{\theta}\right)\right)+\sum_{k=0}^{K-1}\sum_{\xi=1}^{|D|}\alpha_{k,\xi}\left(\boldsymbol{\theta}^{[i]}\right)\log\left(p\left(\mathbf{y}(k)|\mathbf{d}_\xi;\boldsymbol{\theta}\right)\right) \tag{6.42}$$

where

$$\log\left(p\left(\mathbf{y}|\mathbf{d}_p;\boldsymbol{\theta}\right)\right)=-\frac{1}{2}\log\left(2\pi\sigma_{\mathbf{v}}^2\right)-\frac{1}{2\sigma_{\mathbf{v}}^2}\left\|\mathbf{y}\left(k\right)-\tilde{\mathbf{X}}\,\mathbf{P}\times\mathrm{vec}\left(\boldsymbol{\mathcal{H}}\right)\right\|^2 \tag{6.43}$$

Finally,

$$\begin{aligned}Q\left(\boldsymbol{\theta},\boldsymbol{\theta}^{[i]}\right)=g\left(\sigma_{\mathbf{v}}^2\right)&-\tfrac{1}{2\sigma_{\mathbf{v}}^2}\left\|\mathbf{y}\left(k\right)-\tilde{\mathbf{X}}\,\mathbf{P}\times\mathrm{vec}\left(\boldsymbol{\mathcal{H}}\right)\right\|^2\\&-\tfrac{1}{2\sigma_{\mathbf{v}}^2}\sum_{k=0}^{K-1}\sum_{\xi=1}^{|D|}\alpha_{k,\xi}\left(\boldsymbol{\theta}^{[i]}\right)\left\|\mathbf{y}\left(k\right)-\boldsymbol{\mathcal{W}}(k)\boldsymbol{\mathcal{H}}\mathbf{d}_\xi\right\|^2\end{aligned} \tag{6.44}$$

- **M-step**

By zeroing the derivative of equation (6.44) w.r.t. $\mathrm{vec}\left(\boldsymbol{\mathcal{H}}\right)$, we obtain:

$$\begin{aligned}&\mathbf{P}^H\tilde{\mathbf{X}}_p^H\tilde{\mathbf{X}}_p\mathbf{P}\times\mathrm{vec}\left(\boldsymbol{\mathcal{H}}\right)+\sum_{k=0}^{K-1}\sum_{\xi=1}^{|D|}\alpha_{k,\xi}\left(\boldsymbol{\theta}^{[i]}\right)\left(\mathbf{d}_\xi{}^*\mathbf{d}_\xi{}^T\otimes\boldsymbol{\mathcal{W}}(k)^H\boldsymbol{\mathcal{W}}(k)\right)\times\mathrm{vec}\left(\boldsymbol{\mathcal{H}}\right)\\&-\mathbf{P}^H\tilde{\mathbf{X}}_p^H\mathbf{Y}_p-\sum_{k=0}^{K-1}\sum_{\xi=1}^{|D|}\alpha_{k,\xi}\left(\boldsymbol{\theta}^{[i]}\right)\mathrm{vec}\left(\boldsymbol{\mathcal{W}}(k)^H\mathbf{y}\left(k\right)\mathbf{d}_\xi{}^H\right)=0.\end{aligned} \tag{6.45}$$

then leads to :

$$\begin{aligned}\mathrm{vec}\left(\boldsymbol{\mathcal{H}}^{[i+1]}\right)=&\left[\mathbf{P}^H\tilde{\mathbf{X}}_p^H\tilde{\mathbf{X}}_p\mathbf{P}+\sum_{k=0}^{K-1}\sum_{\xi=1}^{|D|}\alpha_{k,\xi}\left(\boldsymbol{\theta}^{[i]}\right)\left(\mathbf{d}_\xi{}^*\mathbf{d}_\xi{}^T\otimes\boldsymbol{\mathcal{W}}(k)^H\boldsymbol{\mathcal{W}}(k)\right)\right]^{-1}\\&\times\left[\mathbf{P}^H\tilde{\mathbf{X}}_p^H\mathbf{Y}_p+\sum_{k=0}^{K-1}\sum_{\xi=1}^{|D|}\alpha_{k,\xi}\left(\boldsymbol{\theta}^{[i]}\right)\mathrm{vec}\left(\boldsymbol{\mathcal{W}}(k)^H\mathbf{y}\left(k\right)\mathbf{d}_\xi{}^H\right)\right].\end{aligned} \tag{6.46}$$

CHAPTER 7

Subspace blind and semi-blind channel estimation

The only way of discovering the limits of the possible is to venture a little way past them into the impossible.

Clarke's Second Law.

Abstract

In this chapter, we propose a semi-blind (SB) subspace channel estimation technique for which an identifiability result is first established for the subspace based criterion. Our algorithm adopts the MIMO-OFDM system model without cyclic prefix and takes advantage of the circulant property of the channel matrix to achieve lower computational complexity and to accelerate the algorithm's convergence by generating a group of sub vectors from each received OFDM symbol. The contributions of this work have been published in national [1] and international [2] conferences.

[1] [93] A. Ladaycia, A. Mokraoui, K. Abed-Meraim, and A. Belouchrani, "Contributions à l'estimation semi-aveugle des canaux MIMO-OFDM," in GRETSI 2017, Sep. 2017, Nice, France.

[2] [94] A. Ladaycia, K. Abed-Meraim, A. Mokraoui, and A. Belouchrani, "Efficient Semi-Blind Subspace Channel Estimation for MIMO-OFDM System," in 2018 26th European Signal Processing Conference (EUSIPCO), Sep. 2018, Rome, Italy.

Chapter content

7.1 Introduction

Research work on semi-blind methods can be divided into two categories. The first category groups works that aim to improve the performance of the channel estimation through the joint use of pilots and data symbols. This is the case, for example, of [95] where the authors used a subspace approach or [26] which proposes a decomposition of the channel matrix into a whitening matrix and another unitary. The second category includes works that focus on reducing the size of the transmitted pilot signals in order to improve the throughput gain (see for example [66]). In [33], the authors exploit the semi-blind approach to reduce the transmitted power ("green communications").

This chapter proposes a semi-blind channel estimation method based on the subspace decomposition (in signal subspace and noise subspace) of the covariance matrix of the received signal. The derivation of subspace methods depends on the matrix system model. In our case, we use an appropriate windowing that increases the convergence rate together with the circular Toeplitz block structure of the system matrix associated with an OFDM symbol. First, we establish a subspace identifiability result linked to this structure before using it for semi-blind channel estimation.

Note that in the literature there exist already several versions of the subspace method, for example [95, 96] differ from the one proposed in this thesis by incorporating the cyclic prefix (CP) and virtual carriers (VC) into the system model which changes the size and structure of the system channel matrix. The latter methods are efficient only for large sample sizes and hence a fast alternative approach has been introduced in [97]. Compared to this last method, our solution does not rely on the presence of VC and has a lower computational complexity. Finally, we present simulation results with comparative study that assess the performance gain achieved by the proposed solution.

7.2 System model

This MIMO-OFDM system adopted in this study is illustrated in Figure 1.1 and described in chapter 1. The received signal $\mathbf{y}$ at the N_r receivers of the MIMO-OFDM system is given by 1 (after CP removal):

$$\mathbf{y} = \boldsymbol{\mathcal{H}}\mathbf{x} + \mathbf{v}, \tag{7.1}$$

where $\mathbf{y} = \left[\mathbf{y}_1^T \cdots \mathbf{y}_{N_r}^T\right]^T$ and $\mathbf{x} = \left[\mathbf{x}_1^T \cdots \mathbf{x}_{N_t}^T\right]^T$. The noise $\mathbf{v} = \left[\mathbf{v}_1^T \cdots \mathbf{v}_{N_r}^T\right]^T$ is assumed to be additive independent white Circular Complex Gaussian (CCG) satisfying $E\left[\mathbf{v}(k)\mathbf{v}(i)^H\right] =$

$\sigma^2_{\mathbf{v}}\mathbf{I}_K\delta_{ki}$; $(.)^H$ being the Hermitian operator; $\sigma^2_{\mathbf{v}}$ the noise variance; $\mathbf{I}_K$ the identity matrix of size $K \times K$. The channel matrix $\boldsymbol{\mathcal{H}}$ is given by:

$$\boldsymbol{\mathcal{H}} = \begin{bmatrix} \mathbf{H}_{1,1} & \cdots & \mathbf{H}_{1,N_t} \\ \vdots & \ddots & \vdots \\ \mathbf{H}_{N_r,1} & \cdots & \mathbf{H}_{N_r,N_t} \end{bmatrix}. \tag{7.2}$$

Each sub-block $\mathbf{H}_{i,j}$ (with $i = 1, \cdots, N_r$ and $j = 1, \cdots, N_t$) of the matrix $\boldsymbol{\mathcal{H}}$ is a circulant $K \times K$ Toeplitz matrix. The first row of the (i,j)-th block contains the propagation channel coefficients between the i-th transmitter and the j-th receiver $\mathbf{h}_{i,j}$ i.e. $\left(\mathbf{h}_{i,j} = [\mathrm{h}_{i,j}(0) \cdots \mathrm{h}_{i,j}(N-1)]^T\right)$, given by: $\begin{bmatrix}\mathrm{h}_{i,j}(0) & \mathbf{0}_{1\times(K-N)} & \mathrm{h}_{i,j}(N-1) \cdots \mathrm{h}_{i,j}(1)\end{bmatrix}$. The signal $\mathbf{x}_i$, sent by the i-th transmitter is an OFDM signal, modulating the data signal $\mathbf{d}_i$, using the inverse Fourier transform IFFT, as follows

$$\mathbf{x}_i = \frac{\mathbf{W}^H}{\sqrt{K}}\mathbf{d}_i, \tag{7.3}$$

where $\mathbf{W}$ represents the K-point Fourier matrix. Equation (7.1), can be rewritten as:

$$\mathbf{y} = \boldsymbol{\mathcal{H}}\boldsymbol{\mathcal{W}}\mathbf{d} + \mathbf{v} = \boldsymbol{\mathcal{A}}\mathbf{d} + \mathbf{v}, \tag{7.4}$$

where $\boldsymbol{\mathcal{A}} = \boldsymbol{\mathcal{H}}\boldsymbol{\mathcal{W}}$ and $\boldsymbol{\mathcal{W}} = \mathbf{I}_{N_t} \otimes \mathbf{W}$ with $\otimes$ referring to the Kronecker product. The transmitted data are regrouped in $\mathbf{d} = \left[\mathbf{d}_1^T \cdots \mathbf{d}_{N_t}^T\right]^T$.

In the sequel the received OFDM symbols are assumed to be i.i.d and the N_p pilots are arranged according to the block-type scheme followed by N_d data OFDM symbols. To take into account the time index (ignored in equations (7.1) and (7.4)), we will refer to the t-th OFDM symbol by $\mathbf{y}(t)$ instead of $\mathbf{y}$.

7.3 MIMO channel estimation

This section first reminds the well known Least Squares estimator, denoted LS, based on the pilot symbols known at the receiver side. Our subspace blind estimator is then introduced to ultimately derive the proposed semi-blind estimation solution. This is formulated by the minimization of a cost function that incorporates both the pilot and the blind (data) part.

7.3.1 Pilot-based channel estimation

In order to derive LS estimator, based on the training sequences, equation (7.1) is rewritten as:

$$\mathbf{y} = \tilde{\mathbf{X}}\mathbf{h} + \mathbf{v}, \tag{7.5}$$

where $\mathbf{h} = \left[\mathbf{h}_1^T \cdots \mathbf{h}_{N_r}^T\right]^T$ is a vector of size $N_r N_t N \times 1$ representing the MIMO channel taps (where $\mathbf{h}_r = \left[\mathbf{h}_{1,r}^T \cdots \mathbf{h}_{N_t,r}^T\right]^T$). $\tilde{\mathbf{X}} = \mathbf{I}_{N_r} \otimes \mathbf{X}$, with $\mathbf{X} = [\mathbf{X}_1 \cdots \mathbf{X}_{N_t}]$ where $\mathbf{X}_i$ is a circulant $K \times N$ Toeplitz matrix containing the elements of $\mathbf{x}_i$. Each column is obtained by a simple down cyclic shift of the previous one with the first column being the vector $\mathbf{x}_i$.

The LS channel estimator $\hat{\mathbf{h}}_{LS}$, using N_p pilot OFDM symbols, $\tilde{\mathbf{X}}_p = \left[\tilde{\mathbf{X}}(1)^T \cdots \tilde{\mathbf{X}}(N_p)^T\right]^T$, is obtained by the minimization of the following cost function:

$$C(\mathbf{h}) = \left\|\tilde{\mathbf{y}}_p - \tilde{\mathbf{X}}_p \mathbf{h}\right\|^2, \tag{7.6}$$

with $\tilde{\mathbf{y}}_p = \left[\mathbf{y}(1)^T \cdots \mathbf{y}(N_p)^T\right]^T$.

Then the LS estimator is given by [21]:

$$\hat{\mathbf{h}}_{LS} = \left(\tilde{\mathbf{X}}_p^H \tilde{\mathbf{X}}_p\right)^{-1} \tilde{\mathbf{X}}_p^H \tilde{\mathbf{y}}_p. \tag{7.7}$$

7.3.2 Subspace based SB channel estimation

In this subsection, we consider the subspace approach for the data model given in equation (7.1). Based on the data model assumptions, the data covariance matrix is equal to:

$$\mathbf{C}_y = E(\mathbf{y}\mathbf{y}^H) = \sigma_{\mathbf{x}}^2 \boldsymbol{\mathcal{H}} \boldsymbol{\mathcal{H}}^H + \sigma_{\mathbf{v}}^2 \mathbf{I}_{KN_r} \tag{7.8}$$

Hence, the signal subspace (principal subspace of $\mathbf{C}_y$) coincides with the range space of $\boldsymbol{\mathcal{H}}$ while the noise subspace is its orthogonal complement. These subspaces can be estimated from the eigenvalue decomposition (EVD) of $\mathbf{C}_y$ according to:

$$\mathbf{C}_y = \mathbf{U}\boldsymbol{\Lambda}\mathbf{U}^H = [\mathbf{U}_s | \mathbf{U}_n] \begin{bmatrix} \boldsymbol{\Lambda}_s & \mathbf{0} \\ \mathbf{0} & \boldsymbol{\Lambda}_n \end{bmatrix} \begin{bmatrix} \mathbf{U}_s^H \\ \mathbf{U}_n^H \end{bmatrix}, \tag{7.9}$$

where $\mathbf{C}_y$ is estimated using N_d data OFDM symbols as follows:

$$\hat{\mathbf{C}}_y = \frac{1}{N_d} \sum_{t=1}^{N_d} \mathbf{y}(t)\mathbf{y}(t)^H. \tag{7.10}$$

$\boldsymbol{\Lambda}$ is a diagonal matrix containing the eigenvalues in descending order, the matrix $\mathbf{U}_s$ of size $KN_r \times KN_t$ contains the eigenvectors associated with the largest eigenvalues representing the signal subspace. The noise subspace $\mathbf{U}_n$ is associated with the $K(N_r - N_t)$ smallest eigenvalues, i.e.:

$$[\mathbf{U}_s | \mathbf{U}_n] = [\mathbf{u}_1 \cdots \mathbf{u}_{KN_t} | \mathbf{u}_{KN_t+1} \cdots \mathbf{u}_{KN_r}]. \tag{7.11}$$

Now, the subspace identification applies only when the range space of matrix $\boldsymbol{\mathcal{H}}$ ($range(\boldsymbol{\mathcal{H}})$) characterizes uniquely the channel vector $\mathbf{h}$ (up to certain inherent indeterminacies [63]). For

this purpose, we have proved the following identifiability result:

Lemma 7.1. *Let $\mathbf{H}(z)$ be the $N_r \times N_t$ polynomial filtering matrix which (i,j)-th entry is given by $\mathbf{h}_{i,j}(z) = \sum_{k=0}^{N} h_{i,j}(k) z^{-k}$. Under the assumption that $\mathbf{H}(z)$ is irreducible (i.e. $rank(\mathbf{H}(z)) = N_t$ for all z), the range space of matrix $\boldsymbol{\mathcal{H}}$ characterizes the channel as follows: For any polynomial matrix $\mathbf{H}'(z)$ of degree N, we have $range(\boldsymbol{\mathcal{H}}') = range(\boldsymbol{\mathcal{H}})$ if and only if $\mathbf{H}'(z) = \mathbf{H}(z)\mathbf{Q}$, where $\mathbf{Q}$ is a constant $N_t \times N_t$ matrix representing the inherent indeterminacy of the blind approach [63].*

Using the previous lemma, we can blindly identify the channel vector through the orthogonality relation between the noise and signal subspaces according to:

$$\mathbf{u}_i^H \boldsymbol{\mathcal{A}} = 0 \quad i = KN_t + 1, \cdots, KN_r, \tag{7.12}$$

where $\boldsymbol{\mathcal{A}}$ is the channel matrix given in equation (7.4).

Solving this orthogonality relation in the least squares sense leads to:

$$C(\boldsymbol{\mathcal{H}}) = \sum_{i=KN_t+1}^{KN_r} \left\| \mathbf{u}_i^H \boldsymbol{\mathcal{A}} \right\|^2 = \sum_{i=KN_t+1}^{KN_r} \left\| \mathbf{u}_i^H \boldsymbol{\mathcal{H}} \boldsymbol{\mathcal{W}} \right\|^2. \tag{7.13}$$

By partitioning vector $\mathbf{u}_i$ of dimension $KN_r \times 1$ into N_r vectors $\mathbf{v}_r^i \, (r = 1, \cdots, N_r)$ of size K as follows:

$$\mathbf{u}_i = \left[\begin{array}{ccc} \mathbf{v}_1^{i\,T} & \cdots & \mathbf{v}_{N_r}^{i\,T} \end{array} \right]^T, \tag{7.14}$$

one can generate the $NN_r \times K$ matrix $\mathbf{V}_i$ as:

$$\mathbf{V}_i = \left[\begin{array}{c} \mathbf{V}_1^i \cdots \mathbf{V}_{N_r}^i \end{array} \right]^T, \tag{7.15}$$

where each matrix $\mathbf{V}_r^i$ is circulant of size $N \times K$ constructed from the vector $\mathbf{v}_r^i$. Each line is obtained by a simple left cyclic shift of the previous one with the first line being the vector $\mathbf{v}_r^{i\,T}$. The cost function given by equation (7.13), can then be rewritten in the following form:

$$C(\underline{\mathbf{H}}) = \sum_{i=KN_t+1}^{KN_r} \left\| \underline{\mathbf{H}}^T \mathbf{V}_i{}^* \boldsymbol{\mathcal{W}} \right\|^2 = \sum_{i=KN_t+1}^{KN_r} \left\| \underline{\mathbf{H}}^T \mathbf{V}_i{}^* \right\|^2, \tag{7.16}$$

where

$$\begin{aligned} \underline{\mathbf{H}} &= [\underline{\mathbf{h}}_1 \cdots \underline{\mathbf{h}}_{N_t}] \\ \underline{\mathbf{h}} &= \left[\underline{\mathbf{h}}_1^T \cdots \underline{\mathbf{h}}_{N_t}^T \right]^T \\ \underline{\mathbf{h}}_i &= \left[\mathrm{h}_{1,i}(0) \cdots \mathrm{h}_{1,i}(N-1) \cdots \mathrm{h}_{N_r,i}(0) \cdots \mathrm{h}_{N_r,i}(N-1) \right]^T. \end{aligned} \tag{7.17}$$

This criterion reduces finally to:

$$\begin{aligned} C(\underline{\mathbf{h}}) = \sum_{i=1}^{N_t} \underline{\mathbf{h}}_i^T \boldsymbol{\Phi} \underline{\mathbf{h}}_i^* &= \underline{\mathbf{h}}^T (\mathbf{I}_{N_t} \otimes \boldsymbol{\Phi}) \underline{\mathbf{h}}^* \\ &= \underline{\mathbf{h}}^H (\mathbf{I}_{N_t} \otimes \boldsymbol{\Phi}^*) \underline{\mathbf{h}}, \end{aligned} \tag{7.18}$$

where

$$\boldsymbol{\Phi} = \sum_{i=KN_t+1}^{KN_r} \mathbf{V}_i{}^* \mathbf{V}_i{}^T, \tag{7.19}$$

The cost function in the semi-blind subspace case is composed of two cost functions: the least squares based on the pilots and the one related to the subspace blind estimation:

$$C(\underline{\mathbf{h}}) = \left\| \tilde{\mathbf{y}}_p - \tilde{\mathbf{X}}_p \mathbf{P} \underline{\mathbf{h}} \right\|^2 + \alpha \underline{\mathbf{h}}^H (\mathbf{I}_{N_t} \otimes \boldsymbol{\Phi}^*) \underline{\mathbf{h}}, \tag{7.20}$$

where α is a weighting factor[3] for the subspace method and $\mathbf{P}$ is a permutation matrix such that $\mathbf{h} = \mathbf{P}\underline{\mathbf{h}}$. The minimization of the latest cost function, leads to the semi-blind channel estimation as:

$$\hat{\underline{\mathbf{h}}} = \left(\mathbf{P}^H \tilde{\mathbf{X}}_p^H \tilde{\mathbf{X}}_p \mathbf{P} + \alpha (\mathbf{I}_{N_t} \otimes \boldsymbol{\Phi}^*) \right)^{-1} \mathbf{P}^H \tilde{\mathbf{X}}^H \tilde{\mathbf{y}}_p. \tag{7.21}$$

The channel estimation performance is strongly related to the estimation quality of covariance matrix, which is relatively poor when the number of data OFDM symbols is small. To alleviate this concern and also to reduce the computational cost (via a reduced size EVD), we introduce next a windowing technique that helps obtaining 'closed to optimal' performance with small number of OFDM symbols.

7.3.3 Fast semi-blind channel estimation

In this part, we propose to subdivide each OFDM symbol into N_g OFDM subvectors, according to a specific shift which will be detailed hereafter. Using one received OFDM symbol $\mathbf{y}$ given in equation (7.1), one can define a set of sub-vectors $\mathbf{y}_{(g)}$ of size $N_r G \times 1$ ($G < K$ being a chosen window size) as follows[4]

$$\mathbf{y}_{(g)} = \left[\mathbf{y}_1(g : g+G-1)^T \cdots \mathbf{y}_{N_r}(g : g+G-1)^T \right]^T, \tag{7.22}$$

where $g = 1, \cdots, K-G+1$. Then, we group the N_g ($N_g = K-G+1$) vectors into one matrix $\mathbf{Y}_G = \left[\mathbf{y}_{(1)} \cdots \mathbf{y}_{(N_G)} \right]$ that is given by:

$$\mathbf{Y}_G = \boldsymbol{\mathcal{H}}_G \mathbf{X}_G + \mathbf{V}_G, \tag{7.23}$$

[3] The optimal weighting can be derived as in [98] using a two step approach.

[4] For simplicity, we adopt here some MATLAB notations.

where the new channel matrix $\mathbf{H}_G$ $(N_rG \times N_tK)$ is extracted from the matrix $\mathbf{H}$ given in (7.2) as:

$$\boldsymbol{\mathcal{H}}_G = \begin{bmatrix} \mathbf{H}_{1,1}(1:G,:) & \cdots & \mathbf{H}_{1,N_t}(1:G,:) \\ \vdots & \ddots & \vdots \\ \mathbf{H}_{N_r,1}(1:G,:) & \cdots & \mathbf{H}_{N_r,N_t}(1:G,:) \end{bmatrix}. \tag{7.24}$$

and the input data matrix is given by $\mathbf{X}_G = \left[\mathbf{x}_{(0)} \cdots \mathbf{x}_{(N_G-1)}\right]$, where $\mathbf{x}_{(g)}$ is obtained from vector $\mathbf{x}$ by applying g up-cyclic shifts.

Using equation (7.3), one can establish the relation between the i-th transmitted signal $\mathbf{x}^i_{(g)}$ and the data $\mathbf{d}_i$ as:

$$\mathbf{x}^i_{(g)} = \frac{\mathbf{W}^H}{\sqrt{K}}\mathbf{D}^g\mathbf{d}_i = \frac{\mathbf{W}^H}{\sqrt{K}}\mathbf{d}^i_{(g)}, \tag{7.25}$$

where $\mathbf{D}^g$ is $(K \times K)$ diagonal phase matrix given by:

$$\mathbf{D}^g = \frac{1}{\sqrt{(K)}}\text{diag}\{e^{j2\pi(g)(0)} \cdots e^{j2\pi(g)(K-1)}\} \tag{7.26}$$

Then, $\mathbf{x}_{(g)} = \boldsymbol{\mathcal{W}}\mathbf{d}_{(g)}$, where $\mathbf{d}_{(g)} = \left[(\mathbf{d}^1_{(g)})^T \cdots (\mathbf{d}^{N_t}_{(g)})^T\right]^T$. Finally, by concatenating all the data vectors in one $N_tK \times N_g$ matrix $\mathbf{D}_G = \left[\mathbf{d}_{(0)} \cdots \mathbf{d}_{(N_G-1)}\right]$, equation (7.23) becomes:

$$\mathbf{Y}_G = \boldsymbol{\mathcal{H}}_G\boldsymbol{\mathcal{W}}\mathbf{D}_G + \mathbf{V}_G \tag{7.27}$$

The estimation of the correlation matrix is done using the N_dN_g vectors (instead of using only N_d vectors), which leads to fast convergence speed:

$$\hat{\mathbf{C}}_G = \frac{1}{N_dN_G}\sum_{t=1}^{N_d}\mathbf{Y}_G(t)\mathbf{Y}_G(t)^H. \tag{7.28}$$

As in the previous section, under the condition that matrix $\boldsymbol{\mathcal{H}}_G$ is full column rank (and hence $GN_r > KN_t$), one can use the subspace orthogonality relation as in (7.12) to estimate the channel vector using the EVD of $\hat{\mathbf{C}}_G$.

7.4 Performance analysis and discussions

Herein, we analyze the performance of the subspace semi-blind channel estimators in terms of the normalized Root Mean Square Error (NRMSE) given by equation (6.32) for the two subspace methods presented in this thesis i.e. when considering one symbol OFDM and the case when we split this OFDM symbol into several subvectors.

The considered MIMO-OFDM wireless system is related to the IEEE 802.11n standard [22] composed of two transmitters $(N_t = 2)$ and three receivers $(N_r = 3)$. The pilot sequences (or

training sequences) correspond to those specified in the IEEE 802.11n standard, where each pilot is represented by one OFDM symbol ($K = 64$ samples) of power $P_{x_p} = 23$ dBm completed by a CP ($L = 16$ samples) at its front. The data signal power is $P_{x_d} = 20$ dBm. The channel model is of type B with path delay [0 10 20 30] μs and an average path gains of [0 -4 -8 -12] dB.

The Signal to Noise Ratio associated with pilots at the reception is defined as

$$SNR = \frac{\|\boldsymbol{\mathcal{H}}\mathbf{x}_p\|^2}{N_r N_p K \sigma_{\mathbf{v}}^2}. \tag{7.29}$$

Figure 7.1 presents a comparison between the proposed SB method, the SB method in [97] ($\mathbf{h}_{SB}^{G=45}$[12]), the LS method ($\mathbf{h}_{LS}$) and the SB Cramèr Rao bound CRB_{SB}, detailed in [32], for $N_p = 4$ and $N_d = 150$. For the subspace method, we considered the full-OFDM symbol case[5] with $G = K = 64$ ($\mathbf{h}_{SB}^{G=64}$) and the windowed case with $G = 45$ ($\mathbf{h}_{SB}^{G=45}$). The curves represent the NMSE versus the SNR for all considered methods. Several observations can be made out of this experiment: First, both SB methods (the proposed one and the SB method in [97]) have the same estimation performance but our algorithm has a reduced computational cost due to the reduced size of matrix $\mathbf{Y}_G$ as compared to the one used in [97] and to the circulant matrix structure which helps reducing the cost of the calculation of matrix $\boldsymbol{\Phi}$ in equation (7.19). Second, by comparing the cases $G = K = 64$ and $G = 45$, one can see that the windowing is of high importance to achieve the SB gain for small sample sizes. Finally, comparing the obtained results with the CRB, we observe a gap of few dBs with the optimal estimation.

Figure 7.2 presents the performance of the SB method with $G = K = 64$ and $G = 45$ versus the number of data OFDM symbols (N_d). Also, as a benchmark, we compare the results with the case where the covariance matrix for $G = K = 64$ is perfectly estimated ($\mathbf{h}_{SB}^{E}$) and given by equation (7.10). One can see that without windowing a large number of OFDM symbols (more that 300) is needed to achieve the gain of the SB approach, while the proposed windowing allows us to converge with about 20 OFDM symbols only. Another observation is that increasing the window size G improves the estimation accuracy when a large number of OFDM symbols is available.

For a given $SNR = 10dB$, Figure 7.3 illustrates the impact of the size of the partitioned OFDM symbol[6] (G) on the estimation performance for the cases $N_d = 40$ (small sample size), $N_d = 150$ (moderate sample size) and $N_d = 300$ (large sample size). We notice that the window size choice has a strong impact on the estimation performance and for small and moderate sample

[5]For this case, the method in [97] does not work without the use of the VC and hence its corresponding plot is not provided.

[6]Note that for $\boldsymbol{\mathcal{H}}_G$ to be tall and full column rank, G belongs to the range [43, 64].

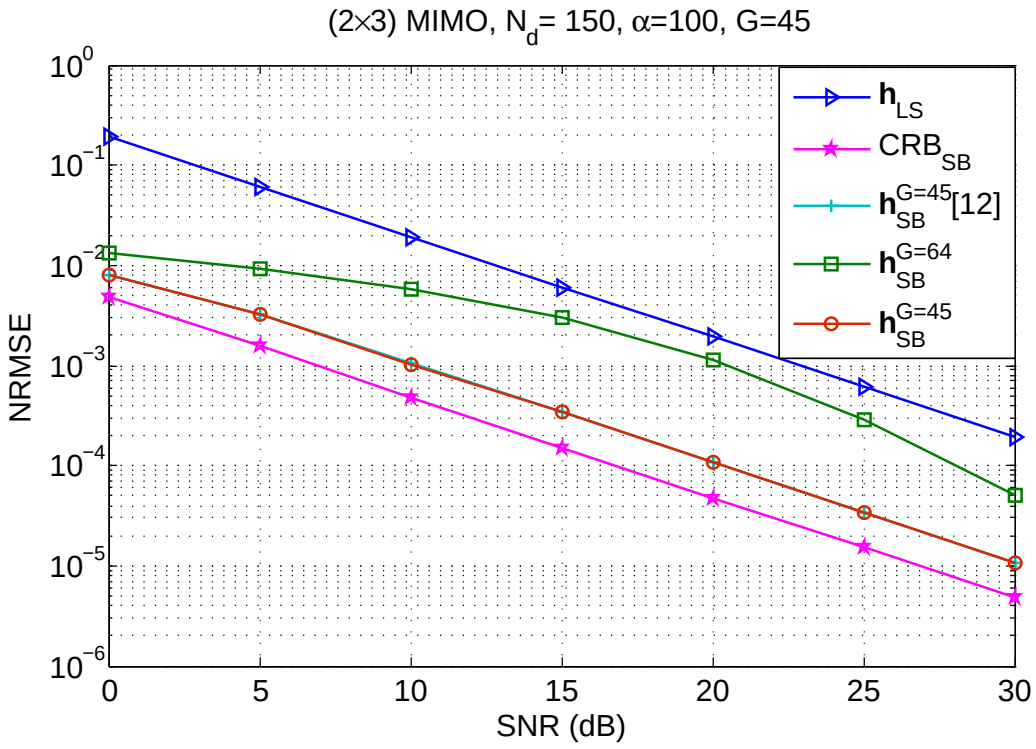

Figure 7.1: *NRMSE versus SNR.*

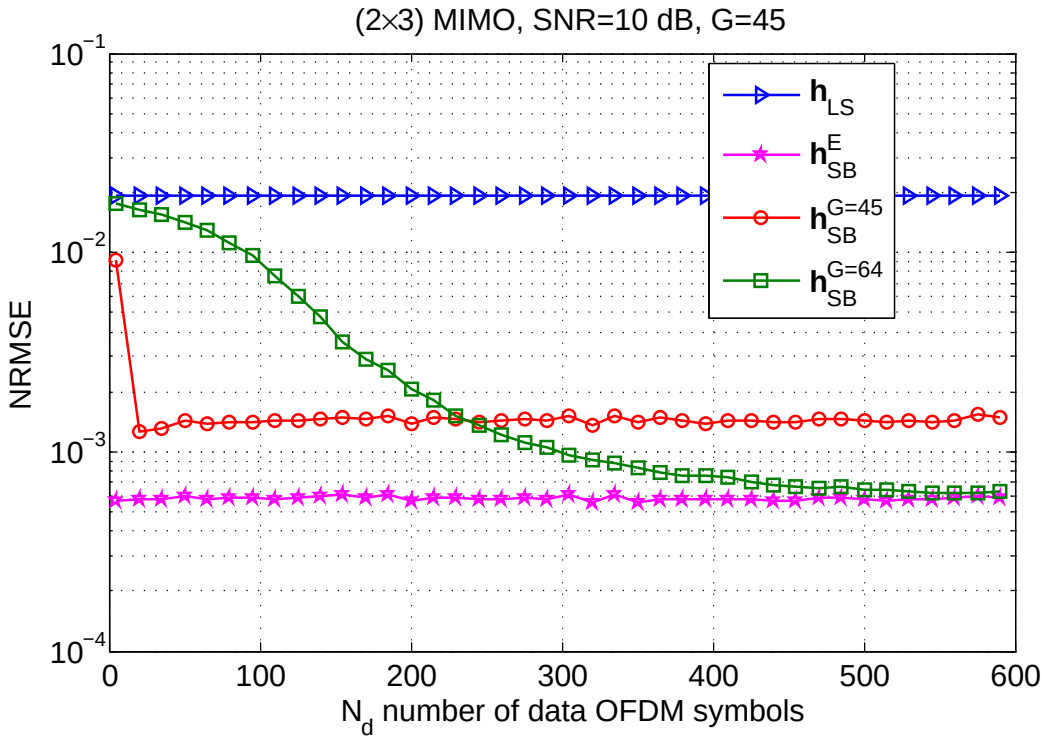

Figure 7.2: *NRMSE versus the number of data OFDM symbols N_d ($SNR = 10$ dB).*

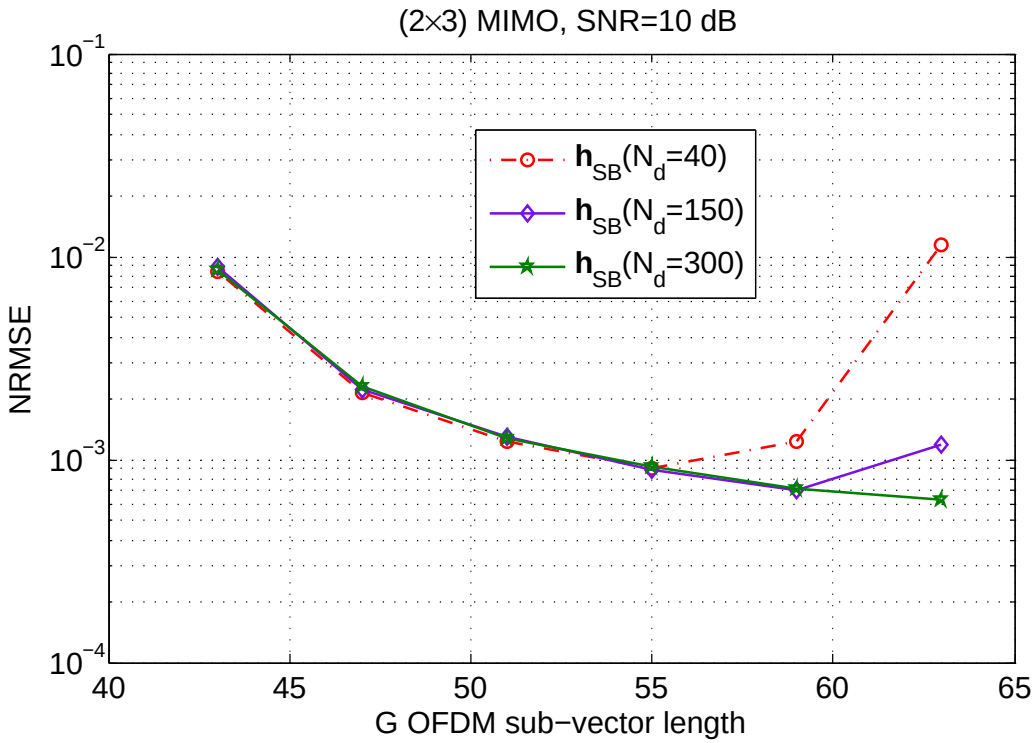

Figure 7.3: *NRMSE versus the Size of the partitioned symbol G.*

sizes, an optimal value of G exists and depends on N_d. For large sample sizes, the optimal window size is $G = K$ which confirms the observation made previously in Figure 7.2.

7.5 Conclusion

A new version of the semi-blind subspace method for channel estimation is proposed in the context of MIMO-OFDM systems. For that, we have introduced a new blind subspace estimation method for which an identifiability result has been established. This SB method exploits the circulant matrix structure to reduce the computational complexity and an appropriate windowing technique to improve the estimation accuracy for small or moderate sample sizes.

CHAPTER 8

Semi-blind estimation for specular channel model

It always seems impossible
until it's done.

Nelson Mandela.

This work has been done in collaboration with Marius Pesavento as part of a mobility to Germany (Darmstadt). It has been published in ICASSP 2019 conference[1].

Abstract

This study deals with semi-blind channel estimation in SISO-OFDM communications system in the case of specular channel model. The proposed algorithm proceeds in two main stages. The first one addresses the pilot-based Time-Of-Arrival (TOA) estimation using subspace methods and then estimates the channel through its specular model. In the second stage, one considers a decision feedback equalizer that is used to refine the channel parameters estimates.

[1] [99] A. Ladaycia, M. Pesavento, A. Mokraoui, K. Abed-Meraim, and A. Belouchrani, "Decision feedback semi-blind estimation algorithm for specular OFDM channels," in 2019 IEEE International Conference on Acoustics, Speech and Signal Processing (ICASSP2019), Accepted.

Chapter content

8.1 Introduction

Channel identification can be done by estimating the channel parameters, i.e. parametric channel estimation [100], or by estimating directly the channel coefficients [82]. Channel estimation approaches based on the parametric channel modeling require Time-Of-Arrival (TOA) (multipath delays) estimation.

Many TOA estimation approaches, based on pilots, have been developed and long established in sensor array processing. Among these methods, one can cite the subspace techniques such MUltiple SIgnal Classification (MUSIC) algorithm [101], [102], root MUSIC (rootMUSIC) [103], [104], [105] and ESPRIT algorithm (Estimation of Signal Parameters via Rotational Invariance Technique) [106]. A new subspace-like algorithm using Partial Relaxation (PR) technique is proposed in [107] and considered here in our work.

The objective of this work is to propose an efficient pilot-based and semi-blind channel estimation algorithms for SISO-OFDM system based on TOA estimation.

The first contribution is related to the TOA estimation using only one OFDM pilot. The latter is used to generate a group of sub vectors, with an appropriate windowing, to which one can apply subspace methods to estimate the TOA.

The second contribution is to incorporate the unknown data on the channel estimation process. The semi-blind TOA estimation is done using a Decision Feedback process [33], where a first estimate of the transmitted data is used with the existing pilot to enhance the TOA estimation performance.

8.2 SISO-OFDM system communications model

The considered SISO-OFDM communications system is illustrated in Figure 8.1. Each OFDM symbol is composed of K samples and is extended in time domain by the insertion of its last L samples in its front considered as a Cyclic Prefix (CP). The CP duration is assumed to be greater than or equal to delay spread. The received signal considered in baseband, after removing the CP, is given in the time domain by the following equation:

$$y(t) = x(t) * \sum_{p=1}^{N} \bar{h}_i \mathrm{sinc}(t - \tau_i) + v(t), \tag{8.1}$$

where $x(t)$ is the transmitted signal, N the number of multipaths, $\bar{h}_i$ and τ_i are respectively the complex gain and the time delay (TOA) of the i-th path.

After sampling the received OFDM signal (using the sampling rate T_s) and taking its K-point

FFT, the received signal can be written as:

$$\mathbf{y} = \mathbf{x} \odot \mathbf{A}(\tau)\bar{\mathbf{h}} + \mathbf{v}, \tag{8.2}$$

where $\mathbf{y}$ (respectively $\mathbf{x}$) is the $K \times 1$ vector for each received (respectively transmitted) OFDM symbol. The $\odot$ symbol denotes the element wise multiplication and $\bar{\mathbf{h}}$ the channel complex gain vector defined as $\bar{\mathbf{h}} = [\bar{h}_1, \cdots, \bar{h}_N]$. The matrix $\mathbf{A}(\tau) \in \mathbb{C}^{K \times N}$ is given by:

$$\mathbf{A}(\tau) = \begin{pmatrix} 1 & \cdots & 1 \\ e^{-\frac{2\pi i \tau_1}{KT_s}} & \cdots & e^{-\frac{2\pi i \tau_N}{KT_s}} \\ \vdots & \ddots & \vdots \\ e^{-\frac{2\pi i (K-1)\tau_1}{KT_s}} & \cdots & e^{-\frac{2\pi i (K-1)\tau_N}{KT_s}} \end{pmatrix}, \tag{8.3}$$

and $\mathbf{v}$ is an additive white Circular Gaussian noise satisfying $E\left[\mathbf{v}(k)\mathbf{v}(i)^H\right] = \sigma^2_{\mathbf{v}}\mathbf{I}_K\delta_{ki}$ where $(.)^H$ is the Hermitian operator; $\sigma^2_{\mathbf{v}}$ the noise variance; $\mathbf{I}_K$ the identity matrix of size $K \times K$.

Denote $\mathbf{h}$ the global transmission channel defined as $\mathbf{h} = \mathbf{A}(\tau)\bar{\mathbf{h}}$. Equation (8.2) then becomes:

$$\mathbf{y} = \mathbf{x} \odot \mathbf{h} + \mathbf{v}. \tag{8.4}$$

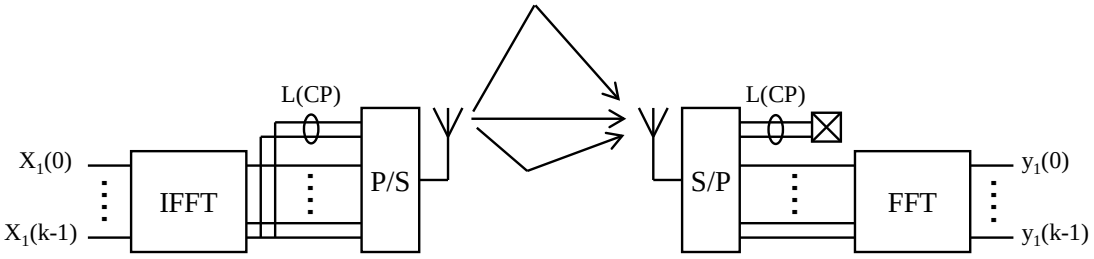

Figure 8.1: *SISO-OFDM communications system*

8.3 Proposed channel estimation

This section concerns the proposed Decision Feedback (DF) semi-blind channel estimation algorithm. This algorithm is based on the concept of Decision Feedback Equalizer technique (DFE) described in [33]. It is composed of two main stages summarized in Figure 8.2. The first one, described in section 8.3.1, provides a coarse estimate of the channel parameters that are used for its first stage equalization. The decision of this stage is then feeded back to the second one, developed in section 8.3.2, to improve the channel estimation performance.

8.3.1 First stage: pilot-based TOA estimation

To identify the channel, the first stage focuses on the estimation issue of the time delays, i.e. τ_i due to multipaths, exploiting the known training sequences. The latter, also referred to as pilots, are organized according to a block-type pilot arrangement where N_p ODFM symbols are dedicated to pilots and N_d OFDM symbols are reserved for data [82]. The known training sequences are then exploited by the receiver to estimate the TOA.

Consider $\oslash$ the element wise division. Each element $\mathbf{y}_i$ of the received signal corresponding to the $i-th$ OFDM symbol, is divided by the $i-th$ OFDM pilot vector $\mathbf{x}_i$. An average is then performed on the N_p division results as follows:

$$\mathbf{z} = \frac{1}{N_p}\sum_{i=1}^{N_p} \mathbf{y}_i \oslash \mathbf{x}_i = \mathbf{A}(\tau)\bar{\mathbf{h}} + \tilde{\mathbf{v}}, \tag{8.5}$$

$\tilde{\mathbf{v}}$ being the resulting average noise term.

To apply the subspace methods, one needs a 'sufficient' number (larger than N) of data vectors satisfying the parametric model in (8.5). For that N_G symbols, i.e. $N_G = K - G + 1$, are built from $\mathbf{z}$ using a shift windowing of size $N < G < K$. As proposed in [94], these shifted symbols are concatenated in one matrix $\mathbf{Z} = [\mathbf{z}_1, \cdots, \mathbf{z}_{N_G}] \in \mathbb{C}^{G \times N_G}$ given by:

$$\mathbf{Z} = [\mathbf{A}_1(\tau)\bar{\mathbf{h}}, \cdots, \mathbf{A}_{N_G}(\tau)\bar{\mathbf{h}}] + \tilde{\mathbf{V}}, \tag{8.6}$$

where $\tilde{\mathbf{V}}$ corresponds to the resulting shifted noise term. One observes that each matrix $\mathbf{A}_g(\tau) \in \mathbb{C}^{G \times N}$ is equal to $\mathbf{A}_1(\tau)$ multiplied by a diagonal matrix $\mathbf{D}^g \in \mathbb{C}^{N \times N}$. The latter is given by:

$$\mathbf{D}^g = \text{diag}\left\{ e^{-\frac{2\pi i(g-1)\tau_1}{KT_s}} \cdots e^{-\frac{2\pi i(g-1)\tau_N}{KT_s}} \right\}. \tag{8.7}$$

with $g = 1, \cdots, N_G$. Therefore, equation (8.6) is rewritten as:

$$\mathbf{Z} = \mathbf{A}_1(\tau)\mathbf{S} + \tilde{\mathbf{V}} \text{ with } \mathbf{S} = [\mathbf{D}^1\bar{\mathbf{h}}, \cdots, \mathbf{D}^{N_G}\bar{\mathbf{h}}]. \tag{8.8}$$

To estimate the TOA, subspace techniques such as MUSIC [101, 102], rootMUSIC [103, 104, 105], ESPRIT [106], and DOA estimation method using Partial Relaxation (PR) [107], [108] are exploited and compared in the sequel. The received OFDM symbols are assumed to be i.i.d. and uncorrelated with the channel noise. An estimate of the covariance matrix $\hat{\mathbf{R}}$ of the processed signal $\mathbf{z}$ is given by:

$$\hat{\mathbf{R}} = \frac{1}{N_G}\mathbf{Z}\mathbf{Z}^H. \tag{8.9}$$

Based on the subspace approach, using eigenvalue decomposition (EVD), the covariance matrix is decomposed:

$$\hat{\mathbf{R}} = \hat{\mathbf{U}}\hat{\mathbf{\Lambda}}\hat{\mathbf{U}}^H = \left[\hat{\mathbf{U}}_s \middle| \hat{\mathbf{U}}_n\right] \begin{bmatrix} \hat{\mathbf{\Lambda}}_s & \mathbf{0} \\ \mathbf{0} & \hat{\mathbf{\Lambda}}_n \end{bmatrix} \begin{bmatrix} \hat{\mathbf{U}}_s^H \\ \hat{\mathbf{U}}_n^H \end{bmatrix}, \tag{8.10}$$

where the diagonal matrix $\hat{\mathbf{\Lambda}}_s$, of size $N \times N$, contains the largest eigenvalues $(\hat{\lambda}_1, \cdots, \hat{\lambda}_N)$; and $\hat{\mathbf{U}}_s \in \mathbb{C}^{G\times N}$ represents the signal subspace containing the corresponding principal eigenvectors of $\hat{\mathbf{R}}$. Similarly, the noise subspace $\hat{\mathbf{U}}_n \in \mathbb{C}^{G\times(G-N)}$ is associated with the $(G-N)$ smallest eigenvalues $\hat{\mathbf{\Lambda}}_n \in \mathbb{C}^{(G-N)\times(G-N)}$.

Remark: Note that instead of averaging the OFDM symbols in (8.5) followed by the windowing of vector $\mathbf{z}$, one can apply first the windowing on each OFDM symbol and average the results through the sample estimate covariance matrix in equation (8.9). The latter approach is more expensive but allows us to slightly improve the estimation accuracy of the TOA parameters.

The standard subspace method (MUSIC algorithm) exploits the orthogonality of the noise and signal subspaces to estimate the TOA according to [101, 102]: $\min_\tau \|\hat{\mathbf{U}}_n^H \mathbf{a}(\tau)\|^2$ where $\mathbf{a}(\tau) = [1, e^{-\frac{2\pi i \tau_1}{KT_s}}, \cdots, e^{-\frac{2\pi i (G-1)\tau_1}{KT_s}}]^T$. To avoid this complex non-linear optimization problem, a simplified subspace approach using polynomial rooting (rootMUSIC) has been proposed in the literature [103, 104, 105]. On the other hand, to improve the estimation accuracy, one should minimize $\|\hat{\mathbf{U}}_n^H \mathbf{A}(\tau)\|^2$ which requires a joint estimation of all TOA parameters. This is obviously, too expensive, and hence an alternative solution is the one given in [107], [108] using partial relaxation.

Once the TOA $\boldsymbol{\tau}$ is estimated, the least-squares estimate of the complex gain vector $\bar{\mathbf{h}}$ and the global channel $\mathbf{h}$, using equation (8.5), is deduced as follows:

$$\begin{aligned} \hat{\bar{\mathbf{h}}} &= \mathbf{A}(\hat{\boldsymbol{\tau}}_{OP})^\sharp \mathbf{z}, \\ \hat{\mathbf{h}}_{OP} &= \mathbf{A}(\hat{\boldsymbol{\tau}}_{OP}) \hat{\bar{\mathbf{h}}}, \end{aligned} \tag{8.11}$$

where $(.)^\sharp$ denotes the pseudo inverse matrix. Once estimating the channel $(\hat{\mathbf{h}}_{OP})$, a linear equalizer is performed and a hard decision is applied to obtain a first estimate of the transmitted signals $(\hat{\mathbf{X}}_d)$. The latter, concatenated to the pilots, are exploited by the second stage as a new training sequence:

$$\mathbf{X}_p = [\mathbf{X}_p \;\; \hat{\mathbf{X}}_d] \in \mathbb{C}^{K\times(N_p+N_d)}. \tag{8.12}$$

8.3.2 Second stage: DF semi-blind channel estimation

The first stage feeds back the estimated data (equation (8.12)) to the second stage. This data is now considered as pilots and is then used to re-estimate the TOA and channel (i.e. $\hat{\boldsymbol{\tau}}_{SB}$, $\hat{\mathbf{h}}_{SB}$).

Three DF approches are derived according to the involved TOA estimation algorithm, namely: the MUSIC algorithm (i.e MUSIC-DF), the rootMUSIC algorithm (rootMUSIC-DF) algorithm or the PR algorithm (PR-DF).

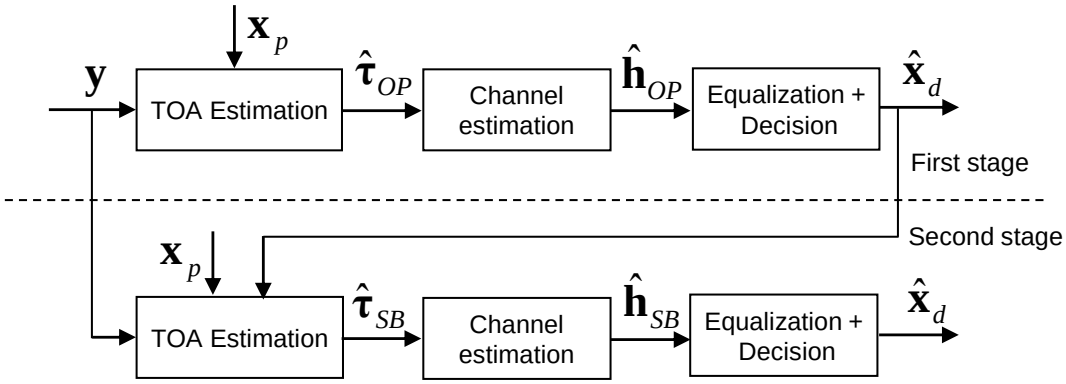

Figure 8.2: *DF semi-blind TOA estimation approach.*

8.4 Simulation results

This section discusses the performance of the proposed DF semi-blind channel estimation algorithm. The pilot sequences correspond to those specified in the IEEE 802.11n standard [22]. The parameters of simulations are summarized in the next table 8.1. The estimation performance is measured in terms of the Normalized Root Mean Square Error (NRMSE), given by:

$$\text{NRMSE} = \sqrt{\frac{1}{N_{mc}} \sum_{i=1}^{N_{mc}} \frac{\left\| \hat{\boldsymbol{\theta}}^{(i)} - \boldsymbol{\theta} \right\|^2}{\|\boldsymbol{\theta}\|^2}}, \tag{8.13}$$

where $\boldsymbol{\theta}$ represents the parameter under performance analysis ($\boldsymbol{\tau}$ or $\mathbf{h}$).

Figures 8.3 and 8.4 compare the performance between MUSIC, Root-MUSIC and PR estimators when using only the first stage with one OFDM pilot symbol and the complete scheme DF semi-blind (i.e. two stages when the data symbols are feeded back).

In Figure 8.3, one can observe that using one OFDM pilot leads to a good estimation of TOA. This estimation is enhanced when DF technique (referred to as MUSIC-DF, rootMUSIC-DF and PR-DF) is applied even at low SNR.

Parameters	**Specifications**
Channel model	IEEE 802.11n
Frequency sampling	$\frac{1}{T_s} = 20MHz$
Number of multipaths	$N = 4$
Time Of Arrivals	$\tau = [2\ 6\ 10\ 15]T_s$
Number of paths	$N = 4$
Number of pilot OFDM symbols	N_p
Number of data OFDM symbols	N_d
Pilot signal power	$P_{x_p} = 23$ dBm
Data signal power	$P_{x_d} = 20$ dBm
Number of subcarriers	$K = 512$
Cyclic prefix	$L = 64$
Size of the partitioned symbol	$G = 128$
Number of equivalent symbols	$N_G = 385$
Number of Monte Carlo realizations	$N_{mc} = 100$

Table 8.1: *Specular channel model simulation parameters.*

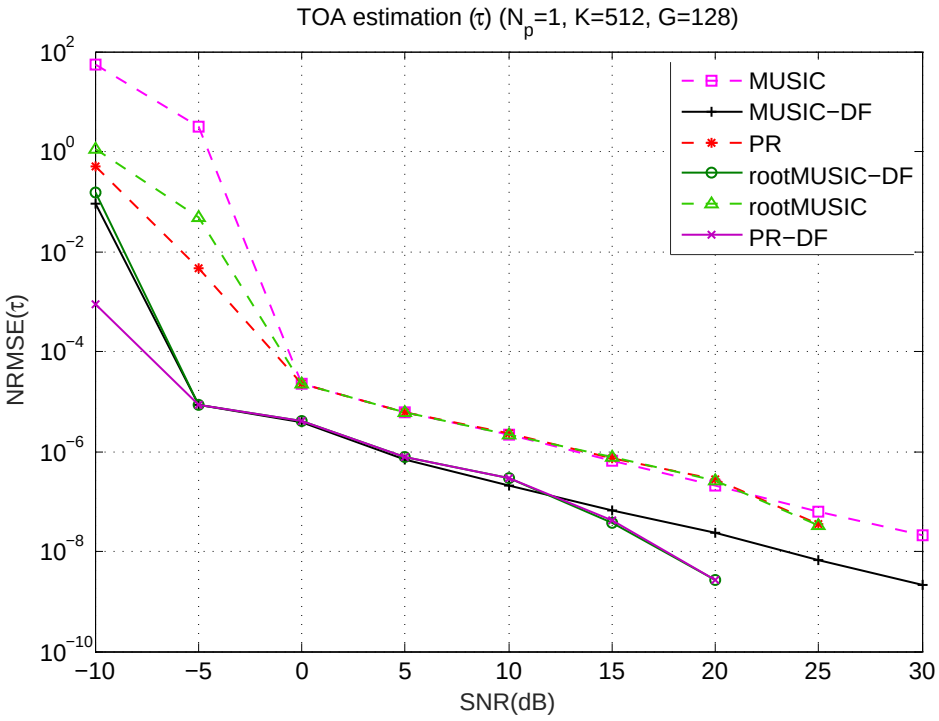

Figure 8.3: *TOA (τ) estimation performances versus SNR when N_p=1 and N_d=8.*

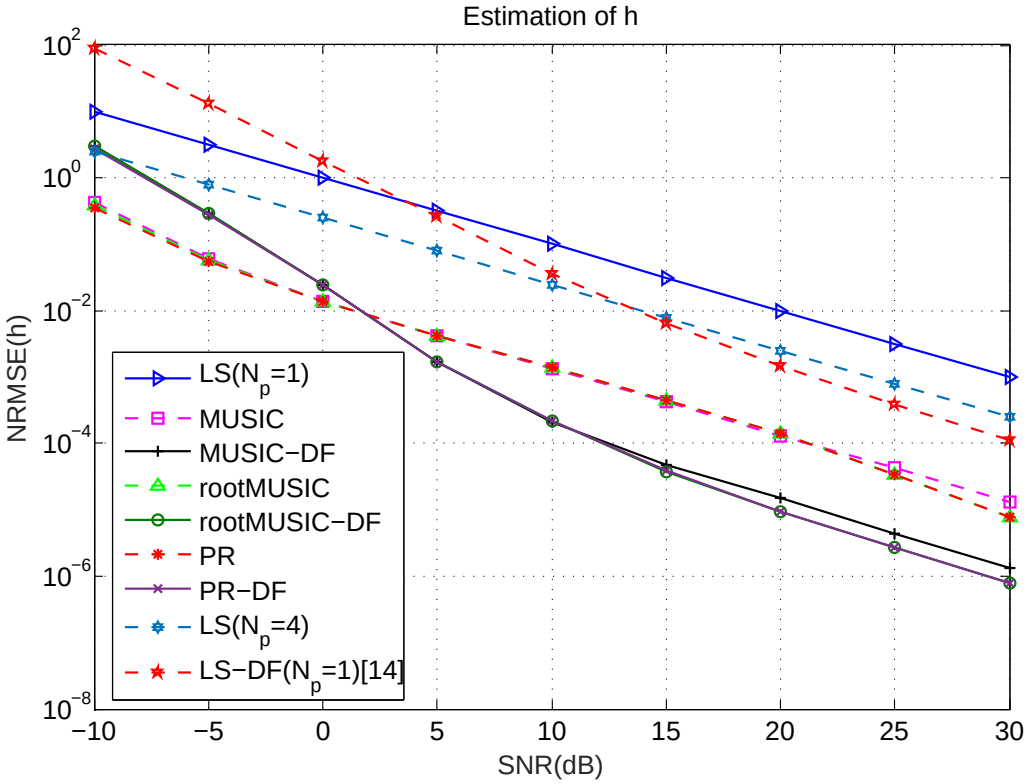

Figure 8.4: *Global channel estimation (***h***) performances versus SNR when N_p=1 and N_d=8.*

Figure 8.4 presents the channel estimation performance. The proposed approach performs well compared to the LS estimator even if the latter uses 4 OFDM pilot symbols instead on 1. Moreover the DF semi-blind approach behaves good even from relatively low SNRs. Note that at very low SNRs (lower than 2 dB), the DF approach becomes inefficient due to the ill channel equalization and hence the high decision error rate in that context. In the same plot, we present a comparison between the proposed approaches and the LS-DF algorithm proposed in [33], where we can observe that a significant gain is obtained in favor of the two methods presented in this thesis. While considering the Symbol Error Ratio (SER) plots of Figure 8.5, one can see also a non-negligible performance gain in favor of the proposed DF-based approach.

At a given SNR=-5dB, Figure 8.6 shows the influence of increasing the number of pilot OFDM symbols N_p in the estimation process on the performance of the pilot-based TOA (i.e. first stage). Indeed the TOA estimation performance is improved when the number of pilot OFDM symbols N_p is increased. Note that using few pilots ($N_p < 3$) PR gives better performance than the two other subspace methods and from $N_p = 4$ the three estimators have the same behavior.

Figure 8.7 illustrates the impact of increasing the number of data OFDM symbols in the DF semi-blind channel estimation, on the performance of the TOA estimation compared to

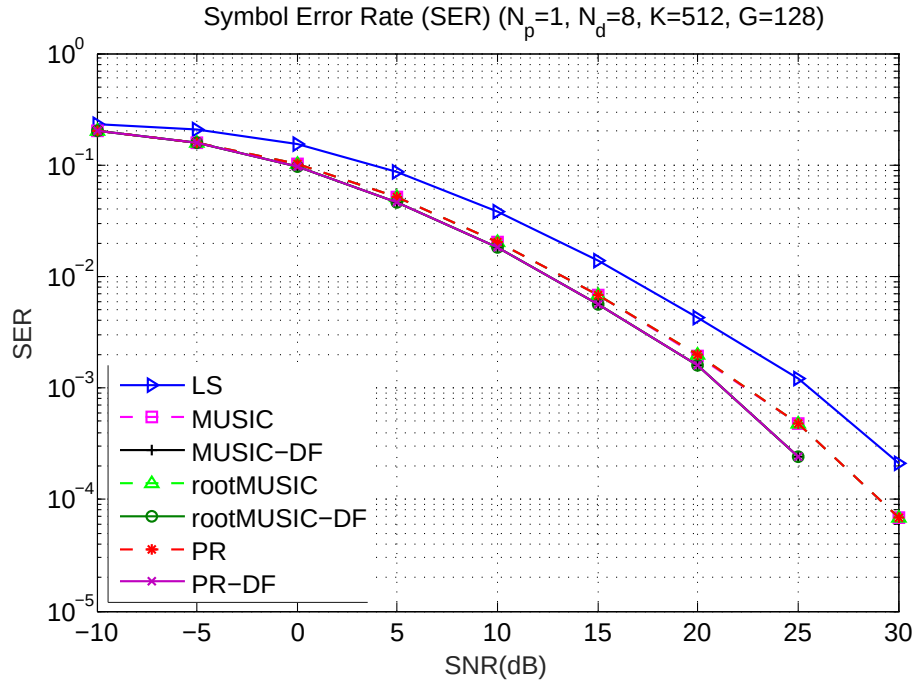

Figure 8.5: *SER versus SNR when N_p=1 and N_d=8.*

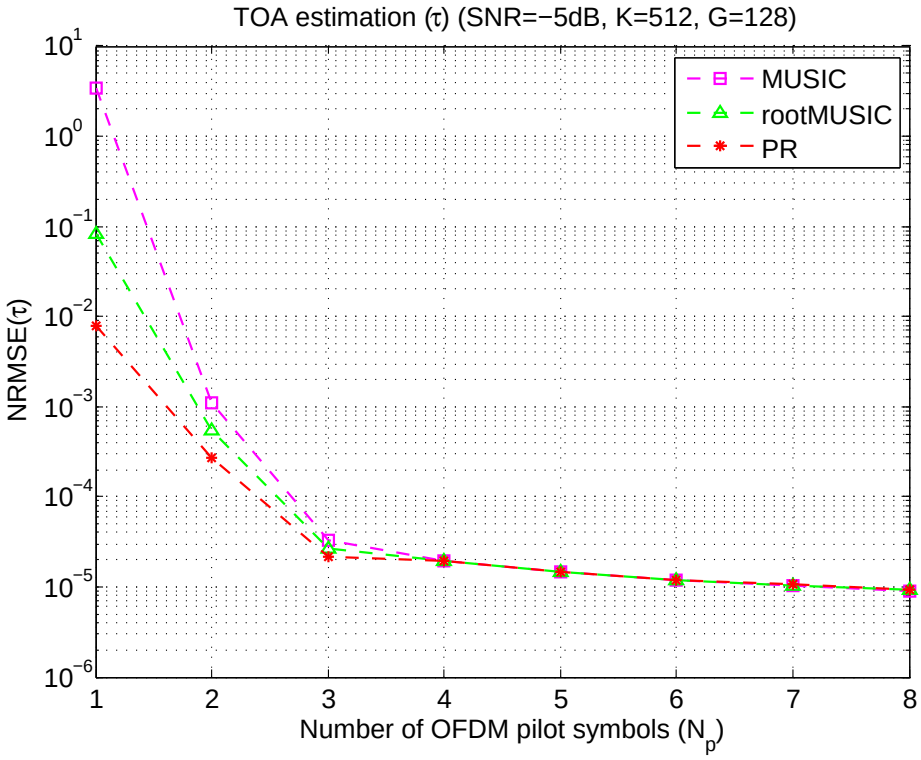

Figure 8.6: *TOA estimation performance versus the number of pilot OFDM symbols N_p for $SNR = -5dB$.*

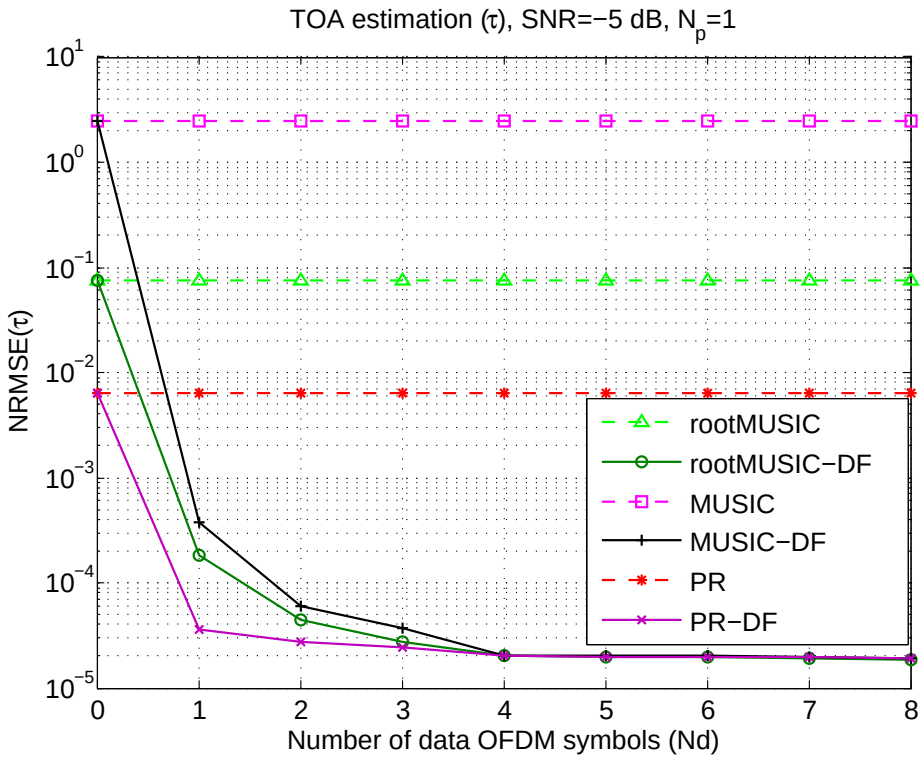

Figure 8.7: *TOA estimation performance versus the number data OFDM symbols N_d when N_p=1 and SNR=-5 dB.*

pilot-based TOA estimation (i.e. only the first stage) represented by horizontal lines. As can be seen, only very few data symbols are needed to achieve most of the semi-blind performance gain.

8.5 Conclusion

This chapter addressed two channel estimation approaches using TOA pilot-based and semi-blind estimation. The first one exploits pilot symbols with a subspace estimation method and the second employed semi-blind approach using a decision feedback (DF). Simulation results showed that good performance can be reached using only one OFDM pilot symbol with appropriate windowing.

Conclusion and future work

CHAPTER 9

Conclusion and future work

We ought not to be embarrassed of appreciating the truth and of obtaining it wherever it comes from, even if it comes from races distant and nations different from us. Nothing should be dearer to the seeker of truth than the truth itself, and there is no deterioration of the truth, nor belittling either of one who speaks it or conveys it.

Al-Kindi.

Chapter content

9.1 Achieved work

Channel estimation is of paramount importance to equalization and symbol detection problems in most wireless communications especially in MIMO-OFDM systems. Hence, it attracts the interest of researchers and system developers since the twentieth century. A spectacular advance has been realized with the development and implementation of pilot-based channel estimation algorithms motivated by its low complexity and feasibility in regards of the available calculators at that time. The appearance of powerful computers (processors) available at the base stations, and the ever increasing demand for higher data rates have led to consider other channel estimation approaches. The proposed approaches, mainly semi-blind (SB) techniques, increase the data rates by reducing the number of transmitted pilots since the latter do not carry information and represent a bandwidth waste. Moreover, many challenging aspects are moderately or weakly investigated in the open literature with respect to semi-blind channel estimation. This thesis is one of the contributions dealing with SB channel identification and its analysis in the context of MIMO-OFDM systems.

Several contributions to the SB channel estimation have been realized in the thesis: the quantification of the maximum rate of reduction of the transmitted pilots using SB channel estimation while ensuring the same pilot-based estimation quality, then the development of efficient SB channel estimators (LS-DF, subspace methods, EM-based algorithms). Moreover, further investigations on the performance bounds of MIMO-OFDM channel estimation have been successfully addressed including the analysis of the effect of CFO on channel estimation performance.

Below, we briefly summarize the overall thesis work, before listing the points corresponding to our main contributions.

First, the theoretical performance limits for the semi-blind and pilot-based channel estimation methods have been addressed in the context of MIMO-OFDM and massive MIMO-OFDM systems. This analysis has been conducted through the analytical derivation of the CRBs for different data models (i.e. CG, NCG and BPSK/QPSK) and for different pilot design patterns (i.e. block-type, lattice-type and comb-type pilot arrangement). The investigation of the derived CRBs shows the huge pilot sample reduction and consequently the throughput gain obtained thanks to the semi-blind approach while maintaining the same pilot-based channel estimation quality. In this thesis, we show that, by properly using SB techniques, the attainable reduction can exceed 95% (BPSK data model) of the original size.

This study has also been extended to large MIMO-OFDM systems (10×10) where we show

that the performance gains are slightly higher than those observed for smaller size MIMO-OFDM systems. Moreover, the same study, in chapter 2, has been generalized to multi-cell massive MIMO-OFDM systems under the effect of pilot contamination. Thereafter, we have shown that, using SB methods, it is possible to solve efficiently the pilot contamination problem when considering finite alphabet communications signals.

Second, we investigated the effect of the CFO on channel estimation performance using the CRB tool. Due to the CFO cyclostationarity propriety, we show that The CFO impacts advantageously the semi-blind channel estimation. In the case of MISO-OFDM communications system based on multi-relay transmission protocols, we have proposed two efficient approaches to jointly estimate transmission channel and CFOs. In the same context, another study has been conducted to evaluate and compare the CRB for the estimation of the subcarrier channel coefficients with and without considering the OFDM structure (i.e. estimating the channel taps in the time domain or in the frequency one). This study highlights the significant gain associated to the time domain approach.

Thirdly, we proposed four SB channel estimation algorithms. We started with the simplest one (LS-DF) which is based on the LS estimator used in conjunction with a decision feedback where the estimated data are re-injected to the channel estimation stage to enhance the estimation performance. In the context of green communications, we shown that, thanks to SB LS-DF algorithm, one can reduce up to 76% of pilot's transmitted power.

The second SB approach is based on the maximum-likelihood (ML) technique, one of the most efficient but also most expensive estimation methods. The optimization of the ML criterion is done through an iterative technique using the EM-algorithm. We proposed three approximation/simplification approaches to deal with the numerical complexity of the classical EM-algorithm. The proposed three approximations (i.e. EM-MISO, S-EM, EM-SIMO) give a good performance at lower computational cost as compared to the standard EM-algorithm.

An intermediate solution (i.e. it is cheaper than the ML but more expensive as well as more efficient than the LS-DF), is the one based on subspace technique introduced in chapter 7.

Finally, for the practical case of specular channel model, we proposed a parametric approach based on TOA estimation using subspace methods for SISO-OFDM systems. The semi-blind TOA estimation is realized using a Decision Feedback process that is considered to enhance the TOA estimation performance starting from a first 'rough' estimate obtained thanks to the existing pilot.

9.2 Thesis contributions

The main contributions of this research are listed below:

- Derivation of the channel estimation CRBs for different data models (i.e. CG, NCG, BPSK/QPSK) and for different pilot design patterns (i.e. block-type, lattice-type and comb-type pilot arrangement) in the case of MIMO-OFDM system.
- For BPSK/QPSK data model, a realistic CRB approximation has been given to bypass the high complexity of the exact CRB computation.
- Proposition of an effective computational technique to deal with the huge-size matrix manipulation needed for the CRB calculation in the large size MIMO scenario and massive MIMO.
- Quantification of rate of reduction of the overhead (pilots) due to the use of SB channel estimation.
- Derivation of the SB channel estimation CRBs for multi-cell massive MIMO-OFDM system under pilot contamination phenomenon.
- Investigation of the effectiveness of SB channel estimation to solve the pilot contamination problem when considering finite alphabet communications signals.
- Contribution to drone protection against blind interception using CRBs analysis in the blind context.
- Derivation of the SB channel estimation CRBs in the presence of CFO in MIMO-OFDM system, and investigation of the positive impact of CFO on channel estimation performance.
- Proposition of two approaches to jointly estimate CFO and channel coefficients.
- Quantification of the performance degradation between estimating the channel coefficients on time or frequency domain.
- Contribution to green communications by quantifying the reduced transmitted power using SB channel estimation.
- Proposition of SB channel estimator based on decision feedback strategy (LS-DF).
- Contribution to SB channel estimation using EM-algorithm in the case of MIMO-OFDM system.

- Derivation of four simplified versions of the SB EM-method.
- Contribution to SB subspace channel estimation for MIMO-OFDM system.
- Derivation of a parametric SB method to estimate channel parameters (TOA) in the case of specular OFDM channel.

9.3 Future work

The research work related to SB channel estimation in MIMO-OFDM systems, carried out in this thesis can be extended in several directions. Some recommendations for future work are listed below.

- Extend the SB channel estimation performance analysis to non-Gaussian noise case, where GMM (Gaussian Mixture Model) can be used to approximate the noise probability density function to a GMM one using EM algorithm. Furthermore, consider the stochastic channel model (instead of deterministic one) where Bayesian approach can be considered to evaluate the CRB for a given channel type.
- As shown in appendix A, the major issue of the OMR protocol in the MISO communications scenario, is the CFO. It will be interesting to evaluate, using the CRB, the maximum allowed CFO to guarantee a target transmission quality.
- Extend the study of chapter 8 to the MIMO-OFDM systems. This study can also be enriched by a performance analysis by deriving the corresponding CRBs.
- Implement the proposed algorithms in this thesis in a real system such as a video transmission system and evaluate in practice the throughput gain due to the use of SB channel estimation approaches.

Appendices

APPENDIX

CFO and channel estimation

Success is not final, failure is not fatal: it is the courage to continue that counts.

Winston Churchill.

This work has been done in collaboration with Ahmed Bader and Mohamed Slim Alouini from KAUST, Saudi Arabia. It has been published in EUSIPCO 2017 conference[1].

Abstract

This study deals with the joint channel and carrier frequency offset (CFO) estimation in a MISO communications system. This problem arises in OFDM based multi-relay transmission protocols such that the geo-routing one proposed by A. Bader et al in 2012. Indeed, the outstanding performance of this multi-hop relaying scheme relies heavily on the channel and CFO estimation quality at the PHY layer. In this work, two approaches are considered: The first is based on estimating the overall channel (including the CFO) as a time-varying one using an adaptive scheme under the assumption of small or moderate CFOs while the second one performs separately, the channel and CFO parameters estimation based on the considered data model.

[1] [109] A. Ladaycia, K. Abed-Meraim, A. Bader and M. S. Alouini, "CFO and channel estimation for MISO-OFDM systems," in 2017 25th European Signal Processing Conference (EUSIPCO), Aug. 2017, pp. 2264-2268, Kos, Greece.

Chapter content

A.1 Introduction

Recently, an efficient beaconless geo-routing based multi-hop relaying protocol, namely OMR (OFDM-based Multi-hop Relaying) protocol, has been proposed in [110], [111]. As for other existing geo-routing protocols, in OMR the nodes can locally make their forwarding decisions using very limited knowledge of the overall network topology. Relaying decisions in OMR are taken in a distributed fashion at any given hop based on location information, in order to alleviate the overhead which rapidly grows with node density. In addition, to deal with the fact that the proposed paradigm leads to the creation of multiple copies of the same packet with different propagation delays, OMR relies on the OFDM which allows correct packet detection at a receiving node thanks to the use of the cyclic prefix (see [110] for more details).

In [111] and [110], it has been shown that the OMR overcomes existing contention based geo-routing relaying protocols in terms of end-to-end performance (throughput and time-space footprint). However, the performance analysis in [110], [112] relies on the assumption of perfect frequency synchronization between the nodes.

In standard OFDM systems, it is well known that frequency desynchronization leads to a carrier frequency offset (CFO) at the receiver node which deteriorates significantly the decoding performance. Fortunately, this problem is well mastered and many solutions exist to track and correct this CFO effect [113], [114].

The existing solutions from the literature are not adequate for our case, as we have several simultaneous transmitters (i.e. we have a particular MISO system where all relays transmit the same data packet through different channels) each with its own CFO and channel. The aim of this study is to provide solutions to this severe problem in order to preserve the end-to-end high performance of the OMR protocol.

A.2 MISO-OFDM communications system model

Consider an OFDM system with K subcarriers and using a cyclic prefix of length L larger than the channel impulse response size N. Assume the received signal is affected by a carrier frequency offset[2] (due generally to desynchronization between the transmitter and receiver's local oscillators). Then, for one single transmitter, after sampling and removing the guard interval, the received discrete baseband signal at time n_s (associated with the n_s-th OFDM symbol) is

[2] In this study, the effect of time desynchronization is neglected.

given by [114]:

$$\mathbf{y}(n_s) = \mathbf{\Gamma}(n_s)\frac{\mathbf{F}^H}{\sqrt{K}}\mathbf{H}\mathbf{x}(n_s) + \mathbf{v}(n_s) \tag{A.1}$$

where $\mathbf{y}(n_s) = [y_0(n_s), \cdots, y_{K-1}(n_s)]^T$, and
$\mathbf{x}(n_s) = [x_0(n_s), \cdots, x_{K-1}(n_s)]^T$ ($x_k(n_s)$ being the transmitted symbol at time n_s and subcarrier k). The noise $\mathbf{v}(n_s)$ at time n_s, is assumed to be additive white Circular Complex Gaussian (CCG) satisfying $E\left[\mathbf{v}(k)\mathbf{v}(i)^H\right] = \sigma^2_{\mathbf{v}}\mathbf{I}_K\delta_{ki}$; $(.)^H$ being the Hermitian operator; $\sigma^2_{\mathbf{v}}$ the noise variance; $\mathbf{I}_K$ the identity matrix of size $K \times K$ and δ_{ki} the Dirac operator.

The channel frequency response matrix $\mathbf{H}$ of size $K \times K$, where channels are assumed constant over the packet transmission period is defined as:

$$\mathbf{H} = \text{diag}\left\{\frac{\mathbf{W}}{\sqrt{K}}\bar{\mathbf{h}}\right\} = \text{diag}\left\{H_0, \cdots, H_{K-1}\right\}, \tag{A.2}$$

H_k is the channel frequency response at the k-th subcarrier. $\bar{\mathbf{h}} = [h(0), \cdots, h(N-1)]^T$, $\mathbf{F}$ is the $(K \times K)$ Discrete Fourier Transform matrix; $\mathbf{W}$ the N first columns of $\mathbf{F}$; and $\mathbf{\Gamma}(n_s)$ the normalized CFO matrix of size $K \times K$ at the n_s-th OFDM symbol given by:

$$\Gamma(n_s) = e^{j2\pi\phi n_s}\text{diag}\left\{1, \cdots, e^{j2\pi\phi(K-1)/K}\right\}. \tag{A.3}$$

$\phi = \Delta f \times T_s$ is the normalized CFO where Δf is the CFO and T_s is the symbol period.

Now, considering a MISO system where N_t nodes transmit simultaneously the same data to a single node as illustrated in Figure A.1, the received signal in (A.1) becomes:

$$\mathbf{y}(n_s) = \sum_{i=1}^{N_t}\mathbf{\Gamma}_i(n_s)\frac{\mathbf{F}^H}{\sqrt{K}}\mathbf{H}_i\mathbf{x}(n_s) + \mathbf{v}(n_s) \tag{A.4}$$

one can write equation (A.4) as:

$$\mathbf{y}(n_s) = \sum_{i=1}^{N_t}\mathbf{\Gamma}_i(n_s)\frac{\mathbf{F}^H}{\sqrt{K}}\mathbf{X}(n_s)\mathbf{h}_i + \mathbf{v}(n_s), \tag{A.5}$$

where

$$\begin{aligned}
\mathbf{X}(n_s) &= \text{diag}\left\{x_0(n_s), \cdots, x_{K-1}(n_s)\right\} \\
\mathbf{h}_i \quad &= \left[H_{i,0}, \cdots, H_{i,K-1}\right]^T \\
\mathbf{\Gamma}_i(n_s) &= e^{j2\pi\phi_i n_s}\text{diag}\left\{1, \cdots, e^{j2\pi\phi_i(K-1)/K}\right\}.
\end{aligned} \tag{A.6}$$

$H_{i,k}$ refers to the frequency response of the i-th channel at the k-th frequency. Equation (A.5) can be re-written as :

$$\mathbf{y}(n_s) = \bar{\mathbf{H}}(n_s)\mathbf{x}(n_s) + \mathbf{v}(n_s), \tag{A.7}$$

where:

$$\bar{\mathbf{H}}(n_s) = \sum_{i=1}^{N_t} \mathbf{\Gamma}_i(n_s) \frac{\mathbf{F}^H}{\sqrt{K}} \mathbf{H}_i \tag{A.8}$$

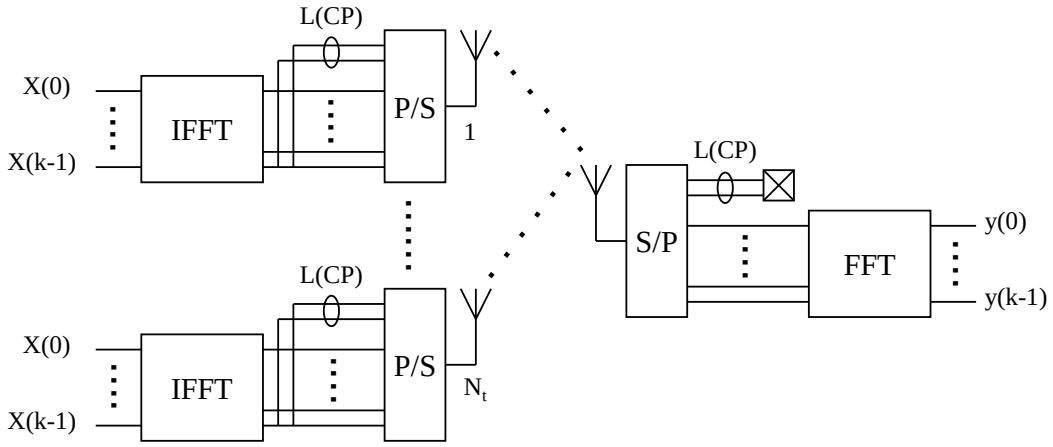

Figure A.1: *MISO-OFDM model.*

A.3 Non-Parametric Channel Estimation

Since the transmitted data is common to all nodes, we consider in this approach the N_t channels with their CFOs as one global time varying channel given in (A.8). Let us assume a slow channel variation (i.e. small CFOs), in such a way the global channel is considered approximately constant over few OFDM symbols. In this case, and after doing the FFT, equation (A.5) can be approximated by :

$$\mathbf{y}(n_s) = \mathbf{X}(n_s)\mathbf{h} + \mathbf{v}, \tag{A.9}$$

$\mathbf{h}$ is the equivalent global time-varying channel vector corresponding to (A.8).

The channel estimation is performed using N_p pilot OFDM symbols[3],

Under Gaussian noise assumption, the (LS) Least Squares (LS coincide with the optimal Maximum Likelihood (ML) estimator in that case) estimation of $\mathbf{h}$ is given by:

$$\hat{\mathbf{h}} = \left(\mathbf{X}_p{}^H \mathbf{X}_p\right)^{-1} \mathbf{X}_p{}^H \mathbf{y_p}. \tag{A.10}$$

Where $\mathbf{y}_p = \left[\mathbf{y}(1)^T \cdots \mathbf{y}(N_p)^T\right]^T$ and
$\mathbf{X}_p = \left[\mathbf{X}(1)^T \cdots \mathbf{X}(N_p)^T\right]^T$.

This algorithm can be implemented efficiently in the following way:

1) It is initialized by sending N_p successive pilot symbols.

[3]We assume the channel approximately invariant over the pilot sequence duration.

2) Use the estimated channel for the equalization and detection of the current data symbol.

3) Then, pilots are replaced in (A.10) by the "decided symbols" using a sliding window of size N_p and following a "decision directed approach", i.e. one replaces $\mathbf{X}(n_s)$ by $\hat{\mathbf{X}}(n_s)$ the decided symbol at time n_s.

The latter estimation method is valid only if the CFOs are small valued in which case the previous algorithm leads to good channel and symbol detection performance[4].

For the most general case where the CFO values are 'non controllable' and not necessarily small, we propose next a more complex but more adequate method for the estimation of the global channel parameters.

A.4 Parametric Channel Estimation

In the case of 'relatively' large CFO values, the slow channel variation assumption is violated and the previous solution fails to provide an appropriate channel estimate. In that case, we need to resort to the direct estimation of the channel parameters (i.e. CFOs and channel impulse responses). Based on the data model in (A.5), one can use a Maximum Likelihood (ML) method for the estimation of the desired parameters. However, the ML cost function being highly non linear, we consider instead a reduced cost estimation method where we neglect the phase variation along one OFDM symbol, so that one can approximate:

$$\mathbf{\Gamma}_i(n_s) \approx e^{j2\pi\phi_i n_s}\mathbf{I}_K \tag{A.11}$$

Equation (A.11) leads to the approximate noise free model

$$\mathbf{y}(n_s) \approx \frac{\mathbf{F}^H}{\sqrt{K}}\mathbf{X}(n_s)\tilde{\mathbf{h}}(n_s), \tag{A.12}$$

where $\tilde{\mathbf{h}}(n_s) = \sum_{i=1}^{N_t} \mathbf{h}_i e^{j2\pi\phi_i n_s}$ refers to the equivalent time varying channel.

Now, by definition, the channel vector $\mathbf{h}_i$ represents the frequency response coefficients of the i-th channel, i.e. $\mathbf{h}_i = \mathbf{W}\bar{\mathbf{h}}_i \big/ \sqrt{K}$. One can rewrite $\tilde{\mathbf{h}}(n_s)$ in matrix form as:

$$\begin{aligned}\tilde{\mathbf{h}}(n_s) &= \frac{\mathbf{W}}{\sqrt{K}}\left[\bar{\mathbf{h}}_1, \cdots, \bar{\mathbf{h}}_{N_t}\right]\mathbf{e}(n_s) \\ &= \frac{\mathbf{W}}{\sqrt{K}}\bar{\mathbf{h}}(n_s),\end{aligned} \tag{A.13}$$

[4]This suggests that one should consider a rough frequency synchronization between all nodes by exchanging for example a known and comon tone signal that can be used to mitigate the frequency offsets.

where $\mathbf{e}(n_s) = \left[e^{j2\pi\phi_1 n_s}, \cdots, e^{j2\pi\phi_{N_t} n_s}\right]^T$ and $\bar{\mathbf{h}}(n_s) = \left[\bar{\mathbf{h}}_1, \cdots, \bar{\mathbf{h}}_{N_t}\right]\mathbf{e}(n_s)$.

The estimate of the channel impulse response $\bar{\mathbf{h}}(n_s)$ can be easily obtained in the LS sense (using pilot symbols) as follows:

$$\mathbf{z}(n_s) = \frac{\mathbf{W}^H}{\sqrt{K}}\mathbf{X}(n_s)^{-1}\frac{\mathbf{F}}{\sqrt{K}}\mathbf{y}(n_s) \approx \bar{\mathbf{h}}(n_s) \tag{A.14}$$

By using N_p successive OFDM pilots, one can hence estimate:

$$\begin{aligned}\mathbf{Z} &= [\mathbf{z}(1), \cdots, \mathbf{z}(N_p)] \\ &\approx \left[\bar{\mathbf{h}}_1, \cdots, \bar{\mathbf{h}}_{N_t}\right]\begin{bmatrix} e^{j2\pi\phi_1} & \cdots & e^{j2\pi N_p\phi_1} \\ \vdots & \ddots & \vdots \\ e^{j2\pi\phi_{N_t}} & \cdots & e^{j2\pi N_p\phi_{N_t}} \end{bmatrix} \\ &= \breve{\mathbf{H}}\mathbf{E}^H\end{aligned} \tag{A.15}$$

From the rows of matrix $\mathbf{Z}$, one can obtain an estimate of the channel's CFO while the column vectors provide an estimate of the channel impulse responses. Since, in general the CFO values are relatively small and hence closely separated and the sample size (i.e. N_p) is small too, one needs to use high resolution techniques for the frequency estimation. One can use ESPRIT[5] method to estimate the frequencies. To this end, by performing a regular SVD decomposition on the composite matrix $\mathbf{Z}$ one can write

$$\mathbf{Z} = \mathbf{U}\mathbf{\Sigma}\mathbf{V}^H \tag{A.16}$$

where, $\mathbf{V} : N_p \times N_t$ is a matrix of principal right singular vectors[6]. Since $\mathbf{E}$ and $\mathbf{V}$ span the same subspace (i.e. the row space of $\mathbf{Z}$), one can write $\mathbf{V} = \mathbf{E}\mathbf{Q}$, where $\mathbf{Q} : N_p \times N_p$ is a non singular unknown matrix.

Let $\mathbf{V}_1 = \mathbf{V}$ (without the last row) and $\mathbf{V}_2 = \mathbf{V}$ (without the first row), then

$$\mathbf{V}_1 = \mathbf{E}_1\mathbf{Q}, \qquad \mathbf{V}_2 = \mathbf{E}_2\mathbf{Q} \tag{A.17}$$

where, $\mathbf{E}_1 = \mathbf{E}$ without the last row and $\mathbf{E}_2 = \mathbf{E}$ without the first row. Hence, one can express $\mathbf{V}_2$ in terms of $\mathbf{E}_1$ as follows

$$\mathbf{E}_2 = \mathbf{E}_1\mathbf{\Phi}, \quad \mathbf{\Phi} = \text{diag}\left\{e^{-j2\pi\phi_1}, \cdots, e^{-j2\pi\phi_{N_t}}\right\} \tag{A.18}$$

[5]ESPRIT stands for Estimation of Subspace Parameters via Rotational Invariance Technique [115].

[6]We assume here that $N_p > N_t$ and that the CFOs are distinct, $\phi_i \neq \phi_j$ if $i \neq j$.

Considering equations (A.17) and (A.18), we write $\mathbf{V}_2$ as:

$$\mathbf{V}_2 = \mathbf{E}_1 \mathbf{\Phi} \mathbf{Q} \tag{A.19}$$

by evaluating $\mathbf{\Psi}$ as

$$\mathbf{\Psi} = \mathbf{V}_1{}^{\#} \mathbf{V}_2 = \mathbf{Q}^{-1} \mathbf{\Phi} \mathbf{Q} \tag{A.20}$$

where $(.)^{\#}$ refers to the pseudo-inverse operator. $\mathbf{\Phi}$ is estimated as the matrix of eigenvalues of $\mathbf{\Psi}$ and the CFOs are obtained from the phase arguments of the eigenvalues. Once $\mathbf{\Phi}$ is obtained, one can estimate $\breve{\mathbf{H}}$ as

$$\breve{\mathbf{H}} \approx \mathbf{Z} \left(\mathbf{E}^H \right)^{\#} \tag{A.21}$$

Remarks:

1) ESPRIT is an expensive method and can be replaced by a Fourier search if the CFOs, are not too close as compared to the resolution limit of the DFT, i.e. $|(\phi_i - \phi_j)| \geq \frac{2}{N_p}$.

2) The channel and CFO estimates in (A.20) and (A.21) can be used to initialize a numerical method for ML optimization (e.g. for example with Levenberg-Marquardt method [116]) in order to improve the estimation performance, especially when the approximation in (A.11) is roughly satisfied.

A.5 Simulations results

This section analyzes the channel estimation performance for the considered MISO-OFDM wireless system. The training sequence used in this work is the Zadoff-Chu sequence considered in the LTE standard [4]. Fig. 1.2a represents the block-type pilot arrangement adopted in this work. Each field (or pilot) is represented by one OFDM symbol ($K = 64$ samples) where a CP ($L = 16$ samples) is added at its front. Simulation parameters are summarized in Table A.1.

The SNR associated with pilots at the receiver is defined as $SNR_p = \frac{\|\mathbf{X}_p \mathbf{h}\|^2}{K N_p \sigma_{\mathbf{v}}^2}$. The SNR, denoted SNR_d (in dB), associated with data is given by: $SNR_d = SNR_p - (Px_p - Px_d)$ where Px_p (respectively Px_d) is the power of pilots (respectively data) in dB.

Figure A.2 compares the NMSE of the estimated data (related to the considered channel estimation methods followed by linear zero-forcing equalization) versus SNR_p at relatively low CFO. The NMSE curves show that the parametric method and the non-parametric one have

Parameters	Specifications
Channel model	Cost 207
Number of transmit antennas	$N_t = 3$
Number of receive antennas	$N_r = 1$
Channel length	$N = 4$
Number of pilot OFDM symbols	$N_p = 4$
Number of data OFDM symbols	$N_d = 5$
Pilot signal power	$P_{x_p} = 23$ dBm
Data signal power	$P_{x_d} = 20$ dBm
Number of sub-carriers	$K = 64$

Table A.1: *MISO system simulation parameters.*

similar performance in this context (for comparison, the plot in blue represents the CFO free context, while the magenta plot is for the channel estimate obtained by 'ignoring' the CFO effect).

One can observe also that the gap with CFO free context increases with the SNR which motivates for considering the ML or other advanced estimation approaches in future works to improve the estimation performance. Figure A.3 presents comparative results but for the symbol error rate with BPSK modulated signal.

In Figures A.4 and A.5, we consider a similar experiment but for high CFO values. In that case the non-parametric approach is not adequate and does not allow correct detection of the data symbols. As in the previous figure, we still observe a large performance gap between the cases with and without CFO suggesting the use of more elaborated methods to compensate this performance loss.

In Figures A.6, A.7 and A.8, we evaluate the Normalized Root Mean Squares Error (NRMSE) of the channel estimate versus the SNR or the pilot sequence size N_p. It is observed that for large SNR or large number of pilot symbols, the parametric approach performance improves significantly. Also, its performance for high CFO values is slightly better than for low CFOs due to the improved frequency resolution. On the other hand, the estimation quality of the non-parametric solution becomes worse for larger training sequences since the assumption that the channel remains invariant over all the pilot duration is not satisfied when N_p increases.

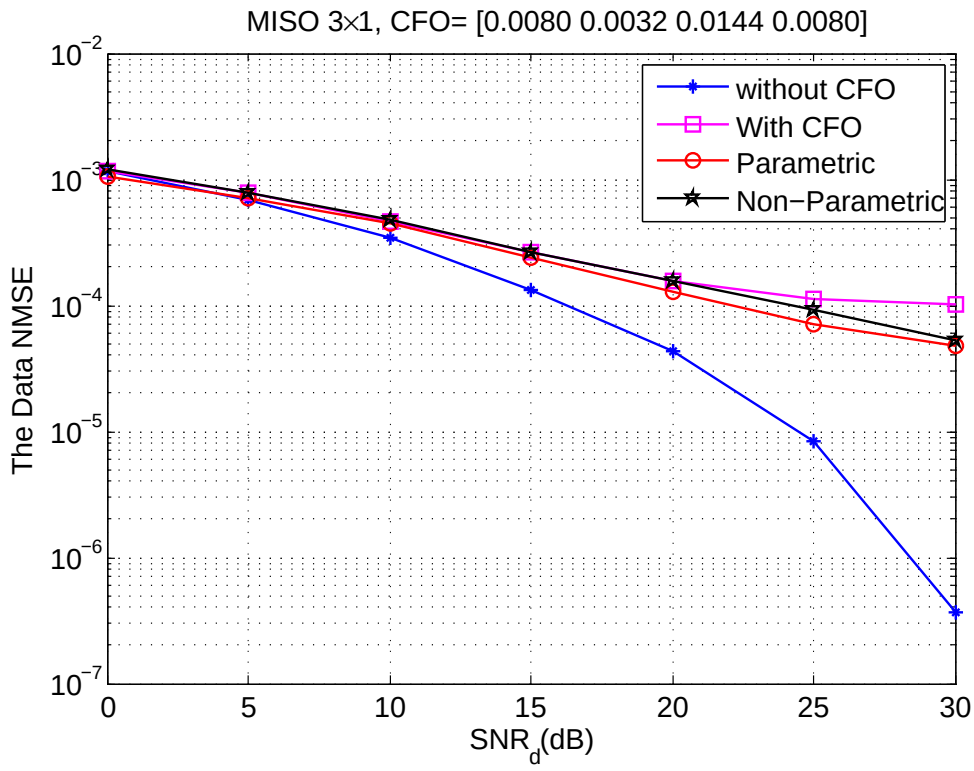

Figure A.2: *NMSE of the data versus SNR_d (with and without CFO) at low CFO*

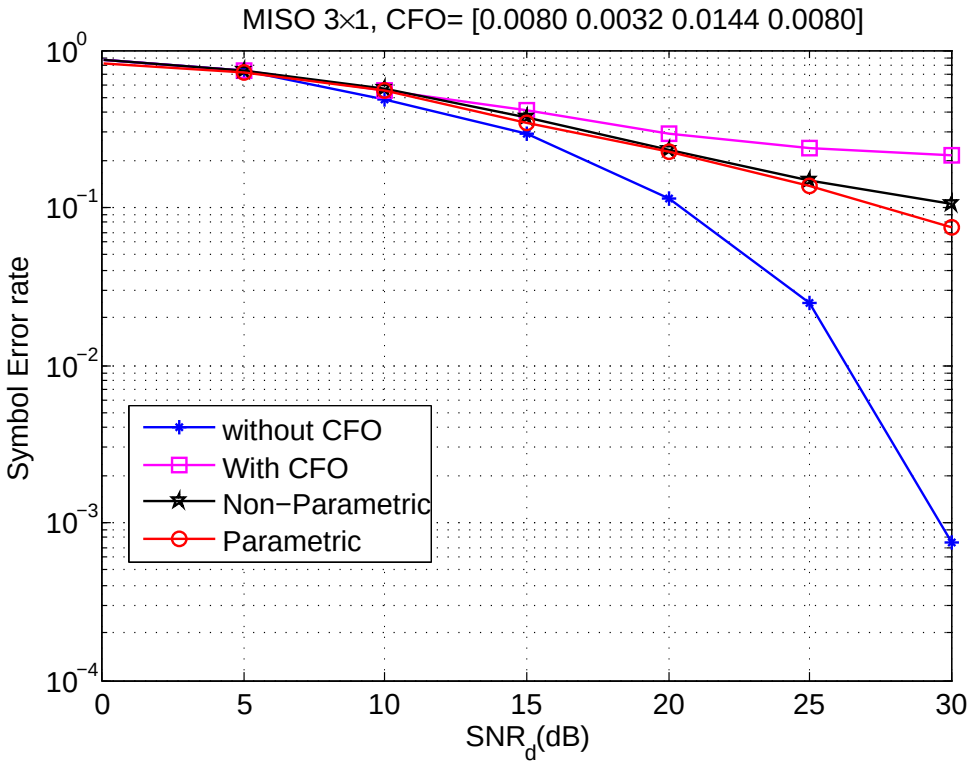

Figure A.3: *Symbol error rate versus SNR_d (with and without CFO) at low CFO*

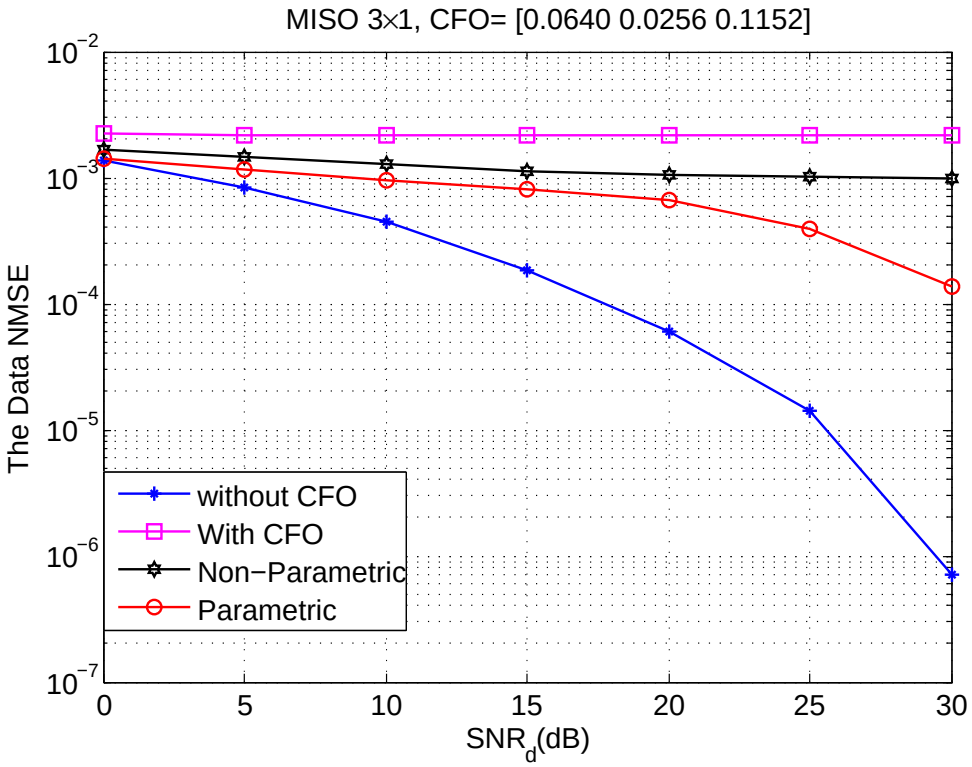

Figure A.4: *NMSE of the data versus SNR_d (with and without CFO) at high CFO*

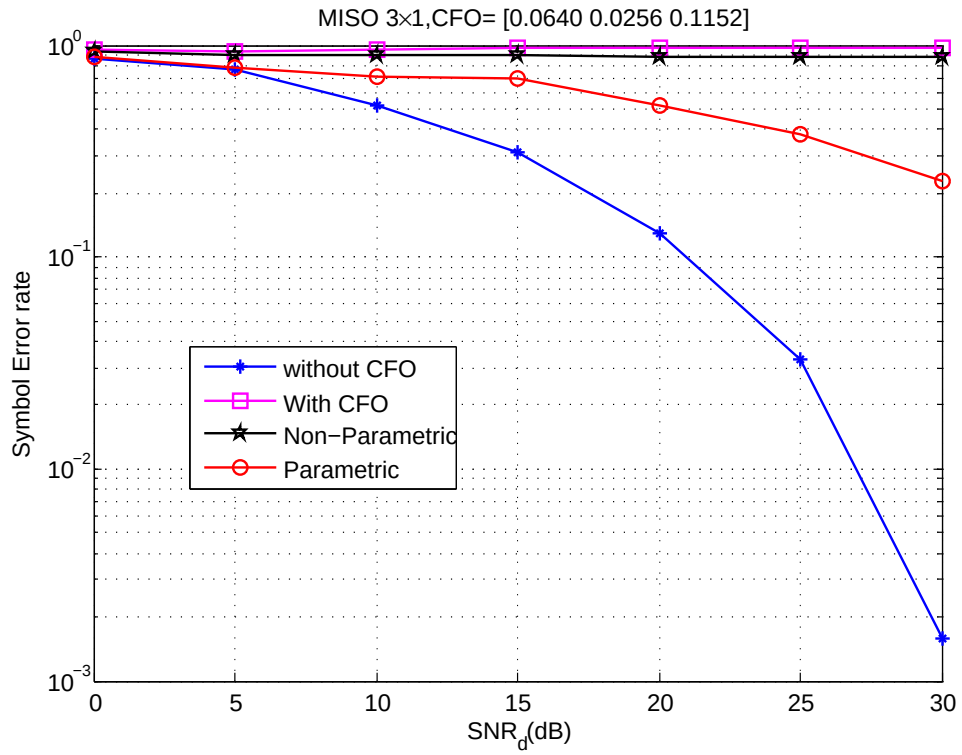

Figure A.5: *Symbol error rate versus SNR_d (with and without CFO) at high CFO*

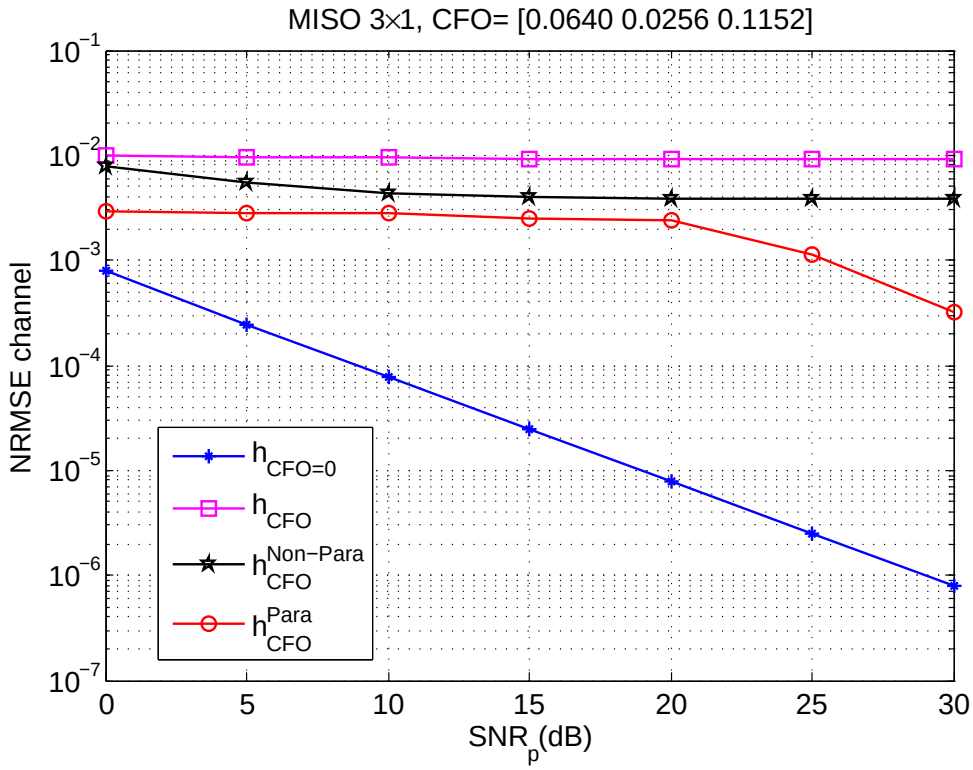

Figure A.6: *NRMSE of the channel estimation versus SNR (with and without CFO).*

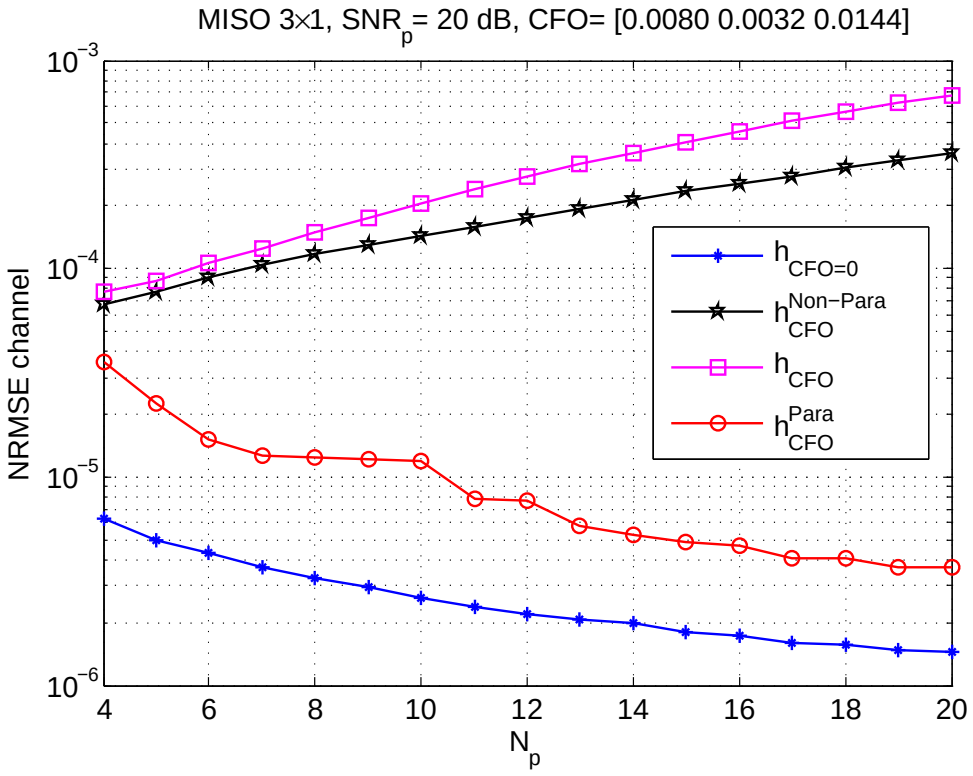

Figure A.7: *NRMSE of the channel estimate versus N_p at low CFO.*

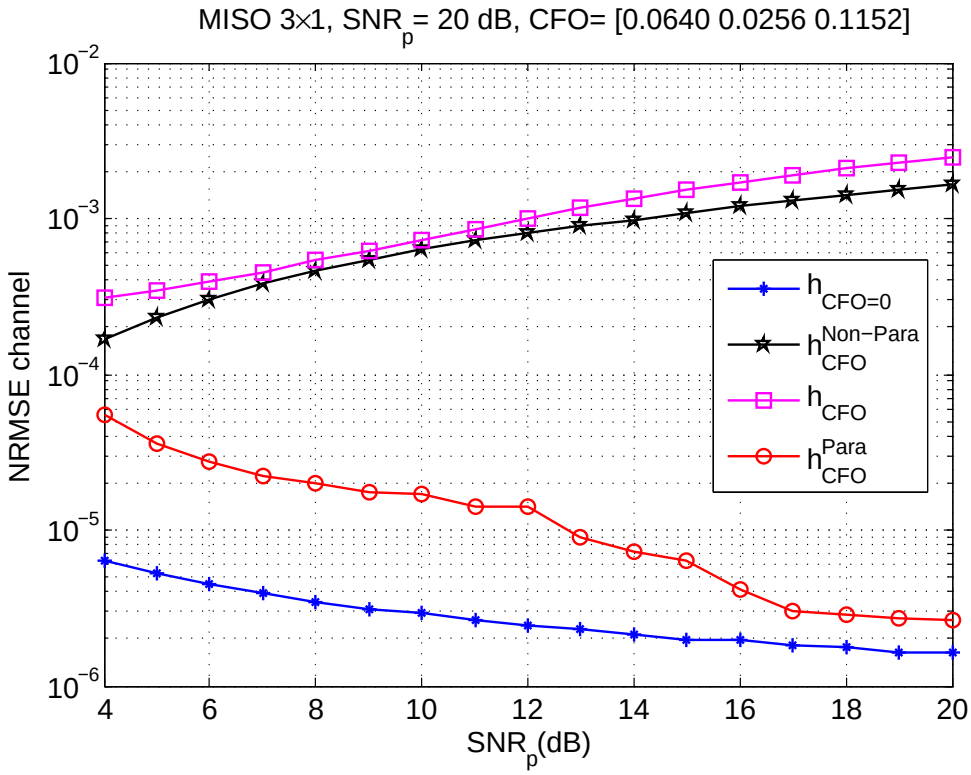

Figure A.8: *NRMSE of the channel estimate versus N_p at high CFO.*

A.6 Conclusion

Based on the above theoretical study as well as on the experimental set-up of Dr Mohamed Tlich (not presented here) [117], we can draw the following remarks:

In this study we proposed a first solution for the channel and CFO estimation that is relatively cheap but can be used only if a rough frequency synchronization between all nodes is available to guarantee the 'small values' of the CFOs and consequently the slow channel variation needed in this approach.

A second solution is provided based on parametric estimation. It is more expensive in terms of computational resources and pilots (i.e. requires longer pilots) but can work without frequency synchronization.

APPENDIX

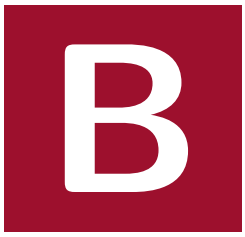

French summary

Chapter content

B.1 Introduction

Au cours des dernières décennies, les communications sans fil ont connu des développements remarquables dans de nombreux domaines distincts. Cela a commencé avec la recherche universitaire, où de nombreuses améliorations et progrès ont été réalisés. Cela est également évident dans les applications militaires, où la guerre et les armes traditionnelles ont été remplacées par des armes autonomes (comme les véhicules aériens sans pilote (UAV)) et la guerre électronique cybernétique. Le domaine civil a également vu sa part de progrès dans les communications sans fil, en ce sens que nos vies sont devenues plus virtuelles et connectées.

L'utilisation de plusieurs antennes au niveau de l'émetteur ou du récepteur, ou des deux (MIMO), peut considérablement améliorer les performances des systèmes de transmission [5, 6]. Les systèmes de communications MIMO offrent des degrés de liberté supplémentaires fournis par la dimension spatiale, qui peuvent être exploités pour transmettre simultanément des flux de données indépendants (multiplexage spatial) augmentant ainsi le débit de données, ou la transmission multiplicative d'un flux de données unique (diversité spatiale) pour augmenter la fiabilité du système [5, 7].

B.1.1 Motivations

L'utilisation sans précédent de téléphones intelligents, tablettes, super-téléphones, etc., équipés d'applications gourmandes en données, telle que la vidéo en streaming, de lourdes interfaces graphiques pour réseaux sociaux et des services de navigation en temps réel, a poussé à des changements révolutionnaires de la 4G à la prochaine génération de systèmes sans fil . Bien que les systèmes 4G puissent être chargés avec beaucoup plus de services, de fonctionnalités en temps réel et de données que les anciens systèmes, il subsiste un écart considérable entre les exigences pratiques de la population et ce que peuvent offrir les technologies 4G. Pour répondre aux fortes demandes de la croissance explosive des utilisateurs de téléphones cellulaires et des services potentiels associés, la norme de la cinquième génération (5G) fait actuellement l'objet d'une enquête et de discussions approfondies. Avec des vitesses pouvant atteindre 10 gigabits par seconde, la 5G devrait être 100 fois plus rapide que la 4G [14]. Les deux technologies principales pour répondre aux exigences de la 5G sont l'utilisation des systèmes à ondes millimétriques (mmWave) et des systèmes MIMO massifs [15].

Avec un nombre plus élevé d'antennes à la station de base (BS), quelques centaines, par rapport aux systèmes MIMO classiques (8 antennes pour le LTE), des systèmes MIMO massifs ou MIMO à grande échelle peuvent offrir un grand gains d'efficacité spectrale et énergétique

[14, 16, 17].

Les systèmes de communications MIMO massifs surmontent plusieurs limitations des systèmes MIMO traditionnels, tel que la sécurité, la robustesse et le débit de traitement [18, 15]. Il a été démontré que les énormes systèmes MIMO promettaient de multiplier par 10 le débit du système tout en desservant simultanément des dizaines d'utilisateurs sur la même ressource temps-fréquence [18]. Pour cela, le débit et la capacité du système seront fortement améliorés afin de satisfaire la quantité croissante d'échange de données et demande de qualité de service pour les futurs réseaux cellulaires.

Pour exploiter pleinement le potentiel des technologies susmentionnées, la connaissance du canal de transmission (CSI) est indispensable. Pour améliorer les performances du système, il est essentiel que la CSI soit disponible à la fois au niveau de l'émetteur et du récepteur. La connaissance de CSI est utilisée pour la détection cohérente des signaux transmis du côté du récepteur. Du côté des émetteurs, la CSI est essentielle pour concevoir des schémas de précodage efficaces pour l'annulation des interférences entre utilisateurs. Cependant, la connaissance parfaite de la CSI n'est pas disponible dans la pratique, elle doit donc être estimée. Cette thèse s'intéresse aux algorithmes d'estimation du canal de transmission et de faible complexité pour les systèmes MIMO-OFDM et les systèmes MIMO-OFDM massifs.

B.1.2 Estimation du canal de transmission

La bonne conduite de la mission du système de communications sans fil dépend en grande partie de la disponibilité de la connaissance de son environnement. L'environnement de propagation fait référence au canal de communications qui assure la connexion entre l'émetteur et le récepteur. Ainsi, l'estimation de canal de transmission est d'une importance primordiale pour l'égalisation et la détection de symboles. Plusieurs modèles de canaux et approches d'estimation de canaux ont été développés dans la littérature en fonction de leurs applications et de la norme sélectionnée. Les méthodes d'estimation peuvent être divisées en trois classes principales discutées ci-dessous.

B.1.2.1 Estimation de canal basée sur les séquences pilotes

En générale, l'estimation du canal de transmission est réalisée en insérant, dans la trame transmise, des séquences d'apprentissage (appelées pilotes) connue a priori par le récepteur, selon une disposition connue dans la trame (bloc, peigne ou réseau) [19, 20, 21]. Côté récepteur, en observant la sortie en correspondance des symboles du pilote, il est possible d'estimer le canal. Cette connaissance est ensuite introduite dans le processus de détection afin de permettre une estimation optimale des données. Cette approche (estimation du canal basée sur les pilotes) est

la plus utilisée dans les normes de communications [22, 13], pour sa faible complexité de calculs et sa robustesse. Son inconvénient réside dans le fait que les symboles pilotes ne contiennent pas d'informations utile, ils représentent donc un gaspillage de bande passante. De plus, la plupart des observations (celles liées aux symboles inconnus) sont ignorées dans le processus d'estimation, ce qui représente une occasion manquée d'améliorer la précision de l'estimation du canal.

B.1.2.2 Estimation aveugle du canal

Contrairement à l'estimation de canal basée sur les séquences pilotes, les méthodes d'estimation de canal aveugle s'appuient entièrement sur les propriétés statistiques des symboles transmis inconnus (c'est-à-dire qu'aucun pilote n'est transmis) [23, 24, 25]. Cette approche réduit le temps de réponse du système, mais nécessite un grand nombre de symboles de données pour les propriétés statistiques et de puissants algorithmes. De plus, les approches basées sur les pilotes donnent de meilleures performances à faible complexité de calculs que les approches d'estimation aveugles.

B.1.2.3 Estimation semi-aveugle du canal

Chaque méthodes d'estimation de canal a ses avantages et ses inconvénients. Généralement, la première classe (c'est-à-dire un estimateur de canal basé sur les pilotes) fournit une estimation de canal plus précise que la classe d'estimation aveugle. Cependant, la seconde classe, dans la plupart des cas, augmente l'efficacité spectrale par rapport à la première. Par conséquent, il serait avantageux de conserver les avantages des deux techniques en utilisant des méthodes d'estimation semi-aveugles [26, 27, 28, 29], exploitant à la fois les données et les pilotes pour identifier le canal de transmission.

B.1.3 Objectifs de la thèse

Un des problèmes majeurs de ces systèmes est le fort niveau d'interférences dû au grand nombre d'émetteurs simultanés. Dans un tel contexte, les solutions 'classiques' de conception de pilotes 'orthogonaux' sont extrêmement coûteuses en débit utile permettant ainsi aux solutions d'identification de canal dites 'aveugles' ou 'semi-aveugles' (abandonnées dans les systèmes de communications civiles) de revenir au-devant de la scène comme solutions intéressantes d'identification ou de déconvolution de ces canaux MIMO.

Dans cette thèse, nous avons commencé, dans la première partie, par une analyse comparative des performances, en se basant sur les bornes de Cramèr-Rao (CRB), afin de mesurer la réduction potentielle de la taille des séquences pilotes en employant les méthodes dites semi-aveugles basées sur l'exploitation conjointe des pilotes et des données. Les résultats d'analyse montrent que nous

pouvons réduire jusqu'à 95% des pilotes sans affecter les performances d'estimation du canal.

Nous avons par la suite, dans la deuxième partie, proposé de nouvelles méthodes d'estimation semi-aveugle du canal, à faible coût, permettant d'approcher les performances limites (CRB). Nous avons proposé un estimateur semi-aveugle, appelé LS-DF (Least Squares-Decision Feedback), basé sur une estimation des moindres carrés avec retour de décision qui permet un bon compromis performance / complexité numérique. Un autre estimateur semi-aveugle de type sous-espace a aussi été proposé ainsi qu'un algorithme basé sur l'approche EM (Expectation Maximization) pour lequel trois versions à coût réduit ont été étudiées. Dans le cas d'un canal spéculaire, nous avons proposé un algorithme d'estimation paramétrique qui s'appuie sur l'estimation des temps d'arrivés combinée avec la technique DF.

Dans cette annexe, nous présentons un résumé en langue Française des travaux réalisés.

B.1.4 Liste des publications

Les travaux de recherche développés dans cette thèse ont donné lieu aux publications suivantes :

Articles de revues :

1) Ladaycia, A. Mokraoui, K. Abed-Meraim, and A. Belouchrani, "Performance bounds analysis for semi-blind channel estimation in MIMO-OFDM communications systems," IEEE Transactions on Wireless Communications, vol. 16, no. 9, pp. 5925-5938, Sep. 2017.

2) A. Ladaycia, A. Belouchrani, K. Abed-Meraim and A. Mokraoui, "Semi-Blind MIMO-OFDM Channel Estimation using EM-like Techniques," IEEE Transactions on Wireless Communications, May. 2019. (submitted).

3) O. Rekik, A. Ladaycia, K. Abed-Meraim, and A. Mokraoui, "Performance Bounds Analysis for Semi-Blind Channel Estimation with Pilot Contamination in Massive MIMO-OFDM Systems," IET Communications, May. 2019. (submitted).

Articles de conférences :

1) A. Ladaycia, A. Mokraoui, K. Abed-Meraim, and A. Belouchrani, "What semi-blind channel estimation brings in terms of throughput gain?" in 2016 10th ICSPCS, Dec. 2016, pp. 1-6, Gold Coast, Australia.

2) A. Ladaycia, A. Belouchrani, K. Abed-Meraim, and A. Mokraoui, "Parameter optimization for defeating blind interception in drone protection," in 2017 Seminar on Detection Systems Architectures and Technologies (DAT), Feb. 2017, pp. 1-6, Alger, Algeria.

3) A. Ladaycia, A. Mokraoui, K. Abed-Meraim, and A. Belouchrani, "Further investigations on the performance bounds of MIMO-OFDM channel estimation," in The 13th International Wireless Communications and Mobile Computing Conference (IWCMC 2017), June 2017, pp. 223-228, Valance, Spain.

4) A. Ladaycia, A. Mokraoui, K. Abed-Meraim, and A. Belouchrani, "Toward green communications using semi-blind channel estimation," in 2017 25th European Signal Processing Conference (EUSIPCO), Aug. 2017, pp. 2254-2258, Kos, Greece.

5) A. Ladaycia, K. Abed-Meraim, A. Bader, and M.S. Alouini, "CFO and channel estimation for MISO-OFDM systems," in 2017 25th European Signal Processing Conference (EUSIPCO), Aug. 2017, pp. 2264-2268, Kos, Greece.

6) A. Ladaycia, A. Mokraoui, K. Abed-Meraim, and A. Belouchrani, "Contributions à l'estimation semi-aveugle des canaux MIMO-OFDM," in GRETSI 2017, Sep. 2017, Nice, France.

7) A. Ladaycia, A. Belouchrani, K. Abed-Meraim, and A. Mokraoui, "EM-based semi-blind MIMO-OFDM channel estimation," in 2018 IEEE International Conference on Acoustics, Speech and Signal Processing (ICASSP2018), Apr. 2018, Alberta, Canada.

8) A. Ladaycia, K. Abed-Meraim, A. Mokraoui, and A. Belouchrani, "Efficient Semi-Blind Subspace Channel Estimation for MIMO-OFDM System," in 2018 26th European Signal Processing Conference (EUSIPCO), Sep. 2018, Rome, Italy.

9) O. Rekik, A. Ladaycia, K. Abed-Meraim, and A. Mokraoui, "Performance Bounds Analysis for Semi-Blind Channel Estimation with Pilot Contamination in Massive MIMO-OFDM Systems," in 2018 26th European Signal Processing Conference (EUSIPCO), Sep. 2018, Rome, Italy.

10) A. Ladaycia, M.Pesavento, A. Mokraoui, K. Abed-Meraim, and A. Belouchrani, "Decision feedback semi-blind estimation algorithm for specular OFDM channels," in 2019 IEEE International Conference on Acoustics, Speech and Signal Processing (ICASSP2019).

11) A. Ladaycia, A. Belouchrani, K. Abed-Meraim, and A. Mokraoui, "Efficient EM-algorithm for MIMO-OFDM semi blind channel estimation," in 2019 Conference on Electrical Engineering (CEE2019).

12) O. Rekik, A. Ladaycia, K. Abed-Meraim, and A. Mokraoui, "Semi-Blind Source Separation based on Multi-Modulus Criterion: Application for Pilot Contamination Mitigation in Massive MIMO Systems," in The 19th ISCIT, Ho Chi Minh City, Vietnam. in The 19th ISCIT, Ho Chi Minh City, Vietnam.

13) A. Ladaycia, A. Belouchrani, K. Abed-Meraim, and A. Mokraoui, "Algorithme EM efficace pour l'estimation semi-aveugle de canal MIMO-OFDM," in GRETSI 2019.

B.2 Analyse de performances limites d'estimation de canal des systèmes de communications MIMO-OFDM

La combinaison de la technologie MIMO et de la modulation OFDM (c'est-à-dire MIMO-OFDM) est largement déployée dans les systèmes de communications sans fil, comme dans le réseau sans fil 802.11n [22], LTE et LTE-A [4]. En effet, l'utilisation de MIMO-OFDM améliore la capacité de canal et la fiabilité des communications. En particulier, il a été montrée dans [14, 16] que grâce au déploiement d'un grand nombre d'antennes dans les stations de base, le système pouvait atteindre un débit de transmission élevé et offrir une efficacité spectrale très élevée.

Dans un tel système, l'estimation de canal de transmission reste une préoccupation actuelle dans la mesure où la performance globale en dépend fortement, en particulier pour les grands systèmes MIMO où l'estimation de canal de transmission devient plus complexe.

Cette section est consacré à l'analyse comparative de performances limites de de l'estimation semi-aveugle et aux approches basées uniquement sur les pilotes de canal de transmission, dans le contexte des systèmes MIMO-OFDM. Pour obtenir des résultats comparatifs généraux indépendamment des algorithmes ou des méthodes d'estimation spécifiques, cette analyse est réalisée à l'aide de la CRB.

Par conséquent, nous commençons par donner plusieurs dérivations de CRB pour différents modèles de données (Gaussienne circulaire (CG), Gaussienne non circulaire (NCG), Binary / Quadratic Phase Shift Keying (BPSK / QPSK)) et différentes organisations des pilotes (blocs, peignes et treillis). Dans le cas particulier des systèmes MIMO de grandes dimensions, nous avons exploité la structure diagonale des blocs des matrices de covariance pour développer une technique numérique rapide qui évite les coûts prohibitifs et les problèmes de mémoire insuffisante (dus aux grandes tailles de matrice) du calcul de la CRB. De plus, dans le cas BPSK / QPSK, une approximation réaliste de la CRB est introduite pour éviter des calculs d'intégrales numériques lourds. Après avoir calculé toutes les CRB nécessaires, nous les utiliserons pour comparer les

performances des approches semi-aveugles et ainsi que celles basées uniquement sur les séquences pilotes.

Il est bien connu que les techniques semi-aveugles peuvent aider à réduire la taille de la séquence d'apprentissage ou à améliorer la qualité de l'estimation [35]. Cependant, il s'agit de la première étude qui quantifie de manière approfondie le taux de réduction de la séquence d'apprentissage lorsque une approche d'estimation semi-aveugle dans le contexte de MIMO-OFDM est utilisée. L'un des principaux résultats de cette analyse est de mettre en évidence le fait qu'en recourant à l'estimation semi-aveugle, on peut se supprimer la plupart des échantillons pilotes sans affecter la qualité de l'identification du canal. Un autre résultat important de cette étude est la possibilité de concevoir facilement des séquences pilotes semi-orthogonales dans le cas de grande dimension MIMO grâce à leur taille réduite.

B.2.1 Systèmes de communications à porteuses multiples : concepts principaux

B.2.1.1 Modèle du système MIMO-OFDM

Le système de communications MIMO, illustré par la Figure B.1, est composé de N_t antennes d'émission et N_r antennes de réception utilisant K sous-porteuses. Le signal émis est supposé OFDM.

Le signal reçu au r-ème antenne, après suppression du cyclic préfixe et après avoir calculé la FFT est donné par :

$$\mathbf{y}_r = \sum_{i=1}^{N_t} \mathbf{F}\, \mathbf{T}(\mathbf{h}_{i,r}) \frac{\mathbf{F}^H}{K} \mathbf{x}_i + \mathbf{v}_r \qquad K \times 1, \tag{B.1}$$

où $\mathbf{F}$ représente la matrice de Fourier; $\mathbf{h}_{i,r}$ est le vecteur des coefficients du canal de transmission; $\mathbf{x}_i$ est le i-ème symbole OFDM; et $\mathbf{T}(\mathbf{h}_{i,r})$ est une matrice circulaire. $\mathbf{v}_r$ représente le bruit, supposé additif Gaussian tel que $E\left[\mathbf{v}_r(k)\mathbf{v}_r(i)^H\right] = \sigma^2_{\mathbf{v}}\mathbf{I}_K\delta_{ki}$; $\sigma^2_{\mathbf{v}}$ la puissance du bruit.

Dans le cas général, l'équation précédente peut se mettre sous les deux formes suivantes :

$$\mathbf{y} = \boldsymbol{\lambda}\mathbf{x} + \mathbf{v}, \tag{B.2}$$

$$\mathbf{y} = \tilde{\mathbf{X}}\mathbf{h} + \mathbf{v}. \tag{B.3}$$

B.2.1.2 Principaux modèles d'arrangement des pilotes

Les séquences pilotes peuvent être structurées en bloc (Figure B.2a), en peigne (comb) (Figure B.2b) ou bien réseaux (lattice) comme le montre la Figure B.2c

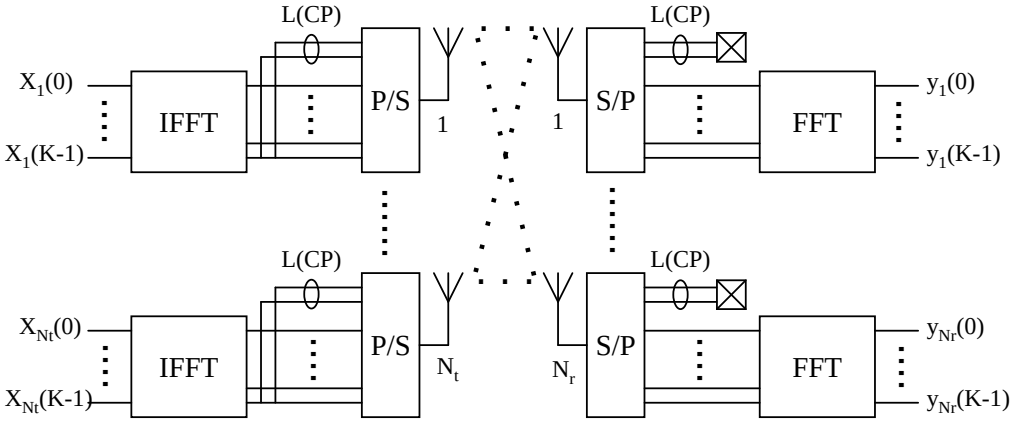

Figure B.1: *Modèle du système MIMO-OFDM*

B.3 CRB pour une estimation de canal basée sur les pilotes arrangés selon le type bloc

La CRB est obtenue en inversant la matrice d'information de Fisher (FIM) notée $\mathbf{J}^{p}_{\boldsymbol{\theta\theta}}$ où $\boldsymbol{\theta}$ est le vecteur des paramètres à estimer $\boldsymbol{\theta} = \mathbf{h}$:

$$\mathbf{J}^{p}_{\boldsymbol{\theta\theta}} = \sum_{i=1}^{N_p} \mathbf{J}^{p_i}_{\boldsymbol{\theta\theta}}, \tag{B.4}$$

avec $\mathbf{J}^{p_i}_{\boldsymbol{\theta\theta}}$ la FIM assossie i-ème pilote donnée par [36, 35] :

$$\mathbf{J}^{p_i}_{\boldsymbol{\theta\theta}} = \mathrm{E}\left\{ \left(\frac{\partial \ln \mathrm{p}(\mathbf{y}(\mathrm{i}), \mathbf{h})}{\partial \boldsymbol{\theta}^*} \right) \left(\frac{\partial \ln \mathrm{p}(\mathbf{y}(\mathrm{i}), \mathbf{h})}{\partial \boldsymbol{\theta}^*} \right)^{\mathrm{H}} \right\}. \tag{B.5}$$

Puis la CRB est comme suit :

$$CRB_{OP} = \sigma^2_{\mathbf{v}} tr\left\{ \left(\tilde{\mathbf{X}}^H_p \tilde{\mathbf{X}}_p \right)^{-1} \right\}. \tag{B.6}$$

B.3.1 CRB pour une estimation semi-aveugle de canal dans le cas des pilotes arrangés selon le type bloc

Pour dériver l'expression de la CRB, trois cas ont été considérés, selon que les données transmises sont stochastiques, gaussiennes circulaires (CG), stochastiques gaussiennes non circulaires (NCG) ou i.i.d. signaux BPSK / QPSK. Les symboles de données et le bruit sont supposés être à la fois i.i.d. et indépendants. Par conséquent, la FIM, notée $\mathbf{J}_{\boldsymbol{\theta\theta}}$, est divisée en deux parties :

$$\mathbf{J}_{\boldsymbol{\theta\theta}} = \mathbf{J}^{p}_{\boldsymbol{\theta\theta}} + \mathbf{J}^{d}_{\boldsymbol{\theta\theta}}, \tag{B.7}$$

où $\mathbf{J}^{p}_{\boldsymbol{\theta\theta}}$ la FIM des pilotes, et $\mathbf{J}^{d}_{\boldsymbol{\theta\theta}}$ est la FIM des données.

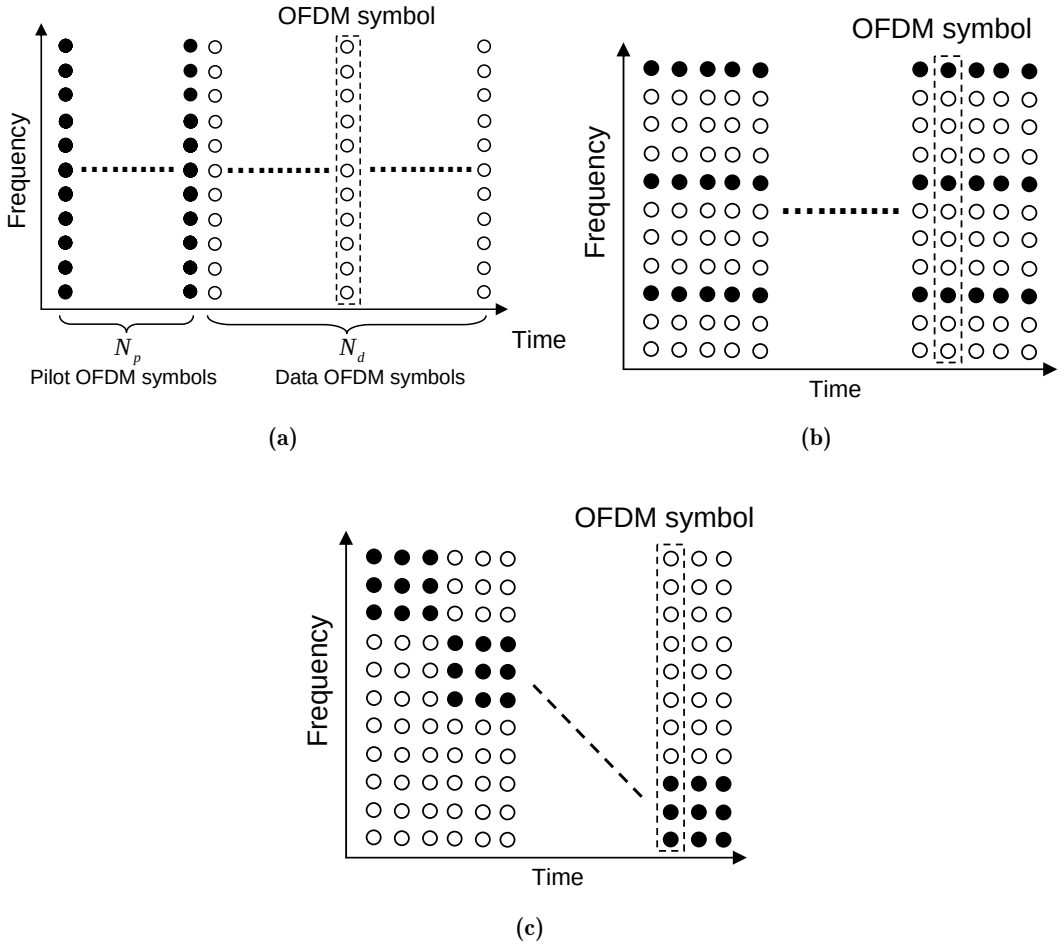

Figure B.2: *Organisation des séquences pilotes: (a) organisation en bloc; (b) en peigne; (c) en réseau.*

Le vecteur des paramètres inconnus $\boldsymbol{\theta}$ est composé des paramètres complexes et réels (i.e $\boldsymbol{\theta}_c$ et $\boldsymbol{\theta}_r$) comme suit :

$$\boldsymbol{\theta} = \left[\boldsymbol{\theta}_c^T \left(\boldsymbol{\theta}_c^*\right)^T \boldsymbol{\theta}_r^T\right]^T, \tag{B.8}$$

B.3.1.1 Modèle de données gaussien circulaire

Le signal est supposé CG centré et de matrice de covariance $\mathbf{C}_{\mathbf{x}} = \text{diag}\left(\boldsymbol{\sigma}_{\mathbf{x}}^2\right)$ avec $\boldsymbol{\sigma}_{\mathbf{x}}^2 \overset{\text{def}}{=} \left[\sigma_{\mathbf{x}_1}^2 \cdots \sigma_{\mathbf{x}_{N_t}}^2\right]^T$. La FIM des données eest égale à la FIM d'un symbole OFDM multiplié par le nombre de symboles OFDM N_d. La matrice de covariance du signal reçu $\mathbf{y}$ est donnée par :

$$\mathbf{C}_{\mathbf{y}} = \sum_{i=1}^{N_t} \sigma_{\mathbf{x}_i}^2 \boldsymbol{\lambda}_i \boldsymbol{\lambda}_i^H + \sigma_{\mathbf{v}}^2 \mathbf{I}_{KN_r}. \tag{B.9}$$

Les paramètres inconnus sont donnés par :

$$\boldsymbol{\theta}_c = \mathbf{h}\,; \qquad \boldsymbol{\theta}_r = \left[\boldsymbol{\sigma}_{\mathbf{x}}^{2\,T} \sigma_{\mathbf{v}}^2\right]^T. \tag{B.10}$$

La FIM est donnée par la trace suivante :

$$\mathbf{J}^{d}_{\boldsymbol{\theta\theta}} = tr\left\{\mathbf{C}_{\mathbf{y}}^{-1}\frac{\partial \mathbf{C}_{\mathbf{y}}}{\partial \boldsymbol{\theta}^{*}}\mathbf{C}_{\mathbf{y}}^{-1}\left(\frac{\partial \mathbf{C}_{\mathbf{y}}}{\partial \boldsymbol{\theta}^{*}}\right)^{H}\right\}. \tag{B.11}$$

B.3.1.2 Modèle de données gaussien non circulaire

Dans ce cas les vecteurs des paramètres sont donnés par :

$$\boldsymbol{\theta}_{c} = \mathbf{h}\,; \qquad \boldsymbol{\theta}_{r} = \left[\boldsymbol{\sigma}_{\mathbf{x}}^{2\,T}\ \boldsymbol{\phi}^{T}\ \rho_{c}\,\sigma_{\mathbf{v}}^{2}\right]^{T}. \tag{B.12}$$

où $0 < \rho_c \leq 1$ et $\boldsymbol{\phi} = [\phi_1 \cdots \phi_{N_t}]^T$ sont le taux et la phase de non-circularité du signal.

Après calculs, la FIM est donnée par:

$$\left[\mathbf{J}^{d}_{\boldsymbol{\theta\theta}}\right]_{i,j} = \frac{1}{2}tr\left\{\tilde{\mathbf{C}}_{\mathbf{y}}^{-1}\frac{\partial \tilde{\mathbf{C}}_{\mathbf{y}}}{\partial \boldsymbol{\theta}^{*}}\tilde{\mathbf{C}}_{\mathbf{y}}^{-1}\left(\frac{\partial \tilde{\mathbf{C}}_{\mathbf{y}}}{\partial \boldsymbol{\theta}^{*}}\right)^{H}\right\}, \tag{B.13}$$

où

$$\tilde{\mathbf{C}}_{\mathbf{y}} = \begin{bmatrix} \mathbf{C}_{\mathbf{y}} & \mathbf{C'}_{\mathbf{y}} \\ \mathbf{C'}^{*}_{\mathbf{y}} & \mathbf{C}^{*}_{\mathbf{y}} \end{bmatrix}, \tag{B.14}$$

$$\mathbf{C'}_{\mathbf{y}} = E\left[\mathbf{y}\mathbf{y}^{T}\right] = \sum_{i=1}^{N_t}\rho_{c}e^{j\phi_i}\sigma_{\mathbf{x}_i}^{2}\boldsymbol{\lambda}_{i}\boldsymbol{\lambda}_{i}^{T}. \tag{B.15}$$

B.3.1.3 Modèle de données BPSK et QPSK

Dans le cas BPSK/QPSK, la fonction de vraisemblance est donnée par :

$$p(\mathbf{y}_{(k)}, \boldsymbol{\theta}) = \frac{1}{Q^{N_t}}\sum_{q=1}^{Q^{N_t}}\frac{1}{(\pi\sigma_{\mathbf{v}}^{2})^{N_r}}e^{-\left\|\mathbf{y}_{(k)}-\boldsymbol{\lambda}_{(k)}\mathbf{C}_{\mathbf{x}}^{\frac{1}{2}}\mathbf{x}_{q}\right\|^{2}/\sigma_{\mathbf{v}}^{2}}, \tag{B.16}$$

avec $\boldsymbol{\lambda}_{(k)} = \left[\boldsymbol{\lambda}_{(k),1}, \cdots, \boldsymbol{\lambda}_{(k),N_t}\right]$ où $\boldsymbol{\lambda}_{(k),i} = \left[\left(\mathbf{W}\mathbf{h}_{i,1}\right)_{k}, \cdots, \left(\mathbf{W}\mathbf{h}_{i,N_r}\right)_{k}\right]^{T}$.

Après calculs, simplifications et approximations à fort SNR, la FIM est donnée par :

$$\mathbf{J}^{d}_{\boldsymbol{\theta\theta}}(k) = \frac{1}{\sigma_{\mathbf{v}}^{2}Q^{N_t}}\sum_{q=1}^{Q^{N_t}}\left(\frac{\partial \boldsymbol{\lambda}_{(k)}\mathbf{C}_{\mathbf{x}}^{\frac{1}{2}}\mathbf{x}_{q}}{\partial \boldsymbol{\theta}^{*}}\right)^{H}\left(\frac{\partial \boldsymbol{\lambda}_{(k)}\mathbf{C}_{\mathbf{x}}^{\frac{1}{2}}\mathbf{x}_{q}}{\partial \boldsymbol{\theta}^{*}}\right), \tag{B.17}$$

$$\begin{aligned} \left[\mathbf{J}^{d}_{\boldsymbol{\theta\theta}}(k)\right]_{i,j} &= \frac{1}{\sigma_{\mathbf{v}}^{2}Q^{N_t}}\sum_{q=1}^{Q^{N_t}}\mathbf{x}_{q}^{H}\left(\frac{\partial \boldsymbol{\lambda}_{(k)}\mathbf{C}_{\mathbf{x}}^{\frac{1}{2}}}{\partial \theta_{i}^{*}}\right)^{H}\left(\frac{\partial \boldsymbol{\lambda}_{(k)}\mathbf{C}_{\mathbf{x}}^{\frac{1}{2}}}{\partial \theta_{j}^{*}}\right)\mathbf{x}_{q}, \\ \left[\mathbf{J}^{d}_{\boldsymbol{\theta\theta}}(k)\right]_{i,j} &= \frac{1}{\sigma_{\mathbf{v}}^{2}Q^{N_t}}\sum_{q,m,l}x_{q}^{*}(m)\,x_{q}(l)\,\boldsymbol{\Gamma}_{m,l}^{i,j} \quad 1 \leq m,\ l \leq N_t, \end{aligned} \tag{B.18}$$

où $\boldsymbol{\Gamma}^{i,j} = \left(\frac{\partial \boldsymbol{\lambda}_{(k)}\mathbf{C}_{\mathbf{x}}^{\frac{1}{2}}}{\partial \theta_{i}^{*}}\right)^{H}\left(\frac{\partial \boldsymbol{\lambda}_{(k)}\mathbf{C}_{\mathbf{x}}^{\frac{1}{2}}}{\partial \theta_{j}^{*}}\right)$.

Paramètres	Spécifications
Modèle du canal	IEEE 802.11n
Nombre de trajets multiples	$N = 4$
Nombre de symboles OFDM pilotes (LTF)	$N_p^{LTF} = 2$
Nombre de symboles OFDM pilotes (HT-LTF)	$N_p^{HT-LTF} = 4$
Nombre de symboles OFDM données	$N_d = 40$
Puissance du signal des pilotes	$\sigma_p^2 = 23$ dBm
Puissance du signal des données	$\boldsymbol{\sigma}_{\mathbf{x}}^2 = [20\ 21\ 18\ 19]$ dBm
nombre de sous porteuse	$K = 64$
Rapport signal sur bruit	SNR_p = [-5:20] dB
Taux de non circularité	$\rho_c = 0.9$
Phases de non circularité	$\boldsymbol{\phi} = \left[\frac{\pi}{4}\ \frac{\pi}{2}\ \frac{\pi}{6}\ \frac{\pi}{3}\right]$

B.3.2 Résultats de simulations

Les simulations ont été réalisées dans le contexte du standard IEEE 802.11n. La trame physique est représentée par la Figure B.3. Les paramètres de simulations sont donnés dans le tableau suivant.

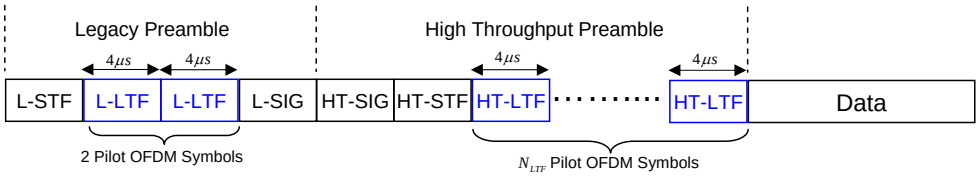

Figure B.3: *Trame physique du standard IEEE 802.11n.*

La Figure B.5 représente les CRBs normalisées $\left(\frac{tr\{CRB\}}{\|\mathbf{h}\|^2}\right)$ en fonction du SNR_p. Les courbes confirment que les CRB de l'estimation semi-aveugle du canal sont inférieures à celles de la CRB lorsque seuls les pilotes sont exploités (CRB_{OP}). Notons que la CRB_{SB}^{NCG} donne de meilleurs résultats que la CRB_{SB}^{CG} et que la CRB_{SB} dans le cas $BPSK$ et $QPSK$ donnent les meilleures performances. Sur la Figure B.6, on présente l'effet d'augmenter le nombre de symboles OFDM sur les performances d'estimation semi-aveugle.

L'approche d'estimation de canal semi-aveugle est traditionnellement utilisée pour améliorer la précision d'identification de canal. Cependant, ce chapitre montre que l'approche semi-aveugle peut être exploitée pour augmenter le débit du système sans fil MIMO-OFDM tout en maintenant la même qualité d'estimation de canal obtenue lors de l'utilisation d'échantillons pilotes. Pour

cela, pour atteindre la CRB_{OP}, la stratégie proposée consiste à réduire le nombre d'échantillons pilotes et à augmenter en conséquence le nombre d'échantillons de données (Figure B.4) pour le cas semi-aveugle, jusqu'à atteindre la même performance d'estimation. Pour cela, on présente sur la Figure B.7 la CRB normalisée semi-aveugle en fonction du nombre de pilotes supprimés. On remarque dans le cas CG on peut supprimer jusqu'à 55% des pilotes et 87% dans le cas NCG et 95% pour les modulations BPSK et QPSK

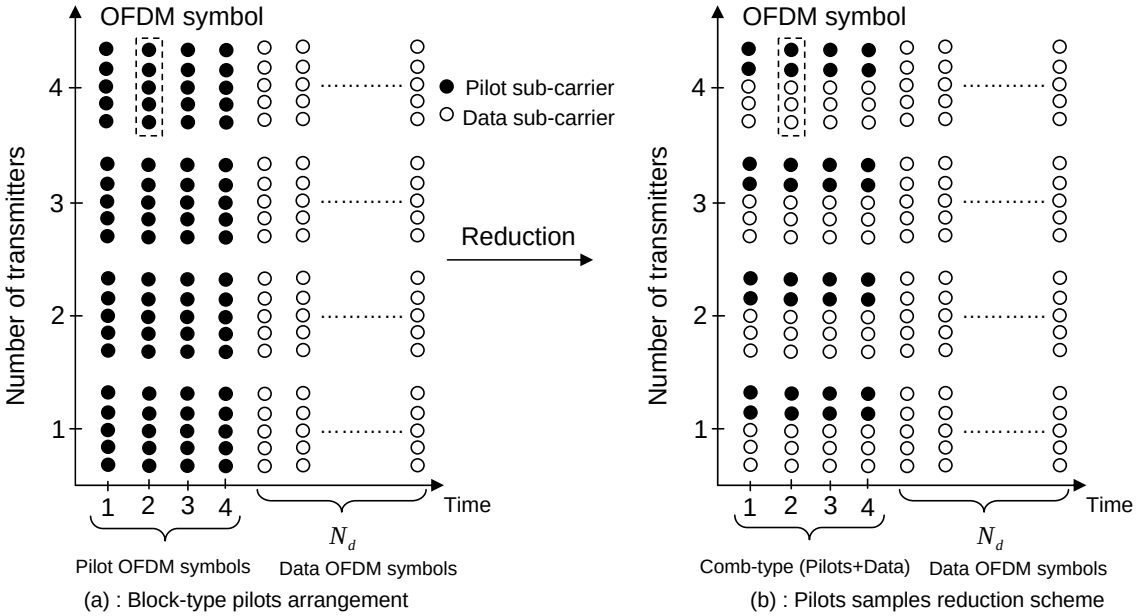

Figure B.4: *Réduction des pilotes*

B.4 Algorithme EM efficace pour l'estimation semi-aveugle de canal MIMO-OFDM

L'estimation semi-aveugle de canal basée sur le Maximum de Vraisemblance (MV) est l'une des approches assez souvent retenue pour ses bonnes performances mais au prix d'une grande complexité de calcul. Dans [84], l'algorithme EM maximise la vraisemblance pour estimer non seulement le canal mais également les données transmises. Les auteurs proposent un précodeur et utilisent des sous-porteuses de données comme pilotes virtuels pour l'estimation du canal. Dans [85], une méthode alternative basée sur l'algorithme EM est introduite pour l'estimation des coefficients du canal dans le domaine fréquentiel. Dans [86], les auteurs ont développé un algorithme EM en supposant que les données inconnues suivent une distribution Gaussienne même lorsque les symboles sont de type QPSK. Bien que l'algorithme EM soit performant, il engendre une lourde charge de calcul. Nous proposons tout d'abord une version exacte de l'algorithme EM pour estimer de manière itérative le canal MIMO dans le contexte semi-aveugle.

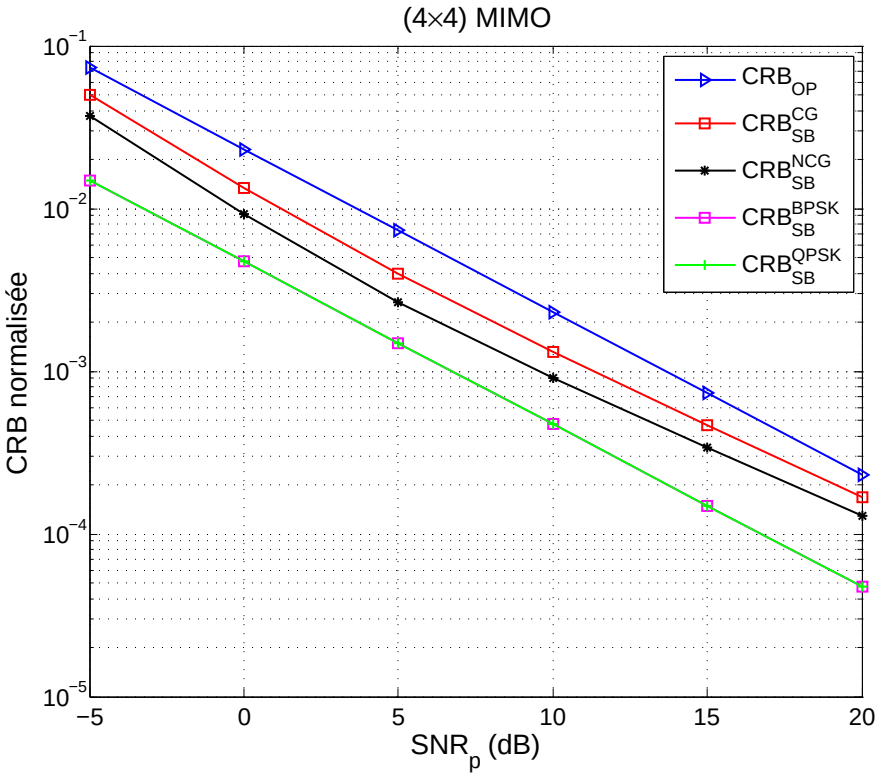

Figure B.5: *CRB normalisée en fonction du $SNR_p(dB)$*

Dans le but de réduire son coût de calcul, le système MIMO-OFDM est ensuite décomposé de façon à transformer le problème initial d'estimation en un problème d'identification de canal des sous-systèmes MISO en parallèle.

B.4.1 Système de communications MIMO-OFDM

Le système de communications MIMO-OFDM considéré est composé de N_t émetteurs et de N_r récepteurs. Soit K le nombre de sous-porteuses. Après suppression du préfixe cyclique et le calcul de la TFD de K- points, le signal $y_r(k)$ reçu sur la k-ème sous-porteuse du r-ème récepteur est donné par:

$$y_r(k) = \sum_{i=1}^{N_t} \sum_{n=0}^{N-1} h_{ri}(n) w_K^{nk} d_i(k) + v_r(k) \quad 0 \leq k \leq K-1, \tag{B.19}$$

où $d_i(k)$ représente les données transmises par le i-ème émetteur sur la k-ème sous porteuse; $\mathbf{v}_r = [v_r(1), \cdots, v_r(K)]$ le bruit supposé additif Gaussien tel que $E\left[\mathbf{v}_r(k)\mathbf{v}_r(i)^H\right] = \sigma_{\mathbf{v}}^2 \mathbf{I}_K \delta_{ki}$; $h_{ri}(n)$ le n-ème coefficients du canal de transmission entre le i-ème émetteur et le r-ème récepteur; et N la longueur du canal. w_K^{nk} représente le (n,k)-ème coefficient de la matrice de Fourier $\mathbf{W}$ de taille $K \times K$.

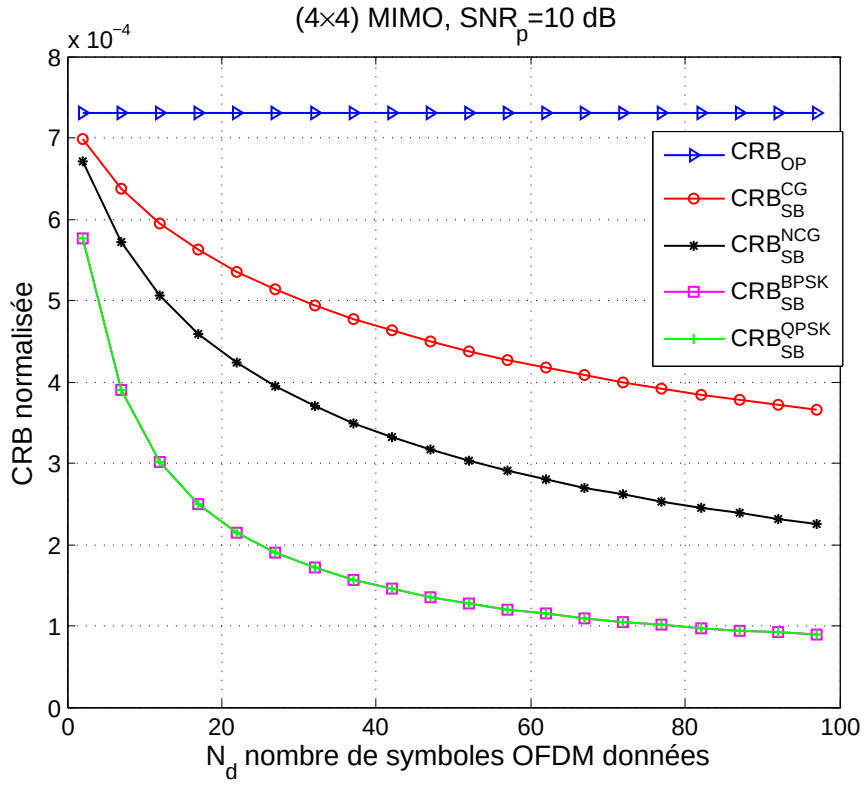

Figure B.6: *CRB normalisé en fonction du nombre des symboles OFDM donnés N_d*

L'équation (B.19) peut se mettre sous forme matricielle :

$$y_r(k) = \mathbf{w}^T(k)\mathbf{H}_r\mathbf{d}(k) + v_r(k), \tag{B.20}$$

avec $\mathbf{d}(k) = [d_1(k), \cdots, d_{N_t}(k)]^T$ les données transmises ; $\mathbf{w}(k) = \left[1 \quad w_K^k, \cdots, w_K^{(N-1)k}\right]^T$; et $\mathbf{H}_r$ la matrice des coefficients du canal définie comme suit :

$$\mathbf{H}_r = \begin{bmatrix} h_{r1}(0) & \cdots & h_{rN_t}(0) \\ \vdots & \ddots & \vdots \\ h_{r1}(N-1) & \cdots & h_{rN_t}(N-1) \end{bmatrix}. \tag{B.21}$$

La représentation vectorielle du signal reçu, c.a.d. $\mathbf{y}(k) = [y_1(k), \cdots, y_{N_r}(k)]^T$ et $\mathbf{v}(k) = [v_1(k), \cdots, v_{N_r}(k)]^T$, permet de réécrire l'équation (B.20) sous une forme compacte :

$$\mathbf{y}(k) = \boldsymbol{\mathcal{W}}(k)\boldsymbol{\mathcal{H}}\mathbf{d}(k) + \mathbf{v}(k), \tag{B.22}$$

où $\boldsymbol{\mathcal{W}}(k) = \mathbf{I}_{N_r} \otimes \mathbf{w}^T(k)$ ($\otimes$ représente le produit de Kronecker) et $\boldsymbol{\mathcal{H}} = [\mathbf{H}_1^T, \cdots, \mathbf{H}_{N_r}^T]^T$.

Dans ce qui suit, les symboles OFDM reçus sont supposés i.i.d. L'algorithme EM est présenté pour une organisation en peigne des symboles OFDM [32]. Notons K_p le nombre de sous-porteuses

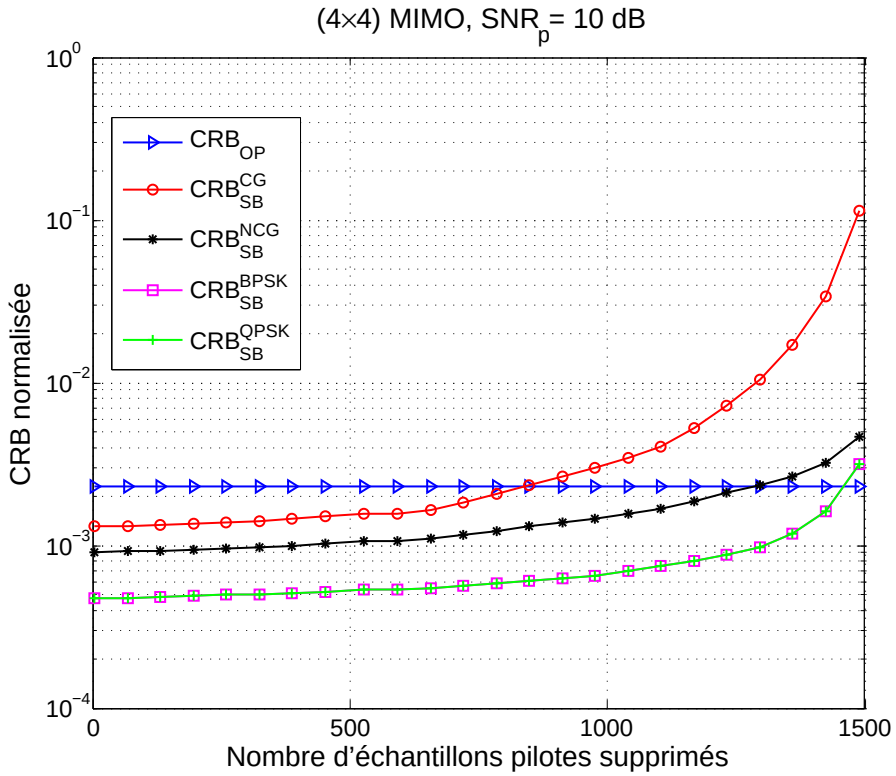

Figure B.7: *CRB normalisée en fonction du nombre des pilotes supprimes*

pilotes et K_d celui des sous-porteuses dédiées aux données. Les données transmises sont supposées appartenir à un alphabet fini. On note $D = \{\mathbf{d}_\xi\}$ (respectivement $|D|$) l'ensemble fini de toutes les réalisations possibles du vecteur de données $\mathbf{d}$ (respectivement son cardinal).

B.4.2 Estimation semi-aveugle de canal MIMO

Avant de présenter l'algorithme EM pour l'estimation semi-aveugle du canal MIMO, rappelons rapidement les grandes lignes de cet algorithme. Le vecteur des paramètres inconnus $\boldsymbol{\theta}$ contient les coefficients du canal de transmission $vec(\boldsymbol{\mathcal{H}})$ ainsi que la puissance du bruit ${\sigma_{\mathbf{v}}}^2$. L'algorithme EM est un processus d'optimisation itératif qui estime les paramètres inconnus en maximisant la vraisemblance marginale des données reçues $\mathbf{y}$. Notons $\mathbf{y}$ les données incomplètes et $\mathbf{d}$ les données cachées. L'algorithme EM est basé sur les deux étapes suivantes :

- Étape d'évaluation de l'espérance (étape-E) – Calcul de la fonction auxiliaire :

$$Q\left(\boldsymbol{\theta}, \boldsymbol{\theta}^{[i]}\right) = E_{\mathbf{d}|\mathbf{y},\boldsymbol{\theta}^{[i]}}\left[\log p\left(\mathbf{y}|\mathbf{d};\boldsymbol{\theta}\right)\right] \tag{B.23}$$

- Étape de maximisation (étape-M) – Calcul de $\boldsymbol{\theta}^{[i+1]}$ qui maximise $Q\left(\boldsymbol{\theta},\boldsymbol{\theta}^{[i]}\right)$ comme :

$$\boldsymbol{\theta}^{[i+1]} = \arg\max_{\boldsymbol{\theta}} Q\left(\boldsymbol{\theta},\boldsymbol{\theta}^{[i]}\right) \tag{B.24}$$

La convergence de l'algorithme EM à un maximum local a été montrée et discutée dans [88].

B.4.2.1 Algorithme EM pour l'estimation semi-aveugle de canal MIMO

Cette section met en oeuvre l'algorithme EM pour l'estimation semi-aveugle du canal MIMO. La fonction du maximum de vraisemblance est donnée par :

$$p\left(\mathbf{y};\boldsymbol{\theta}\right) = \prod_{k=0}^{K_p-1} p\left(\mathbf{y}\left(k\right);\boldsymbol{\theta}\right) \prod_{k=K_p}^{K-1} p\left(\mathbf{y}\left(k\right);\boldsymbol{\theta}\right), \tag{B.25}$$

où $p\left(\mathbf{y}\left(k\right);\boldsymbol{\theta}\right) \sim \mathcal{N}\left(\boldsymbol{\mathcal{W}}(k)\boldsymbol{\mathcal{H}}\mathbf{d}_p(k), \sigma_{\mathbf{v}}^2\mathbf{I}\right)$, pour
$k = 0, \cdots, K_p - 1$, $\mathbf{d}_p(k)$ est le vecteur contenant la séquence pilote de la k-ème sous-porteuse; et pour $k = K_p, \cdots K-1$, on a :

$$p\left(\mathbf{y}\left(k\right);\boldsymbol{\theta}\right) = \sum_{\xi=1}^{|D|} p\left(\mathbf{y}\left(k\right)|\mathbf{d}_\xi;\boldsymbol{\theta}\right) p\left(\mathbf{d}_\xi\right), \tag{B.26}$$

avec $p\left(\mathbf{y}\left(k\right)|\mathbf{d}_\xi;\boldsymbol{\theta}\right) \sim \mathcal{N}\left(\boldsymbol{\mathcal{W}}(k)\boldsymbol{\mathcal{H}}\mathbf{d}_\xi, \sigma_{\mathbf{v}}^2\mathbf{I}\right)$.

Étape-E : Après simplification, $Q\left(\boldsymbol{\theta},\boldsymbol{\theta}^{[i]}\right)$ devient :

$$Q\left(\boldsymbol{\theta},\boldsymbol{\theta}^{[i]}\right) = \sum_{k=0}^{K_p-1} \log p\left(\mathbf{y}(k)|\mathbf{d}_p(k);\boldsymbol{\theta}\right) + \sum_{k=K_p}^{K-1} \sum_{\xi=1}^{|D|} \alpha_{k,\xi}\left(\boldsymbol{\theta}^{[i]}\right) \log p\left(\mathbf{y}(k)|\mathbf{d}_\xi;\boldsymbol{\theta}\right), \tag{B.27}$$

où

$$\alpha_{k,\xi}\left(\boldsymbol{\theta}^{[i]}\right) = \frac{p\left(\mathbf{y}\left(k\right)|\mathbf{d}_\xi;\boldsymbol{\theta}^{[i]}\right) p\left(\mathbf{d}_\xi\right)}{\sum_{\xi'=1}^{|D|} p\left(\mathbf{y}\left(k\right)|\mathbf{d}_{\xi'};\boldsymbol{\theta}^{[i]}\right) p\left(\mathbf{d}_{\xi'}\right)}. \tag{B.28}$$

Dans ce travail, toutes les réalisations $\mathbf{d}_\xi$ sont équiprobables. Le terme $p\left(\mathbf{d}_\xi\right)$ est alors ignoré dans l'équation (B.28).

Étape-M : Cette étape estime $\boldsymbol{\theta}$, c.a.d. la matrice des coefficients du canal $\boldsymbol{\mathcal{H}}$ et la puissance du bruit $\sigma_{\mathbf{v}}^2$ en maximisant la fonction auxiliaire :

$$\boldsymbol{\theta}^{[i+1]} = \arg\max_{\boldsymbol{\theta}} Q\left(\boldsymbol{\theta},\boldsymbol{\theta}^{[i]}\right). \tag{B.29}$$

En mettant à zéro la dérivée de $Q\left(\boldsymbol{\theta},\boldsymbol{\theta}^{[i]}\right)$, donnée par l'équation (B.27), par rapport à $\boldsymbol{\mathcal{H}}$ et en utilisant la propriété suivante de l'opérateur *vec* :
$vec\left(\mathbf{ACB}\right) = \left(\mathbf{B}^T \otimes \mathbf{A}\right) vec\left(\mathbf{C}\right)$, on obtient :

$$vec\left(\boldsymbol{\mathcal{H}}^{[i+1]}\right) = \left[\sum_{k=0}^{K_p-1}\left(\mathbf{d}_p(k)^*\mathbf{d}_p(k)^T \otimes \boldsymbol{\mathcal{W}}(k)^H\boldsymbol{\mathcal{W}}(k)\right) + \sum_{k=K_p}^{K-1}\sum_{\xi=1}^{|D|} \alpha_{k,\xi}\left(\boldsymbol{\theta}^{[i]}\right)\left(\mathbf{d}_\xi{}^*\mathbf{d}_\xi{}^T \otimes \boldsymbol{\mathcal{W}}(k)^H\boldsymbol{\mathcal{W}}(k)\right)\right]^{-1}$$
$$\times \left[\sum_{k=0}^{K_p-1} vec\left(\boldsymbol{\mathcal{W}}(k)^H\mathbf{y}_p\left(k\right)\mathbf{d}_p(k)^H\right) + \sum_{k=K_p}^{K-1}\sum_{\xi=1}^{|D|} \alpha_{k,\xi}\left(\boldsymbol{\theta}^{[i]}\right) vec\left(\boldsymbol{\mathcal{W}}(k)^H\mathbf{y}\left(k\right)\mathbf{d}_\xi{}^H\right)\right]. \tag{B.30}$$

De même, la mise à zéro de la dérivée de $Q\left(\boldsymbol{\theta},\boldsymbol{\theta}^{[i]}\right)$ par rapport à ${\sigma_{\mathbf{v}}}^2$ donne :

$$\{{\sigma_{\mathbf{v}}}^2\}^{[i+1]} = \frac{1}{K}\left(\sum_{k=0}^{K_p-1}\left\|\mathbf{y}_p(k)-\boldsymbol{\mathcal{W}}(k)\boldsymbol{\mathcal{H}}^{[i+1]}\mathbf{d}_p(k)\right\|^2+\sum_{k=K_p}^{K-1}\sum_{\xi=1}^{|D|}\alpha_{k,\xi}\left(\boldsymbol{\theta}^{[i]}\right)\left\|\mathbf{y}(k)-\boldsymbol{\mathcal{W}}(k)\boldsymbol{\mathcal{H}}^{[i+1]}\mathbf{d}_\xi\right\|^2\right). \tag{B.31}$$

L'algorithme est résumé comme suit :

Algorithm 3 *estimation du canal par l'algorithme SA-EM-MIMO*

Initialisation :

1: $i=0$;

2: $\boldsymbol{\theta}^{[0]}=\left[vec\left(\boldsymbol{\mathcal{H}}^{[0]}\right)^T,\{\sigma_{\mathbf{v}}^2\}^{[0]}\right]$ qui représentent les estimés du canal de transmission et de la puissance du bruit en se basant que sur les séquences pilotes ;

Traitement :

3: Estimation de $\boldsymbol{\mathcal{H}}^{[i+1]}$ utilisant $\boldsymbol{\mathcal{H}}^{[i]}$ et $\{\sigma_{\mathbf{v}}^2\}^{[i]}$ selon l'équation (B.30) ;

4: Estimation de $\{\sigma_{\mathbf{v}}^2\}^{[i+1]}$ utilisant $\boldsymbol{\mathcal{H}}^{[i+1]}$, $\boldsymbol{\mathcal{H}}^{[i]}$ et $\{\sigma_{\mathbf{v}}^2\}^{[i]}$ selon l'équation (B.31) ;

5: Remplacer $\boldsymbol{\theta}^{[i]}=\boldsymbol{\theta}^{[i+1]}$;

6: Tant que $\left(\|\boldsymbol{\mathcal{H}}^{[i+1]}-\boldsymbol{\mathcal{H}}^{[i]}\|>\epsilon\right)$ répéter à partir de l'étape 3 ;
Sinon : $\hat{\boldsymbol{\mathcal{H}}}=\boldsymbol{\mathcal{H}}^{[i+1]}$ et $\hat{\sigma}_{\mathbf{v}}^2=\{\sigma_{\mathbf{v}}^2\}^{[i+1]}$.

B.4.2.2 Algorithme EM pour l'estimation semi-aveugle de canal des sous-systèmes

La sommation sur toutes les réalisations possibles du vecteur $\mathbf{d}$ (c.a.d. $|D|$ introduite dans les équations (B.30) et (B.31)) engendre une lourde charge de calcul croissante de manière exponentielle avec N_t. Pour réduire cette charge de calcul, nous proposons de décomposer le système MIMO-OFDM en N_{CPU} sous-systèmes MIMO-OFDM de taille $(N_s \times N_r)$ avec $N_s < N_t$. Cette stratégie est pertinente lorsque la station de base est dotée de calculateurs équipées de N_{CPU} processeurs en parallèle. Ainsi, au lieu d'estimer le canal MIMO comme un seul système, la complexité des calculs est répartie entre tous les processeurs du système N_{CPU}. L'algorithme EM est appliqué sur tous les sous-systèmes MIMO-OFDM (en parallèle), où chaque sous-système est composé de N_s émetteurs et de N_r récepteurs, où N_s est la partie entière de N_t/N_{CPU} ($\lfloor N_t/N_{CPU}\rfloor$) ou $\lfloor N_t/N_{CPU}\rfloor+1$.

A chaque itération (sur les sous-systèmes), les coefficients du canal du u-ème ($u=1\cdots N_{CPU}$) sous-système sont estimés après avoir supprimé les autres signaux reçus des autres (N_t-N_s) émetteurs en utilisant l'égaliseur DFE (voir Figure B.8). Ce dernier estime tout d'abord le canal en s'appuyant sur les séquences pilotes avec l'estimateur LS ($\hat{\boldsymbol{h}}_{OP}$). L'algorithme de détection, développé dans [91], est ensuite appliqué afin d'estimer les données transmises $(\hat{\mathbf{d}}_1\ \cdots\ \hat{\mathbf{d}}_{N_t})$.

Pour estimer le canal du u-ème sous-système MIMO, les signaux transmis par les autres émetteurs sont considérés comme interférences et par conséquent sont soustraits au signal reçu comme suit :

$$\begin{aligned}\mathbf{y}_u^{sub-MIMO}(k) &= \mathbf{y}(k) - \boldsymbol{\mathcal{W}}(k)\hat{\boldsymbol{\mathcal{H}}}_{\bar{u}}\hat{\mathbf{d}}_{\bar{u}}(k) \\ &= \boldsymbol{\mathcal{W}}(k)\boldsymbol{\mathcal{H}}_u\mathbf{d}_u(k) + \mathbf{z}_u(k),\end{aligned} \tag{B.32}$$

où $\mathbf{y}_u^{sub-MIMO}(k)$ est un estimé du signal reçu uniquement des N_s utilisateurs du u-ème sous-système, $\boldsymbol{\mathcal{H}}_u$ représente les N_s colonnes de la matrice $\boldsymbol{\mathcal{H}}$ correspondant aux coefficients du canal de transmission du u-ème sous-système. $\hat{\boldsymbol{\mathcal{H}}}_{\bar{u}}$ est l'estimée de la matrice du canal des $(N_t - N_s)$ utilisateurs interférants, c.a.d. $\hat{\boldsymbol{\mathcal{H}}}_{\bar{u}}$ est égale à $\hat{\boldsymbol{\mathcal{H}}}$ dans laquelle les N_s colonnes qui correspondent au u-ème sous-système sont supprimés.

$\mathbf{z}_u(k)$ représente le bruit et les termes résiduels d'interférence. Sous l'hypothèse que $\mathbf{z}_u(k) \sim \mathcal{N}(0, \sigma^2_{\mathbf{z}_u}\mathbf{I})$, on peut écrire :

$$p\left(\mathbf{y}_u^{sub-MIMO}(k); \boldsymbol{\theta}_u\right) \sim \mathcal{N}\left(\boldsymbol{\mathcal{W}}(k)\boldsymbol{\mathcal{H}}_u d_u(k), \sigma^2_{\mathbf{z}_u}\mathbf{I}\right), \tag{B.33}$$

où $\boldsymbol{\theta}_u = \left[\boldsymbol{\mathcal{H}}_u^T, \sigma^2_{\mathbf{z}_u}\right]^T$ est le vecteur des paramètres inconnus.

En faisant ce traitement, on obtient N_{CPU} sous-systèmes MIMO-OFDM pouvant être traités indépendamment, en parallèle, selon l'algorithme EM itératif suivant :

Pour $u = 1, \cdots, N_{CPU}$:

Etape-E : La fonction auxiliaire $Q\left(\boldsymbol{\theta}_u, \boldsymbol{\theta}_u^{[i]}\right)$ est écrite comme suit :

$$Q\left(\boldsymbol{\theta}_u, \boldsymbol{\theta}_u^{[i]}\right) = \sum_{k=0}^{K_p-1} \log p\left(\mathbf{y}_{p,u}^{sub-MIMO}(k) | \mathbf{d}_{p,u}(k); \boldsymbol{\theta}_u\right) + \sum_{k=K_p}^{K-1}\sum_{\xi=1}^{|D_u|} \alpha_{k,\xi}\left(\boldsymbol{\theta}_u^{[i]}\right) \log p\left(\mathbf{y}_u^{sub-MIMO}(k) | \mathbf{d}_\xi; \boldsymbol{\theta}_u\right), \tag{B.34}$$

où $\{\mathbf{d}_{p,u}(k)\}$ représente les symboles pilotes, $|D_u|$ est l'ensemble des réalisations possibles des symboles du u-ème sous-système avec :

$$p\left(\mathbf{y}_{p,u}^{sub-MIMO}(k) | \mathbf{d}_{p,u}(k); \boldsymbol{\theta}_u\right) \sim \mathcal{N}\left(\boldsymbol{\mathcal{W}}(k)\boldsymbol{\mathcal{H}}_u\mathbf{d}_{p,u}(k), \sigma^2_{\mathbf{z}_u}\mathbf{I}\right), \tag{B.35}$$

$$p\left(\mathbf{y}_u^{sub-MIMO}(k) | \mathbf{d}_\xi; \boldsymbol{\theta}_u\right) \sim \mathcal{N}\left(\boldsymbol{\mathcal{W}}(k)\boldsymbol{\mathcal{H}}_u\mathbf{d}_\xi, \sigma^2_{\mathbf{z}_u}\mathbf{I}\right), \tag{B.36}$$

$$\alpha_{k,\xi}\left(\boldsymbol{\theta}_u^{[i]}\right) = \frac{p\left(\mathbf{y}_u^{sub-MIMO}(k) | \mathbf{d}_\xi; \boldsymbol{\theta}_u^{[i]}\right) p\left(\mathbf{d}_\xi\right)}{\sum_{\xi'=1}^{|D_u|} p\left(\mathbf{y}_u^{sub-MIMO}(k) | \mathbf{d}_{\xi'}; \boldsymbol{\theta}_u^{[i]}\right) p\left(\mathbf{d}_{\xi'}\right)}. \tag{B.37}$$

Étape-M : En mettant à zero la dérivée de $Q\left(\boldsymbol{\theta}_u, \boldsymbol{\theta}_u^{[i]}\right)$ donnée dans l'équation (B.34) par rapport à $\boldsymbol{\mathcal{H}}_u$, on obtient :

$$\begin{aligned}\boldsymbol{\mathcal{H}}_u^{[i+1]} = &\left[\sum_{k=0}^{K_p-1} \boldsymbol{\mathcal{W}}(k)^H\boldsymbol{\mathcal{W}}(k)\mathbf{d}_{p_t,u}(k)\mathbf{d}_{p_t,u}^*(k) + \sum_{k=K_p}^{K-1}\sum_{\xi=1}^{|D_u|}\alpha_{k,\xi,t}\left(\boldsymbol{\theta}_u^{[i]}\right)\boldsymbol{\mathcal{W}}(k)^H\boldsymbol{\mathcal{W}}(k)\mathbf{d}_\xi\mathbf{d}_\xi^*\right]^{-1} \\ &\times\left(\sum_{k=0}^{K_p-1}\boldsymbol{\mathcal{W}}(k)^H\mathbf{y}_{p_t,u}^{sub-MIMO}(k)\,\mathbf{d}_{p_t,u}^*(k) + \sum_{k=K_p}^{K-1}\sum_{\xi=1}^{|D_u|}\alpha_{k,\xi,t}\left(\boldsymbol{\theta}_u^{[i]}\right)\boldsymbol{\mathcal{W}}(k)^H\mathbf{y}_{u,t}^{sub-MIMO}(k)\,\mathbf{d}_\xi^*\right).\end{aligned} \tag{B.38}$$

De même, la mise à zero de la dérivée de $Q\left(\boldsymbol{\theta}_u, \boldsymbol{\theta}_u^{[i]}\right)$ donnée par l'équation (B.34) par rapport à $\sigma^2_{\mathbf{z}_u}$, permet d'obtenir :

$$\begin{aligned}\{{\sigma_{\mathbf{z}_u}}^2\}^{[i+1]} = \frac{1}{K}\Bigg(&\sum_{k=0}^{K_p-1}\left\|\mathbf{y}_{p_t,u}^{sub-MIMO}(k) - \boldsymbol{\mathcal{W}}(k)\boldsymbol{\mathcal{H}}_u^{[i+1]}\mathbf{d}_{p_t,u}(k)\right\|^2 \\ &+\sum_{k=K_p}^{K-1}\sum_{\xi=1}^{|D_u|}\alpha_{k,\xi,t}\left(\boldsymbol{\theta}_u^{[i]}\right)\left\|\mathbf{y}_{u,t}^{sub-MIMO}(k) - \boldsymbol{\mathcal{W}}(k)\boldsymbol{\mathcal{H}}_u^{[i+1]}\mathbf{d}_{\xi}\right\|^2\Bigg).\end{aligned} \tag{B.39}$$

L'algorithme d'estimation semi-aveugle EM-MIMO basé sur N_{CPU} EM-MIMO est résumé par la Figure B.8.

Algorithm 4 *Estimateur SA-EM basé sur N_{CPU} EM-MIMO*

Initialisation :

1: Estimation basée que sur les pilotes (LS) (i.e. $\hat{\boldsymbol{h}}_{OP}$) ;

2: Estimation des données transmises (i.e. $\hat{\mathbf{d}}$) utilisant des algorithmes de détection et décision [91] ;

3: Annulation des Interférences : Considérons un $(N_s \times N_r)$ sous-système MIMO en éliminant les autres signaux reçus des autres émetteurs (interférences) ;

4: Initialisation de $\boldsymbol{\theta}_u^{[0]} = \left[\boldsymbol{\mathcal{H}}_u^{[0]}, \{\sigma^2_{\mathbf{z}_u}\}^{[0]}\right]$, $u = 1, \cdots, N_{CPU}$ par leurs estimés obtenus par les pilotes seuls ;

Traitement : Pour $u = 1 : N_{CPU}$

5: Estimation de $\boldsymbol{\mathcal{H}}_u^{[i+1]}$ utilisant $\boldsymbol{\mathcal{H}}_u^{[i]}$ et $\{\sigma^2_{\mathbf{z}_u}\}^{[i]}$ selon l'équation (B.38) ;

6: Estimation de $\{\sigma^2_{\mathbf{z}_u}\}^{[i+1]}$ utilisant $\{\sigma^2_{\mathbf{z}_u}\}^{[i]}$, $\boldsymbol{\mathcal{H}}_u^{[i]}$, et $\boldsymbol{\mathcal{H}}_u^{[i+1]}$ selon l'équation (B.39);

7: Mettre $\boldsymbol{\theta}_u^{[i]} = \boldsymbol{\theta}_u^{[i+1]}$;

8: Tant que $\left(\|\boldsymbol{\mathcal{H}}_u^{[i+1]} - \boldsymbol{\mathcal{H}}_u^{[i]}\| > \epsilon\right)$ répéter à partir de l'étape 5 ;
Sinon : $\hat{\boldsymbol{\mathcal{H}}}_u = \boldsymbol{\mathcal{H}}_u^{[i+1]}$ et $\hat{\sigma}^2_{\mathbf{z}_u} = \{\sigma^2_{\mathbf{z}_u}\}^{[i+1]}$; Fin pour

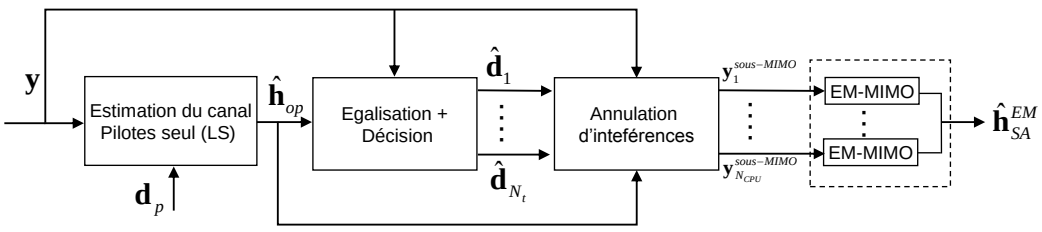

Figure B.8: *Estimation semi-aveugle basée sur N_{CPU} sous-systèmes.*

B.4.3 Analyse des performances

Les simulations s'appuient sur un système de communications sans fil (4×4)-MIMO. Les séquences pilotes correspondent à celles spécifiées dans le standard IEEE 802.11n [22] avec $K = 64$ et $K_p = 8$. Le canal de propagation multi-trajet est représenté par un canal de type B avec un retard de propagation [0 10 20 30] μs et une atténuation moyenne de [0 -4 -8 -12] dB. Notons ($\mathbf{h}_{SA}^{MIMO}$) la version exacte de l'algorithme EM ; ($\mathbf{h}_{SA}^{sous-MIMO}$) l'algorithme EM d'estimation avec une décomposition du système en $N_{CPU} = 2$ MIMO-OFDM sous-systèmes. Les performances de ces algorithmes sont mesurées en termes d'erreur quadratique moyenne normalisée (NRMSE).

La Figure B.9 compare les performances des deux estimateurs à la borne de Cramér-Rao (CRB_{SA}) [32] en fonction du SNR (dB). Les courbes confirment bien que l'estimation semi-aveugle donne de meilleures performances comparées aux méthodes classiques basées uniquement sur les séquences pilotes ($\mathbf{h}_{OP}$). De plus, l'algorithme semi-aveugle proposé, dans lequel le système MIMO-OFDM est décomposé en 2 sous-systèmes MIMO (2×4), donne de bons résultats avec une réduction significative du temps d'exécution (de moitié).

La Figure B.10 compare l'influence de l'augmentation du nombre de symboles OFDM N_d sur les performances d'estimation des canaux mesurées en termes de NRMSE pour un $SNR = 10$ dB. Les courbes montrent que les performances de l'estimation semi-aveugle s'améliorent au fur et à mesure que le nombre de symboles OFDM N_d augmente.

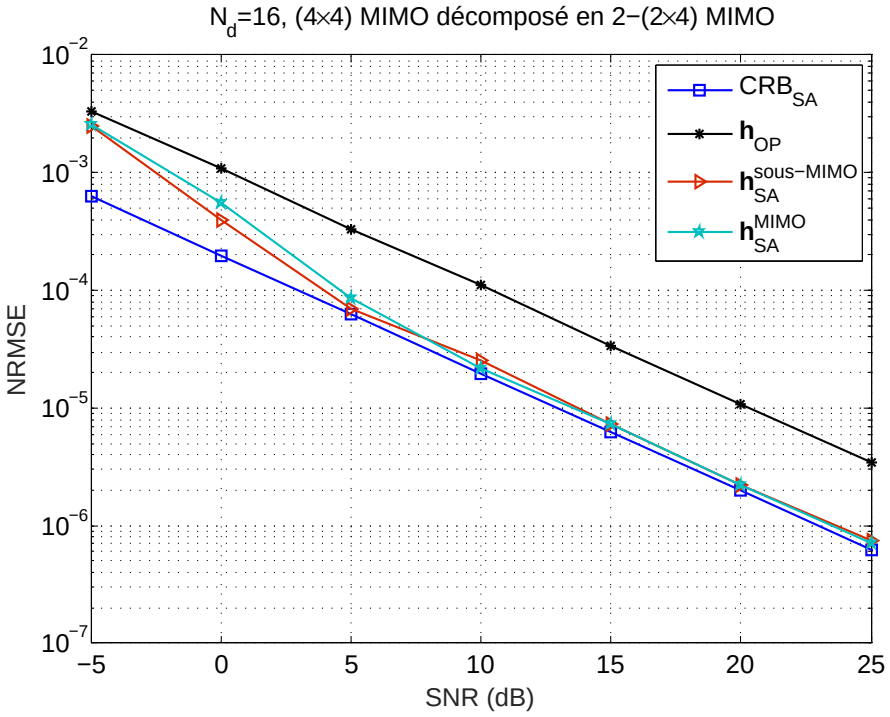

Figure B.9: *Comparaison des performances d'estimation.*

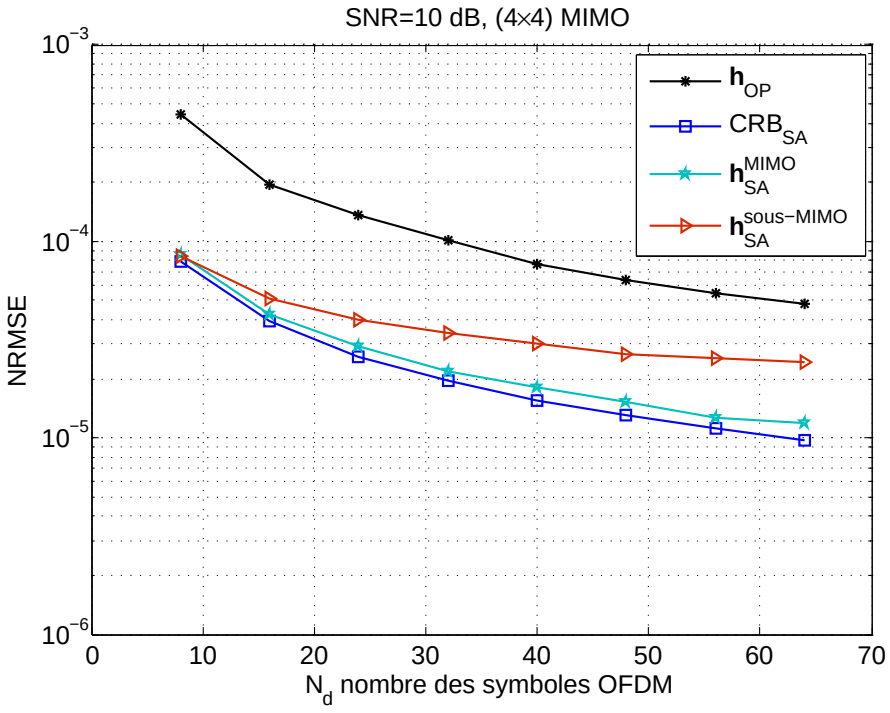

Figure B.10: *Performances en fonction de N_d.*

B.5 Conclusion

L'estimation du canal est d'une importance capitale pour l'égalisation et la détection des symboles dans la plupart des systèmes de communications sans fil, en particulier dans les systèmes MIMO-OFDM. Il suscite dès lors l'intérêt des chercheurs et des développeurs de systèmes depuis le XXe siècle. Une avancée spectaculaire a été réalisée avec le développement et la mise en œuvre d'algorithmes d'estimation de canal basés sur les pilotes, motivés par sa faible complexité et sa faisabilité en ce qui concerne les calculateurs disponibles à cette époque. L'apparition d'ordinateurs puissants (processeurs) disponibles aux stations de base et la forte demande en débits de données plus élevés ont conduit à envisager d'autres approches d'estimation de canaux. Les approches proposées, principalement les techniques semi-aveugles, augmentent le débit de données en réduisant le nombre de pilotes transmis, car ces derniers ne transmettent pas d'informations et représentent un gaspillage de la bande passante. En outre, de nombreux problématiques sont faiblement étudiés dans la littérature en ce qui concerne l'estimation du canal semi-aveugle. Cette thèse est l'une des contributions traitant de l'identification de canaux de de transmission en semi-aveugle et de son analyse dans le contexte des systèmes MIMO-OFDM.

Plusieurs contributions à l'estimation semi-aveugle du canal de transmission ont été réalisées dans cette thèse : la quantification du taux maximum de réduction des pilotes transmis en utilisant l'estimation semi-aveugle du canal tout en garantissant la même qualité d'estimation basée sur les pilotes, puis le développement d'estimateurs semi-aveugles efficaces du canal (LS-DF, méthodes sous-espace, algorithmes basés sur l'algorithme EM). De plus, d'autres études sur les limites de performance de l'estimation de canal MIMO-OFDM ont été abordées, notamment l'analyse de l'effet du CFO sur les performances de l'estimation de canal. Ci-dessous, nous résumons brièvement le travail réalisé dans de cette thèse.

Premièrement, les limites de performance théoriques pour les méthodes d'estimation de canaux semi-aveugles et basées sur des pilotes ont été abordées dans le contexte des systèmes MIMO-OFDM et des systèmes massifs MIMO-OFDM. Cette analyse a été réalisée par le biais de la dérivation analytique des CRB pour différents modèles de données (CG, NCG et BPSK / QPSK) et pour différents modèles de conception pilotes (par exemple, agencement pilote de type bloc, type réseau et type peigne). L'étude des CRB dérivés montre l'énorme réduction du nombre d'échantillons pilotes et, par conséquent, le gain en débit obtenu grâce à l'approche semi-aveugle, tout en conservant la même qualité d'estimation de canal en utilisant que les pilotes. Dans cette thèse, nous montrons que, en utilisant les techniques semi-aveugle, la réduction peut dépasser 95% (modèle de données BPSK) de la taille originale.

Cette étude a également été étendue aux grands systèmes MIMO-OFDM (10×10), où nous montrons que les gains de performance sont légèrement supérieurs à ceux observés pour les systèmes MIMO-OFDM de taille plus petite. De plus, la même étude, a été généralisée aux systèmes massifs multi-cellules MIMO-OFDM sous l'effet de la contamination des pilotes. Par la suite, nous avons montré qu'en utilisant les méthodes semi-aveugle, il est possible de résoudre efficacement le problème de contamination des pilotes lorsqu'on considère des signaux de communications en alphabet fini.

Deuxièmement, nous avons étudié l'effet du CFO sur les performances de l'estimation de canal à l'aide de l'outil CRB. En raison de la propriété de cyclostationnarité du CFO, nous montrons que le CFO impacte avantageusement l'estimation du canal semi-aveugle. Dans le cas du système de communications MISO-OFDM basé sur des protocoles de transmission à relais multiples, nous avons proposé deux approches efficaces pour estimer conjointement le canal de transmission et les CFO. Dans le même contexte, une autre étude a été menée pour évaluer et comparer les CRB pour l'estimation des coefficients de canal de sous-porteuse avec et sans considération de la structure OFDM (c'est-à-dire l'estimation des coefficients de canal dans le domaine temporel ou fréquentiel). Cette étude met en évidence le gain significatif associé à l'approche du domaine temporel.

Troisièmement, nous avons proposé quatre algorithmes d'estimation semi-aveugle de canal. Nous avons commencé par le plus simple (LS-DF) qui repose sur l'estimateur LS utilisé conjointement avec un retour de décision dans lequel les données estimées sont réinjectées à l'étape d'estimation de canal pour améliorer les performances de l'estimation. Dans le contexte des communications écologiques, nous avons montré que, grâce à l'algorithme semi-aveugle LS-DF, on pouvait réduire jusqu'à 76% de la puissance transmise par les pilotes.

La seconde approche semi-aveugle repose sur la technique du maximum de vraisemblance (ML), l'une des méthodes d'estimation les plus efficaces mais aussi les plus coûteuses. L'optimisation du critère ML se fait par une technique itérative utilisant l'algorithme EM. Nous avons proposé trois approches d'approximation/simplification pour traiter la complexité numérique de l'algorithme EM classique. Les trois approximations proposées (à savoir EM-MISO, S-EM, EM-SIMO) donnent de bonnes performances à un coût de calcul inférieur par rapport à l'algorithme EM classique.

Enfin, pour le cas pratique du modèle à canal spéculaire, nous avons proposé une approche paramétrique basée sur une estimation des temps d'arrivés (TOA) utilisant des méthodes sous-espace pour les systèmes SISO-OFDM. L'estimation semi-aveugle des TOAs est réalisée à l'aide

d'un processus de retour de décision qui améliore les performances de l'estimation des TOAs à partir d'une première estimation obtenue grâce aux pilotes existants. Les principales contributions de cette thèse sont énumérées ci-dessous :

- Dérivation des CRB d'estimation de canal pour différents modèles de données (CG, NCG, BPSK / QPSK) et pour différents modèles de conception pilote (agencement pilote de type bloc, type réseau et type peigne) dans le cas du système MIMO-OFDM .
- Pour le modèle de données BPSK / QPSK, une approximation réaliste du CRB a été donnée pour contourner la grande complexité du calcul exact du CRB.
- Proposition d'une technique de calcul efficace pour traiter la manipulation des matrices de grande taille nécessaire pour le calcul des CRBs dans le scénario MIMO de grande taille et le MIMO massif.
- Quantification du taux de réduction des séquences pilotes grâce à l'utilisation de l'estimation semi-aveugle du canal.
- Dérivation des CRB d'estimation semi-aveugle du canal pour un système MIMO-OFDM massif multicellulaire en tenant en compte le phénomène de contamination des pilotes.
- Étude de l'efficacité de l'estimation semi-aveugle du canal de transmission pour résoudre le problème de contamination des pilotes.
- Contribution à la protection des drones contre l'interception aveugle à l'aide de l'analyse des CRBs dans le contexte aveugle.
- Dérivation des CRB d'estimation semi-aveugle de canal en présence de CFO dans le système MIMO-OFDM et l'étude de l'impact positif de CFO sur les performances de l'estimation de canal.
- Proposition de deux approches pour estimer conjointement les coefficients CFO et le canal de transmission.
- Quantification de la dégradation des performances entre l'estimation des coefficients de canal dans le domaine temporel ou fréquentiel.
- Contribution aux communications écologiques en quantifiant la réduction de la puissance transmise à l'aide d'une estimation semi-aveugle de canal.

- Proposition de un estimateur semi-aveugle de canal basé sur la stratégie de retour de décision (LS-DF).
- Contribution à l'estimation semi-aveugle du canal en utilisant l'algorithme EM dans le cas du système MIMO-OFDM.
- Dérivation de quatre versions simplifiées de l'algorithme semi-aveugle EM classique.
- Contribution à l'estimation semi-aveugle sous-espace du canal pour le système MIMO-OFDM.
- Dérivation d'une méthode semi-aveugle paramétrique pour estimer les paramètres de canal (TOA) dans le cas d'un canal OFDM spéculaire.

Bibliography

[1] J. A. del Peral-Rosado, R. Raulefs, J. A. López-Salcedo, and G. Seco-Granados, "Survey of cellular mobile radio localization methods: From 1G to 5G," *IEEE Communications Surveys Tutorials*, vol. 20, no. 2, pp. 1124–1148, 2018.

[2] G. Gu and G. Peng, "The survey of GSM wireless communication system," in *2010 International Conference on Computer and Information Application*, Dec 2010, pp. 121–124.

[3] L. L. Hanzo, L.-L. Yang, E.-L. Kuan, and K. Yen, *Overview of Multicarrier CDMA*. IEEE, 2004. [Online]. Available: https://ieeexplore.ieee.org/document/5732959

[4] F. W. Y. Bouguen, E. Hardouin, *LTE et les réseaux 4G*. Paris, France: Editions Eyrolles, 2013.

[5] A. J. PAULRAJ, D. A. GORE, R. U. NABAR, and H. BOLCSKEI, "An overview of MIMO communications - a key to gigabit wireless," *Proceedings of the IEEE*, vol. 92, no. 2, pp. 198–218, Feb 2004.

[6] K. Choi and H. Liu, *MIMO System - Part II: Spatial Multiplexing*. IEEE, 2016. [Online]. Available: https://ieeexplore.ieee.org/document/7435069

[7] F. D. Flaviis, L. Jofre, J. Romeu, and A. Grau, *Multiantenna Systems for MIMO Communications*. Morgan and Claypool, 2013. [Online]. Available: https://ieeexplore.ieee.org/document/6812510

[8] A. Narasimhamurthy, M. Banavar, and C. Tepedelenliouglu, *OFDM Systems for Wireless Communications*. Morgan and Claypool, 2010. [Online]. Available: https://ieeexplore.ieee.org/document/6812632

[9] C. O. B. Clerckx, *MIMO wireless networks*. The Boulevard, Langford Lane, Kindlinton, Oxford, OX51 GB: ACADEMIC PRESS, 2013.

[10] M. Jiang and L. Hanzo, "Multiuser MIMO-OFDM for next-generation wireless systems," *Proceedings of the IEEE*, vol. 95, no. 7, pp. 1430–1469, July 2007.

[11] S. Aust, R. V. Prasad, and I. G. M. M. Niemegeers, "Outdoor long-range wlans: A lesson for ieee 802.11ah," *IEEE Communications Surveys Tutorials*, vol. 17, no. 3, pp. 1761–1775, thirdquarter 2015.

[12] B. P. Crow, I. Widjaja, J. G. Kim, and P. T. Sakai, "Ieee 802.11 wireless local area networks," *IEEE Communications Magazine*, vol. 35, no. 9, pp. 116–126, Sep. 1997.

[13] I.-T. Lu and K.-J. Tsai, "Channel estimation in a proposed IEEE802.11n OFDM MIMO WLAN system," in *IEEE Sarnoff Symposium*, April 2007, pp. 1–5.

[14] E. G. Larsson, O. Edfors, F. Tufvesson, and T. L. Marzetta, "Massive MIMO for next generation wireless systems," *IEEE Communications Magazine*, vol. 52, no. 2, pp. 186–195, February 2014.

[15] R. Vannithamby and S. Talwar, *Massive MIMO Communications*. Wiley, 2017. [Online]. Available: https://ieeexplore.ieee.org/document/8042298

[16] F. Rusek, D. Persson, B. K. Lau, E. G. Larsson, T. L. Marzetta, O. Edfors, and F. Tufvesson, "Scaling up MIMO: Opportunities and challenges with very large arrays," *IEEE Signal Processing Magazine*, vol. 30, no. 1, pp. 40–60, Jan 2013.

[17] T. L. Marzetta, "Noncooperative cellular wireless with unlimited numbers of base station antennas," *IEEE Transactions on Wireless Communications*, vol. 9, no. 11, pp. 3590–3600, 2010.

[18] H. Q. Ngo, E. G. Larsson, and T. L. Marzetta, "Energy and spectral efficiency of very large multiuser MIMO systems," *IEEE Transactions on Communications*, vol. 61, no. 4, pp. 1436–1449, 2013.

[19] O. Simeone, Y. Bar-Ness, and U. Spagnolini, "Pilot-based channel estimation for OFDM systems by tracking the delay-subspace," *IEEE Trans. on Wireless Communications*, vol. 3, no. 1, pp. 315–325, Jan 2004.

[20] W. Zhang, X. G. Xia, and P. C. Ching, "Optimal training and pilot pattern design for OFDM systems in Rayleigh fading," *IEEE Trans. on Broadcasting*, vol. 52, no. 4, pp. 505–514, Dec 2006.

[21] G. B. Jency and S. J. Gladwin, "Channel estimation using optimized pilot placement in OFDM system," in *Communications and Signal Processing (ICCSP), 2014 International Conference on.* IEEE, 2014, pp. 1529–1534.

[22] R. S. E. Perahi, *Next Generation Wireless LANS.* New York, USA: Cambridge University Press, 2008.

[23] S. Noh, Y. Sung, and M. D. Zoltowski, "A new precoder design for blind channel estimation in MIMO-OFDM systems," *IEEE Trans. on Wireless Communications*, vol. 13, no. 12, pp. 7011–7024, Dec 2014.

[24] L. Tong, G. Xu, and T. Kailath, "Blind identification and equalization based on second-order statistics: a time domain approach," *IEEE Trans. on Information Theory.*, Mar 1994.

[25] C. Shin, R. W. Heath, and E. J. Powers, "Blind channel estimation for MIMO-OFDM systems," *IEEE Trans. on Vehicular Technology*, vol. 56, no. 2, pp. 670–685, March 2007.

[26] A. K. Jagannatham and B. D. Rao, "Whitening-rotation-based semi-blind MIMO channel estimation," *IEEE Trans. on Signal Processing*, vol. 54, no. 3, pp. 861–869, March 2006.

[27] K. Liu, J. P. C. L. da Costa, H. C. So, and A. L. F. de Almeida, "Semi-blind receivers for joint symbol and channel estimation in space-time-frequency MIMO-OFDM systems," *IEEE Trans. on Signal Processing*, vol. 61, no. 21, pp. 5444–5457, Nov 2013.

[28] G. Favier and A. L. F. de Almeida, "Tensor space-time-frequency coding with semi-blind receivers for MIMO wireless communication systems," *IEEE Trans. on Signal Processing*, vol. 62, no. 22, pp. 5987–6002, Nov 2014.

[29] W. Yang, Y. Cai, and Y. Xun, "Semi-blind channel estimation for OFDM systems," in *IEEE 63rd Vehicular Technology Conference*, vol. 1, May 2006, pp. 226–230.

[30] R. C. de Lamare, "Massive MIMO systems: Signal processing challenges and research trends," *arXiv preprint arXiv:1310.7282*, 2013.

[31] N. Hassan and X. Fernando, "Massive MIMO wireless networks: An overview," *Electronics*, vol. 6, no. 3, p. 63, 2017.

[32] A. Ladaycia, A. Mokraoui, K. Abed-Meraim, and A. Belouchrani, "Performance bounds analysis for semi-blind channel estimation in MIMO-OFDM communications systems," *IEEE Trans. on Wireless Communications*, vol. 16, no. 9, pp. 5925–5938, Sept 2017.

[33] ——, "Toward green communications using semi-blind channel estimation," in *25th European Signal Processing Conference (EUSIPCO)*, Aug 2017, pp. 2254–2258.

[34] A. K. Jagannatham and B. D. Rao, "Complex constrained CRB and its application to semi-blind MIMO and OFDM channel estimation," in *Processing Workshop Proceedings, 2004 Sensor Array and Multichannel Signal*, July 2004, pp. 397–401.

[35] S.-M. Omar, D. Slock, and O. Bazzi, "Bayesian and deterministic crbs for semi-blind channel estimation in SIMO single carrier cyclic prefix systems," in *IEEE 22nd International Symposium on Personal Indoor and Mobile Radio Communications (PIMRC)*, Sept 2011, pp. 1682–1686.

[36] S. M. Kay, *Fundamentals of Statistical signal processing, Estimation Theory.* Upper Saddle River, New Jersey 07458, USA: Prentice Hall PTR, INC, 1993.

[37] D.-T. Do and D.-T. Vu, "New orthogonal pilot scheme for semi-blind channel estimation in MIMO systems," in *International Conference on Networking and Information Technology*, June 2010, pp. 235–238.

[38] S. Park, E. Serpedin, and K. Qaraqe, "Gaussian assumption: The least favorable but the most useful [lecture notes]," *IEEE Signal Processing Magazine*, vol. 30, no. 3, pp. 183–186, May 2013.

[39] T. Menni, E. Chaumette, P. Larzabal, and J. Barbot, "New results on deterministic cramer-rao bounds for real and complex parameters," *IEEE Trans. on Signal Processing*, vol. 60, no. 3, pp. 1032–1049, March 2012.

[40] L. Berriche and K. Abed-Meraim, "Stochastic Cramér-Rao bounds for semiblind MIMO channel estimation," in *IEEE International Symposium on Signal Processing and Information Technology*, Dec 2004, pp. 119–122.

[41] J. P. Delmas and H. Abeida, "Stochastic cramer-rao bound for noncircular signals with application to DOA estimation," *IEEE Trans. on Signal Processing*, vol. 52, no. 11, pp. 3192–3199, Nov 2004.

[42] K. Lee, J. Kim, J. Jung, and I. Lee, "Zadoff-chu sequence based signature identification for OFDM," *IEEE Trans. on Wireless Communications*, vol. 12, no. 10, pp. 4932–4942, October 2013.

[43] H. Yin, D. Gesbert, M. C. Filippou, and Y. Liu, "Decontaminating pilots in massive MIMO systems," in *IEEE International Conference on Communications (ICC)*, June 2013, pp. 3170–3175.

[44] X. Zheng, H. Zhang, W. Xu, and X. You, "Semi-orthogonal pilot design for massive MIMO systems using successive interference cancellation," in *IEEE Global Communications Conference*, Dec 2014, pp. 3719–3724.

[45] O. Rekik, A. Ladaycia, K. Abed-Meraim, and A. Mokraoui, "Performance bounds analysis for semi-blind channel estimation with pilot contamination in massive MIMO-OFDM systems," in *26th European Signal Processing Conference (EUSIPCO)*, Sep 2018.

[46] F. Boccardi, R. W. Heath, A. Lozano, T. L. Marzetta, and P. Popovski, "Five disruptive technology directions for 5G," *IEEE Communications Magazine*, vol. 52, no. 2, pp. 74–80, 2014.

[47] J. Jose, A. Ashikhmin, T. L. Marzetta, and S. Vishwanath, "Pilot contamination problem in multi-cell TDD systems," in *International Symposium on Information Theory (ISIT)*. IEEE, 2009, pp. 2184–2188.

[48] F. Fernandes, A. Ashikhmin, and T. L. Marzetta, "Inter-cell interference in noncooperative TDD large scale antenna systems," *IEEE Journal on Selected Areas in Communications*, vol. 31, no. 2, pp. 192–201, 2013.

[49] J. Hoydis, S. Ten Brink, and M. Debbah, "Massive MIMO in the UL/DL of cellular networks: How many antennas do we need?" *IEEE Journal on selected Areas in Communications*, vol. 31, no. 2, pp. 160–171, 2013.

[50] H. Yin, D. Gesbert, M. Filippou, and Y. Liu, "A coordinated approach to channel estimation in large-scale multiple-antenna systems," *IEEE Journal on Selected Areas in Communications*, vol. 31, no. 2, pp. 264–273, 2013.

[51] J. Ma and L. Ping, "Data-aided channel estimation in large antenna systems," in *International Conference on Communications (ICC)*. IEEE, 2014, pp. 4626–4631.

[52] A. Ashikhmin and T. Marzetta, "Pilot contamination precoding in multi-cell large scale antenna systems," in *International Symposium on Information Theory (ISIT)*. IEEE, 2012, pp. 1137–1141.

[53] L. Li, A. Ashikhmin, and T. Marzetta, "Pilot contamination precoding for interference reduction in large scale antenna systems," in *51st Annual Allerton Conference on Communication, Control, and Computing*. IEEE, 2013, pp. 226–232.

[54] J. Fan, W. Li, and Y. Zhang, "Pilot contamination mitigation by fractional pilot reuse with threshold optimization in massive MIMO systems," *Digital Signal Processing*, 2018.

[55] T. Peken, G. Vanhoy, and T. Bose, "Blind channel estimation for massive MIMO," *Analog Integrated Circuits and Signal Processing*, vol. 91, no. 2, pp. 257–266, 2017.

[56] E. Amiri, R. Mueller, and W. Gerstacker, "Blind pilot decontamination in massive MIMO by Independent Component Analysis," in *Globecom Workshops*. IEEE, 2017, pp. 1–5.

[57] D. Hu, L. He, and X. Wang, "Semi-blind pilot decontamination for massive MIMO systems," *IEEE Transactions on Wireless Communications*, vol. 15, no. 1, pp. 525–536, 2016.

[58] A. S. Alwakeel and A. H. Mehana, "Semi-blind channel estimation and interference alignment for massive MIMO network," in *Global Communications Conference GLOBECOM*. IEEE, 2017, pp. 1–6.

[59] N. Fatema, Y. Xiang, and I. Natgunanathan, "Analysis of a semi-blind pilot decontamination method in massive MIMO," in *27th International Telecommunication Networks and Applications Conference (ITNAC)*. IEEE, 2017, pp. 1–6.

[60] T. L. Marzetta, "How much training is required for multiuser MIMO?" in *40th Asilomar Conference on Signals, Systems and Computers (ACSSC)*. IEEE, 2006, pp. 359–363.

[61] G. Caire, N. Jindal, M. Kobayashi, and N. Ravindran, "Multiuser MIMO achievable rates with downlink training and channel state feedback," *IEEE Transactions on Information Theory*, vol. 56, no. 6, pp. 2845–2866, 2010.

[62] H. Abeida and J.-P. Delmas, "Gaussian Cramer-Rao bound for direction estimation of noncircular signals in unknown noise fields," *IEEE Transactions on Signal Processing*, vol. 53, no. 12, pp. 4610–4618, 2005.

[63] K. Abed-Meraim, P. Loubaton, and E. Moulines, "A subspace algorithm for certain blind identification problems," *IEEE Trans. on Information Theory*, vol. 43, no. 2, pp. 499–511, Mar 1997.

[64] K. Abed-Meraim, W. Qiu, and Y. Hua, "Blind system identification," *Proceedings of the IEEE*, vol. 85, no. 8, pp. 1310–1322, Aug 1997.

[65] P. Comon, "Independent Component Analysis, a new concept?" *Signal processing*, vol. 36, no. 3, pp. 287–314, 1994.

[66] A. Ladaycia, A. Mokraoui, K. Abed-Meraim, and A. Belouchrani, "What semi-blind channel estimation brings in terms of throughput gain ?" in *10th ICSPCS*, Dec 2016, pp. 1–6.

[67] A. Ladaycia, A. Belouchrani, K. Abed-Meraim, and A. Mokraoui, "Parameter optimization for defeating blind interception in drone protection," in *2017 Seminar on Detection Systems Architectures and Technologies (DAT)*, Feb 2017, pp. 1–6.

[68] S.-M. Omar, D. Slock, and O. Bazzi, "Recent insights in the bayesian and deterministic crb for blind SIMO channel estimation," in *IEEE International Conference on Acoustics, Speech and Signal Processing (ICASSP)*, March 2012, pp. 3549–3552.

[69] H. Liu and G. Xu, "Closed-form blind symbol estimation in digital communications," *IEEE Transactions on Signal Processing*, vol. 43, no. 11, pp. 2714–2723, Nov 1995.

[70] D. I. Iglesia, C. J. Escudero, and L. Castedo, "Cramer-rao bound for blind channel estimation in multi-carrier CDMA systems," in *Signal Processing Conference, 2000 10th European*, Sept 2000, pp. 1–4.

[71] A. Ladaycia, A. Mokraoui, K. Abed-Meraim, and A. Belouchrani, "Further investigations on the performance bounds of MIMO-OFDM channel estimation," in *13th International Wireless Communications and Mobile Computing Conference (IWCMC)*, June 2017, pp. 223–228.

[72] D. Huang and K. B. Letaief, "Carrier frequency offset estimation for ofdm systems using subcarriers," *IEEE Trans. on Communications*, vol. 54, no. 5, pp. 813–823, May 2006.

[73] J. Lei and T.-S. Ng, "A consistent OFDM carrier frequency offset estimator based on distinctively spaced pilot tones," *IEEE Trans. on Wireless Communications*, vol. 3, no. 2, pp. 588–599, March 2004.

[74] H. Minn, Y. Li, N. Al-Dhahir, and R. Calderbank, "Pilot designs for consistent frequency offset estimation in ofdm systems," in *IEEE International Conference on Communications*, vol. 10, June 2006, pp. 4566–4571.

[75] K. Lee and I. Lee, "Robust pilot designs for consistent frequency offset estimation in ofdm systems," in *IEEE Global Telecommunications Conference (GLOBECOM 2010)*, Dec 2010, pp. 1–5.

[76] Y. J. Liang and J. F. Chang, "Noniterative joint frequency offset and channel estimation for mimo ofdm systems using cascaded orthogonal pilots," *IEEE Trans. on Vehicular Technology*, vol. 59, no. 8, pp. 4151–4156, Oct 2010.

[77] Y. Shen and E. Martinez, "Channel estimation in OFDM systems," Freescale Semiconductor, Tech. Rep., 2006.

[78] Y. Chen, S. Zhang, S. Xu, and G. Y. Li, "Fundamental trade-offs on green wireless networks," *IEEE Commun. Magazine*, June 2011.

[79] D. Feng, C. Jiang, G. Lim, L. J. Cimini, G. Feng, and G. Y. Li, "A survey of energy-efficient wireless communications," *IEEE Commun. Surveys Tutorials*, vol. 15, no. 1, pp. 167–178, 2013.

[80] K. Qian and W. Q. Wang, "Energy-efficient antenna selection in green MIMO relaying communication systems," *Journal of Communications and Networks*, vol. 18, no. 3, pp. 320–326, June 2016.

[81] T. Dong, V. Dobrev, T. Kolev, R. Rieben, S. Tomov, and J. Dongarra, "A step towards energy efficient computing: Redesigning a hydrodynamic application on cpu-gpu," in *IEEE 28th Int. Parallel and Distributed Processing Symposium*, May 2014, pp. 972–981.

[82] A. Ladaycia, A. Belouchrani, K. Abed-Meraim, and A. Mokraoui, "EM-based semi-blind MIMO-OFDM channel estimation," in *2018 IEEE International Conference on Acoustics, Speech and Signal Processing (ICASSP)*, April 2018, pp. 3899–3903.

[83] ——, "Semi-blind MIMO-OFDM channel estimation using EM-like techniques," *IEEE Trans. on Signal processing (submitted)*, July 2018.

[84] S. Park, J. W. Choi, J. Y. Seol, and B. Shim, "Expectation-maximization-based channel estimation for multiuser MIMO systems," *IEEE Trans. on Communications*, vol. 65, no. 6, pp. 2397–2410, June 2017.

[85] G. Hu and D. Li, "EM-based channel estimation for MIMO OFDM system," in *International Conference on Networks Security, Wireless Communications and Trusted Computing*, vol. 1, April 2009, pp. 159–162.

[86] E. Nayebi and B. D. Rao, "Semi-blind channel estimation for multiuser massive MIMO systems," *IEEE Trans. on Signal Processing*, vol. 66, no. 2, pp. 540–553, Jan 2018.

[87] ——, "Semi-blind channel estimation in massive MIMO systems with different priors on data symbols," in *43rd International Conference on Acoustics, Speech and Signal Processing (ICASSP)*, Apr 2018.

[88] N. M. L. A. P. Dempster and D. B. Rubin, "Maximum likelihood from incomplete data via the EM algorithm," *Journal of the Royal Statistical Society. Series B (Methodological)*, vol. 39, no. 1, pp. 1–38, 1977.

[89] P. Comon and M. Rajih, "Blind identification of under-determined mixtures based on the characteristic function," in *IEEE International Conference on Acoustics, Speech, and Signal Processing*, vol. 4, March 2005, pp. iv/1005–iv/1008 Vol. 4.

[90] J. A. Fessler and A. O. Hero, "Space-alternating generalized expectation-maximization algorithm," *IEEE Trans. on Signal Processing*, vol. 42, no. 10, pp. 2664–2677, Oct 1994.

[91] M. O. Damen, H. E. Gamal, and G. Caire, "On maximum-likelihood detection and the search for the closest lattice point," *IEEE Trans. on Information Theory*, vol. 49, no. 10, pp. 2389–2402, Oct 2003.

[92] W. Abediseid and M. S. Alouini, "On lattice sequential decoding for the unconstrained AWGN channel," *IEEE Trans. on Communications*, vol. 61, no. 6, pp. 2446–2456, June 2013.

[93] A. Ladaycia, K. Abed-Meraim, A. Mokraoui, and A. Belouchrani, "Contributions à l'estimation semi-aveugle des canaux MIMO-OFDM," in *GRETSI 2017*, Sep 2017.

[94] ——, "Efficient semi-blind subspace channel estimation for MIMO-OFDM system," in *26th European Signal Processing Conference (EUSIPCO)*, Sep 2018.

[95] C. Shin, R. W. Heath, and E. J. Powers, "Blind channel estimation for MIMO-OFDM systems," *IEEE Tran. on Vehicular Tech.*, March 2007.

[96] B. Muquet, M. de Courville, and P. Duhamel, "Subspace-based blind and semi-blind channel estimation for OFDM systems," *IEEE Tran. on Signal Processing*, Jul 2002.

[97] J. L. Yu and W. R. Kuo, "Fast semi-blind channel estimation for MIMO-OFDM systems with virtual carriers," in *1st IEEE International Conference on Communications in China (ICCC)*, Aug 2012, pp. 356–361.

[98] A. Kammoun, K. Abed-Meraim, and S. Affes, "Quasi-convexity of the asymptotic channel MSE in regularized semi blind estimation," *IEEE Trans. on Information Theory*, vol. 57, no. 7, pp. 4732–4739, July 2011.

[99] A. Ladaycia, M. Pesavento, A. Mokraoui, K. Abed-Meraim, and A. Belouchrani, "Decision feedback semi-blind estimation algorithm for specular OFDM channels," in *2018 IEEE International Conference on Acoustics, Speech and Signal Processing (ICASSP) (submitted)*, October 2018, pp. 3899–3903.

[100] M. R. Raghavendra, S. Bhashyam, and K. Giridhar, "Exploiting hopping pilots for parametric channel estimation in OFDM systems," *IEEE Signal Processing Letters*, vol. 12, no. 11, pp. 737–740, Nov 2005.

[101] R. Schmidt, "Multiple emitter location and signal parameter estimation," *IEEE Trans. on Antennas and Propagation*, vol. 34, no. 3, pp. 276–280, Mar 1986.

[102] K. V. Rangarao and S. Venkatanarasimhan, "gold-MUSIC: A variation on MUSIC to accurately determine peaks of the spectrum," *IEEE Trans. on Antennas and Propagation*, vol. 61, no. 4, pp. 2263–2268, April 2013.

[103] B. D. Rao and K. V. S. Hari, "Performance analysis of root-MUSIC," *IEEE Trans. on Acoustics, Speech, and Signal Processing*, vol. 37, no. 12, pp. 1939–1949, Dec 1989.

[104] W. Suleiman, M. Pesavento, and A. Zoubir, "Performance analysis of direction-of-arrival estimation using the decentralized root-MUSIC," in *IEEE 6th International Workshop on Computational Advances in Multi-Sensor Adaptive Processing (CAMSAP)*, Dec 2015, pp. 329–332.

[105] M. V. Athi and S. A. Zekavat, "Real-time root-MUSIC DOA estimation via a parallel polynomial rooting method," in *IEEE 25th Annual International Symposium on Personal, Indoor, and Mobile Radio Communication (PIMRC)*, Sept 2014, pp. 290–295.

[106] R. Roy and T. Kailath, "Esprit-estimation of signal parameters via rotational invariance techniques," *IEEE Trans. on Acoustics, Speech, and Signal Processing*, vol. 37, no. 7, pp. 984–995, Jul 1989.

[107] M. Trinh-Hoang, M. Viberg, and M. Pesavento, "An improved DOA estimator based on partial relaxation approach," in *43rd International Conference on Acoustics, Speech and Signal Processing (ICASSP)*, Apr 2018.

[108] ——, "Partial relaxation approach: An eigenvalue-based DOA estimator framework," *IEEE Transactions on Signal Processing*, pp. 1–1, 2018.

[109] A. Ladaycia, K. Abed-Meraim, A. Bader, and M. S. Alouini, "Cfo and channel estimation for miso-ofdm systems," in *25th European Signal Processing Conference (EUSIPCO)*, Aug 2017, pp. 2521–2525.

[110] A. Bader, "Contention-free multi-relay beaconless geo-routing"," *Ph.D. dessertation, Telecom ParisTech*, 2013.

[111] A. Bader, K. Abed-Meraim, and M. S. Alouini, "An efficient multi-carrier position-based packet forwarding protocol for wireless sensor networks," *IEEE Trans. on Wireless Communications*, vol. 11, no. 1, pp. 305–315, January 2012.

[112] ——, "Beaconless georouting under the spotlight: Practical link models and application scenarios," *IEEE Systems Journal*, vol. 9, no. 3, pp. 785–796, Sept 2015.

[113] R. O'Donnell, "Prolog to synchronization techniques for orthogonal frequency division multiple access (ofdma): A tutorial review," *Proceedings of the IEEE*, vol. 95, no. 7, pp. 1392–1393, July 2007.

[114] D. Huang and K. B. Letaief, "Carrier frequency offset estimation for ofdm systems using subcarriers," *IEEE Trans. on Communications*, vol. 54, no. 5, pp. 813–823, May 2006.

[115] R. Roy and T. Kailath, "Esprit-estimation of signal parameters via rotational invariance techniques," *IEEE Trans. on Acoustics, Speech, and Signal Processing*, vol. 37, no. 7, pp. 984–995, Jul 1989.

[116] D. W. Marquardt, "An algorithm for least-squares estimation of nonlinear parameters." *Journal of the society for Industrial and Applied Mathematics*, vol. 11, no. 2, p. 431–441, 1963.

[117] M. Tlich and M. S. Alouini, "Design and optimization of multi-node multihop relaying techniques using cross-layer approach," *Technical report for the KACST project under Grant RGC/3/1801-01-01, KAUST, KSA*, 2015.

Titre : **Annulation d'interférences dans les systèmes MIMO et MIMO massifs (Massive MIMO).**

Mots clefs : MIMO/ massive MIMO, OFDM, CRB, semi-aveugle, méthode sous-espace, algorithme EM, LS-DF, canal spéculaire.

Résumé : Les systèmes de communications MIMO utilisent des réseaux de capteurs qui peuvent s'étendre à de grandes dimensions (MIMO massifs) et qui sont pressentis comme solution potentielle pour les futurs standards de communications à très hauts débits. Un des problème majeur de ces systèmes est le fort niveau d'interférences dû au grand nombre d'émetteurs simultanés. Dans un tel contexte, les solutions 'classiques' de conception de pilotes 'orthogonaux' sont extrêmement coûteuses en débit utile permettant ainsi aux solutions d'identification de canal dites 'aveugles' ou 'semi-aveugles' de revenir au-devant de la scène comme solutions intéressantes d'identification ou de déconvolution de ces canaux MIMO.
Dans cette thèse, nous avons commencé par une analyse comparative des performances, en nous basant sur les CRB, afin de mesurer la réduction potentielle de la taille des séquences pilotes et ce en employant les méthodes dites semi-aveugles. Les résultats d'analyse montrent que nous pouvons réduire jusqu'à 95% des pilotes sans affecter les performances d'estimation du canal. Nous avons par la suite proposé de nouvelles méthodes d'estimation semi-aveugle du canal, permettant d'approcher la CRB. Nous avons proposé un estimateur semi-aveugle, LS-DF qui permet un bon compromis performance / complexité numérique. Un autre estimateur semi-aveugle de type sous-espace a aussi été proposé ainsi qu'un algorithme basé sur l'approche EM pour lequel trois versions à coût réduit ont été étudiées. Dans le cas d'un canal spéculaire, nous avons proposé un algorithme d'estimation paramétrique se basant sur l'estimation des temps d'arrivés combinée avec la technique DF.

Title : **Interference cancellation in MIMO and massive MIMO systems**

Keywords : Geostrophic equilibrium, low Froude number, hyperbolic system, finite volume method, Godunov scheme, numerical diffusion, well-balanced scheme, Coriolis force.

Abstract : MIMO systems use sensor arrays that can be of large-scale (massive MIMO) and are seen as a potential candidate for future digital communications standards at very high throughput. A major problem of these systems is the high level of interference due to the large number of simultaneous transmitters. In such a context, 'conventional' orthogonal pilot design solutions are expensive in terms of throughput, thus allowing for the so-called 'blind' or 'semi-blind' channel identification solutions to come back to the forefront as interesting solutions for identifying or deconvolving these MIMO channels.
In this thesis, we started with a comparative performance analysis, based on CRB, to quantify the potential size reduction of the pilot sequences when using semi-blind methods that jointly exploit the pilots and data. Our analysis shows that, up to 95% of the pilot samples can be suppressed without affecting the channel estimation performance when such semi-blind solutions are considered. After that, we proposed new methods for semi-blind channel estimation, that allow to approach the CRB. At first, we have proposed a SB estimator, LS-DF which allows a good compromise between performance and numerical complexity. Other SB estimators have also been introduced based on the subspace technique and on the ML approach, respectively. The latter is optimized via an EM algorithm for which three reduced cost versions are proposed. In the case of a specular channel model, we considered a parametric estimation method based on times of arrival estimation combined with the DF technique.

Université Paris-13, Sorbonne Paris Cité

Laboratoire de Traitement et Transport de l'Information (L2TI)

Villetaneusse, France